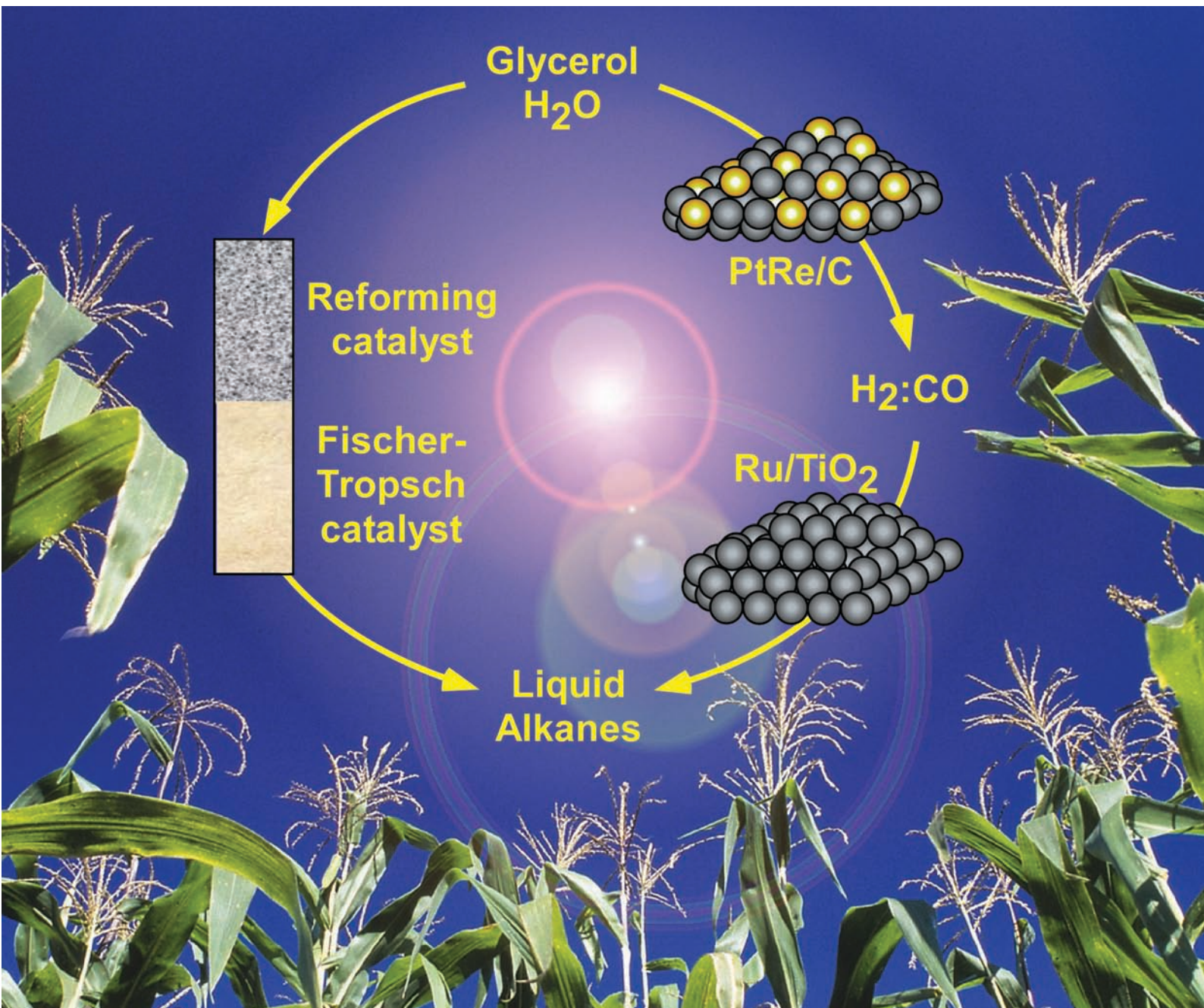


# Green Chemistry

Cutting-edge research for a greener sustainable future

[www.rsc.org/greenchem](http://www.rsc.org/greenchem)

Volume 9 | Number 10 | October 2007 | Pages 1029–1144



ISSN 1463-9262

Chen *et al.*  
Efficient and controlled  
polymerization of lactide

Simonetti *et al.*  
Coupling of glycerol processing with  
Fischer–Tropsch synthesis

Mack *et al.*  
Solvent-free method for the  
reduction of esters

Sheldrake and Schleck  
Dicationic molten salts as re-usable  
media for pyrolysis of cellulose



1463-9262(2007)9:10;1-T

RSC Publishing



## *The must-have primary research journal for environmental issues*

Comprehensive and high quality coverage of multidisciplinary, international research relating to the measurement, pathways, impact and management of contaminants in all environments.



- Highly visible and cited in MEDLINE
- Accelerated publication rates, typically around 80 days
- Dedicated to the measurement of natural and anthropogenic sources of pollution with a view to assessing environmental and human health effects

## Submit your work to JEM today

RSC Publishing

[www.rsc.org/jem](http://www.rsc.org/jem)

Registered Charity Number 207890



# Green Chemistry

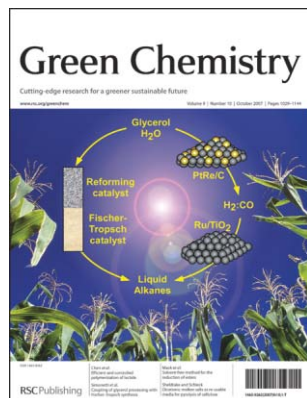
Cutting-edge research for a greener sustainable future

[www.rsc.org/greenchem](http://www.rsc.org/greenchem)

RSC Publishing is a not-for-profit publisher and a division of the Royal Society of Chemistry. Any surplus made is used to support charitable activities aimed at advancing the chemical sciences. Full details are available from [www.rsc.org](http://www.rsc.org)

## IN THIS ISSUE

ISSN 1463-9262 CODEN GRCHFJ 9(10) 1029–1144 (2007)



### Cover

See Simonetti *et al.*, pp. 1073–1083.

A new process that couples catalytic conversion of glycerol with Fischer–Tropsch synthesis can produce liquid alkanes from biomass-derived feedstocks.

Image reproduced by permission of James A. Dumesic from *Green Chem.*, 2007, **9**, 1073.

## CHEMICAL TECHNOLOGY

T73

Chemical Technology highlights the latest applications and technological aspects of research across the chemical sciences.

## Chemical Technology

October 2007/Volume 4/Issue 10

[www.rsc.org/chemicaltechnology](http://www.rsc.org/chemicaltechnology)

## COMMUNICATIONS

1038



### Efficient and controlled polymerization of lactide under mild conditions with a sodium-based catalyst

Hsuan-Ying Chen, Jubo Zhang, Chu-Chieh Lin,\*  
Joseph H. Reibenspies and Stephen A. Miller\*

A common phenolic antioxidant provides the ligand scaffold in the first discrete sodium-based catalyst for the highly active and controlled ring-opening polymerization of lactide.



## EDITORIAL STAFF

**Editor**

Sarah Ruthven

**Assistant editor**

Sarah Dixon

**Publishing assistant**

Ruth Bircham

**Team leader, serials production**

Stephen Wilkes

**Technical editor**

Edward Morgan

**Production administration coordinator**

Sonya Spring

**Administration assistants**

Clare Davies, Donna Fordham, Julie Thompson

**Publisher**

Emma Wilson

Green Chemistry (print: ISSN 1463-9262; electronic: ISSN 1463-9270) is published 12 times a year by the Royal Society of Chemistry, Thomas Graham House, Science Park, Milton Road, Cambridge, UK CB4 0WF.

All orders, with cheques made payable to the Royal Society of Chemistry, should be sent to RSC Distribution Services, c/o Portland Customer Services, Commerce Way, Colchester, Essex, UK CO2 8HP. Tel +44 (0) 1206 226050; E-mail [sales@rscdistribution.org](mailto:sales@rscdistribution.org)

2007 Annual (print + electronic) subscription price: £902; US\$1705. 2007 Annual (electronic) subscription price: £812; US\$1534. Customers in Canada will be subject to a surcharge to cover GST. Customers in the EU subscribing to the electronic version only will be charged VAT.

If you take an institutional subscription to any RSC journal you are entitled to free, site-wide web access to that journal. You can arrange access via Internet Protocol (IP) address at [www.rsc.org/ip](http://www.rsc.org/ip). Customers should make payments by cheque in sterling payable on a UK clearing bank or in US dollars payable on a US clearing bank. Periodicals postage paid at Rahway, NJ, USA and at additional mailing offices. Airfreight and mailing in the USA by Mercury Airfreight International Ltd., 365 Blair Road, Avenel, NJ 07001, USA.

US Postmaster: send address changes to Green Chemistry, c/o Mercury Airfreight International Ltd., 365 Blair Road, Avenel, NJ 07001. All despatches outside the UK by Consolidated Airfreight.

PRINTED IN THE UK

**Advertisement sales:** Tel +44 (0) 1223 432246; Fax +44 (0) 1223 426017; E-mail [advertising@rsc.org](mailto:advertising@rsc.org)

# Green Chemistry

Cutting-edge research for a greener sustainable future

[www.rsc.org/greenchem](http://www.rsc.org/greenchem)

Green Chemistry focuses on cutting-edge research that attempts to reduce the environmental impact of the chemical enterprise by developing a technology base that is inherently non-toxic to living things and the environment.

## EDITORIAL BOARD

**Chair**

Professor Martyn Poliakoff  
Nottingham, UK

**Scientific Editor**

Professor Walter Leitner  
RWTH-Aachen, Germany

**Associate Editors**

Professor C. J. Li  
McGill University, Canada  
Professor Kyoko Nozaki  
Kyoto University, Japan

**Members**

Professor Paul Anastas  
Yale University, USA  
Professor Joan Brennecke  
University of Notre Dame, USA  
Professor Mike Green  
Sasol, South Africa  
Professor Buxing Han  
Chinese Academy of Sciences,  
China  
Professor Roshan Jachuck  
Clarkson University, USA

Dr Alexei Lapkin  
Bath University, UK  
Dr Janet Scott  
Unilever, UK  
Professor Tom Welton  
Imperial College, UK

## ADVISORY BOARD

James Clark, York, UK  
Avelino Corma, Universidad  
Politécnica de Valencia, Spain  
Mark Harmer, DuPont Central  
R&D, USA  
Herbert Hugl, Lanxess Fine  
Chemicals, Germany  
Makoto Misono, nite,  
Japan  
Colin Raston,  
University of Western Australia,  
Australia

Robin D. Rogers, Centre for Green  
Manufacturing, USA  
Kenneth Seddon, Queen's  
University, Belfast, UK  
Roger Sheldon, Delft University of  
Technology, The Netherlands  
Gary Sheldrake, Queen's  
University, Belfast, UK  
Pietro Tundo, Università ca  
Foscari di Venezia, Italy

## INFORMATION FOR AUTHORS

Full details of how to submit material for publication in Green Chemistry are given in the Instructions for Authors (available from <http://www.rsc.org/authors>). Submissions should be sent via ReSource: <http://www.rsc.org/resource>.

Authors may reproduce/republish portions of their published contribution without seeking permission from the RSC, provided that any such republication is accompanied by an acknowledgement in the form: (Original citation) – Reproduced by permission of the Royal Society of Chemistry.

© The Royal Society of Chemistry 2007. Apart from fair dealing for the purposes of research or private study for non-commercial purposes, or criticism or review, as permitted under the Copyright, Designs and Patents Act 1988 and the Copyright and Related Rights Regulations 2003, this publication may only be reproduced, stored or transmitted, in any form or by any means, with the prior permission in writing of the Publishers or in the case of reprographic reproduction in accordance with the terms of licences issued by the Copyright Licensing Agency in the UK. US copyright law is applicable to users in the USA.

The Royal Society of Chemistry takes reasonable care in the preparation of this publication but does not accept liability for the consequences of any errors or omissions.

Ⓢ The paper used in this publication meets the requirements of ANSI/NISO Z39.48-1992 (Permanence of Paper).

Royal Society of Chemistry: Registered Charity No. 207890



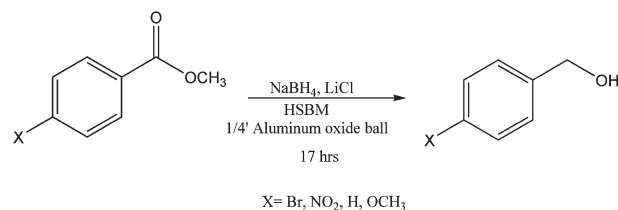
## COMMUNICATIONS

1041

**The first solvent-free method for the reduction of esters**

James Mack,\* Dennis Fulmer, Sam Stofel and Natalie Santos

We found aldehydes, ketones and esters can be reduced easily using solvent-free ball milling conditions. To the best of our knowledge this represents the first solvent-free method for the reduction of esters.

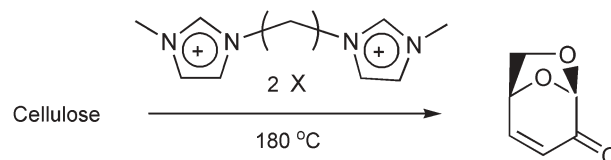


1044

**Dicationic molten salts (ionic liquids) as re-usable media for the controlled pyrolysis of cellulose to anhydrosugars**

Gary N. Sheldrake\* and David Schleck

Di-imidazolium dihalides ( $\text{X} = \text{Cl}, \text{Br}$ ) with short alkyl linker chains ( $n = 4-6$ ) are re-usable media for the controlled pyrolysis of cellulose to anhydrosugars, mainly levoglucosenone, at relatively low temperatures with no added acid or base.



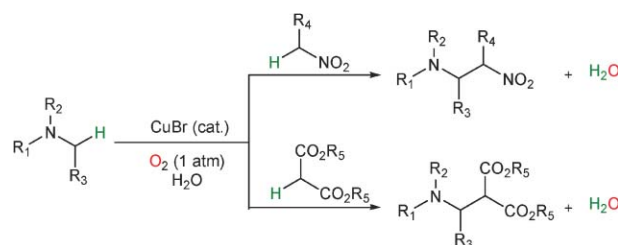
## PAPERS

1047

**Copper catalyzed oxidative alkylation of  $\text{sp}^3$  C–H bond adjacent to a nitrogen atom using molecular oxygen in water**

Olivier Baslé and Chao-Jun Li\*

A simple and highly efficient C–C bond formation was developed by the reaction of two  $\text{sp}^3$  C–H bonds catalyzed by copper bromide under an oxygen atmosphere in water. The aerobic and aqueous version of the cross-dehydrogenative-coupling (CDC) reaction provides formation of  $\beta$ -nitroamines and  $\beta$ -diester amines under safe and mild conditions.

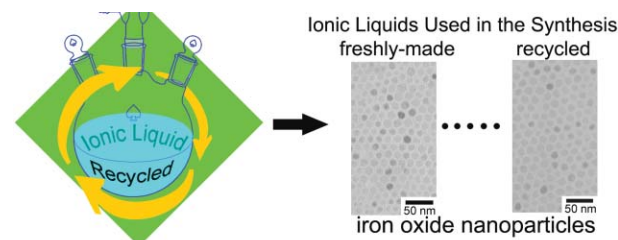


1051

**Synthesis of iron oxide nanoparticles using a freshly-made or recycled imidazolium-based ionic liquid**

Yong Wang, Sean Maksimuk, Rui Shen and Hong Yang

A new solvent recyclable process has been developed for an imidazolium-based ionic liquid,  $[\text{BMIM}][\text{Tf}_2\text{N}]$ , in the synthesis of monodisperse superparamagnetic iron oxide nanoparticles.



1057

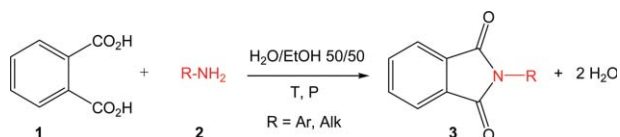


### Surface modification of lignocellulosic fibres in atmospheric air pressure plasma

Alexis Baltazar-Y-Jimenez and Alexander Bismarck\*

The potential use of atmospheric air pressure plasma as a swift, economic and environmentally sound surface treatment for lignocellulosic fibres to improve the interaction to renewable polymers was studied.

1067

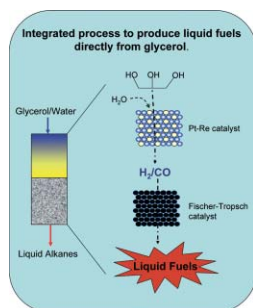


### Rapid and clean synthesis of phthalimide derivatives in high-temperature, high-pressure H<sub>2</sub>O/EtOH mixtures

Joan Fraga-Dubreuil,\* Gürbüz Çomak, Alasdair W. Taylor and Martyn Poliakoff\*

An alternative and clean method for the preparation of a wide variety of *N*-substituted phthalimides is reported using high-temperature, high-pressure water/EtOH mixtures (HTHP-H<sub>2</sub>O/EtOH), often yielding pure crystals *without* any work up.

1073

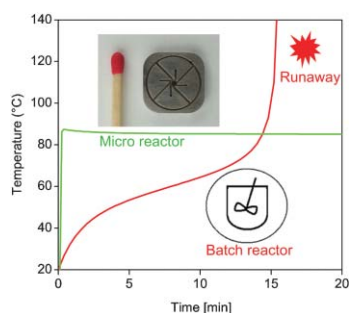


### Coupling of glycerol processing with Fischer–Tropsch synthesis for production of liquid fuels

Dante A. Simonetti, Jeppe Rass-Hansen, Edward L. Kunkes, Ricardo R. Soares and James A. Dumesic\*

Liquid fuels can be produced in a single reactor by coupling the low-temperature conversion of glycerol to synthesis gas with the formation of liquid alkanes by Fischer–Tropsch synthesis.

1084



### Synthesis of ionic liquids in micro-reactors—a process intensification study

Daniel A. Waterkamp, Michael Heiland, Michael Schlüter, Janelle C. Sauvageau, Tom Beyersdorff and Jorg Thöming\*

To intensify the synthesis of ionic liquids, a continuously operating micro-reactor system is introduced. As presented for 1-butyl-3-methylimidazolium bromide, a high product purity could be achieved at a twentyfold increase of space–time–yield compared to a conventional batch process.

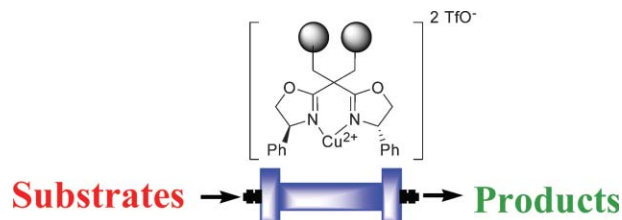
## PAPERS

1091

**Bisoxazoline-functionalised enantioselective monolithic mini-flow-reactors: development of efficient processes from batch to flow conditions**

M. Isabel Burguete, Alfonso Cornejo, Eduardo García-Verdugo,\* Juan García, Maria José Gil, Santiago V. Luis,\* Victor Martínez-Merino, Jose Antonio Mayoral and Maia Sokolova

Monolithic polymers functionalised with BOX-Cu moieties can be applied for the cyclopropanation reaction under batch and flow conditions using either conventional or supercritical solvents.

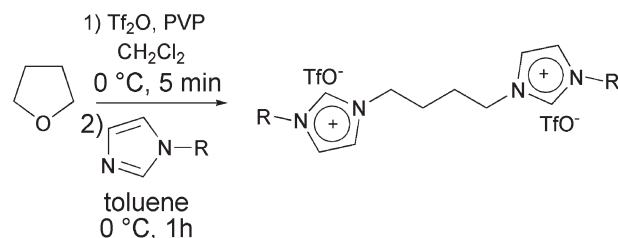


1097

**Halide-free highly-pure imidazolium triflate ionic liquids: Preparation and use in palladium-catalysed allylic alkylation**

Loïc Leclercq, Isabelle Suisse, Guy Nowogrocki and Francine Agbossou-Niedercorn\*

Several halide free imidazolium triflate salts have been prepared. The halide free ionic liquids were applied successfully as solvents in the palladium catalysed allylic alkylation.

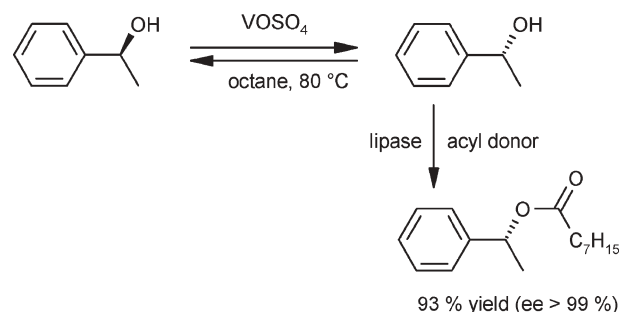


1104

**Heterogeneous vanadium catalysts for racemization and chemoenzymatic dynamic kinetic resolution of benzylic alcohols**

S. Wuyts, J. Wahlen, P. A. Jacobs\* and D. E. De Vos

Vanadyl sulfate is a heterogeneous racemization catalyst that can be combined with a lipase for the dynamic kinetic resolution of racemic benzylic alcohols.

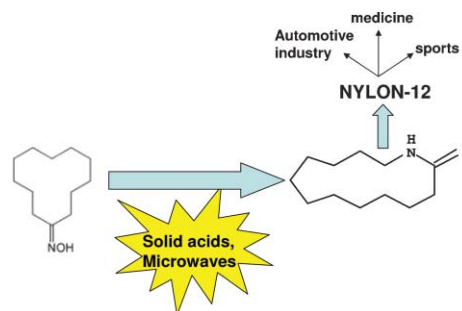


1109

**A microwave approach to the selective synthesis of  $\omega$ -laurolactam**

Tomas D. Conesa, Juan M. Campelo, James H. Clark, Rafael Luque,\* Duncan J. Macquarrie and Antonio A. Romero\*

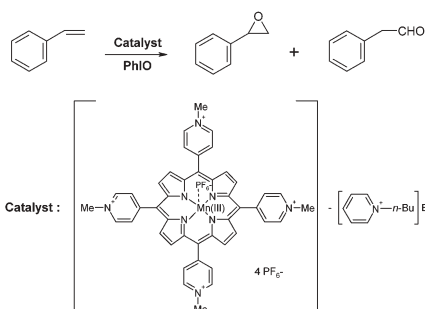
Different micro- and mesoporous materials were found to be extremely active in the production of  $\omega$ -laurolactam under microwave conditions in a very short period of time (typically 5 min).





## PAPERS

1114

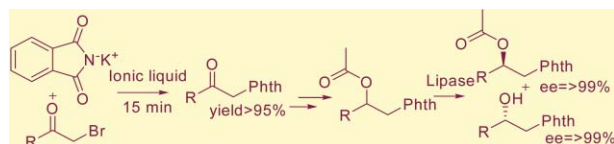


### Mild oxidation of styrene and its derivatives catalyzed by ionic manganese porphyrin embedded in a similar structured ionic liquid

Ye Liu, Hong-Jiao Zhang, Yong Lu,\* Yue-Qin Cai and Xiu-Li Liu

Multi-component ionic liquids functionalized with manganese porphyrin were applied as the catalyst for the oxidation of styrene (derivatives) with the advantages of suppression of oxidation degradation and self-aggregation, improved recyclability and no requirement for additional axial ligands and organic solvents.

1120

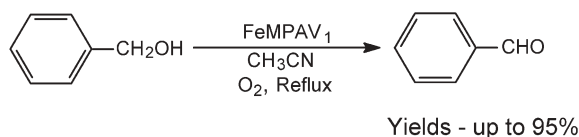


### A facile approach towards enantiomerically pure masked $\beta$ -amino alcohols

Pankaj Gupta, Bhahwal Ali Shah, Rajinder Parshad, Ghulam Nabi Qazi and Subhash Chandra Taneja\*

$\beta$ -Amino alcohols in the form of phthalimide alcohols prepared *via* a fast coupling reaction in an ionic liquid together with an efficient biocatalytic resolution offer a green methodology for enantiomers ( $ee \geq 99\%$ ,  $50 \text{ g L}^{-1}$ ).

1126

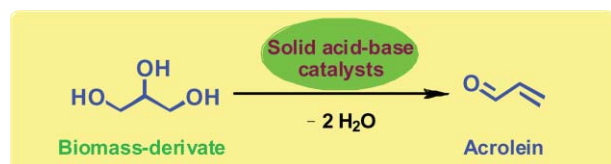


### Iron and vanadium containing molybdophosphoric acid catalyst for selective oxidation of alcohols with molecular oxygen

P. Nagaraju, Nayeem Pasha, P. S. Sai Prasad and N. Lingaiah\*

Oxidation of various alcohols over heterogeneous iron and vanadium containing molybdophosphoric acid catalyst with molecular oxygen as oxidant afford the corresponding carbonyl compounds with excellent yields.

1130



### Sustainable production of acrolein: investigation of solid acid–base catalysts for gas-phase dehydration of glycerol

Song-Hai Chai, Hao-Peng Wang, Yu Liang and Bo-Qing Xu\*

Sustainable synthesis of acrolein by catalytic gas-phase dehydration of biomass-derivate glycerol was attempted using various solid catalysts with a wide range of acid–base properties. The most selective catalysts showed Hammett acidities at  $-8.2 \leq H_0 \leq -3.0$ .

## PAPERS

1137

**An efficient microwave-assisted green transformation of cellulose into levoglucosenone. Advantages of the use of an experimental design approach**

Ariel M. Sarotti, Rolando A. Spanevello and Alejandra G. Suárez\*

The microwave-assisted pyrolysis of cellulose towards its conversion into levoglucosenone is reported. The optimisation of the processes was carried out employing an experimental design approach.



## ADDITIONS AND CORRECTIONS

1141

**An efficient synthesis of 1,5-benzodiazepine derivatives catalyzed by silver nitrate**

Rupesh Kumar, Preeti Chaudhary, Surendra Nimesh, Akhilesh K. Verma and Ramesh Chandra

## AUTHOR INDEX

- |                                     |                               |                               |                               |
|-------------------------------------|-------------------------------|-------------------------------|-------------------------------|
| Agbossou-Niedercorn, Francine, 1097 | García, Juan, 1091            | Martínez-Merino, Victor, 1091 | Shen, Rui, 1051               |
| Baltazar-Y-Jimenez, Alexis, 1057    | García-Verdugo, Eduardo, 1091 | Mayoral, Jose Antonio, 1091   | Simonetti, Dante A., 1073     |
| Baslé, Olivier, 1047                | Gil, Maria José, 1091         | Miller, Stephen A., 1038      | Soares, Ricardo R., 1073      |
| Beyersdorff, Tom, 1084              | Gupta, Pankaj, 1120           | Nagaraju, P., 1126            | Sokolova, Maia, 1091          |
| Bismarck, Alexander, 1057           | Heiland, Michael, 1084        | Nowogrocki, Guy, 1097         | Spanevello, Rolando A., 1137  |
| Burguete, M. Isabel, 1091           | Jacobs, P. A., 1104           | Parshad, Rajinder, 1120       | Stofel, Sam, 1041             |
| Cai, Yue-Qin, 1114                  | Kunkes, Edward L., 1073       | Pasha, Nayeem, 1126           | Suárez, Alejandra G., 1137    |
| Campelo, Juan M., 1109              | Leclercq, Loïc, 1097          | Poliakoff, Martyn, 1067       | Suisse, Isabelle, 1097        |
| Chai, Song-Hai, 1130                | Li, Chao-Jun, 1047            | Prasad, P. S. Sai, 1126       | Taneja, Subhash Chandra, 1120 |
| Chen, Hsuan-Ying, 1038              | Liang, Yu, 1130               | Qazi, Ghulam Nabi, 1120       | Taylor, Alasdair W., 1067     |
| Clark, James H., 1109               | Lin, Chu-Chieh, 1038          | Rass-Hansen, Jeppe, 1073      | Thöming, Jorg, 1084           |
| Çomak, Gürbüz, 1067                 | Lingaiah, N., 1126            | Reibenspies, Joseph H., 1038  | Wahlen, J., 1104              |
| Conesa, Tomas D., 1109              | Liu, Xiu-Li, 1114             | Romero, Antonio A., 1109      | Wang, Hao-Peng, 1130          |
| Cornejo, Alfonso, 1091              | Liu, Ye, 1114                 | Santos, Natalie, 1041         | Wang, Yong, 1051              |
| De Vos, D. E., 1104                 | Lu, Yong, 1114                | Sarotti, Ariel M., 1137       | Waterkamp, Daniel A., 1084    |
| Dumesic, James A., 1073             | Luis, Santiago V., 1091       | Sauvageau, Janelle C., 1084   | Wuyts, S., 1104               |
| Fraga-Dubreuil, Joan, 1067          | Luque, Rafael, 1109           | Schleck, David, 1044          | Xu, Bo-Qing, 1130             |
| Fulmer, Dennis, 1041                | Mack, James, 1041             | Schlüter, Michael, 1084       | Yang, Hong, 1051              |
|                                     | Macquarrie, Duncan J., 1109   | Shah, Bhahwal Ali, 1120       | Zhang, Hong-Jiao, 1114        |
|                                     | Maksimuk, Sean, 1051          | Sheldrake, Gary N., 1044      | Zhang, Jubo, 1038             |

## FREE E-MAIL ALERTS AND RSS FEEDS

Contents lists in advance of publication are available on the web *via* [www.rsc.org/greenchem](http://www.rsc.org/greenchem) - or take advantage of our free e-mail alerting service ([www.rsc.org/ej\\_alert](http://www.rsc.org/ej_alert)) to receive notification each time a new list becomes available.



Try our RSS feeds for up-to-the-minute news of the latest research. By setting up RSS feeds, preferably using feed reader software, you can be alerted to the latest Advance Articles published on the RSC web site. Visit [www.rsc.org/publishing/technology/rss.asp](http://www.rsc.org/publishing/technology/rss.asp) for details.

## ADVANCE ARTICLES AND ELECTRONIC JOURNAL

Free site-wide access to Advance Articles and the electronic form of this journal is provided with a full-rate institutional subscription. See [www.rsc.org/ejs](http://www.rsc.org/ejs) for more information.

\* Indicates the author for correspondence: see article for details.



Electronic supplementary information (ESI) is available *via* the online article (see <http://www.rsc.org/esi> for general information about ESI).

# Chemical Technology

## Simply measuring particle size gives a good estimate of risk Sizing up the danger of volcanic ash

Analysing the grain size of volcanic ash particles might provide a quick and easy way to calculate their potential threat to human health, according to a British scientist.

Although the primary hazards of a volcanic eruption, such as pyroclastic flows, are of major concern after a volcanic eruption, secondary hazards, such as the short term and long term effects of the dust and ash ejected, are also a major problem. Volcanic ash may cause acute respiratory diseases and has the potential to cause chronic diseases, such as lung cancer. But assessing this risk can be difficult, as conventional medical studies may take months, years or even decades to conclude whether a dust is toxic or not.

What is certain, however, is that the ash cannot be harmful if the particles are too large to enter the lung. Therefore, Claire Horwell at the Institute of Hazard and Risk Research at Durham University developed a method that allowed her to estimate the amount of fine particles in volcanic ash without



needing state of the art instruments.

By characterising the grain size distribution of volcanic ash after eruptions, Horwell developed an equation for estimating the quantity of health-pertinent fractions when state-of-the-art techniques are unavailable. By focussing on techniques that allow cheap and quick assessment of the health hazards posed by volcanic emissions, Horwell hopes to provide hazard managers with a new tool to rapidly assess how bad

**Ash and dust can cause chronic and acute respiratory diseases**

**Reference**  
C Horwell, *J. Environ. Monit.*, 2007, DOI: 10.1039/b710583p

an eruption is for the health.

'At the onset of future eruptions, local scientists can simply sieve the ash and immediately calculate the percentage of ash that is fine enough to enter the lung. This means that a preliminary assessment of the potential health hazard can be carried out in a matter of minutes rather than waiting for laboratory results. Hazard managers can then rapidly decide whether to distribute dust masks to a population or even to evacuate an area until ash fall has ceased,' explained Horwell.

Further research is needed to establish what actual health risk volcanic ash might pose. The biggest challenge, however, is bringing together scientists from across several disciplines (such as medics, mineralogists or toxicologists) to definitively determine the health risks of volcanic ash. In the meantime, Horwell's technique may help hazard managers make more informed decisions.

*Edward Morgan*

PHOTODISC

## In this issue

### Finding fission by-products

Vaporisation and ICPMS combine to detect radionuclides

### Wet, not wet, wet

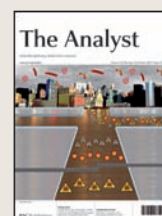
Smart surface changes hydrophobicity at the flick of a switch

### Instant insight: Science and art in harmony

Marc Aucouturier illustrates the benefit of a multidisciplinary approach to preserving our cultural heritage

### Interview: Chemical conservation

David Saunders explains to Joanne Thomson how chemistry can be used to preserve ancient artefacts



The latest applications and technological aspects of research across the chemical sciences



# Application highlights

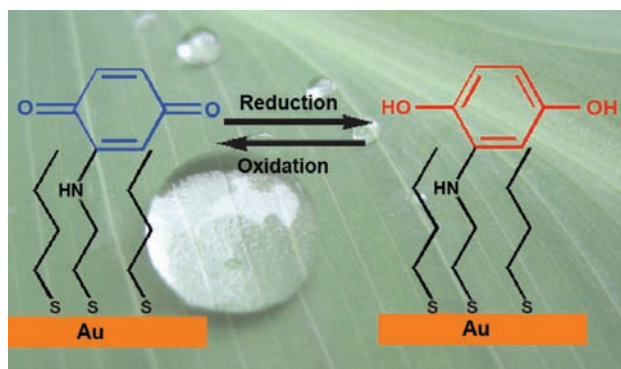
Smart surface changes hydrophobicity at the flick of a switch

## Wet, not wet, wet

Bored of bath-cleaning? Wearied by window-washing? Thanks to a group of scientists in Israel these mundane chores could soon be consigned to the past.

Itamar Willner and colleagues at the Hebrew University of Jerusalem have made a quinine-coated 'smart surface' whose wettability can be switched using either an electrical or a chemical trigger. Such surfaces are inspired by self-cleaning systems in nature. The lotus leaf, for example, has a hydrophobic surface that allows water droplets to roll off the leaf, removing dirt from its surface.

Willner and his team coated a gold surface with hydrophobic benzoquinone, which is reduced to hydrophilic hydroquinone using either an applied voltage or a chemical reducing agent. Hydroquinone has two hydroxyl groups that interact strongly with the water, causing the surface to



**Benzoquinone (blue) repels water, but the reduced hydroquinone (red) does not**

### Reference

A Wieckowska, A B Braunschweig and I Willner, *Chem. Commun.*, 2007, DOI: 10.1039/b710540a

become 'wetter' when reduced.

'The hydroquinone/benzoquinone surface evolved from a much more complex system that, after a lot of effort, did not work at all. We were still surprised with how robust the [simple] system [was] and how dramatic the changes were that we observed,' said Willner.

The team's smart surface is easily prepared and the small size

of quinone means that a lot of molecules can be packed into the surface, causing large macroscopic changes in the surface wettability.

Aside from self-cleaning applications, these clever surfaces may be used in microfluidic devices that could provide new analytical procedures for clinical diagnostics. For example, if the inner part of a capillary was coated with a conductive film functionalized with Willner's quinine monolayer it could be used to suck minute volumes of fluid from cells or organs.

'A smart idea to create a smart surface,' said Jilie Kong, a microfluidics expert at Fudan University, Shanghai. 'The reversible change of hydrophobicity/hydrophilicity is promising in the design of novel microfluidic chips or biosensors,' said Kong.

Ruth Doherty

Ultramicroelectrode probes coated by CVD to give uniform layer

## Diamonds are for electron microscopy

A team of UK scientists have developed a way of controlling the chemical vapour deposition of diamond to uniformly coat ultramicroelectrodes. These electrodes often have a diameter of less than 25 microns, ideally suited for scanning electrochemical microscopy (SECM).

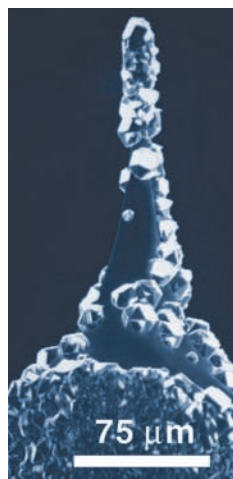
SECM is a type of microscopy that images surfaces using a physical probe. By mechanically moving the probe across a surface, an accurate image of the surface can be mapped. The electrodes that are used as probes are known as ultramicroelectrodes (UMEs).

Diamond is an attractive material for electrodes because of its electrochemical characteristics and chemical inertness. However, up until now diamond UMEs could not be made using conventional chemical vapour deposition techniques. The team led by John Foord at the

University of Oxford successfully modified the deposition process to produce diamond-coated ultramicroelectrodes. By combining efficient nucleation methods and an electrochemical bias during growth, the electrode can be coated with a uniform, polycrystalline diamond layer.

The team have been working in the area of diamond electrochemistry for a number of years and aim to produce diamond electrodes for probing biological media. Foord explained the challenge: 'Conventional microelectrodes fail to function in biological media because of adsorption of biological media, which foul the electrode,' he said. Diamond can be chemically functionalised to make it more stable than other electrodes under these conditions, he said, making it an ideal target material.

Frank Marken from the



**Diamond's chemical properties make it ideal for use as electrodes**

University of Bath is an expert in novel electrode design and believes this work could have a wide impact. 'The availability of sharp, conducting diamond tools could be of wider significance... tools to "dissect" and image individual biological cells and their content could be envisaged as future developments,' he said.

However, Foord believes that more work is needed before the full potential of these ultramicroelectrodes is realised. A thin insulating coating for the body of the electrode is needed, which can be removed from the electrode tip without damaging it. The group are currently exploring the use of polymer coatings for this purpose.

May Copsey

### Reference

J Hu, J S Foord and K B Holt, *Phys. Chem. Chem. Phys.*, 2007, DOI: 10.1039/b710241k

## Electrothermal vaporisation and ICPMS combine to detect radionuclides

# Finding fission by-products

Researchers in Canada have developed a method to rapidly measure ultra-trace amounts of strontium 90 ( $^{90}\text{Sr}$ ) in environmental samples.

$^{90}\text{Sr}$  is a by-product of the fission of uranium and plutonium in nuclear reactors and nuclear weapons, with a half-life of 29 years. It was widely dispersed into the environment during nuclear weapons testing in the 1950s and '60s. It is chemically similar to calcium so it accumulates in bone and blood-forming tissue. Exposure to  $^{90}\text{Sr}$  may be linked to certain cancers.

Patricia Grinberg and coworkers at the Institute for National Measurements Standards in Ottawa used ICPMS combined with electrothermal vaporisation and dynamic reaction cell technology to measure  $^{90}\text{Sr}$  concentrations as low as 3.5 picograms per gram. The method was tested by measuring natural Sr in marine sediments,



river water and biological material and the recovery of  $^{90}\text{Sr}$  spikes added to the samples.

'The determination of  $^{90}\text{Sr}$  is non-trivial both as a consequence of its extremely low concentration levels and because it suffers from interferences, frequently necessitating laborious separation procedures, which can cause

**Strontium 90 was dispersed into the atmosphere during nuclear testing**

#### Reference

P Grinberg, S Willie and R E Sturgeon, *J. Anal. At. Spectrom.*, 2007, DOI: 10.1039/b708018b

contamination and increase the analysis time,' said Grinberg.

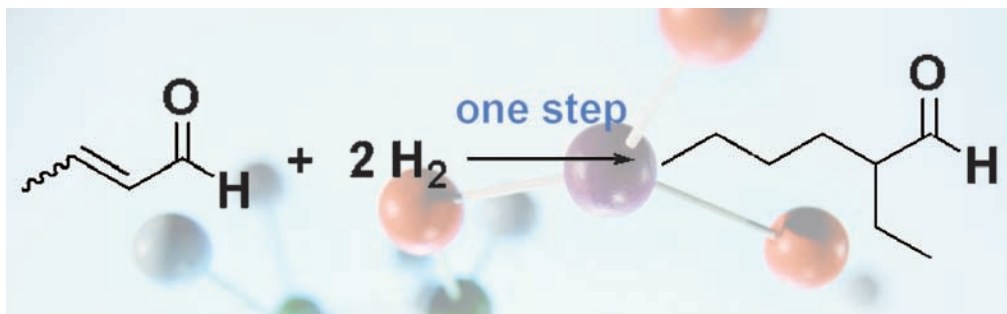
Grinberg's method takes advantage of the ability of electrothermal vaporisation systems to use thermal programming to selectively remove interferences and simplify sample preparation procedures.

The work is part of a project financed by the Chemical Radiological and Nuclear Research Technology Initiative (CRTI) in Canada on the development of new technologies for the rapid detection and identification of radionuclides.

'Radionuclides have traditionally been measured using radiometric techniques which are not ideally suited to rapid and/or accurate determination,' said Grinberg. 'Rapid determination is crucial in the event of a nuclear or radiological accident so as to assess and minimize adverse health, economic and environmental effects,' she continued. *Joanna Stevens*

## Carbon dioxide solvent and palladium catalyst improve synthesis

# Organic synthesis goes supercritical



Swiss chemists have developed a greener and more efficient way of making an industrially important aldehyde.

2-Ethylhexanal is a key compound in the manufacture of perfumes and paints. Until now, its large-scale synthesis was dogged by the need for several consecutive reaction steps, poor yields or the need for large excesses of certain reagents.

Alfons Baiker and his colleagues at the Swiss Federal Institute of Technology (ETH) in Zürich have now developed a method of making it in a highly selective way and in a single step from crotonaldehyde (but-2-enal) using only a small excess of hydrogen.

Supercritical carbon dioxide (where it is in a fluid state that is mid-way in character between a gas and a liquid) at 60°C and 16 MPa

pressure is used as the reaction medium for the starting materials, and the reaction takes place by passing it over a palladium catalyst at a constant flow rate.

According to Baiker, 'the catalyst exhibits high activity, selectivity and a long lifetime', adding that the only by-product, butyraldehyde, is also industrially useful and easily separated by distillation.

'The ... method ... may provide a promising alternative for the industrial production of [these] two important aldehydes,' he said.

Martyn Poliakoff, a fellow of clean technology at the University of Nottingham and chair of Green Chemistry's editorial board, considers Baiker's work an 'interesting development'. He added that he saw 'considerable potential for [the development of] sustainable chemical processes'.

*David Parker*

**One step ahead: previous routes have several steps or give poor yields**

#### Reference

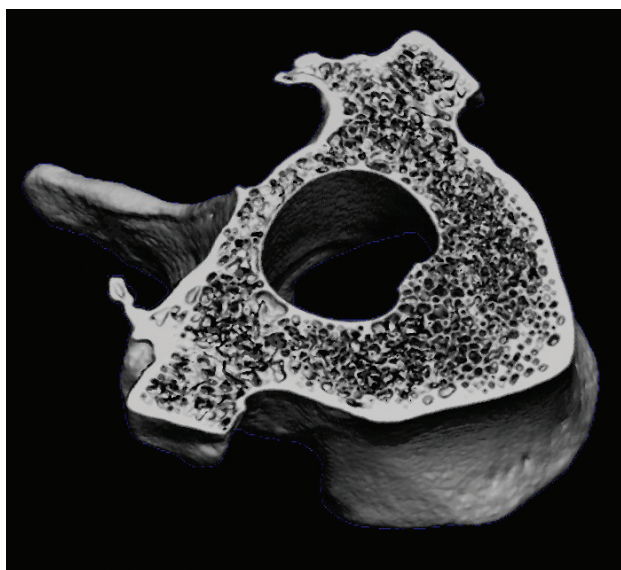
T Seki, J-D Grunwaldt and A Baiker, *Chem. Commun.*, 2007, DOI: 10.1039/b710129e

Reference materials allow more localized investigation of bone density

## The phantom of the bone scanners

Research by Swiss scientists could open the way to better diagnosis and treatment for osteoporosis sufferers.

Susanne Schweizer and colleagues at ETH Zurich in Switzerland have synthesised reference materials – or ‘phantoms’ – that allow micro-computed tomography ( $\mu$ -CT) to be used for measuring mineral content of individual bone struts. Scans currently used to diagnose osteoporosis measure the mineral density of bones over a relatively large area. Knowledge of the mineral density of patient's bones on a more local scale should aid the diagnosis of osteoporosis at an earlier stage, and help determine the most appropriate treatment, explained Schweizer.



Micro-computed tomography can already image bone in 3D

$\mu$ -CT is a well established research technique for studying bones in three dimensions. Previous attempts to use it in accurate measurements of bone density were hindered by a lack of good phantoms needed to calibrate the machine for this purpose, explained Schweizer. She has now overcome the hurdles, making phantoms that properly mimic the way bones reflect X-rays from the scanner.

Schweizer said that these phantoms are already being used in  $\mu$ -CT studies of live rodents, with clinical applications being the end goal.

Nina Athey-Pollard

### Reference

S Schweizer et al, *Analyst*, 2007, DOI: 10.1039/b703220j

Keeping catalysts apart enables them to perform at their best

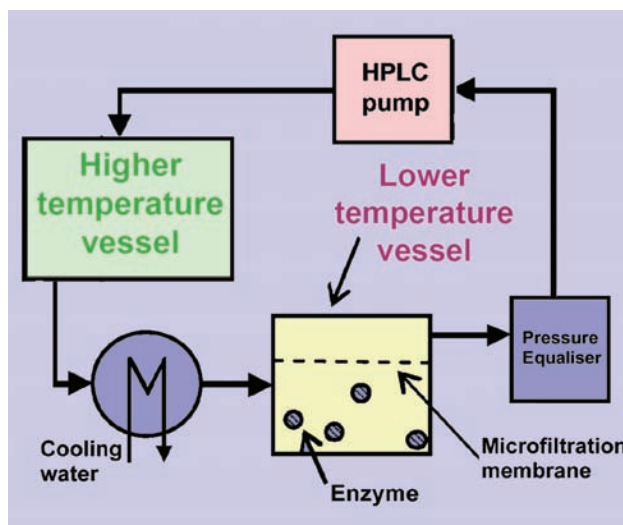
## Membranes do the trick

Researchers in the UK and New Zealand have shown that using a membrane could help catalysts operating in the same system work more efficiently.

The team, led by Paul Taylor at the University of Warwick and Andrew Livingston at Imperial College London, used a membrane to keep catalysts in environments where they work best.

Taylor explained that in a process where two or more catalytic steps are combined in one operation, called a tandem catalytic process, the catalysts normally have to compromise on their performance. This is because the same operating conditions are imposed on both catalysts. ‘We use technological tricks to avoid the compromise,’ he said, ‘and allow the catalysts to operate under their respective optimum conditions, while in terms of the process they are in the same synthetic operation.’

The team used the membrane in a tandem catalytic process



called dynamic kinetic resolution, a process used to make enantiomerically enriched products. Jonathan Williams, professor of organic chemistry at the University of Bath, explained that, although there are many

**The enzyme stays in the cold while the metal catalyst feels the heat**

opportunities for using catalysts in tandem catalytic processes, there are practical problems associated with their use because of the different conditions they require. ‘These researchers have provided an elegant solution to this problem by using a membrane to retain an enzyme catalyst in a lower temperature vessel whilst metal-catalysed racemisation occurs in a higher temperature vessel, leading to an effective dynamic kinetic resolution process,’ he said.

The partnership involved collaboration between chemists interested in tandem catalysis and chemical engineers interested in membrane technology. Taylor explained that the collaboration resulted from effective networking with colleagues in industry interested in membrane separation. Katherine Davies

### Reference

C Roengpihya et al, *Chem. Commun.*, 2007, DOI: 10.1039/b709035h



## Instant insight

# Science and art in harmony

Marc Aucouturier, Centre for Research and Restoration of the Museums of France, and Evelyne Darque-Ceretti, Paris School of Mines, illustrate the benefit of a multidisciplinary approach to preserving our cultural heritage

The understanding and preservation of cultural heritage has been a major challenge for all civilisations. The most modern tools of materials science are rising to the challenge. Knowing the composition and rebuilding the history of an artefact needs sophisticated laboratory instruments and a long enquiry involving intensive collaboration between materials scientists and art historians. Data on the physical constitution of an artefact, its authenticity, its history, the circumstances of its discovery, its treatment after being abandoned and/or stored, are useful not only to increase our knowledge of civilisation and art history, but also to inform conservation policy.

The study of cultural heritage artefacts and their preservation and restoration begins with – and is often limited to – a comprehensive characterisation of their surface by non-destructive methods. The application of surface science to cultural heritage materials has undergone a dramatic development in the past few decades, thanks to the impressive improvement of analysis and investigation equipment.

One example of objects recently submitted to in depth investigation are beautiful ancient ceramics with a metallic lustre decoration. This technique was born in the 9th century in factories created by the Arabs during their conquests in Mesopotamia, Egypt and Persia. With the passing of the centuries, Arab potters spread their know-how all over the Islamic world. It reached Spain and was finally transmitted to the workshops of the Italian Renaissance at the end of the 15th century, giving rise to what is known as majolica ceramics.



Lustrated ceramics attracted the attention of conservators and scientists on account of the structure of the thin surface film that is responsible for their specific aspect. They exhibit an iridescent shine that sometimes imitates a gold, silver or copper deposit in specular reflection and appears from deep red to bright yellow by diffused light observation. In order to understand this very sophisticated technique and trace its propagation through the ages, a series of investigation were conducted in several materials science laboratories. They showed that the surface film is made of vitreous matter in which nanoparticles of metallic silver and/or copper are embedded. In other words, ancient Islamic potters invented nanotechnology eleven centuries before our solid state physicists.

Another example of an ancient decoration technique that is still not fully understood is 'black bronze'. It is the result of intentional surface treatments by ancient craftsmen in order to change the surface aspect and colour of bronze artefacts. It was discovered on bronze artefacts from Egypt (2nd millennium BC), the Roman Empire (1st century AD), China (4th century AD) and Japan (14th century AD). It consists of a chemical treatment applied to

**All that glitters is not gold: the iridescent sheen on this pottery is the work of ancient nanoscientists.**

specific copper alloys containing always gold (1 to 8 wt%) and/or silver (1 to 4 wt%) in order to give them a black or velvet colour. A comprehensive study has been conducted recently on a large body of Egyptian and Roman Empire pieces from the Louvre museum in France. Most of the black patina appears to be pure cuprite,  $\text{Cu}_2\text{O}$ , containing small amounts of gold and/or silver. The natural colour of cuprite is red, and the research on the role of the precious metals on its black coloration is still under investigation.

Many other examples could be given, such as the fruitful application of Raman spectroscopy to the identification of pigments and the restoration of painted artefacts, the use of analytical spectroscopy to organise a preservation policy for the Swedish warship Vasa, the study of environmental degradation of medieval stained glass windows by secondary ion mass spectroscopy or the identification of degradation mechanisms of old paper manuscripts by spectrophotometry and atomic force microscopy.

*Read the full Tutorial Review 'The surface of cultural heritage artefacts: physico-chemical investigations for their knowledge and their conservation' in issue 10 of Chemical Society Reviews.*

#### Reference

M Aucouturier and E Darque-Ceretti, *Chem. Soc. Rev.*, 2007, **36**, 1605, DOI: 10.1039/b605304c

## Interview

# Chemical conservation

*David Saunders explains to Joanne Thomson how chemistry can be used to preserve ancient artefacts*



**David Saunders**

David Saunders is Keeper of the Department of Conservation, Documentation and Science at the British Museum, London. His research focuses on the scientific examination of artefacts, principally using non-destructive imaging and spectroscopic techniques.

**What inspired you to develop a career in the analytical sciences?**

I was inspired to specialise in chemistry by a teacher at school whose enthusiasm for the subject caught my imagination. I have also had a longstanding interest in museums since my father took me to them as a child.

When I was coming to the end of my postgraduate studies, I was very interested in the way that science is applied to the arts and archaeology. When I was doing post doctoral work, I saw a job opportunity at the National Gallery in London and that was really how I started in the field.

**History and not chemistry springs to mind when most people think of museums. How big a role does chemistry play at the British Museum?**

Chemistry is involved in two aspects of the museum's activities. Firstly, it is used in the preservation and restoration of the collections. Secondly, through the chemical analysis of the objects, we bring another aspect into their interpretation that augments the history side. We can shed light on how objects were made, what they're made of and how cultures have changed, developed and traded. Increasingly, we're finding the public are engaged by this type of information.

**What techniques do you use to examine artefacts?**

We begin by using simple microscopy to magnify an object. We then use scanning electron microscopy (SEM) to look at objects at much higher magnification. With this we have the potential to conduct energy dispersive X-ray analysis (SEM-EDX), which is an absolute workhorse for the department. This can give us some elemental information.

We also use other X-ray techniques like X-ray fluorescence and diffraction and X-radiography. X-Radiography is very important – we use it routinely to look inside objects that we can't otherwise look in.

We use various spectroscopic techniques, including Raman spectroscopy. This has been the big new thing for museums in the last 10–15 years, particularly Raman microscopy, where the Raman is directed through the optics of a microscope.

The fingerprinting of various materials by Raman has become of sufficient significance that the organisation that was putting together the infrared library of museum-related materials has extended it into Raman.

**What is the most rewarding aspect of your work?**

It's adding to the sum total of something that's known about an object. Preservation is, of course, enormously important but it is the intellectual enquiry that I find most rewarding. I enjoy using the documentary sources together with the knowledge of specialist art historians and archaeologists to piece together what the science is telling us about the object with what we know about the object from other sources.

**Do you have a message for young scientists?**

Don't get too narrow. Read around; look at what is happening in other fields. You can't be an expert in everything but you can have a broader knowledge and that's when you start to see the interconnections. Bringing in the best of other fields is a terribly important facet of how scientists can think within an organisation.

**Which scientist do you most admire and why?**

Michael Faraday, because he was heavily involved in the development of science in museums and galleries in Britain. Everyone knows Faraday for his very straight scientific work but he got involved in everything. He was involved in the commission that looked at relocating museums out of London in the mid-19th century because of fears about pollution damage to the collections. Although he was engaged in very serious study in a single area, it didn't stop him retaining that breadth.

**If you weren't a scientist, what would you be?**

I have always regretted giving up history at such an early stage. I would quite like to be a historian. If I couldn't give up the science completely, perhaps I'd end up doing history of science. Maybe I would go the whole way and become an art historian or an archaeologist, although the idea of being knee deep in mud in an archaeological site doesn't necessarily appeal!

# Easier and more efficient than traditional LLE

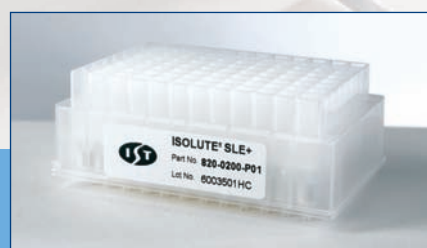
## ... SLE+ Supported Liquid Extraction Plates

Supported Liquid Extraction (SLE) provides an easier to automate alternative to liquid-liquid extraction (LLE), with no off-line steps (e.g. mixing or centrifuging) required. Problems including emulsion formation, and separation of liquid layers are eliminated.

ISOLUTE® SLE+ Supported Liquid Extraction Plates are optimized for simultaneous processing of 96 samples (extract up to 200 µL of plasma or urine per well), using a generic methodology for extraction of neutral, acidic and basic compounds.

ISOLUTE® SLE+ is available in the industry standard 2 mL fixed well 'SPE' plate format and is compatible with all commercially available automated liquid handling systems.

For more information or to request a free sample visit [www.biotage.com](http://www.biotage.com).



### NEW! ISOLUTE SLE+ Plates

Improve productivity and maximize analyte recovery with this new more efficient alternative to traditional liquid-liquid extraction.

- No emulsion formation
- Easy to automate
- Rapidly transfer methods from traditional LLE to ISOLUTE SLE+
- Excellent flow characteristics improve reproducibility

  
**Biotage**  
[www.biotage.com](http://www.biotage.com)



# Essential elements

## And the winner is...



Left to right - Richard Kidd, Richard Gedye and Bernard Donovan

Months of hard work were rewarded recently as *RSC Project Prospect* was named as winner of the 2007 ALPSP/Charlesworth Award for Publishing Innovation.

In making the award, which recognises a significantly innovative approach to any

aspect of scholarly publication, the judges described *RSC Project Prospect* as 'the clear winner ... journals incorporate standard metadata within the full text of articles and combine this with an elegant and intuitive on-screen manifestation of the advantages of including

this metadata. As a result, sophisticated and effective searching of the literature is greatly improved and the value gained from reading each article is significantly enhanced. It is delightfully simple to use and benefits to authors and readers are immediately obvious.'

Receiving the award at the ALPSP Annual Dinner in London on September 13th, project manager Richard Kidd declared: 'RSC Publishing is proud to win the 2007 award, which is great recognition for the work our publishing staff and academic partners have put into the development and evolution of *Project Prospect*.'

This is the first time that RSC Publishing has received the award for publishing innovation, and staff are understandably delighted.

Read more about *RSC Project Prospect* on the website: [www.projectprospect.org](http://www.projectprospect.org)

## And finally...

We are pleased to announce that the *RSC eBook Collection* has been updated to include the first set of 2007 titles.

Since its launch in March 2007 the *RSC eBook Collection* has enjoyed a lot of attention from libraries across the globe keen to expand their chemical science book collections.



Access to over 740 high quality, digitalised books is combined with powerful search engines to enable scientists to find the information they need, when they need it. Newly published books within the collection can be found by browsing by publication date, or alternatively, subject area and the first chapter of each book is available free for anyone visiting the site. Further new titles and functionality will be added to the *RSC eBook Collection* at different stages throughout the year.

To find out more about our ebook services visit [www.rsc.org/ebooks](http://www.rsc.org/ebooks)

## You say, we display!

You told us that you wanted direct access to the latest research ... and now, thanks to the latest update of the RSC Journals website, that's exactly what we are delivering.

The contents list for each current issue now appears on the journal's homepage, delivering the content you want to see as soon as you arrive at the site. Graphical abstracts are included

as standard, to enable readers to browse content much more conveniently. A more prominent and easy-to-use search box also makes finding published research much more intuitive.

The changes are being introduced following feedback from readers and through extensive user testing; further evidence of the continued investment and development of

our online platform. Since the website re-launch in summer 2005, RSC Publishing has introduced RSS feeds, alerting you to new content as and when it is published, and the award-winning *RSC Project Prospect* has provided powerful HTML enhancements in journal articles.

To see for yourself visit [www.rsc.org/journals](http://www.rsc.org/journals) and select your favourite RSC journal.

*Chemical Technology* (ISSN:1744-1560) is published monthly by the Royal Society of Chemistry, Thomas Graham House, Science Park, Milton Road, Cambridge UK CB4 0WF. It is distributed free with *Chemical Communications*, *Journal of Materials Chemistry*, *The Analyst*, *Lab on a Chip*, *Journal of Environmental Monitoring*, *Green Chemistry*, *CrysEngComm*, *Physical Chemistry Chemical Physics* and *Analytical Abstracts*. *Chemical Technology* can also be purchased separately. 2007 annual subscription rate: £199; US \$376. All orders accompanied by payment should be sent to Sales and Customer Services, RSC (address above). Tel +44 (0) 1223 432360, Fax +44 (0) 1223 426017. Email: [sales@rsc.org](mailto:sales@rsc.org)

**Editor:** Neil Withers

**Associate editors:** Nicola Nugent, Celia Clarke

**Interviews editor:** Joanne Thomson

**Essential Elements:** Valerie Simpson, Caroline Wain and Melanie Charles

**Publishing assistant:** Jackie Cockrill

**Publisher:** Graham McCann

Apart from fair dealing for the purposes of research or private study for non-commercial purposes, or criticism or review, as permitted under the Copyright, Designs and Patents Act 1988 and the copyright and Related Rights Regulations 2003, this publication may only be reproduced, stored or transmitted, in any form or by any means, with the prior permission of the Publisher or in the case of reprographic reproduction in accordance with the terms of licences issued by the Copyright Licensing Agency in the UK. US copyright law is applicable to users in the USA.

The Royal Society of Chemistry takes reasonable care in the preparation of this publication but does not accept liability for the consequences of any errors or omissions.

Royal Society of Chemistry: Registered Charity No. 207890.

# RSC Publishing

©The Royal Society of Chemistry 2007

# Efficient and controlled polymerization of lactide under mild conditions with a sodium-based catalyst†

Hsuan-Ying Chen,<sup>ab</sup> Jubo Zhang,<sup>a</sup> Chu-Chieh Lin,<sup>\*b</sup> Joseph H. Reibenspies<sup>a</sup> and Stephen A. Miller<sup>\*a</sup>

Received 13th April 2007, Accepted 25th June 2007

First published as an Advance Article on the web 10th July 2007

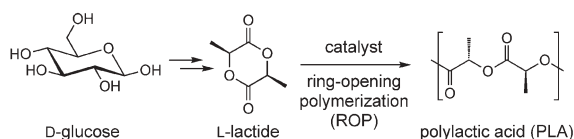
DOI: 10.1039/b705622b

A common phenolic antioxidant provides the ligand scaffold in the first discrete sodium-based catalyst for the highly active and controlled ring-opening polymerization of lactide.

The biorenewability, biodegradability, and biocompatibility of polylactic acid (PLA) have contributed to its increasing number of applications, many of which are in the medical field.<sup>1</sup> The ring-opening polymerization (ROP) of lactide—commonly made *via* glucose fermentation—is the principal method for synthesizing PLA (Fig. 1).<sup>2,3</sup>

While aluminum alkoxides<sup>4</sup> are effective initiators for the controlled ROP of lactones, they exhibit low activity in lactide polymerization. Zinc,<sup>5</sup> tin,<sup>6</sup> and lanthanide<sup>7</sup> derivatives are effective lactone/lactide ROP initiators, affording polymers with high molecular weights in high yields. Although Sn(II) initiators are employed commercially with approval by the U.S. Food and Drug Administration,<sup>8</sup> they are difficult to remove from the resultant polymer and there are growing concerns about tin cytotoxicity;<sup>1</sup> thus, they have limited utility in the preparation of medical-grade polymers.<sup>9</sup> Efforts to address this issue have resulted in recent magnesium,<sup>5,10</sup> calcium,<sup>11</sup> iron,<sup>12</sup> and highly active metal-free<sup>13</sup> catalysts that are competent for the ROP of lactide.

Sodium is the most abundant metal in seawater (1.1%), the sixth most abundant element in the earth's crust (2.3%), and the ninth most abundant element in the human body (0.14%).<sup>14</sup> The ubiquity, accessibility, and biocompatibility of sodium are strong motivations for investigating its potential in ROP catalysis. We report herein the synthesis, characterization, and catalytic behavior of the first discrete sodium-based catalyst for the efficient and controlled ring-opening polymerization of lactide.



**Fig. 1** Poly(lactic acid) (PLA) is typically prepared by the ring-opening polymerization of lactide, catalyzed by various metal-based initiators.

<sup>a</sup>Department of Chemistry, Texas A&M University, College Station, Texas, 77843-3255, U. S. A. E-mail: samiller@mail.chem.tamu.edu; Fax: +1-979-845-9452; Tel: +1-979-845-2543

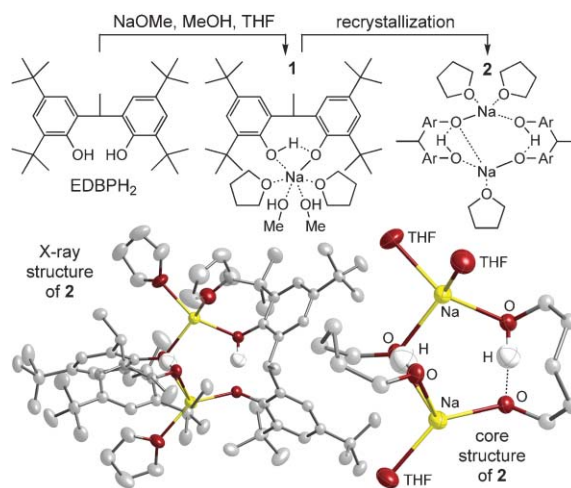
<sup>b</sup>Department of Chemistry, National Chung-Hsing University, Taichung 402, Taiwan, R. O. C. E-mail: cchlin@mail.nchu.edu.tw; Tel: +886-4-22840411 ext 718

† Electronic supplementary information (ESI) available: Catalyst synthesis and characterization data (including X-ray crystallography for **2**), polymer characterization data and details of the kinetic study. See DOI: 10.1039/b705622b

Alkali metal alkoxides such as lithium *tert*-butoxide<sup>15</sup> have shown commendable catalytic activity toward the ROP of lactones and lactide. However, since these metal alkoxides function as simple anionic initiators, they typically suffer from undesirable back-biting and transesterification reactions, leading to macrocycles, catalyst inhomogeneity, and broad or multimodal polymer molecular weight distributions. Such side reactions can be minimized through the use of sterically demanding ligands. In consideration of this and our previous studies with lithium,<sup>16,17</sup> we targeted sodium complexes of 2,2'-ethyldene-bis(4,6-di-*tert*-butyl-phenol) (EDBPH<sub>2</sub>), which are unknown despite the ligand's commercial availability and meagre cost. Moreover, EDBPH<sub>2</sub> is an attractive ligand because it has been approved as an indirect food additive (as an antioxidant in polymer packaging) by the U.S. Food and Drug Administration.<sup>18</sup>

Fig. 2 describes the synthesis of (EDBPH)Na(MeOH)<sub>2</sub>(THF)<sub>2</sub> (**1**), a *bis*-methanol adduct<sup>19</sup> which can be made directly from EDBPH<sub>2</sub>. Recrystallization of **1** afforded the aggregated disodium complex [(EDBPH)Na(THF)<sub>2</sub>]<sub>2</sub>[Na(THF)(EDBPH)] (**2**) with loss of THF and methanol. The solid state structure of **2**† implies certain structural features to be present in **1**, including a mono-deprotonated *bis*-phenol ligand.

The ring-opening polymerization of L-lactide employing **1** (2.5 mM) as initiator was systematically examined to produce the results in Table 1. In toluene, complex **1** is a highly efficient catalyst, polymerizing approximately 200 equivalents of L-lactide in 8 minutes at room temperature (20 °C). This turnover frequency



**Fig. 2** Synthesis of precatalyst **1**, which loses all MeOH and some THF upon recrystallization to afford **2** (50% probability ellipsoids, hydrogen atoms omitted except for ArOH).

**Table 1** Ring-opening polymerization of L-lactide initiated by **1**<sup>a</sup>

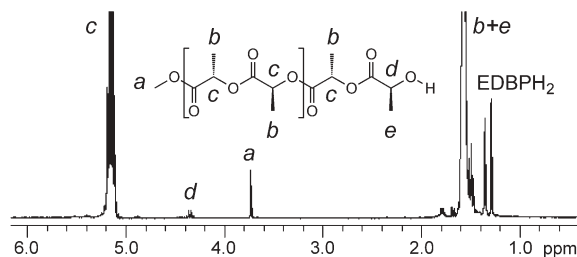
Entry	[M] <sub>0</sub> /[I] <sub>0</sub>	Time/min	Conv. (%) <sup>b</sup>	<i>M</i> <sub>n</sub> <sup>c</sup> GPC <sup>c</sup>	<i>M</i> <sub>w</sub> / <i>M</i> <sub>n</sub> <sup>c</sup>	<i>M</i> <sub>n</sub> calc. <sup>d</sup>	<i>M</i> <sub>n</sub> NMR <sup>b</sup>
1	62	8	>99	6500	1.38	4400	5500
2	134	8	99	14 500	1.33	9600	10 100
3	200	3	81	20 300	1.25	11 700	11 800
4	200	8	98	23 100	1.11	14 100	15 300
5	230	8	95	26 500	1.27	15 700	16 000
6 <sup>e</sup>	200	8	11	1600	1.10	1600	2600
7 <sup>e</sup>	200	240	53	5500	1.13	7700	7700
8 <sup>e</sup>	100	1320	96	8900	1.16	6900	8000
9 <sup>f</sup>	200	8	13	1600	1.10	1900	3800
10 <sup>f</sup>	200	240	51	7300	1.08	7400	8500
11 <sup>f</sup>	100	1320	96	9600	1.08	6900	7700

<sup>a</sup> In 20 mL toluene at 20 °C; 0.034 g **1**; quenched with acetic acid in hexane. <sup>b</sup> By <sup>1</sup>H NMR analysis. <sup>c</sup> GPC vs. calibrated PS standards using a correction factor of 0.58.<sup>23</sup> <sup>d</sup> By (F.W.<sub>-lactide</sub>[M]<sub>0</sub>/2[I]<sub>0</sub>)(% conversion). <sup>e</sup> In tetrahydrofuran. <sup>f</sup> In 1,2-dichloroethane.

of 25 min<sup>-1</sup> compares favorably with the most heralded (but synthetically complex) metal-based catalysts and has only been excelled in a few instances under comparable, mild reaction conditions: [Ca], 180 min<sup>-1</sup> (20 °C);<sup>11</sup> [Zn], 125 min<sup>-1</sup> (25 °C);<sup>20</sup> [Mg], 96 min<sup>-1</sup> (20 °C);<sup>5</sup> [Mg], 36 min<sup>-1</sup> (20 °C);<sup>11</sup> [Zn], 10 min<sup>-1</sup> (20 °C);<sup>5</sup> [Al], 1.2 min<sup>-1</sup> (70 °C);<sup>21</sup> [Sn], 0.02 min<sup>-1</sup> (20 °C).<sup>22</sup> However, the turnover frequency for **1** is markedly lower (~3 min<sup>-1</sup>) in polar solvents such as tetrahydrofuran (entries 6–8) or 1,2-dichloroethane (entries 9–11)—possibly because of competitive solvent complexation to the sodium catalyst. For comparison, NaOMe was tested and found to be essentially inactive in toluene and relatively sluggish in tetrahydrofuran, producing PLA in only 20–40% yield under the conditions of Table 1, entry 8 (~0.02 min<sup>-1</sup>). The previously reported lithium complex (EDBPH)Li(C<sub>6</sub>H<sub>5</sub>CH<sub>2</sub>OH)(THF)<sub>2</sub> was less active than **1** with 94% conversion in 45 minutes under conditions similar to those of Table 1, entry 4 (~4 min<sup>-1</sup>).<sup>17</sup>

The low polydispersity indices (*M*<sub>w</sub>/*M*<sub>n</sub> = 1.11–1.38), linear relationship between *M*<sub>n</sub> (NMR) and *M*<sub>n</sub> (calculated) (*R*<sup>2</sup> = 0.9885), and high degree of isotacticity (*[m]* > 98%; *T*<sub>m</sub> = 160–171 °C) suggest a controlled, sodium-mediated polymerization mechanism in toluene (entries 1–5). End group analysis by <sup>1</sup>H NMR (Fig. 3, sample from Table 1, entry 1) reveals the presence of one methyl ester group per polymer chain and a degree of polymerization approximately half that of the [L-lactide]/[**1**] quotient. This is consistent with an initiation mechanism wherein each of the two methanol molecules of **1** initiates a chain *via* ring-opening of lactide.

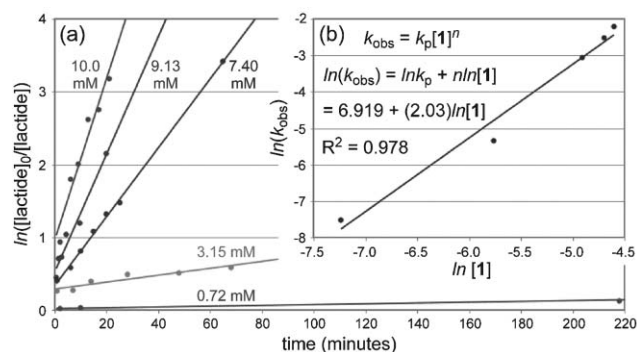
A kinetic study in tetrahydrofuran at 20 °C was conducted to establish the reaction order with respect to monomer and catalyst (aliquots analyzed by <sup>1</sup>H NMR). As expected, plots of



**Fig. 3** <sup>1</sup>H NMR spectrum of methyl ester terminated PLA (Table 1, entry 1). [L-lactide]/[**1**] = 62 and the degree of polymerization is 38, suggesting that each methanol present in **1** can initiate a chain.

ln([lactide]<sub>0</sub>/[lactide]) vs. time for a wide range of [**1**] are linear, indicating the usual first order dependence on monomer concentration (Fig. 4a). Thus, the rate expression can be written as d[lactide]/dt = *k*<sub>p</sub>[lactide]<sup>1</sup>[**1**]<sup>*n*</sup> = *k*<sub>obs</sub>[lactide]<sup>1</sup>, where *k*<sub>obs</sub> = *k*<sub>p</sub>[**1**]<sup>*n*</sup>. A plot of ln(*k*<sub>obs</sub>) vs. ln[**1**] (Fig. 4b) allows the determination of *k*<sub>p</sub> and *n*. The *y*-intercept of the regression line (6.919) equals ln *k*<sub>p</sub>, and thus the polymerization rate constant, *k*<sub>p</sub>, is 1011 M<sup>-2</sup>min<sup>-1</sup> or 16.9 M<sup>-2</sup>s<sup>-1</sup>. The slope of the regression line (2.03) equals *n* and thus the reaction is *second order* in catalyst, **1**. The overall rate expression d[lactide]/dt = *k*<sub>p</sub>[lactide]<sup>1</sup>[**1**]<sup>2</sup> is quite unusual because of the second order dependence on the catalyst. Typical lactide ring-opening polymerizations are first order in monomer and first order in catalyst, although non-integral orders with respect to catalyst less than 1.0 and up to 1.56 have been observed.<sup>5</sup> Such complex kinetic orders have been attributed to aggregation of metal initiators or growing polymer chains.<sup>5,20,24</sup> In the present case, the second order dependence on [**1**] suggests that two monosodium species are involved in the transition state for the propagation event. One mechanistic interpretation is that the chain is appended to one sodium metal—*via* the alcohol terminus—and a second sodium complex activates the lactide monomer *via* carbonyl coordination. Additional mechanistic work will be required to validate this hypothesis.

In conclusion, we have synthesized and employed the first well-defined sodium-based catalyst for the controlled and highly efficient ring-opening polymerization of L-lactide.<sup>25</sup> It is easily



**Fig. 4** (a) Linear plots of ln([lactide]<sub>0</sub>/[lactide]) vs. time demonstrating the first order dependence on monomer concentration (0.72 mM ≤ [**1**] ≤ 10.0 mM). (b) Linear plot of ln(*k*<sub>obs</sub>) vs. ln[**1**] demonstrating the second order dependence on catalyst concentration (*n* = 2.03). All polymerizations performed in THF at 20 °C with [lactide]<sub>0</sub> = 0.20 M.



synthesized in one step from sodium methoxide and a commercially available ligand that is approved for food contact by the U.S.F.D.A. Under the mild conditions tested (ambient temperature and pressure), only a few metal-based catalysts are known to exhibit higher activity, but each of these requires a multi-step synthesis for its preparation. Since a classical anionic mechanism<sup>26–28</sup> is avoided, epimerization and indiscriminate transesterification are minimal—affording isotactic polylactic acid with a narrow molecular weight distribution. Polymer characterization data are consistent with a controlled polymerization system wherein chain growth occurs from the alcohol-terminated polymer, two of which are bound to the sodium catalyst. Initial kinetic studies have revealed an unprecedented second order dependence on catalyst concentration. Future mechanistic studies will be greatly facilitated by the steric and electronic versatility possible with the ancillary ligand employed. Finally, this sodium-based catalyst should enable the synthesis of specialized grades of PLA containing essentially benign residual catalyst.

This research is supported by The Robert A. Welch Foundation (No. A-1537) and the National Science Foundation (NSF-CHE CAREER 0548197). H.-Y. C. would like to thank the National Science Council of the Republic of China for an international travel fellowship.

## Notes and references

‡ CCDC reference number 615697. For crystallographic data in CIF or other electronic format see DOI: 10.1039/b705622b. X-ray crystallographic data were obtained on a Bruker SMART 1000 diffractometer (Mo-K $\alpha$ ,  $\lambda$  = 0.71073 Å; graphite monochromator). The molecular structure was solved by direct methods and was refined employing the SHELXS-97 and SHELXL-97 programs.<sup>29,30</sup> Colorless crystals of **2** were grown from toluene. Crystal data: monoclinic,  $P2_1/n$ ,  $a$  = 16.035(5) Å,  $b$  = 19.797(5) Å,  $c$  = 24.936(5) Å,  $\alpha$  = 90°,  $\beta$  = 104.979(5)°,  $\gamma$  = 90°,  $V$  = 7647(3) Å<sup>3</sup>,  $Z$  = 4,  $T$  = 110(2) K,  $R_1$ (on  $F_0$ ) = 0.0631,  $wR_2$ (on  $F_0^2$ ) = 0.1693, GOF = 1.099 for 821 parameters and 13244 unique data.

- 1 K. E. Uhrich, S. M. Cannizzaro, R. S. Langer and K. M. Shakesheff, *Chem. Rev.*, 1999, **99**, 3181–3198.
- 2 O. Dechy-Cabaret, B. Martin-Vaca and D. Bourissou, *Chem. Rev.*, 2004, **104**, 6147–6176.
- 3 B. J. O'Keefe, M. A. Hillmyer and W. B. Tolman, *J. Chem. Soc., Dalton Trans.*, 2001, 2215–2224.
- 4 Y.-C. Liu, B.-T. Ko and C.-C. Lin, *Macromolecules*, 2001, **34**, 6196–6201.
- 5 B. M. Chamberlain, M. Cheng, D. R. Moore, T. M. O'vitt, E. B. Lobkovsky and G. W. Coates, *J. Am. Chem. Soc.*, 2001, **123**, 3229–3238.
- 6 K. B. Aubrecht, M. A. Hillmyer and W. B. Tolman, *Macromolecules*, 2002, **35**, 644–650.
- 7 H. Ma, T. P. Spaniol and J. Okuda, *Dalton Trans.*, 2003, 4770–4780.
- 8 W. H. Wong and D. J. Mooney, *Synthetic Biodegradable Polymer Scaffolds*, ed. A. Atala and D. J. Mooney, Birkhauser, Boston, MA, 1997, pp. 51–82.
- 9 A.-C. Albertsson and I. K. Varma, *Biomacromolecules*, 2003, **4**, 1466–1486.
- 10 T.-L. Yu, C.-C. Wu, C.-C. Chen, B.-H. Huang, J. Wu and C.-C. Lin, *Polymer*, 2005, **46**, 5909–5917.
- 11 M. H. Chisholm, J. C. Gallucci and K. Phomphrai, *Inorg. Chem.*, 2004, **43**, 6717–6725.
- 12 B. J. O'Keefe, L. E. Breyfogle, M. A. Hillmyer and W. B. Tolman, *J. Am. Chem. Soc.*, 2002, **124**, 4384–4393.
- 13 R. C. Pratt, B. G. G. Lohmeijer, D. A. Long, R. M. Waymouth and J. L. Hedrick, *J. Am. Chem. Soc.*, 2006, **128**, 4556–4557.
- 14 Percentages by mass. J. Emsley, *The Elements*, Clarendon Press, Oxford, 1998, pp. 194–195.
- 15 J. E. Kasperczyk, *Macromolecules*, 1995, **28**, 3937–3939.
- 16 B.-T. Ko and C.-C. Lin, *J. Am. Chem. Soc.*, 2001, **123**, 7973–7977.
- 17 M.-L. Hsueh, B.-H. Huang, J. Wu and C.-C. Lin, *Macromolecules*, 2005, **38**, 9482–9487.
- 18 U.S.F.D.A. Code of Federal Regulations, Title 21, Volume 3, Section 178.2010, Revised April 1, 2006; *Federal Register*, 1986, **51** (193), 35511–35512; *Federal Register*, 1983, **48** (132), 31382–31383; *Federal Register*, 1982, **47** (101, Bk. 1), 22512–22513.
- 19 Both terminal MeOH-Na adducts and Na-( $\mu$ -MeOH)-Na motifs have been observed by X-ray crystallography. E. M. McCarron and R. L. Harlow, *Acta Cryst., Sect. C: Cryst. Struct. Commun.*, 1984, **C40**, 1140–1141.
- 20 C. K. Williams, L. E. Breyfogle, S. K. Choi, W. Nam, V. G. Young, Jr., M. A. Hillmyer and W. B. Tolman, *J. Am. Chem. Soc.*, 2003, **125**, 11350–11359.
- 21 N. Nomura, R. Ishii, M. Akakura and K. Aoi, *J. Am. Chem. Soc.*, 2002, **124**, 5938–5939.
- 22 A. P. Dove, V. C. Gibson, E. L. Marshall, A. J. P. White and D. J. Williams, *Chem. Commun.*, 2001, 283–284.
- 23 A. Kowalski, A. Duda and S. Penczek, *Macromolecules*, 1998, **31**, 2114–2122.
- 24 A. Kowalski, J. Libiszowski, A. Duda and S. Penczek, *Macromolecules*, 2000, **33**, 1964–1971.
- 25 A bimetallic Na/Fe catalyst has been reported: D. S. McGuinness, E. L. Marshall, V. C. Gibson and J. W. Steed, *J. Polym. Sci., Part A: Polym. Chem.*, 2003, **41**, 3798–3803.
- 26 KOPh is not a strong enough base for the anionic polymerization of lactide, but KOtBu is and provides PLA in 77% yield in 1 hour (20 °C, toluene) with 20% racemization. H. R. Kricheldorf and I. Kreiser-Saunders, *Makromol. Chem.*, 1990, **191**, 1057–1066.
- 27 Z. Jedlinski, W. Walach, P. Kurock and G. Adamus, *Makromol. Chem.*, 1991, **192**, 2051–2057.
- 28 Z. Jedlinski, P. Kurock, W. Walach, H. Janeczek and I. Radecka, *Makromol. Chem.*, 1993, **194**, 1681–1689.
- 29 G. M. Sheldrick, *SHELXS-97, Program for solution of crystal structures*, University of Göttingen, Germany, 1997.
- 30 G. M. Sheldrick, *SHELXL-97, Program for refinement of crystal structures*, University of Göttingen, Germany, 1997.



# The first solvent-free method for the reduction of esters†

James Mack,\* Dennis Fulmer, Sam Stofel and Natalie Santos

Received 24th April 2007, Accepted 15th June 2007

First published as an Advance Article on the web 27th June 2007

DOI: 10.1039/b706167f

Utilizing the novel technique of high-speed ball milling, we herein report the first solvent-free reduction of esters.

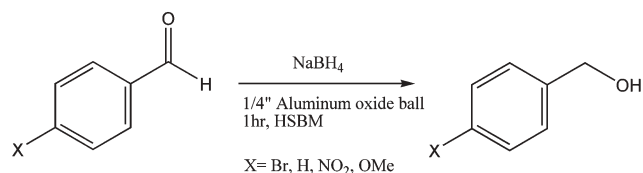
## Introduction

Environmental concerns about solvent-based chemistry have stimulated a renewed interest in the study of chemical reactions under solvent-free conditions. Although most of the research conducted in this area has been performed by using a mortar and pestle,<sup>1–3</sup> high speed ball milling (HSBM) is an attractive solvent-free method that has started to gain attention. In the HSBM method, a ball bearing is placed inside a vessel that is shaken at high speeds.<sup>4,5</sup> The high speed attained by the ball-bearing has enough force to make an amorphous mixture of the reagents which subsequently facilitates a chemical reaction. This method has been studied in metal alloying and for the generation of inorganic salts; however, few organic reactions have been performed by this process.<sup>6–11</sup> We look to further examine the nuances of this solvent-free technique and apply it directly to various organic reactions. We recently demonstrated an increase in rate of the Baylis–Hillman reaction using these unique conditions.<sup>12</sup> In this work, we look to focus on the reduction of aldehydes, ketones and esters by the HSBM approach.

## Results and discussion

Our initial studies focused on the sodium borohydride reduction of various *p*-substituted aryl aldehydes (Scheme 1).

The reactions were conducted in a custom made 0.5 × 2.0 inch screw-capped stainless steel vial and milled with a 0.250 inch aluminium oxide ball-bearing in a Spex certiprep mixer/mill 8000 M for one hour. At the conclusion of the reaction the products were washed with 10% HCl and the remaining solids were dried over a Hirsch funnel. Liquid products were isolated from extraction with the minimal amount of ethyl acetate instead of filtration. Upon isolation <sup>1</sup>H NMR, <sup>13</sup>C NMR and GC-MS



**Scheme 1** Reduction of *p*-substituted aryl aldehydes by HSBM.

University of Cincinnati, Cincinnati, OH, USA.

E-mail: james.mack@uc.edu; Fax: +1 513 556 9239; Tel: +1 513 556 9249

† Electronic supplementary information (ESI) available: Spectral data for all compounds and experimental details. See DOI: 10.1039/b706167f

were compared to literature values to confirm product formation. Our results are summarized in Table 1.

Using one full equivalent of sodium borohydride and milling for 1 h we were able to successfully reduce aldehydes in high yields. The reduction was also successful with ¼ equivalent of sodium borohydride; however much longer reaction times were needed in order to achieve comparable yields.

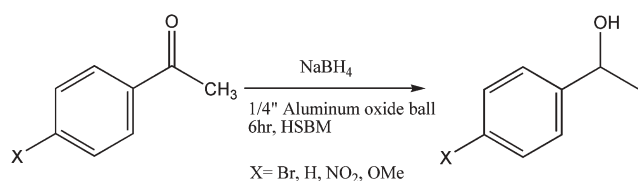
Given the rapid reduction of aldehydes by HSBM, we next studied the reduction of ketones (Scheme 2). Toda *et al.* previously reported the solvent-free sodium borohydride reduction of ketones using a mortar and pestle requires five days of grinding, an inert atmosphere and a large excess of sodium borohydride.<sup>13</sup> Conversely, using ball milling in open atmosphere we have been able to reduce various ketones in six hours in high yields. Our results are summarized in Table 2.

In addition to this report, other solvent-free methods have been developed for the reduction of aldehydes and ketones,<sup>14–17</sup> yet to

**Table 1** Reduction of *p*-substituted aryl aldehydes with sodium borohydride

Entry	Substrate	Time/h	% Conversion <sup>a</sup>	% Yield <sup>b</sup>
1		1	— <sup>c</sup>	— <sup>c</sup>
2		1	>95%	70
3		1	>95%	70
4		1	>95%	65

<sup>a</sup> Conversion data was reported relative to the amount of recovered starting material. <sup>b</sup> Isolated yield is reported as the yield after full work-up. <sup>c</sup> The solid state reduction of sodium borohydride and *p*-nitrobenzaldehyde led to a highly exothermic reaction; neither isolated yields or % conversion could be accurately attained.



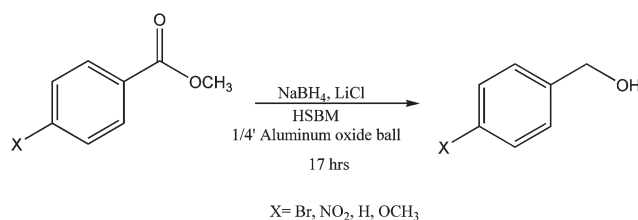
**Scheme 2** Reduction of *p*-substituted aryl ketones by HSBM.

**Table 2** Reductions of *p*-substituted aryl ketones with sodium borohydride

Entry	Substrate	Time/h	% Conversion	% Yield
1		6	>95%	70
2		6	>95%	73
3		6	>95%	70
4		6	>95%	65

the best of our knowledge none are known for the reduction of esters. Unlike aldehydes and ketones, esters are not typically reduced with sodium borohydride; more powerful and hazardous reducing agents such as lithium aluminium hydride are generally necessary. Given our success with the reduction of aldehydes and ketones using HSBM, we focused our attention on developing a safe solvent-free method for the reduction of esters (Scheme 3).

Aside from lithium aluminium hydride, lithium borohydride has been shown to be a powerful reducing agent for esters.<sup>18–20</sup> Although lithium borohydride is a powerful reducing agent, it is expensive,<sup>21</sup> cumbersome to prepare<sup>18,22</sup> and it has been known to readily combust in humid air.<sup>23</sup> Through the use of high speed ball



**Scheme 3** Solvent-free reduction of esters by HSBM.

**Table 3** Reactions of *p*-substituted aryl methyl benzoates with sodium borohydride and lithium chloride

Entry	Substrate	Time/h	% Conversion	% Yield
1		17	>90	69
2		17	>90	85
3		17	>90	67
4		17	38	32

milling, we were able to easily generate lithium borohydride from sodium borohydride and lithium chloride. Using this combination we reduced esters to their respective alcohol in moderate to high yields.

The reactions were conducted in a custom made 0.5 × 2.0 inch screw-capped stainless steel vial and milled with an 0.250 inch aluminium oxide ball-bearing in a Spex certiprep mixer/mill 8000 M for approximately 17 h. Various *p*-substituted aryl methyl benzoates (Scheme 3) were reduced using a 5 : 1 ratio of lithium chloride : sodium borohydride. At the conclusion of the reaction, the products were washed with 10% HCl and the remaining solids were dried over a Hirsch funnel. Liquid products were isolated by extraction from the minimal amount of ethyl acetate. Upon isolation <sup>1</sup>H NMR, <sup>13</sup>C NMR and GC-MS were used to confirm products which were compared to literature values. Our results are summarized in Table 3. Similar to the experimental conditions for the reduction of aldehydes and ketones, all of the ester reductions were run in open atmosphere with no special precautions taken. Further, upon quenching the reaction with dilute acid there was no sign of trace lithium borohydride remaining in the vessel. This suggests all the lithium borohydride generated is completely consumed in the reaction. To the best of our knowledge this represents the first solvent-free method for the reduction of esters.

## Conclusion

In conclusion, we report a practical method for the solvent free reduction of aldehydes and ketones by HSBM in open atmosphere. We further extended our conditions to the reduction of esters with the addition of lithium chloride. Currently, we are tailoring our method for the reduction of amides, carboxylic acids

and nitriles. We are also in the process of developing asymmetric versions of these conditions for the asymmetric reductions. Ball milling is a process that can have a large impact on the field of organic synthesis. We are looking to demonstrate a firm understanding of the guiding principles of HSBM. With a firm understanding we will be able to utilize this process better and adapt it to various other organic reactions creating more general environmentally benign reactions.

## Acknowledgements

We thank the National Science Foundation (CHE-0548150) and the URC at the University of Cincinnati for financial support of this research.

## Notes and references

- 1 K. Tanaka, *Solvent-Free Organic Synthesis*, Wiley-VCH, Cambridge, 2003.
- 2 K. Tanaka and F. Toda, *Chem. Rev.*, 2000, **100**, 1025–1074.
- 3 G. Rothenberg, A. P. Downie, C. L. Raston and J. L. Scott, *J. Am. Chem. Soc.*, 2001, **123**, 8701–8708.
- 4 C. Suryanarayana, *Prog. Mater. Sci.*, 2000, **46**, 1–184.
- 5 L. Takacs, *Prog. Mater. Sci.*, 2002, **47**, 355–414.
- 6 G. Kaupp, *Top. Curr. Chem.*, 2005, **254**, 95–183.
- 7 V. P. Balema, J. W. Wiench, M. Pruski and V. K. Pecharsky, *Chem. Commun.*, 2002, 724–725.
- 8 V. P. Balema, J. W. Wiench, M. Pruski and V. K. Pecharsky, *Chem. Commun.*, 2002, 1606–1607.
- 9 V. P. Balema, J. W. Wiench, M. Pruski and V. K. Pecharsky, *J. Am. Chem. Soc.*, 2002, **124**, 6244–6245.
- 10 K. Komatsu, K. Fujiwara and Y. Murata, *Chem. Commun.*, 2000, 1583–1584.
- 11 K. Komatsu, G.-W. Wang, Y. Murata, T. Tanaka, K. Fujiwara, K. Yamamoto and M. Saunders, *J. Org. Chem.*, 1998, **63**, 9358–9366.
- 12 J. Mack and M. Shumba, *Green Chem.*, 2007, **9**, 328–330.
- 13 F. Toda, K. Kiyoshige and M. Yagi, *Angew. Chem., Int. Ed. Engl.*, 1989, **28**, 320.
- 14 B. Zeynizadeh and T. Behyar, *J. Braz. Chem. Soc.*, 2005, **16**, 1200–1209.
- 15 G. W. Wang and L. Liu, *Chin. Chem. Lett.*, 2004, **15**, 587–590.
- 16 B. T. Cho, S. K. Kang, M. S. Kim, S. R. Ryu and D. K. An, *Tetrahedron*, 2006, **62**, 8164–8168.
- 17 R. S. Varma and R. K. Saini, *Tetrahedron Lett.*, 1997, **38**, 4337–4338.
- 18 H. C. Brown and S. Narasimhan, *J. Org. Chem.*, 1982, **47**, 1604–1606.
- 19 H. C. Brown, S. Narasimhan and Y. M. Choi, *J. Org. Chem.*, 1982, **47**, 4702–4708.
- 20 H. C. Brown and S. Narasimhan, *J. Org. Chem.*, 1984, **49**, 3891–3898.
- 21 Lithium borohydride purchased from Alfa-Aesar is \$7.94 for 1 g as compared to sodium borohydride (\$0.45 for 1 g) and lithium chloride (\$0.11 for 1 g).
- 22 H. C. Brown, Y. M. Choi and S. Narasimhan, *Inorg. Chem.*, 1982, **21**, 3657–3661.
- 23 R. F. Nystrom, S. W. Chaikin and W. G. Brown, *J. Am. Chem. Soc.*, 1949, **71**, 3245–3246.

# Dicationic molten salts (ionic liquids) as re-usable media for the controlled pyrolysis of cellulose to anhydrosugars†

Gary N. Sheldrake\* and David Schleck

Received 5th April 2007, Accepted 25th June 2007

First published as an Advance Article on the web 5th July 2007

DOI: 10.1039/b705241c

Molten dicationic imidazolium chloride or bromide salts, with short alkyl linker chains, have been found to be stable, re-usable media for the controlled pyrolysis of cellulose without acid pre-treatment to give anhydrosugars, primarily levoglucosenone, at a substantially lower temperature (180 °C) than most previously reported methods (typically > 300 °C).

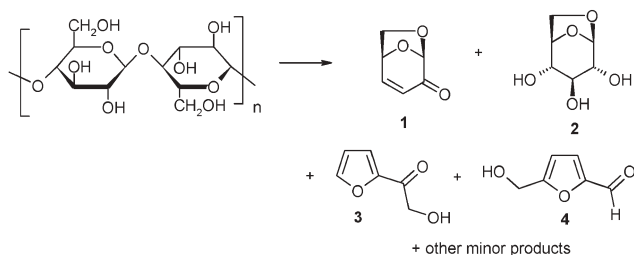
Lignocellulosic biomass has the potential to provide a large percentage of the fine chemical requirements for a sustainable chemical industry based on renewable raw materials. Many sources, for example the much-quoted road map produced by the US Department of Energy,<sup>1</sup> have identified carbohydrates derived from cellulose, hemicellulose and starch as by far the major biomass resource towards this end. There are several potential approaches to the use of cellulose as a raw material and, given the complexity of demand of a mature fine chemical intermediates market, a variety of methods and pathways will be required. The controlled pyrolysis of cellulose to give anhydrosugars (Scheme 1) is one method of producing chiral intermediates from cellulose that has been examined sporadically since the 1970s when much of the basic chemistry was elucidated by Shafizadeh and others.<sup>2</sup>

Levoglucosenone **1** is a synthetically versatile cyclic enone, with D-glucose series stereochemistry, which has been used to prepare such structurally diverse targets as hongconin,<sup>3</sup> (–)-δ-multistriatin<sup>4</sup> and (–)-tetrodotoxin.<sup>5</sup> The lack of free hydroxy groups in levoglucosenone and the relative stability of the intramolecular acetal also facilitate the atom efficient preparation of glucose and glycoside analogues with the minimum of protection/deprotection cycles.<sup>6</sup> However, the synthetic exploitation of levoglucosenone has been limited and has not led to large-scale, commercialised

processes for a number of reasons. Firstly, levoglucosenone is not available directly from nature and its preparation from monosaccharide precursors requires several uneconomic steps. The only practicable published method for the preparation of levoglucosenone is by the pyrolysis of cellulose which has been pre-treated with a mineral acid. This process has been largely confined to relatively small scale (<1 kg) laboratory preparations<sup>7</sup> because of the high temperatures required (typically > 300 °C), the very low yields from cellulose (ca. 1–5%), the large amounts of charred residue and the difficult separation of a product mixture containing at least four significant by-products. Many attempts have been made to improve both the conversion and selectivity of cellulose pyrolysis for levoglucosenone but no published method has overcome all of the practical difficulties. It has been claimed in some more recent work<sup>8</sup> that there is less or no charring of the cellulose, and a higher conversion to anhydrosugars, if the cellulose dissolves in a solvent, e.g. sulfolane, before or during the pyrolysis reaction. However, the low concentration of cellulose and the difficulty of separating the products from the solvent limit this as a preparative approach.

The report by Rogers and co-workers on the dissolution, in relatively high concentrations, of cellulose in ionic liquids containing halide anions<sup>9</sup> suggested to us the prospect of a dissolved-cellulose pyrolysis with continuous removal of the volatile anhydrosugar products by vacuum distillation. From the limited amount of published thermochemical data,<sup>10</sup> many ionic liquids have been reported to be thermally stable over a wide range of temperatures up to and including the reported onset of cellulose pyrolysis.

Preliminary investigations using 1-butyl-3-methylimidazolium chloride and bromide ([C<sub>4</sub>mim]Cl, **5a**, and [C<sub>4</sub>mim]Br, **5b**) were not encouraging, with the ionic liquids degrading extensively under the pyrolysis conditions (>250 °C). However, there was more



Scheme 1

School of Chemistry and Chemical Engineering, David Keir Building, Queen's University of Belfast, N. Ireland, UK.

E-mail: g.sheldrake@qub.ac.uk; Tel: +44 28 9097 4593

† Electronic supplementary information (ESI) available: General preparative methods for the dicationic salts; NMR spectroscopic data for compounds **1**, **3**, **4**, **6a–e** and **7**. See DOI: 10.1039/b705241c

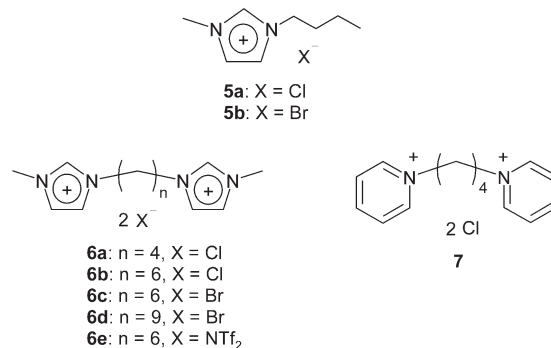


Fig. 1 Structures of imidazolium salts used.



**Table 1** Cellulose pyrolyses

Entry	Pyrolysis medium <sup>a</sup>	T/°C	Time/min	Yield <sup>b</sup> (wt%)	<b>1</b> (wt%)	<b>3</b> (wt%)	<b>4</b> (wt%)
1	<b>6a</b>	180	20	5.5	3.4	1.0	1.0
2	<b>6a</b> <sup>c</sup>	180	20	5.0	3.0	0.9	0.9
3	<b>6a</b> <sup>c,d</sup>	180	20	5.0	3.0	0.9	0.9
4	<b>6b</b>	180	20	2.5	1.5	0.5	0.5
5	<b>6c</b>	180	20	2.5	1.5	0.5	0.5
6	<b>6d</b>	190	30	<0.1	0	0	0
7	<b>6e</b>	190	30	0	0	0	0
8	<b>5a/6e</b> <sup>e</sup>	180	20	—	<sup>f</sup>	—	—
9	— <sup>g</sup>	350	20	3.0	1.9	<0.1	1.0
10	<b>7</b>	220	15	0 <sup>h</sup>	—	—	—
11	<b>5a</b>	180	20	0 <sup>h</sup>	—	—	—
12	<b>5b</b>	180	20	0 <sup>h</sup>	—	—	—

<sup>a</sup> All experiments used 1 g microcrystalline cellulose and 3 g reaction medium except where indicated. <sup>b</sup> Total organic distillate after removal of water. <sup>c</sup> 10 g cellulose, 30 g molten salt. <sup>d</sup> Using recycled [C<sub>4</sub>(mim)<sub>2</sub>]Cl<sub>2</sub>. <sup>e</sup> [C<sub>4</sub>mim]Cl (10 g), [C<sub>4</sub>(mim)<sub>2</sub>](NTf<sub>2</sub>)<sub>2</sub> (1 g), cellulose (0.7 g).

<sup>f</sup> Levoglucosenone identified in the distillate by NMR spectroscopy and GC-MS but not separated from the ionic liquid decomposition products. <sup>g</sup> 3 g cellulose pretreated with 4% (w/w) 90% H<sub>3</sub>PO<sub>4</sub>, no other reaction medium. <sup>h</sup> No anhydrosugars observed, only decomposition products from the salt.

success with the dicationic salts **6**, first introduced by Armstrong *et al.* and reported to have much higher thermal stability.<sup>11</sup> Using [C<sub>4</sub>(mim)<sub>2</sub>]Cl<sub>2</sub> (Fig. 1)† for the pyrolysis of cellulose gave levoglucosenone **1** as the main anhydrosugar product at substantially lower temperatures (optimally 180 °C) than the conventional acid-promoted process (Table 1). Apart from **1**, the distillate contained only water and two other significant organic products, the anhydrosugars 1-(2-furanyl)-2-hydroxyethanone **3** and 5-(hydroxymethyl)furfural **4**. The distillate did not require the neutralisation and work-up normally employed for the phosphoric acid process.<sup>7</sup>

For analytical purposes, the products were purified by silica gel chromatography but the distillates were stable without further treatment for several weeks in a refrigerator. The isolated yields of levoglucosenone after purification, while still disappointing at this stage of development, were comparable with many of the reported mineral acid processes and better than the control reaction in our apparatus (Table 1, entry 9). Surprisingly, and in contrast to most previous cellulose pyrolyses, we have been unable to detect levoglucosan **2** in any of our experiments, either in the distillate or in the residual salt/char mix.

While dicationic imidazolium salts are prepared atom efficiently using relatively inexpensive reactants, the process would be economically unviable and would have no green advantage over previous methods if the salts required disposal after each pyrolysis. Addition of water to the viscous black residue dissolved the salt and allowed removal of the charcoal and other solid cellulose-derived material by filtration or centrifugation. Removal of water from the aqueous filtrate/supernatant regenerated the dicationic salt with 100% mass balance. The salt was unchanged according to NMR spectroscopic analysis and behaved identically in a second pyrolysis (Table 1, entry 3). This recycle has now been repeated four times with no measurable effect on the course of the subsequent pyrolyses.

The range of anhydrosugar products obtained is consistent with an acid-catalysed pyrolysis process but without the need for acid pre-treatment of the cellulose. Imidazolium halide salts are known to exhibit acidic properties in the liquid phase and it could be argued that the salts are providing nothing more than general acid catalysis. However, the significant reduction in pyrolysis temperature suggests a more direct interaction between the salt

and cellulose. We have examined only a narrow range of salts so far, but cellulose pyrolysis has only been observed when a number of key requirements are met. Firstly, an imidazolium dication is required; the dipyridinium dichloride **7** did not support pyrolysis (Table 1, entry 10). Secondly, a halide anion is required, probably to enable dissolution of cellulose; the hydrophobic salt [C<sub>4</sub>(mim)<sub>2</sub>][NTf<sub>2</sub>]<sub>2</sub> (**6e**) produced no anhydrosugar products, but mixing **6e** with [C<sub>4</sub>mim]Cl (**5a**) as a halide source produced some levoglucosenone (Table 1, entry 8). This result is particularly significant because neither salt supports cellulose pyrolysis on its own. Thirdly, the length of the alkyl linker chain is important; [C<sub>6</sub>(mim)<sub>2</sub>]Cl<sub>2</sub> (**6b**) and [C<sub>6</sub>(mim)<sub>2</sub>]Br<sub>2</sub> (**6c**) both gave anhydrosugars, but with reduced yield, and [C<sub>9</sub>(mim)<sub>2</sub>]Br<sub>2</sub> (**6d**) gave no product at all (Table 1, entries 5–7). This result suggests that the interatomic distance between the cations is important for the pyrolysis. As yet we can offer no clear mechanistic rationalisation of these observations and considerably more experimentation is required.

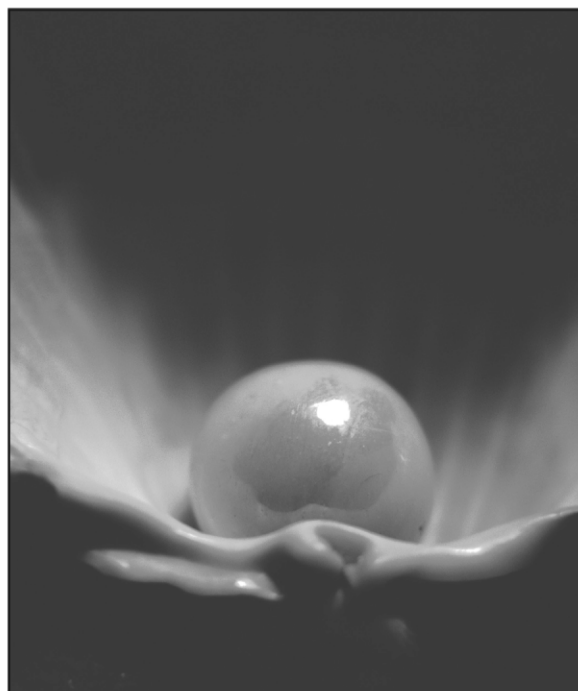
While there is still considerable scope for further development of the conversion and yield of this process, the unique properties of the dicationic molten salts offer several benefits over previous methods for the pyrolysis of cellulose to anhydrosugars.

## Notes and references

† Various reaction configurations have been tried but the most convenient preparations are carried out in a Büchi Kugelrohr short path distillation apparatus. In a typical procedure, [C<sub>4</sub>(mim)<sub>2</sub>]Cl<sub>2</sub> (**6a**, 3 g, prepared using the method described by Armstrong *et al.*<sup>11</sup>) and microcrystalline cellulose (1 g, purchased from Alfa Aesar) were charged to the 25 ml distillation bulb. The apparatus was evacuated (0.1 Torr) and the oven temperature raised to 180 °C. The salt began to melt at ca. 155 °C and distillation was observed almost immediately. Heating and vacuum were maintained for 20 minutes during which time the distillate (0.52 g) was collected in a receiver bulb cooled in a shallow bath of dry ice and acetone. The crude distillate, containing water and the anhydrosugars, was either (a) diluted with CH<sub>2</sub>Cl<sub>2</sub>, dried (anhyd. MgSO<sub>4</sub>) and separated by silica gel chromatography (hexane–CH<sub>2</sub>Cl<sub>2</sub>) or (b) combined with subsequent distillates and separated by fractional vacuum distillation.

- 1 *Top Added Value Chemicals from Biomass Vol. 1: Results of Screening for Potential Candidates from Sugars and Synthesis Gas*, ed. T. Werpy and G. Peterson, U.S. DoE, August 2004.
- 2 (a) Y. Halpern, R. Riffer and A. Broido, *J. Org. Chem.*, 1973, **38**, 204–209; (b) F. Shafizadeh and P. P. S. Chin, *Carbohydr. Res.*, 1977, **58**,

- 79–87; (c) F. Shafizadeh, *J. Anal. Appl. Pyrolysis*, 1982, **3**, 283–305; (d) F. Shafizadeh, *Adv. Chem. Ser.*, 1984, 491–529.
- 3 J. S. Swenton, J. N. Freskos, P. Dalidowicz and M. L. Kerns, *J. Org. Chem.*, 1996, **61**, 459–464.
  - 4 Z. J. Witczak and Y. Li, *Tetrahedron Lett.*, 1995, **36**, 2595–2598.
  - 5 T. Nishikawa, M. Asai, N. Ohya, N. Yamamoto, Y. Fukuda and M. Isobe, *Tetrahedron*, 2001, **57**, 3875–3883.
  - 6 Z. J. Witczak, *ACS Symp. Ser.*, 2003, **841**, 1–19.
  - 7 M. E. Jung and M. Kiankarimi, *J. Org. Chem.*, 1998, **63**, 8133–8144.
  - 8 (a) H. Kawamoto, W. Hatanaka and S. Saka, *J. Anal. Appl. Pyrolysis*, 2003, **70**, 303–313; (b) H. Kawamoto and S. Saka, *J. Anal. Appl. Pyrolysis*, 2006, **76**, 280–284.
  - 9 R. P. Swatowski, S. K. Spear, J. D. Holbrey and R. D. Rogers, *J. Am. Chem. Soc.*, 2002, **124**, 4974–4975.
  - 10 C. P. Fredlake, J. M. Crosthwaite, D. G. Hert, S. N. V. K. Aki and J. F. Brennecke, *J. Chem. Eng. Data*, 2004, **49**, 954–964.
  - 11 (a) J. L. Anderson, R. Ding, A. Ellern and D. W. Armstrong, *J. Am. Chem. Soc.*, 2005, **127**, 593; (b) X. Han and D. W. Armstrong, *Org. Lett.*, 2005, **7**, 4205.



## Looking for that **special** chemical biology research paper?

TRY this free news service:

### Chemical Biology

- highlights of newsworthy and significant advances in chemical biology from across RSC journals
- free online access
- updated daily
- free access to the original research paper from every online article
- also available as a free print supplement in selected RSC journals.\*

\*A separately issued print subscription is also available.

Registered Charity Number: 207890

RSC Publishing

[www.rsc.org/chembiology](http://www.rsc.org/chembiology)

22030681

# Copper catalyzed oxidative alkylation of $sp^3$ C–H bond adjacent to a nitrogen atom using molecular oxygen in water

Olivier Baslé and Chao-Jun Li\*

Received 22nd May 2007, Accepted 13th June 2007

First published as an Advance Article on the web 9th July 2007

DOI: 10.1039/b707745a

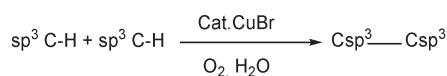
A simple and highly efficient C–C bond formation was developed by the activation of two  $sp^3$  C–H.

Environmental consciousness and safety concerns have given rise to much interest in the use of water as a reaction media in organic synthesis.<sup>1</sup> Due to its unique physical and chemical properties, water has emerged as a powerful solvent for intermolecular C–C bond formation by accelerating the rate and increasing the selectivity of the reaction.<sup>2</sup> Nevertheless, C–C bond formation *via* catalytic C–H bond activation in water remains rare. Recently, we<sup>3</sup> and others<sup>4</sup> described the Grignard-type addition of alkyne to aldehyde in order to generate propargyl alcohol *via* C–H bond activation in water. Equally important is the three-component aldehyde–amine–alkyne ( $A^3$  coupling) reaction<sup>5</sup> to generate the corresponding propargyl amines. However, to the best of our knowledge, C–C coupling by the reaction of  $sp^3$  C–H bond in water has never been reported. In recent years, direct functionalizations of  $sp^3$  C–H have received particular interest.<sup>6</sup> In our own studies, we have developed various cross-dehydrogenative-coupling (CDC) reactions between two different  $sp^3$  C–H bonds by using *tert*-BuOOH as an oxidizing reagent.<sup>7</sup> The replacement of peroxides by molecular oxygen (and in water) would offer a more atom-economical and safer process.<sup>8</sup> Herein, we report a highly efficient CDC reaction between two  $sp^3$  C–H bonds in water catalyzed by copper bromide under one atmosphere of oxygen (Scheme 1).

Previously, we reported the CDC reaction between tertiary amines and nitroalkane to generate  $\beta$ -nitroamines.<sup>7</sup> Such compounds can be readily reduced to 1,2-diamines,<sup>9</sup> which are important molecules in medicinal chemistry and are useful ligands for catalysis.<sup>10</sup> Tetrahydroisoquinoline, a common sub-structure in natural products, was the tertiary amine of choice. Inspired by the work of Murahashi and co-workers on ruthenium-catalyzed oxidation of tetrahydroisoquinolines by oxygen,<sup>11</sup> we examined the CDC reaction between such compounds with nitromethane in the presence of 5 mol% of ruthenium chloride and under one-atmosphere of oxygen gas in water to give 45% yield of the desired CDC reaction product

in 18 h. Encouraged by this initial result, we began to optimize the reaction (Table 1). The addition of 1 mol% of CuBr significantly increased the yield of the desired product (nearly the same as the result obtained with 10 mol%  $RuCl_3$ ). With 5 mol%  $RuCl_3$  and 5 mol% CuBr as co-catalysts, 90% of the corresponding CDC product was obtained after 18 h. Interestingly, the use of 5 mol% of CuBr in the absence of  $RuCl_3$  increased the rate of the reaction to generate 90% of the desired product after 16 h in both methanol and water. It is important to note that the CDC reaction also proceeded efficiently in air and water without the need of oxygen gas, albeit with a reduced reaction rate. After 24 h, 85% of the desired product was obtained with a 99% conversion of the starting material.

Subsequently, oxidative cross-dehydrogenative-coupling between various tertiary amines and nitro-alkanes were examined under the standard conditions of 1 atm oxygen gas in water (Table 2). The reaction of 1,2,3,4-tetrahydroisoquinoline derivatives with two equivalents of nitromethane generated the desired coupling products **3a** and **3e** in excellent yield (entries 1 and 5). Similar excellent results were obtained in the presence of five equivalents of nitroethane or nitropropane (the ratio of the two diastereoisomers is 3 : 2) (entries 2, 3, 5 and 6). Substrate **1b** with an *N*-*p*-methoxyphenyl substituent was found to be more reactive than the simple phenyl substituted analog for the CDC reaction. In this case, the reactions were highly effective, even at 40 °C (entries 4, 5, and



**Scheme 1** Oxidative cross-dehydrogenative-coupling between two  $sp^3$  C–H bonds with oxygen in water.

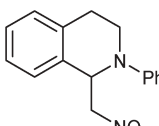
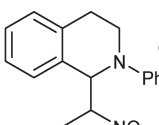
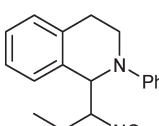
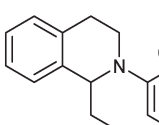
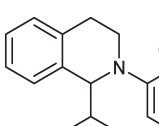
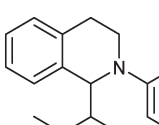
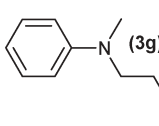
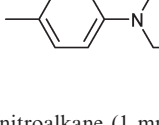
**Table 1** Optimization of reaction conditions<sup>a</sup>

Entry	Solvent	$RuCl_3$ (mol%)	CuBr (mol%)	Time/h	Yield <sup>b</sup>
1	H <sub>2</sub> O	5	0	18	45
2	H <sub>2</sub> O	10	0	18	67
3	H <sub>2</sub> O	5	1	18	62
4	H <sub>2</sub> O	5	2	18	73
5	H <sub>2</sub> O	5	5	18	90
6	H <sub>2</sub> O	0	5	16	90
7	MeOH	0	5	16	90

<sup>a</sup> Tertiary amine (0.2 mmol) and nitroalkane (0.4 mmol) were stirred under O<sub>2</sub> (1 atm) at 60 °C in 0.6 mL of water. <sup>b</sup> NMR yields based on tetrahydroisoquinoline using an internal standard.

Department of Chemistry, McGill University, 801 Sherbrooke Street West, Montreal, Quebec, H3A 2K6, Canada. E-mail: cj.li@mcgill.ca

**Table 2** Catalytic CDC reactions between tertiary amines with nitroalkanes with oxygen in water<sup>d</sup>

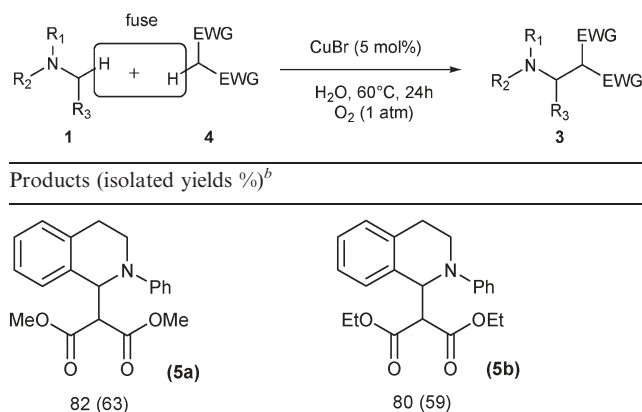
Entry	Nitroalkanes	<i>T</i> /°C	Products	Yield (%) <sup>d</sup>
1	MeNO <sub>2</sub> <b>2a</b>	60	 ( <b>3a</b> )	90 (79) <sup>b</sup>
2	EtNO <sub>2</sub> <b>2b</b>	60	 ( <b>3b</b> )	90 (75)
3	PrNO <sub>2</sub> <b>2c</b>	60	 ( <b>3c</b> )	95 (82)
4	<b>2a</b>	40	 ( <b>3d</b> )	95 (72) <sup>b</sup>
5	<b>2b</b>	40	 ( <b>3e</b> )	80 (67)
6	<b>2c</b>	40	 ( <b>3f</b> )	85 (69)
7	<b>2a</b>	60	 ( <b>3g</b> )	(30) <sup>c</sup>
8	<b>2a</b>	60	 ( <b>3h</b> )	75 (63) <sup>c</sup>

<sup>a</sup> Tertiary amine (0.2 mmol), nitroalkane (1 mmol), CuBr (5 mol%), under O<sub>2</sub> (1 atm) at 60 °C for 16 h in 0.6 mL of water.

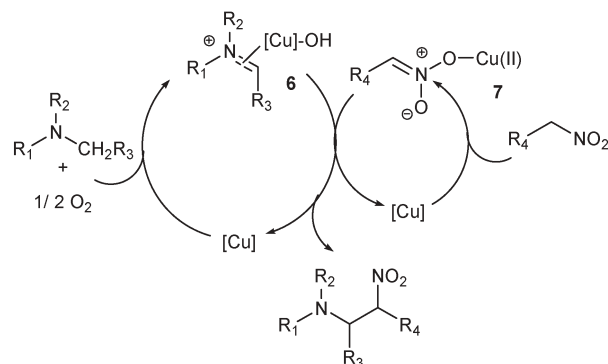
<sup>b</sup> Nitromethane (0.2 mmol) was used. <sup>c</sup> Nitromethane (1.0 mL, 92 equiv) was used. <sup>d</sup> NMR yields based on tertiary amines with an internal standard (isolated yield are given in parentheses).

6). For the symmetrical *N,N*-dimethyltoluidine, although there is a great potential for forming the bisalkylation by-product, the use of 1 mL (92 equiv.) of nitromethane with 0.2 mmol of *N,N*-dimethyltoluidine offered product **3h** with good yield in water (entry 8). Nevertheless, in the case of *N,N*-dimethylaniline, the reaction was less efficient. The selectivity for the formation of the CDC product in the absence of a 4-substituted *N,N*-dimethylaniline derivative decreased considerably.

In addition to nitroalkanes, the oxidative CDC reaction in water with oxygen was also applicable to dialkyl malonate derivatives (Table 3).<sup>12</sup> The reactions of dimethyl- and

**Table 3** CDC reaction of tetrahydroisoquinoline with malonate<sup>a</sup>

<sup>a</sup> Tetrahydroisoquinoline (0.2 mmol) and malonate (0.2 mmol) under O<sub>2</sub> at 60 °C for 24 h in water. <sup>b</sup> NMR yields based on tertiary amines with an internal standard (isolated yield are given in parentheses).

**Scheme 2** Possible mechanism.

diethylmalonate with 2-phenyl-1,2,3,4-tetrahydroisoquinoline generated  $\beta$ -diester products in good yields in water and with oxygen gas.

In order to explore the reaction mechanism, measurement of the molecular oxygen uptake was undertaken (see Experimental). This study showed that 0.5 mol of molecular oxygen is consumed for the oxidation of 1 mol of 2-phenyl-1,2,3,4-tetrahydroisoquinoline under the standard reaction conditions. This result suggests that the reaction proceeds via the copper-catalyzed generation of a possible imine-type intermediate (**6**) with half of an oxygen molecule.<sup>11</sup> Then, copper also catalyzes a subsequent Henry-type reaction *in situ* by facilitating the deprotonation of nitroalkanes to generate intermediate **7** (Scheme 2), as reported earlier by Evans.<sup>13</sup>

In conclusion, a simple and highly efficient C–C bond formation was developed by the reaction of two sp<sup>3</sup> C–H bonds catalyzed by copper bromide under an oxygen atmosphere in water. The oxidative CDC reaction appears to be a combination of a copper-catalyzed oxidative transformation of amines to imine-type intermediates followed by a copper-catalyzed Henry-type reaction. The scope, mechanism, and synthetic applications are under investigation.



## Experimental

$^1\text{H}$  NMR spectra were recorded on Varian 300 and 400 MHz spectrometers in  $\text{CDCl}_3$  solution and the chemical shifts were reported in parts per million ( $\delta$ ) referenced to the internal solvent signal (peak at 7.26 ppm).  $^{13}\text{C}$  NMR were obtained at 75 MHz and referenced to the internal solvent signal (central peak is 77.00 ppm). MS data were obtained by Agilent 6890N Network GC/System/Agilent 5973 Mass Selective Detector. HRMS were made by McGill University. IR spectra were recorded by an ABB Bomem MB100 instrument. Flash column chromatography was performed over SORBENT silica gel 30–60  $\mu\text{m}$ . Thin layer chromatography was performed using Sorbent Silica Gel 60  $\text{F}_{254}$  TLC plates and visualized with ultraviolet light. All reagents were weighed and handled in air, and backfilled under an inert atmosphere of nitrogen at room temperature. All reagents were purchased from Aldrich and Acros and used without further purification. 2-Aryl-1,2,3,4-tetrahydro-isoquinolines were prepared by the literature method.<sup>14</sup>

### General procedure

To a mixture of CuBr (1.4 mg, 0.01 mmol), 2-phenyl-tetrahydroisoquinoline (42 mg, 0.2 mmol), 0.6 mL of distilled water and (21.5  $\mu\text{L}$ , 0.4 mmol)  $\text{CH}_3\text{NO}_2$  was added. Then the 20 mL test-tube was sealed and filled up with molecular oxygen. The reaction was stirred using a magnetic stirrer at 60  $^\circ\text{C}$  for 16 h. The resulting mixture was extracted with ethyl acetate and filtered through a short layer of silica gel and eluted with ethyl acetate. Solvent was evaporated and the residue was purified by column chromatography on silica gel (eluent: hexane–ethyl acetate = 5 : 1), and the fraction with an  $R_f$  = 0.5 was collected and concentrated to give the desired product **3a**.

### 1,2,3,4-Tetrahydro-1-(nitromethyl)-2-phenylisoquinoline (**3a**)<sup>7</sup>

Isolated by flash column chromatography (hexane–ethyl acetate = 5 : 1,  $R_f$  = 0.5).  $^1\text{H}$  NMR (400 MHz, ppm)  $\delta$  7.25–7.20 (m, 2H), 7.18 (dd,  $J$  = 4.4, 1.6 Hz, 1H), 7.16–7.13 (m, 2H), 7.08 (d,  $J$  = 7.6 Hz, 1H), 6.94 (d,  $J$  = 8.0 Hz, 2H), 6.81 (dd,  $J$  = 7.4, 7.4 Hz, 1H), 5.51 (dd,  $J$  = 7.6, 6.8 Hz, 1H), 4.81 (dd,  $J$  = 12.0, 7.6 Hz, 1H), 4.50 (dd,  $J$  = 12.0, 6.8 Hz, 1H), 3.64–3.53 (m, 2H), 3.04 (ddd,  $J$  = 14.0, 8.6, 5.2 Hz, 1H), 2.74 (dt,  $J$  = 16.4, 4.8 Hz, 1H).

### 1,2,3,4-Tetrahydro-1-(1-nitroethyl)-2-phenylisoquinoline (**3b**)<sup>7</sup>

The ratio of isolated diastereoisomers is 1.7. Isolated by flash column chromatography (hexane–ethyl acetate = 5 : 1,  $R_f$  = 0.6). The major isomer:  $^1\text{H}$  NMR (300 MHz, ppm)  $\delta$  5.21 (d,  $J$  = 7.8 Hz, 1H), 5.03 (dq,  $J$  = 8.4, 6.6 Hz, 1H), 3.62–3.49 (m, 2H), 1.53 (d,  $J$  = 6.6 Hz, 3H); The minor isomer:  $^1\text{H}$  NMR (300 MHz, ppm)  $\delta$  5.24 (d,  $J$  = 7.8 Hz, 1H), 4.87 (dq,  $J$  = 8.7, 6.9 Hz, 1H), 3.82 (ddd,  $J$  = 13.5, 8.1, 5.7 Hz, 2H), 1.69 (d,  $J$  = 6.9 Hz, 3H); Other overlapped peaks:  $^1\text{H}$  NMR (300 MHz, ppm)  $\delta$  7.28–7.18 (m), 7.16–7.06 (m), 7.00–6.95 (m), 6.83–6.76 (m), 3.09–2.99 (m), 2.94–2.81 (m).

### 1,2,3,4-Tetrahydro-1-(1-nitropropyl)-2-phenyl-isoquinoline (**3c**)

Isolated by flash column chromatography (hexane–ethyl acetate = 5 : 1,  $R_f$  = 0.6). The ratio of diastereomers is 1.4. IR (neat liquid):  $\nu_{\text{max}}$  3061, 3036, 3024, 2973, 2936, 2879, 2856, 1598, 1577, 1549, 1503, 1494, 1475, 1457, 1438, 1390, 1370, 1346, 1320, 1298, 1269, 1218, 1149, 1122, 1111, 1081, 986  $\text{cm}^{-1}$ ; The major isomer:  $^1\text{H}$  NMR (400 MHz, ppm)  $\delta$  5.15 (d,  $J$  = 9.6 Hz, 1H), 4.88 (t,  $J$  = 9 Hz, 1H), 3.88–3.83 (m, 1H);  $^{13}\text{C}$  NMR (75 MHz, ppm) 149.4, 135.8, 132.8, 129.7, 129.5, 128.9, 128.4, 126.2, 119.7, 116.1, 93.3, 62.5, 42.6; The minor isomer:  $^1\text{H}$  NMR (400 MHz, ppm)  $\delta$  5.26 (d, 9.6 Hz, 1H), 4.67 (t, 9 Hz, 1H).  $^{13}\text{C}$  NMR (75 MHz, ppm)  $\delta$  149.3, 135.0, 134.2, 129.6, 128.9, 128.5, 127.5, 126.9, 118.9, 114.4, 96.4, 61.0, 43.8, 27.1, 25.3, 11.0. Other overlapped peaks:  $^1\text{H}$  NMR (400 MHz, ppm)  $\delta$  3.71–3.51 (m), 3.13–2.85 (m), 2.27–2.09 (m), 1.88–1.80 (m), 0.98–0.93 (m);  $^{13}\text{C}$  NMR (75 MHz, ppm)  $\delta$  129.9, 129.6, 129.5, 128.9, 128.9, 128.5, 128.4, 127.5, 126.9, 126.2, 27.1, 26.0, 25.3, 24.9, 10.9. MS (EI)  $m/z$  (%) 296, 221, 208, 165, 115, 128, 104, 89, 77, 51; HRMS calcd for  $\text{C}_{18}\text{H}_{20}\text{O}_2\text{N}_2$ : 296.1525; found: 296.1511.

### 1,2,3,4-Tetrahydro-2-(4-methoxyphenyl)-1-(nitromethyl)-isoquinoline (**3d**)<sup>7</sup>

Isolated by flash column chromatography (hexane–ethyl acetate = 5 : 1,  $R_f$  = 0.4).  $^1\text{H}$  NMR (400 MHz, ppm)  $\delta$  7.24–7.17 (m, 2H), 7.16–7.11 (m, 2H), 6.89 (d,  $J$  = 8.8 Hz, 2H), 6.79 (d,  $J$  = 8.8 Hz, 2H), 5.37 (dd,  $J$  = 8.4, 6.0 Hz, 1H), 4.80 (dd,  $J$  = 12.0, 8.8 Hz, 1H), 4.54 (dd,  $J$  = 12.0, 6.0 Hz, 1H), 3.73 (s, 3H), 3.60–3.50 (m, 2H), 3.00 (ddd,  $J$  = 16.4, 8.8, 6.4 Hz, 1H), 2.68 (dt,  $J$  = 16.4, 4.0 Hz, 1H).

### 1,2,3,4-Tetrahydro-2-(4-methoxyphenyl)-1-(1-nitroethyl)-isoquinoline (**3e**)<sup>7</sup>

The ratio of isolated diastereoisomers is 1.7. Isolated by flash column chromatography (hexane–ethyl acetate = 5 : 1,  $R_f$  = 0.4). The major isomer:  $^1\text{H}$  NMR (300 MHz, ppm)  $\delta$  3.72 (s, 3H), 3.53–3.44 (m, 2H), 1.52 (d,  $J$  = 6.6 Hz, 3H); The minor isomer:  $^1\text{H}$  NMR (300 MHz, ppm)  $\delta$  4.85 (dq,  $J$  = 8.6, 6.6 Hz, 1H), 3.81–3.75 (m, 2H), 3.74 (s, 3H), 1.67 (d,  $J$  = 6.9 Hz, 3H); Other overlapped peaks:  $^1\text{H}$  NMR (300 MHz, ppm)  $\delta$  7.25–7.07 (m), 7.01–6.98 (m), 6.92–6.87 (m), 6.83–6.75 (m), 5.06–4.93 (m), 3.02–2.92 (m), 2.84–2.72 (m).

### 1,2,3,4-Tetrahydro-2-(4-methoxyphenyl)-1-(1-nitropropyl)-isoquinoline (**3f**)

Isolated by flash column chromatography (eluent: hexane–ethyl acetate = 5 : 1,  $R_f$  = 0.4). The ratio of diastereomers is 1.4. IR (neat liquid):  $\nu_{\text{max}}$  3062, 3042, 3021, 2952, 2932, 2852, 2834, 1607, 1581, 1556, 1553, 1549, 1514, 1506, 1493, 1463, 1441, 1386, 1371, 1347, 1293, 1267, 1246, 1183, 1146, 1120, 1038  $\text{cm}^{-1}$ ; The major isomer:  $^1\text{H}$  NMR (300 MHz, ppm)  $\delta$  4.93–4.8 (m, 2H);  $^{13}\text{C}$  NMR (75 MHz, ppm)  $\delta$  154.1, 136.0, 132.8, 129.0, 128.3, 126.1, 119.4, 114.7, 93.5, 63.2, 55.8, 43.8, 25.6, 24.9, 11.0. The minor isomer:  $^1\text{H}$  NMR (300 MHz, ppm)  $\delta$  5.03 (d,  $J$  = 9 Hz, 1H), 4.67 (m, 1H).  $^{13}\text{C}$  NMR (75 MHz, ppm) 153.5, 135.1, 134.0, 129.1, 127.5, 126.8, 117.8, 115.0, 96.3, 61.8, 55.9, 44.9, 26.5, 25.2, 10.9. Other overlapped peaks:

$^1\text{H}$  NMR (300 MHz, ppm)  $\delta$  7.26–7.18 (m), 7.16–6.74 (m), 3.87–3.72 (m), 3.61–3.47 (m), 3.06–2.95 (m), 2.83–2.73 (m), 1.86–1.80 (m), 0.97–0.94 (m);  $^{13}\text{C}$  NMR (75 MHz, ppm)  $\delta$  144.0, 129.7. MS (EI)  $m/z$  (%) 326, 251, 236, 206, 193, 149, 128, 115, 103, 77, 54; HRMS calcd for  $\text{C}_{19}\text{H}_{22}\text{O}_3\text{N}_2$ : 326.1630; found: 326.1617.

### *N*-Methyl-*N*-(2-nitroethyl)benzenamine (3g)<sup>7</sup>

Isolated by flash column chromatography (hexane–ethyl acetate = 5 : 1,  $R_f$  = 0.4).  $^1\text{H}$  NMR (300 MHz, ppm)  $\delta$  7.28–7.22(m, 2H), 6.78 (dd,  $J$  = 7.2, 7.2 Hz, 1H), 6.72 (dd,  $J$  = 9.0, 0.9 Hz, 2H), 4.56(t,  $J$  = 6.3 Hz, 2H), 4.00 (td,  $J$  = 6.6 Hz, 2H), 2.98 (s, 3H).

### *N*,4-Dimethyl-*N*-(2-nitroethyl)benzenamine (3h)<sup>7</sup>

Isolated by flash column chromatography (hexane–ethyl acetate = 5 : 1,  $R_f$  = 0.5).  $^1\text{H}$  NMR (300 MHz, ppm)  $\delta$  7.05 (d,  $J$  = 8.7 Hz, 2H), 6.64 (d,  $J$  = 8.7 Hz, 2H), 4.52 (t,  $J$  = 6.3 Hz, 2H), 3.93 (t,  $J$  = 6.3 Hz, 2H), 2.92 (s, 3H), 2.25 (s, 3H).

### 2-(2-Phenyl-1,2,3,4-tetrahydro-isoquinolin-1-yl)-malonic acid dimethyl ester (5a)<sup>12</sup>

Isolated by flash column chromatography (hexane–ethyl acetate = 5 : 1,  $R_f$  = 0.5).  $^1\text{H}$  NMR (400 MHz,  $\text{CDCl}_3$ , 25 °C, ppm)  $\delta$  = 7.23–7.17(m, 3H), 7.14–7.05(m, 3H), 6.98(d,  $J$  = 8.0 Hz, 2H), 6.76(dd,  $J$  = 7.2, 7.2 Hz, 1H), 5.70(d,  $J$  = 9.2 Hz, 1H), 3.95(d,  $J$  = 9.2 Hz, 1H), 3.76–3.60(m, 2H), 3.66(s, 3H), 3.55(s, 3H), 3.08(ddd,  $J$  = 16.0, 8.4, 6.3 Hz, 1H), 2.90(dt,  $J$  = 16.0, 5.1 Hz, 1H).

### 2-(2-Phenyl-1,2,3,4-tetrahydro-isoquinolin-1-yl)-malonic acid diethyl ester (5b)<sup>12</sup>

Isolated by flash column chromatography (hexane–ethyl acetate = 5 : 1,  $R_f$  = 0.5).  $^1\text{H}$  NMR (300 MHz,  $\text{CDCl}_3$ , 25 °C, ppm)  $\delta$  = 7.24–7.05 (m, 6H), 6.96 (d,  $J$  = 8.1 Hz, 2H), 6.72 (dd,  $J$  = 7.2, 7.2 Hz, 1H), 5.71 (d,  $J$  = 9.3 Hz, 1H), 4.17–3.93 (m, 4H), 3.88 (d,  $J$  = 9.0 Hz, 1H), 3.74–3.58 (m, 2H), 3.06(ddd,  $J$  = 15.9, 8.7, 6.3 Hz, 1H), 2.87 (dt,  $J$  = 16.5, 5.1 Hz, 1H), 1.16 (t,  $J$  = 7.2 Hz, 3H), 1.08 (t,  $J$  = 7.2 Hz, 3H).

### Measurement of oxygen uptake for copper-catalyzed oxidative alkylation of $\text{sp}^3$ C–H bond adjacent to a nitrogen atom using molecular oxygen in water

In a 10 mL schlenk flask equipped with a magnetic stirring bar and connected to a gas pressure sensor (Vernier; GPS-BTA), CuBr (1.4 mg, 0.01 mmol) was added. After the reaction was flashed with molecular oxygen (1 atm), methanol (0.6 mL) was added. After the flask was immersed in an oil bath at 60 °C

for 1 h to stabilize, 2-phenyl-1,2,3,4-tetrahydro-isoquinoline (0.042 g, 0.2 mmol) dissolved in nitromethane (54  $\mu\text{L}$ , 5 eq.) was injected with a 100  $\mu\text{L}$  syringe to start the reaction. The consumption of oxygen was monitored every minute using Logger Pro 3.0. The absorption of  $\text{O}_2$  stopped after 0.1 mmol was consumed (ca. 16 h).

## References

- (a) C.-J. Li and T. H. Chan, *Organic Reactions in Aqueous Media*, John Wiley, New York, 1997; (b) U. M. Lindstrom, *Chem. Rev.*, 2002, **102**, 2751; (c) C.-J. Li, *Chem. Rev.*, 2005, **105**, 3095; (d) C.-J. Li, *Chem. Rev.*, 1993, **93**, 2023; (e) C.-J. Li and L. Chen, *Chem. Soc. Rev.*, 2006, **35**, 68; (f) *Organic Synthesis in Water*, ed. P. A. Grieco, Thomson Science, Glasgow, 1998.
- (a) S. Narayan, J. Muldoon, M. G. Finn, V. V. Fokin, H. C. Kolb and K. B. Sharpless, *Angew. Chem., Int. Ed.*, 2005, **44**, 3275; (b) D. C. Rideout and R. Breslow, *J. Am. Chem. Soc.*, 1980, **102**, 7816.
- (a) C.-J. Li, *Acc. Chem. Res.*, 2002, **35**, 533; (b) C. Wei and C.-J. Li, *Green Chem.*, 2002, **4**, 39; (c) C.-J. Li and C. Wei, *Chem. Commun.*, 2002, 268; (d) J. Zhang, C. Wei and C.-J. Li, *Tetrahedron Lett.*, 2002, **43**, 5731.
- (a) D. E. Frantz, R. Faessler, C. S. Tomooka and E. M. Carreira, *Acc. Chem. Res.*, 2000, **33**, 373, see also: G. Lu, X. Li, W. L. Chan and A. S. C. Chan, *Chem. Commun.*, 2002, 172(b) Z. Chen, W. Xiong and B. Jiang, *Chem. Commun.*, 2002, 2098.
- (a) C. Wei and C.-J. Li, *J. Am. Chem. Soc.*, 2002, **124**, 5638; (b) C. Wei and C.-J. Li, *J. Am. Chem. Soc.*, 2003, **125**, 9584; (c) C. Koradin, K. Polborn and P. Knochel, *Angew. Chem., Int. Ed.*, 2002, **41**, 2535.
- (a) S. J. Pastine, D. V. Gribkov and D. Sames, *J. Am. Chem. Soc.*, 2006, **128**, 14220; (b) X. Chen, C. E. Goodhue and J.-Q. Yu, *J. Am. Chem. Soc.*, 2006, **128**, 12634; (c) H.-Y. Thu, W.-Y. Yu and C.-M. Che, *J. Am. Chem. Soc.*, 2006, **128**, 9048; (d) C.-G. Dong and Q.-S. Hu, *Angew. Chem., Int. Ed.*, 2006, **45**, 2289; (e) L. Shi, Y.-Q. Tu, M. Wang, F.-M. Zhang, C.-A. Fan, Y.-M. Zhao and W.-J. Xia, *J. Am. Chem. Soc.*, 2005, **127**, 10836; (f) B. Deboef, S. J. Pastine and D. Sames, *J. Am. Chem. Soc.*, 2004, **126**, 6556; (g) Z. Li and C.-J. Li, *Org. Lett.*, 2004, **6**, 4997; (h) Z. Li and C.-J. Li, *J. Am. Chem. Soc.*, 2004, **126**, 11810; (i) S.-I. Murahashi, N. Komiya and H. Terai, *Angew. Chem., Int. Ed.*, 2005, **44**, 6931; (j) S. Doye, *Angew. Chem., Int. Ed.*, 2001, **40**, 3351.
- Z. Li and C.-J. Li, *J. Am. Chem. Soc.*, 2005, **127**, 3672. Caution: *tert*-BuOOH is potentially explosive.
- (a) B. M. Trost, *Science*, 1991, **254**, 1471; (b) B. M. Trost, *Acc. Chem. Res.*, 2002, **35**, 695.
- (a) L. Bernardi, B. F. Bonini, E. Capito, G. Dessole, M. Comes-Franchini, M. Fochi and A. Ricci, *J. Org. Chem.*, 2004, **69**, 8168 and references therein; (b) H. Adams, J. C. Anderson, S. Peace and A. M. K. Pennell, *J. Org. Chem.*, 1998, **63**, 9932.
- D. Lucet, T. Le Gall and C. Mioskowski, *Angew. Chem., Int. Ed.*, 1998, **37**, 2580.
- S.-I. Murahashi, N. Komiya, H. Terai and T. Nakae, *J. Am. Chem. Soc.*, 2003, **125**, 15312.
- Z. Li and C.-J. Li, *Eur. J. Org. Chem.*, 2005, 3173.
- D. A. Evans, D. Seidel, M. Rueping, H. W. Lam, J. T. Shaw and C. W. Downey, *J. Am. Chem. Soc.*, 2003, **125**, 12692 For a recent copper (I)-catalyzed Henry reaction: T. Arai, M. Watanabe, N. Fujiwara and A. Yanagisawa, *Angew. Chem., Int. Ed.*, 2006, **45**, 5978.
- F. Y. Kwong, A. Klapars and S. L. Buchwald, *Org. Lett.*, 2002, **4**, 581.

# Synthesis of iron oxide nanoparticles using a freshly-made or recycled imidazolium-based ionic liquid

Yong Wang, Sean Maksimuk, Rui Shen and Hong Yang

Received 2nd January 2007, Accepted 21st May 2007

First published as an Advance Article on the web 8th June 2007

DOI: 10.1039/b618933d

This paper reports the synthesis of iron oxide nanoparticles using a freshly-made or recycled 1-butyl-3-methylimidazolium bis(triflylmethylsulfonyl)imide ([BMIM][Tf<sub>2</sub>N]) ionic liquid (IL). Iron pentacarbonyl (Fe(CO)<sub>5</sub>), which dissolves in [BMIM][Tf<sub>2</sub>N], thermally decomposed and subsequently oxidized to form iron oxide nanoparticles. These nanoparticles separated out automatically from the imidazolium-based ionic liquid mixtures. Multiple additional runs were tested in making iron oxide nanoparticles using recycled ionic liquid. The iron oxide nanoparticles made were characterized with transmission electron microscopy (TEM), high resolution TEM (HR-TEM) and powder X-ray diffraction (PXRD). The structure and thermal stability of the IL was examined using Fourier transform infrared (FT-IR) spectroscopy and thermal gravimetric analysis (TGA). We found that iron oxide nanoparticles with a narrow size distribution could be obtained. The [BMIM][Tf<sub>2</sub>N] ionic liquid showed no degradation based on the TGA and FT-IR study. The solvent-recyclable process of making size-controlled nanoparticles should have a broad impact on the application of imidazolium-based ionic liquids in the synthesis of nanomaterials.

## Introduction

Room temperature ionic liquids (ILs) are salts that exist in liquid form typically at below 100 °C. They can be used as thermally stable and non-volatile solvents, which can be beneficial to the reduction of solvent emission in comparison to conventional volatile organic compounds (VOCs), although the full environmental impact of ILs is still a debatable issue.<sup>1</sup> Several imidazolium-based ionic liquids, including [BMIM][Tf<sub>2</sub>N], are not only non-flammable but also stable in a broad temperature range from room temperature to over 400 °C.<sup>1,2</sup> Recent research results suggest that ionic liquids are quite useful in the synthesis of nanostructured materials because of their unique solvent properties, such as extended hydrogen bonding.<sup>3</sup> They have been used in making several classes of nanostructured materials including mesoporous metal oxides, metal nanoparticles and sheets, microrods, and composition-controlled metal alloys.<sup>4</sup> In some of these examples, the structures and compositions have not been obtained readily in conventional solvents.

Imidazolium-based ionic liquids are immiscible with a number of conventional non-polar organic solvents.<sup>1d,2</sup> Noticeably, both polar solvents, such as water, and non-polar organic media, such as hexane, are poorly soluble in [BMIM][Tf<sub>2</sub>N]. This rather interesting solubility or solvation property has been used to facilitate the post-synthesis separation of metal nanoparticles made from [BMIM][Tf<sub>2</sub>N] IL mixtures.<sup>4c</sup> The observation that high-quality and surfactant capped nanoparticles can be readily separated out from the

[BMIM][Tf<sub>2</sub>N] IL through a settling process without the use of any antisolvent suggests that it may be feasible to develop a solvent-recyclable process of making nanoparticles using imidazolium-based ionic liquids. In comparison with some other synthetic methods of nanoparticles in ILs, this newly developed approach can produce monodisperse nanoparticles, which also have an excellent dispersity in a number of conventional molecular solvents because of the surfactant capping groups. Such a process should have broad ramifications in applying ionic liquids in material processing.

Iron oxide particles are an important class of magnetic materials.<sup>5</sup> They have been widely used in ferrofluids for sealing and precision polishing, dampers and shock absorbers.<sup>6</sup> It has been demonstrated that iron oxide nanoparticles are the essential components in the design of recyclable catalytic systems.<sup>7</sup> Iron oxide nanoparticles have also been used in different biological applications, which include detection of interactions between single molecules in living systems, imaging and separation of proteins and DNAs.<sup>6,8</sup> As size and size distribution are important in determining the property of magnetic nanoparticles, new opportunities can be expected with the availability of high quality magnetic nanoparticles. In the past several years, various progresses have been made in making monodisperse iron oxide nanoparticles through the non-hydrolytic solution phase reaction.<sup>6,9</sup> Development of a solvent-recyclable method further increases the possibility for a broader application of these ionic liquids.

This paper presents the first synthesis of iron oxide nanoparticles in a [BMIM][Tf<sub>2</sub>N] ionic liquid. We show that this ionic liquid can be recycled and reused without detrimental effects on size and size distribution of the particles made.

Department of Chemical Engineering, University of Rochester, Gavett Hall 206, Rochester, NY, 14627, USA.  
E-mail: hongyang@che.rochester.edu; Fax: +1 585 273 1348;  
Tel: +1 585 275 2110



## Experimental

### Chemicals

Iron pentacarbonyl (99.999%), oleic acid (99.99%), oleylamine (70%, tech. grade), 1,2-hexadecanediol (90%, tech. grade), hexane (anhydrous, 95+%), and lithium bistrifluoromethanesulfonimide ( $\geq 99.95\%$ ) were purchased from Aldrich. Acetone (HPLC grade), 1-chlorobutane (99.5+%), and 1-methylimidazole (99%) were provided by Alfa Aesar. All reagents were used as received without further purifications. [BMIM][Tf<sub>2</sub>N] was made in-house as reported elsewhere.<sup>4g</sup> Its structure was confirmed by proton NMR. The water content in freshly made [BMIM][Tf<sub>2</sub>N] was less than 0.03%, determined by the Karl Fisher coulometry method. The chlorine content was not detectable ( $<0.3\%$  by weight) using potentiometric titration with silver nitrate.

### Synthesis of iron oxide nanoparticles in freshly-made IL

In a typical synthesis of iron oxide nanoparticles, freshly dried and colorless [BMIM][Tf<sub>2</sub>N] (5 mL) was mixed with iron pentacarbonyl (Fe(CO)<sub>5</sub>, 33  $\mu$ L or 0.25 mmol) in a 25 mL three-neck flask at room temperature. The bright yellowish reaction mixture was stirred vigorously using a magnetic stirrer. This mixture was heated at 2 °C min<sup>-1</sup> with a heating mantle controlled by a J-KEM 210 temperature controller in an argon atmosphere. The reaction mixture gradually turned brown, and then black at 150–160 °C. Oleic acid (120  $\mu$ L or 0.38 mmol) was injected into the vessel at 165 °C using a micro-syringe. Black products deposited on the wall of the flask quickly after the injection of oleic acid. This mixture was heated to 280 °C and kept at this temperature for another 1 h before the reaction was terminated. A transparent light yellowish liquid could be readily separated out from the black solid on the wall by decantation. The solid product was collected by washing with 4 mL of hexane that contained 40  $\mu$ L of oleic acid. A suspension of the product in hexane (0.2 mL) was further diluted with 0.3 mL of hexane and then mixed with 1.5 mL of ethanol, followed by centrifuging at 5000 rpm for 7 min. The black precipitant was collected and re-dispersed in hexane.

The effect of secondary capping agents on the particle size was examined using a reaction mixture of 33  $\mu$ L (0.25 mmol) of Fe(CO)<sub>5</sub>, 64  $\mu$ L (0.20 mmol) of oleic acid, 13  $\mu$ L (0.03 mmol) of oleylamine, and 98 mg (0.34 mmol) of 1,2-hexadecanediol in 5 mL of [BMIM][Tf<sub>2</sub>N]. In a typical procedure, freshly dried [BMIM][Tf<sub>2</sub>N] (5 mL) was mixed with oleic acid, oleylamine and 1,2-hexadecanediol in a flask. This mixture was heated with a heating mantle under the protection of argon and stirred vigorously by a magnetic stirrer. The mixture turned into a colorless transparent solution at 75 °C after 1,2-hexadecanediol dissolved. Iron pentacarbonyl (33  $\mu$ L or 0.25 mmol) was then added into the flask at 110 °C using a micro-syringe. The reaction was conducted using the same heating profile described previously, so was the procedure for recovering the nanoparticles.

### Synthesis of iron oxide nanoparticles in recycled IL

The IL collected after each synthesis was distributed into five 2 mL centrifuge tubes and then mixed with equal volume of

hexane, respectively. These mixtures were agitated by a vortex mixer (VWR) for several minutes before they were centrifuged at 11 000 rpm for ten minutes. After centrifuging, the IL and hexane separated into two layers, the top hexane layer was replaced by equal amount of new hexane. The above procedures were repeated for two additional cycles. The resultant IL was treated under vacuum to remove hexane. In general, at least 90% (v/v) of the original ionic liquid used in the reaction could be recovered using this procedure. The loss of IL was mainly due to the transfer of ILs between containers. In the following round of synthesis, 100% recycled IL was used to synthesize nanoparticles while keeping all chemical concentrations constant. Synthesis of nanoparticles in 60% (v/v) recycled IL was also tested using the similar procedures.

### Characterization

Specimens of nanoparticles were prepared using their corresponding suspensions in hexane. The transmission electron microscopy (TEM) images and electron diffraction (ED) patterns were recorded on a JEOL JEM 2000EX microscope at an accelerating voltage of 200 kV. High resolution TEM (HR-TEM) images were recorded on a FEI Tecnai G20 transmission electron microscope operating at 200 kV. Powder X-ray diffraction (PXRD) patterns were recorded on a Philips MPD diffractometer with a Cu K $\alpha$  X-ray source ( $\lambda = 1.54056$  Å). The PXRD patterns were fit using the Xfit software program. The FT-IR spectra were collected on a Shimadzu FTIR 8400S spectrometer. The thermal gravimetric analysis (TGA) was conducted on a Q600 SDT DSC-TGA system from TA Instrument. The magnetic properties of iron oxide nanoparticles were determined using a Quantum Design AC and DC Superconducting Quantum Interference Device (AC/DC SQUID; Model MPMS XL) magnetometer with a field scan range between  $\pm 55$  kOe. FT-IR spectra in the range of 500–4000 cm<sup>-1</sup> were collected on a Shimadzu FTIR-8400S spectrophotometer. Thirty-two scans at an effective resolution of 2 cm<sup>-1</sup> were measured for each sample. The particle size analysis was done by measuring about 200 particles on each specimen using the ImageJ.

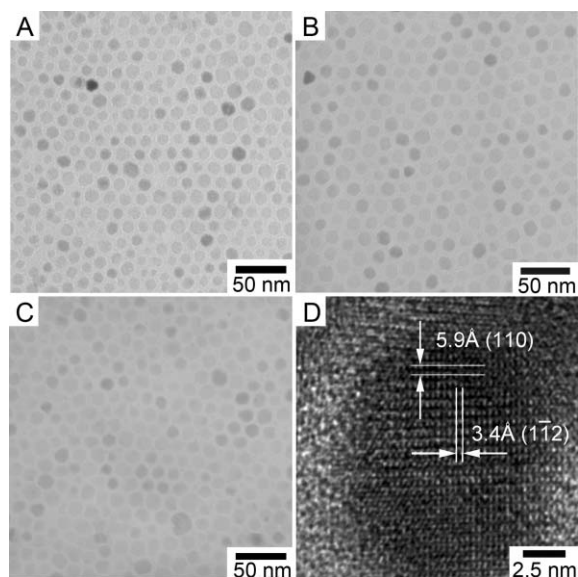
## Results and discussion

Iron pentacarbonyl was used as the precursor because of its good solubility in imidazolium-based ionic liquids.<sup>10,11</sup> In this synthetic procedure, oleic acid was in excess and saturated in [BMIM][Tf<sub>2</sub>N]. Under such reaction conditions, the concentration of oleic acid in the IL remained constant during the reaction. After [BMIM][Tf<sub>2</sub>N] IL was mixed with Fe(CO)<sub>5</sub> in a flask, a transparent bright-yellow solution formed. With the increase of temperature, the reaction mixture gradually turned brown and eventually black at 160 °C. This observation indicated the decomposition of Fe(CO)<sub>5</sub> to intermediate products that were stable in [BMIM][Tf<sub>2</sub>N]. Upon adding oleic acid at 165 °C, a black solid formed immediately and settled out from the reaction mixture, a sign typically indicating the formation of nanoparticles. After the temperature of the mixture reached at 280 °C, the reaction was allowed to continue for about an hour. We observed that the nanoparticles could separate out from [BMIM][Tf<sub>2</sub>N] ILs



automatically through a settling process after the reaction was completed, similar to the case for surfactant-capped metal particles,<sup>4e</sup> and the ILs could be readily recovered by decantation. The formed nanoparticles were typically deposited on the wall of reaction flask and could be collected using various common solvents, such as hexane.

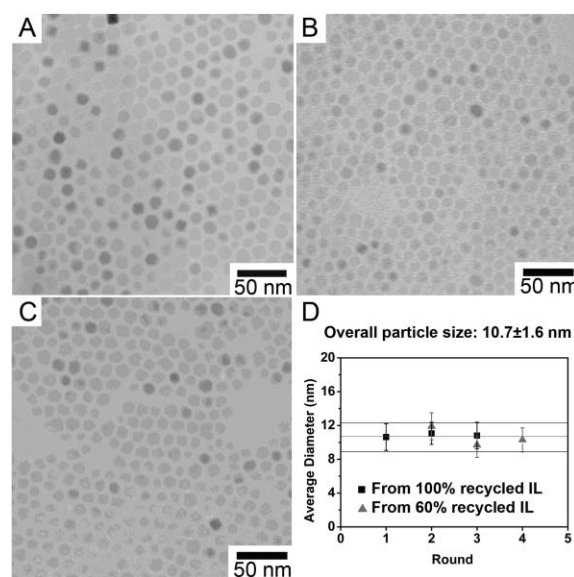
Fig. 1 shows representative TEM images of the nanoparticles obtained from three consecutive syntheses at  $\text{Fe}(\text{CO})_5$  concentration of 0.05 M and  $\text{Fe}(\text{CO})_5$ /oleic acid molar ratio of 0.66. The hexagonal array of nanoparticles could be readily observed, indicating a narrow size distribution and excellent solvent dispersity of these nanoparticles. The ease of such particles in dispersing in an organic solvent was most likely due to oleic acid capping agents, which made the surface of these iron oxide nanoparticles hydrophobic and protected them from aggregating in non-polar organic solvents. Thus, surfactant played an important role in this separation process, which differed from those methods without the use of capping agents. In the latter case, the particles tend not to disperse well in conventional solvents. For those nanoparticles obtained using freshly-prepared  $[\text{BMIM}][\text{Tf}_2\text{N}]$  ionic liquid as solvent, the average diameter was  $10.6 \pm 1.6$  nm. Fig. 1B and 1C show TEM images of the nanoparticles made using IL recovered from the second and third rounds of syntheses, respectively. The particle size analysis shows the average diameters of the nanoparticles were  $11.1 \pm 1.3$  and  $10.8 \pm 1.6$  nm, respectively. The observed size and size distribution could be considered the same, within the error of measurement, to those made by using freshly made  $[\text{BMIM}][\text{Tf}_2\text{N}]$ . Fig. 1D shows a HR-TEM image of a representative nanoparticle. The particle was highly crystalline, even though it had a sphere-like shape. The two sets of lattice fringes were normal to each other and with the distances of 3.4 Å and 5.9 Å, respectively. They could be indexed to (1-12) and (110) planes of maghemite ( $\gamma\text{-Fe}_2\text{O}_3$ ).



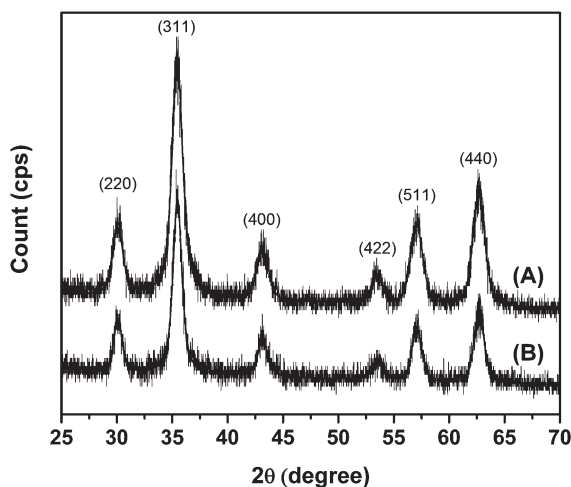
**Fig. 1** TEM images of the nanoparticles obtained using (A) freshly-made, (B) first and (C) second recycled  $[\text{BMIM}][\text{Tf}_2\text{N}]$  ionic liquids, and (D) HR-TEM image of a maghemite nanoparticle showing the lattice fringes.

To systematically examine both the nanoparticles and the ILs recovered from the corresponding reaction mixtures, we also made the particles using ionic liquids at 60% (v/v) recycling ratio, and kept the remaining ionic liquids for characterization. Fig. 2 shows the TEM images of particles made in three consecutive runs using such partially-recycled ionic liquids. The overall average diameter of the particles obtained was  $10.6 \pm 1.7$  nm for these three runs. The average diameters of the nanoparticles ranged between 9.7 and 11.9 nm with an average size distribution within 15% in all these samples. Particles that were made in the first round of recycled IL shown in Fig. 2A had a slightly larger average diameter than those obtained from the other rounds, but well within the experimentally controllable size range. The high level of control over the size and size distribution could arise from the observations that oleic acid remained oversaturated in the IL mixtures throughout the reaction and the particle could settle out from the solution phase once they reached a certain size governed by the reaction conditions and reactant ratios.

Fig. 3 shows the PXRD patterns of the iron oxide nanoparticles obtained using the freshly-made and 60% (v/v) recycled ILs. The two sets of X-ray diffraction patterns were identical in the entire measurement range. The formation of maghemite from iron carbonyl happened most likely through air oxidation similar to those reported by Cheon and co-workers.<sup>8k</sup> Iron diffusion from the core to the surface of the nanoparticles was thought to be involved in the oxidation process.<sup>12,13</sup> As the freshly-made  $[\text{BMIM}][\text{Tf}_2\text{N}]$  IL was heated to 110 °C under vacuum prior to the reaction and water content in such IL was less than 0.03% determined by the Karl Fisher coulometry method, the potential effect of moisture on the composition of iron oxide should be limited. Uniform spherical nanoparticles could still be made from  $\text{Fe}(\text{CO})_5$  in  $[\text{BMIM}][\text{Tf}_2\text{N}]$  IL under ambient air condition; while poly-dispersed nanoparticles formed in this IL over-saturated with



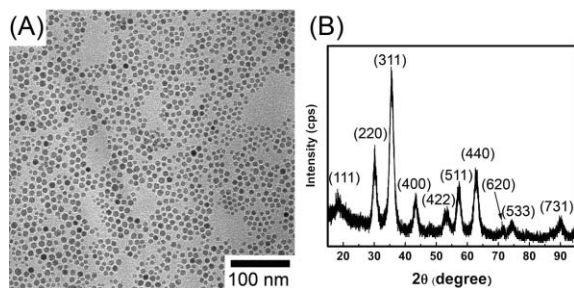
**Fig. 2** TEM images of the iron oxide nanoparticles obtained from 60% (v/v) recycled ILs after (A) first, (B) second and (C) third uses, respectively. (D) The average sizes and size distributions.



**Fig. 3** PXRD patterns of maghemite nanoparticles made using (A) freshly-made and (B) 60% (v/v) recycled [BMIM][Tf<sub>2</sub>N] ionic liquids, respectively.

water. Thus, the major sources for the oxidation of mono-disperse iron oxide nanoparticles could be air or the trace amount of oxygen in argon. The use of oleic acid did not seem to prevent the oxidation.

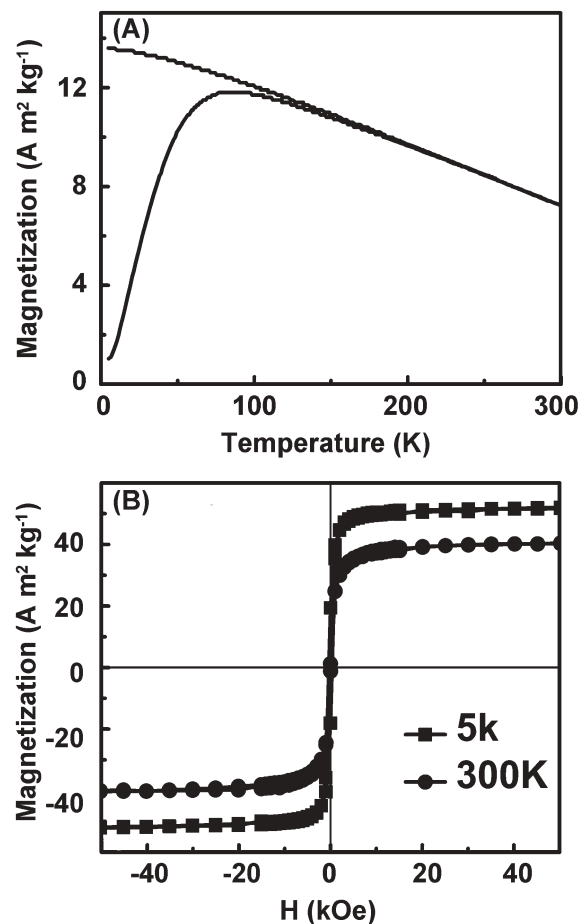
The formed nanoparticles had a fixed average diameter for a reaction mixture under a given condition. The main reason for this size focusing could be due to the settling process of the particles from IL mixtures. We therefore examined if other sizes of iron oxide nanoparticles could be obtained by changing the reactants of the mixtures, since the most stable size of the nanoparticles should be controllable by using different capping agents. Oleylamine and 1,2-hexadecandiol, the two other common additives, were used for this purpose. The reaction was conducted using a modified procedure, where the capping reagents were first mixed with the IL at room temperature and then 0.25 mmol of Fe(CO)<sub>5</sub> was added at 110 °C in 5-mL IL at a Fe(CO)<sub>5</sub> : hexadecandiol : oleic acid : oleylamine molar ratio of 2 : 2.7 : 1.6 : 0.2. Relatively uniform nanoparticles could be generated readily, as indicated in the TEM image shown in Fig. 4A. These particles could also be oxidized into maghemite, judging by the PXRD pattern, Fig. 4B. The nanoparticles had a similar shape as those obtained with only oleic acid used, but with an average diameter of  $8 \pm 1$  nm.



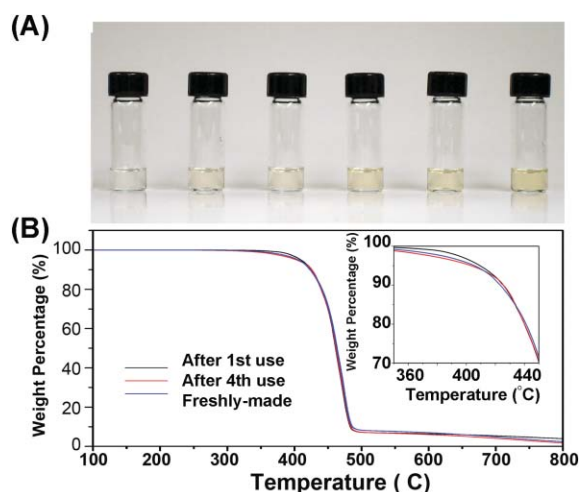
**Fig. 4** (A) TEM image and (B) PXRD pattern of 8 nm iron oxide nanoparticles made in the presence of 1,2-hexadecandiol, oleic acid and oleylamine.

The magnetic properties of the 8 nm nanoparticles were examined using a SQUID magnetometer with a measurement field range between  $\pm 55$  kOe. Fig. 5 shows the field cool/zero field cool (FC/ZFC) magnetization *versus* applied field curves, and the hysteresis loops of these nanoparticles at two different temperatures. They exhibited the typical superparamagnetic behavior with a blocking temperature,  $T_B$  of 88 K. Based on the equation  $K_u = 25k_B T_B / V$ , where  $V$  is the volume of a single particle and  $k_B$  is the Boltzmann constant ( $1.38 \times 10^{-23} \text{ m}^2 \text{ kg s}^{-2} \text{ K}^{-1}$  or  $1.38 \times 10^{-16} \text{ erg K}^{-1}$ ), we obtained the crystalline magnetoanisotropy constant,  $K_u$ , to be  $1.4 \times 10^4 \text{ kg s}^{-2} \text{ m}^{-1}$  or  $1.4 \times 10^5 \text{ erg cm}^{-3}$ . The  $K_u$  for bulk and nanoparticles  $\gamma\text{-Fe}_2\text{O}_3$  were reported to be  $4.7 \times 10^4 \text{ erg cm}^{-3}$  and  $3.0 \times 10^5 \text{ erg cm}^{-3}$ , respectively.<sup>14,15</sup> The coercivity of these nanoparticles was 360 Oe at 5 K, Fig. 5B. The saturated magnetization,  $M_s$ , was found to be  $\sim 50 \text{ emu g}^{-1}$  at 5 K. These values were within the range typically observed for spherical  $\gamma\text{-Fe}_2\text{O}_3$  nanoparticles of this size.

The chemical and physical properties of freshly-made [BMIM][Tf<sub>2</sub>N] and the IL mixtures after the reactions were examined using colorimetric photography, TGA and FT-IR spectroscopy. A gradual but slight coloration of IL was observed after the repeating cycles of synthesis, Fig. 6A. The



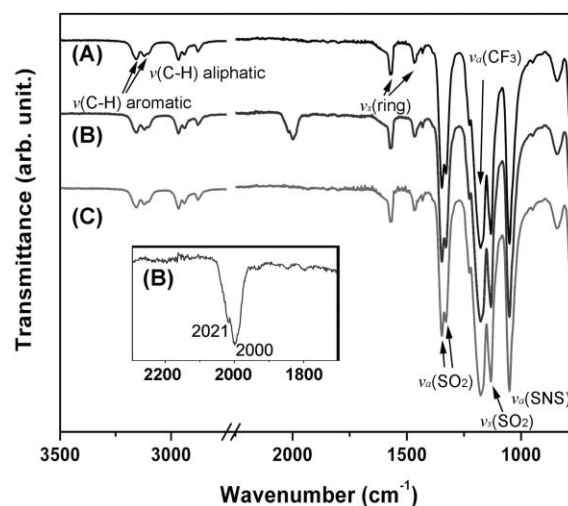
**Fig. 5** (A) The FC/ZFC curve and (B) magnetic hysteresis loops of 8 nm iron oxide particles measured using a SQUID magnetometer (model: MPMS XL). The applied external field was 100 Oe for the field-cooled measurement.



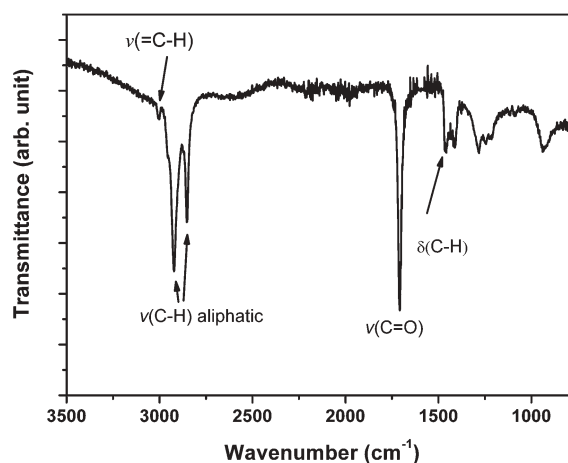
**Fig. 6** (A) Photograph and (B) TGA traces of freshly-made and the recycled [BMIM][Tf<sub>2</sub>N] ILs. The vials from the left to right shown in Panel A were the freshly-made IL and those after first, second, third, fourth and fifth usages at 60% (v/v) recycling ratio, respectively. Inset of Fig. 6B is the enlarged TGA data between 350 and 450 °C.

colorless ionic liquid became slightly yellow after subsequent cycles of reaction. The coloration was generally attributed to the existence of even trace amount of impurities.<sup>1a</sup> The thermal property of the recycled ionic liquids was examined using TGA, as the onset temperature of thermal decomposition of ILs was a good indicator of their thermal stability, Fig. 6B. The onset for pure [BMIM][Tf<sub>2</sub>N] was measured to be 439 °C, similar to those reported in the literature. There was no obvious change in the TGA curve after the first or fourth use of this IL. The onset temperature for decomposition of the IL remained the same as the freshly made one, inset of Fig. 6B. The coloration apparently did not affect of the thermal stability of this ionic liquid, nor did it cause the changes in size and size distribution of the nanoparticles.

FT-IR spectroscopy was used to examine the interactions between different species and changes in chemical compositions of the mixtures. Fig. 7 shows the FT-IR spectra for freshly-made [BMIM][Tf<sub>2</sub>N] IL, Fe(CO)<sub>5</sub>/IL mixture, and the recycled IL after being used in the third cycle. The concentration of Fe(CO)<sub>5</sub> used was the same as those for the synthesis of 11 nm particles. Besides the different stretch modes from the various segments of [BMIM][Tf<sub>2</sub>N], the symmetric and asymmetric stretching modes for the carbonyls could be observed at 2000 and 2021 cm<sup>-1</sup>, respectively, for the mixture of Fe(CO)<sub>5</sub> and [BMIM][Tf<sub>2</sub>N] IL.<sup>11,16</sup> They shifted slightly in comparison to those in toluene, which were centered at 1999 and 2017 cm<sup>-1</sup>. Such shifts have been attributed to the interaction between [BMIM]<sup>+</sup> cation and the carbonyl groups of Fe(CO)<sub>5</sub>. This interaction might facilitate the dissolution of Fe(CO)<sub>5</sub> in [BMIM][Tf<sub>2</sub>N] IL. The IR spectra of the IL mixture after the reactions show an almost identical pattern with that of pure [BMIM][Tf<sub>2</sub>N]. Oleic acid did not cause noticeable changes in the FT-IR spectrum of IL after the reaction, suggesting the limited solubility of oleic acid in this ionic liquid. The relatively good miscibility of Fe(CO)<sub>5</sub> and low solubility of oleic acid in [BMIM][Tf<sub>2</sub>N] could contribute



**Fig. 7** FT-IR spectra of (A) freshly-made [BMIM][Tf<sub>2</sub>N] IL, (B) the mixture of IL and Fe(CO)<sub>5</sub>, and (C) the [BMIM][Tf<sub>2</sub>N] IL recovered from the third usage.



**Fig. 8** FT-IR spectrum of the iron oxide nanoparticles.

to the settling process, as iron oxide nanoparticles were stabilized by oleic acid. The oleic acid capped nanoparticles could not disperse well in the [BMIM][Tf<sub>2</sub>N] IL mixture partially due to the low solubility of oleic acid. Thus, upon the completion of reaction the ionic liquid contained only a small amount of saturated oleic acid. FT-IR spectrum was also used to study the surface chemistry of the resultant iron oxide nanoparticles, Fig. 8. The characteristic bands of the imidazole ring and bistrifluoro-methanesulfonimide ion were not observed, suggesting that the particles obtained from this process should be free from IL.<sup>17,18</sup> The observed strong bands from aliphatic chain and C=O on carboxylic group indicates the presence of oleic acid on the surface of these iron oxide nanoparticles.<sup>16</sup>

## Conclusions

In summary, uniform maghemite nanoparticles can be synthesized in a freshly-made or recycled [BMIM][Tf<sub>2</sub>N] ionic liquid. The nanoparticles obtained exhibited well-controllable size and size distribution. The recycling procedure is simple



and the recycled IL keeps its excellent thermal stability. The feasibility of using both freshly-made and recycled ionic liquids as solvents in making high quality nanoparticles may pave the way for the development of ionic liquid-based technology for particle processing.

## Acknowledgements

This work was supported in part by National Science Foundation (CTS-041722 and DMR-0449849) and Environmental Protection Agency (R831722). This work made use of the MSERC Shared Experimental Facilities at MIT Center for Materials Science and Engineering and at Cornell Centre for Materials Research supported by NSF. We are grateful for Dr Fangcheng Chou and Mr Patrick Boisvert of MIT for the SQUID measurements, and Mr John Grazul of Cornell University for the assistance in running the HR-TEM. We thank Dr Xiaowei Teng, Mr Brian McIntyre and Mr Dalton Labarg for help.

## References

- (a) P. Wasserscheid and T. Welton, *Ionic Liquids in Synthesis*, Wiley-VCH, Weinheim, 1st edn, 2003; (b) K. R. Seddon, *J. Chem. Technol. Biotechnol.*, 1997, **68**, 351–356; (c) J. Dupont, R. F. de Souza and P. A. Z. Suarez, *Chem. Rev.*, 2002, **102**, 3667–3691; (d) J. G. Huddleston, A. E. Visser, W. M. Reichert, H. D. Willauer, G. A. Broker and R. D. Rogers, *Green Chem.*, 2001, **3**, 156–164; (e) G. A. Baker, S. N. Baker, S. Pandey and F. V. Bright, *Analyst*, 2005, **130**, 800–808.
- (a) P. Bonhôte, A. P. Dias, N. Papageorgiou, K. Kalyanasundaram and M. Gratzel, *Inorg. Chem.*, 1996, **35**, 1168–1178; (b) C. P. Fredlake, J. M. Crosthwaite, D. G. Hert, S. Aki and J. F. Brennecke, *J. Chem. Eng. Data*, 2004, **49**, 954–964.
- M. Antonietti, D. B. Kuang, B. Smarsly and Z. Yong, *Angew. Chem., Int. Ed.*, 2004, **43**, 4988–4992.
- (a) A. Taubert, *Angew. Chem., Int. Ed.*, 2004, **43**, 5380–5382; (b) Y. Zhou and M. Antonietti, *J. Am. Chem. Soc.*, 2003, **125**, 14960–14961; (c) Y. J. Zhu, W. W. Wang, R. J. Qi and X. L. Hu, *Angew. Chem., Int. Ed.*, 2004, **43**, 1410–1414; (d) Z. H. Li, Z. M. Liu, J. L. Zhang, B. X. Han, J. M. Du, Y. N. Gao and T. Jiang, *J. Phys. Chem. B*, 2005, **109**, 14445–14448; (e) Y. Wang and H. Yang, *Chem. Commun.*, 2006, 2545–2547; (f) Z. G. Li, H. L. Zhang, J. M. Du, B. X. Han and J. Q. Wang, *Colloid Surf., A*, 2006, **286**, 117–120; (g) Y. Wang and H. Yang, *J. Am. Chem. Soc.*, 2005, **127**, 5316–5317; (h) D. B. Zhao, Z. F. Fe, W. H. Ang and P. J. Dyson, *Small*, 2006, **2**, 879–883.
- (a) R. M. Cornell and U. Schwertmann, *The Iron Oxides: Structure, Properties, Reactions, Occurrences and Uses*, Wiley-VCH, Weinheim, 2nd edn, 2003; (b) C. H. Griffiths, M. P. Ohoro and T. W. Smith, *J. Appl. Phys.*, 1979, **50**, 7108–7115; (c) D. L. Huber, *Small*, 2005, **1**, 482–501.
- U. Jeong, X. W. Teng, Y. Wang, H. Yang and Y. N. Xia, *Adv. Mater.*, 2007, **19**, 33–60.
- (a) D. K. Yi, S. S. Lee and J. Y. Ying, *Chem. Mater.*, 2006, **18**, 2459–2461; (b) M. Kotani, T. Koike, K. Yamaguchi and N. Mizuno, *Green Chem.*, 2006, **8**, 735–741.
- (a) H. W. Gu, K. M. Xu, C. J. Xu and B. Xu, *Chem. Commun.*, 2006, 941–949; (b) J. Xie, S. Peng, N. Brower, N. Pourmand, S. X. Wang and S. H. Sun, *Pure Appl. Chem.*, 2006, **78**, 1003–1014; (c) I. Safarik and M. Safarikova, *Monatsh. Chem.*, 2002, **133**, 737–759; (d) U. Hafeli, W. Schutt, J. Teller and M. Zborowski, *Scientific and Clinical Applications of Magnetic Carriers*, Plenum Press, New York, 1998; (e) X. Q. Liu, Y. P. Guan, Y. Yang, Z. Y. Ma, X. B. Wu and H. Z. Liu, *J. Appl. Polym. Sci.*, 2004, **94**, 2205–2211; (f) F. R. Cunha and Y. D. Sobral, *Physica A*, 2004, **343**, 36–64; (g) I. Hilger, A. Kiessling, E. Romanus, R. Hiergeist, H. T. Rudolf, W. Andra, M. Roskos, W. Linss, P. Weber, W. Weitschies and W. A. Kaiser, *Nanotechnology*, 2004, **15**, 1027–1032; (h) S. Huth, J. Lausier, S. W. Gersting, C. Rudolph, C. Plank, U. Welsch and J. Rosenecker, *J. Gene Med.*, 2004, **6**, 923–936; (i) X. Xie, X. Zhang, H. Zhang, D. P. Chen and W. Y. Fei, *J. Magn. Magn. Mater.*, 2004, **277**, 16–23; (j) J. Won, M. Kim, Y. W. Yi, Y. H. Kim, N. Jung and T. K. Kim, *Science*, 2005, **309**, 121–125; (k) Y. W. Jun, Y. M. Huh, J. S. Choi, J. H. Lee, H. T. Song, S. Kim, S. Yoon, K. S. Kim, J. S. Shin and J. S. Suh and J. Cheon, *J. Am. Chem. Soc.*, 2005, **127**, 5732–5733.
- (a) S. H. Sun and H. Zeng, *J. Am. Chem. Soc.*, 2002, **124**, 8204–8205; (b) Y. N. Xia, P. D. Yang, Y. G. Sun, Y. Y. Wu, B. Mayers, B. Gates, Y. D. Yin, F. Kim and Y. Q. Yan, *Adv. Mater.*, 2003, **15**, 353–389; (c) T. Hyeon, S. S. Lee, J. Park, Y. Chung and H. Bin Na, *J. Am. Chem. Soc.*, 2001, **123**, 12798–12801; (d) J. Park, E. Lee, N. M. Hwang, M. S. Kang, S. C. Kim, Y. Hwang, J. G. Park, H. J. Noh, J. Y. Kini, J. H. Park and T. Hyeon, *Angew. Chem., Int. Ed.*, 2005, **44**, 2872–2877; (e) D. Farrell, Y. Cheng, R. W. McCallum, M. Sachan and S. A. Majetich, *J. Phys. Chem. B*, 2005, **109**, 13409–13419; (f) F. X. Redl, C. T. Black, G. C. Papaefthymiou, R. L. Sandstrom, M. Yin, H. Zeng, C. B. Murray and S. P. O'Brien, *J. Am. Chem. Soc.*, 2004, **126**, 14583–14599; (g) J. Rockenberger, E. C. Scher and A. P. Alivisatos, *J. Am. Chem. Soc.*, 1999, **121**, 11595–11596; (h) Y. Li, M. Afzaal and P. O'Brien, *J. Mater. Chem.*, 2006, **16**, 2175–2180; (i) N. R. Jana, Y. F. Chen and X. G. Peng, *Chem. Mater.*, 2004, **16**, 3931–3935; (j) X. W. Teng and H. Yang, *J. Mater. Chem.*, 2004, **14**, 774–779.
- D. S. Jacob, V. Kahlenberg, K. Wurst, L. A. Solovoyov, I. Felner, L. Shimon, H. E. Gottlieb and A. Gedanken, *Eur. J. Inorg. Chem.*, 2005, 522–528.
- G. H. Tao, M. Zou, X. H. Wang, Z. Y. Chen, D. G. Evans and Y. Kou, *Aust. J. Chem.*, 2005, **58**, 327–331.
- J. Tang, M. Myers, K. A. Bosnick and L. E. Brus, *J. Phys. Chem. B*, 2003, **107**, 7501–7506.
- P. S. Sidhu, R. J. Gilkes and A. M. Posner, *J. Inorg. Nucl. Chem.*, 1977, **39**, 1953–1958.
- O. Jarjayes, P. H. Fries and G. Bidan, *J. Magn. Magn. Mater.*, 1994, **137**, 205–218.
- G. Bate, *Magnetic Oxide*, Wiley-VCH, London, 1975.
- The Aldrich Library of FT-IR Spectra*, Sigma-Aldrich Co., Milwaukee, 2nd edn, 1997.
- J. F. Huang, G. A. Baker, H. M. Luo, K. L. Hong, Q. F. Li, N. J. Bjerrum and S. Dai, *Green Chem.*, 2006, **8**, 599–602.
- S. Tait and R. A. Osteryoung, *Inorg. Chem.*, 1984, **23**, 4352–4360.



# Surface modification of lignocellulosic fibres in atmospheric air pressure plasma

Alexis Baltazar-Y-Jimenez and Alexander Bismarck\*

Received 18th December 2006, Accepted 18th June 2007

First published as an Advance Article on the web 9th July 2007

DOI: 10.1039/b618398k

New applications of lignocellulosic fibres have been driven by numerous factors, including pressure from environmental groups, stringent environmental laws, waste minimisation efforts, recycling and cost reduction initiatives and responsible social awareness. However, the exploitation of such fibres in, for instance, fibre-reinforced composites or in the textile industry is hindered by the presence of waxy layers on the surfaces of lignocellulosic fibres. Many surface treatments are traditionally used to optimise the surface properties of natural fibres. A potential and environmentally sound surface treatment regards the use of atmospheric air pressure plasma (AAPP). The surfaces of various lignocellulosic fibres were modified using AAPP. We investigated the effect of AAPP treatment duration (*i.e.* 1 min and 3 min) on the surface properties of the lignocellulosic fibres using wetting and electrokinetic measurements. The critical surface tension of the untreated and AAPP-treated fibres was determined from wetting measurements using the capillary rise technique, whereas the changes in the surface chemistry were characterised by means of zeta ( $\zeta$ )-potential measurements. A slight increase in the critical surface tension of the lignocellulosic fibres was found with prolonged treatment time, with the exception of abaca fibres. The post-treated fibres show a larger degree of hydrophilicity measured from the difference,  $\Delta\zeta$ , in the decay of the  $\zeta$ -potential measured as function of time, with the exception of hemp fibres. Finally,  $\zeta$ -potential measurements as function of pH validated the performance of both AAPP treatments.

## 1.0 Introduction

Lignocellulosic fibres, such as abaca, flax, hemp and sisal are agro-based resources that offer several advantages over their synthetic counterparts, especially with respect to their low cost, low density, high strength-to-weight-ratio, renewability and recyclability. New applications for these kinds of fibres have been driven by increasingly more stringent environmental laws, such as the European Directives 2000/53/EC on the disposal of end-of-life vehicles and 1999/31/EC on the landfill of waste, which aim to serve the environment by enforcing waste minimisation and increased levels of recycling and recovery. Despite the apparent advantages of lignocellulosic fibres, their high water absorption causes the fibres to swell and their low microbial resistance affects the fibre's properties and the performance of the composites reinforced with them. Moreover, their biggest drawback is their inherent variability of their dimensions and mechanical properties.<sup>1</sup>

At a microscopic level, lignocellulosic fibres themselves are composites which are primarily composed of highly crystalline cellulose fibrils, providing stiffness and strength, which are surrounded by a complex matrix composed of amorphous hemicelluloses, holocelluloses and lignin, with minor amounts of free sugars, starch, proteins, other organic and inorganic

mineral salts.<sup>2</sup> The chemical composition of the lignocellulosic fibres varies from plant to plant, and even within different parts of the same plant. Moreover, the time of harvest, as well as the method used to extract (retting) and separate the fibres affects the chemical composition, strength, fineness and colour of the lignocellulosic fibres.<sup>3</sup> The different retting methods are discussed elsewhere.<sup>4</sup>

Low-pressure plasma treatments have been reported in the past as a cost effective surface modification methods to chemically modify or clean the surface of a wide range of materials, including natural fibres.<sup>5</sup> Atmospheric air pressure plasma (AAPP) is a promising surface modification method to reduce, as far as possible, the negative effects on the environment of other commonly used methods, such as caustic treatment (NaOH), acetylation, silanisation, polymer grafting, *etc.* Plasma treatment techniques remove the need of exposing lignocellulosic fibres to solvents and solutions that otherwise need to be disposed of after treatment.

It is usually accepted that during any plasma treatment at least two combined effects take place: an etching process that sputters the surface and removes weakly attached layers, such as oils and waxes adhering to the material being treated, and the formation of new functional groups<sup>6</sup>. The nature of these functional groups created depends on the feed gas used to produce the plasma.

Of particular interest is the possibility of improving the wetting behaviour and the adhesive properties of lignocellulosic fibres using AAPP treatments to remove non-cellulose substances attached to the surfaces of the plant cell walls. We characterised the effectiveness of AAPP treatment

Department of Chemical Engineering, Polymer & Composite Engineering (PaCE) Group, Imperial College London, South Kensington Campus, London, UK SW7 2AZ.  
E-mail: a.bismarck@imperial.ac.uk; Fax: +44 (0) 20 7594 5638;  
Tel: +44 (0) 20 7594 557

on different lignocellulosic fibres by means of the capillary rise and the streaming potential measurements.

## 2.0 Experimental

### 2.1. Materials

A variety of commercially important lignocellulosic fibres including abaca, flax, hemp and sisal were selected in order to compare the effects of AAPP treatment duration (*i.e.* 1 min and 3 min) on the wettability and electrokinetic properties. Only technical grade fibre bundles were analysed. Abaca (*Musa textilis* Nee) fibres were kindly supplied by Heritage Arts & Crafts (Kalibo, Aklan, the Philippines) obtained from local growers of the Aklan province. The fibres were extracted and separated from the woody core of the plant by hand pulling, washed and sun-dried for one day (Legaspi, 2005, 2006, Heritage Arts & Crafts, personal communication). Dew-retted flax (*Linum usitatissimum*) fibres were obtained from Belgian producers and supplied by Wigglesworth & Co. (London, UK) and dew-retted sisal (*Agave sisalana*) fibres were obtained from a local market in San Luis Potosí, Mexico. During dew retting the fibres are partially rotten, softened and separated by leaving the crop in the field for 3 to 4 weeks in order to allow the combined action of temperature, moisture, bacteria and fungi to remove the cellulose fibres from the surrounding cementing substances, mainly hemicelluloses, lignin and pectins.<sup>7</sup> In the case of flax, the fibres were separated from the stalk by a breaking, scutching and hackling process (Paula Brazier, 2004, Wigglesworth & Co, personal communication). Sisal fibres were separated from the leaves of the crop by placing them individually in a rudimentary tool made of wood where the fibres were pulled out by hand, washed and sun-dried for one day.

Decorticated hemp (*Cannabis sativa*) fibres were kindly provided by Hemcore Ltd (Bishops Stortford, Hertfordshire, UK) from plants harvested near Colchester in the UK (Hobson, 2004, Hemcore Ltd, personal communication). During the decortication process, the wooden stems of hemp have to be disaggregated in order to loosen the adhesion between the fibres and the woody stalk. This is performed by using automated paired breaking rollers and carding systems (Hobson, 2006, Hemcore Ltd, personal communication). The fibres extracted using this method were predominantly short fibres of approximately 1 cm in length mixed with some woody core.

Before any measurement, all fibres were rinsed with distilled water for 10 min to remove water-soluble matter and subsequently vacuum-dried for 48 h at 70 °C. The properties of the test liquids, such as the surface tension, density and viscosity, used for the characterisation of the wetting behaviour of the fibres can be found elsewhere.<sup>8</sup>

### 2.2 Atmospheric air pressure plasma treatment

An Openair plasma system (Plasmatreat GmbH, Steinhagen, Germany) was used to functionalise the surface of lignocellulosic fibres. The AAPP treatment was carried out at maximum power (10 kW), with duration of 1 min and 3 min. A small number of technical fibres (approx. 3 g) were fixed longitudinally inside an inverted glass T-piece. The middle

inlet was positioned under the plasma nozzle in an attempt to confine the active plasma species around the fibres during the duration of the treatment. The distance between the plasma nozzle and the fibres inside the glass cylinder was set to 30 mm in order to avoid the thermal degradation which took place at shorter distances between the fibres and the nozzle.

### 2.3 Determination of wetting properties and fibre surface tension

The wetting behaviour of a packed bed of lignocellulosic fibres can be characterised using the capillary rise method, which is based on the Washburn equation for single capillary combined with the Laplace equation and the Hagen–Poiseuille equation for steady flow conditions.<sup>8</sup> A tensiometer (K100, Krüss GmbH, Hamburg, Germany) was used to measure the weight gain as function of time of at least five fibre bed samples ( $0.5 \pm 0.05$  g) packed inside a cylindrical holder (Krüss GmbH, Hamburg, Germany) at 20 °C. The precise procedure used can be found in ref. 8. It is possible to obtain the critical surface tension of the fibres  $\gamma_c$  in analogy to a Zisman plot by determining the maximum of a plot of the normalised wetting rate over the surface tension of the test liquids by Gaussian fit to the experimental data.<sup>8</sup>

### 2.4 $\zeta$ -Potential measurements

The  $\zeta$ -potential of the untreated and AAPP-treated lignocellulosic fibres was measured using the streaming potential method applied in an electrokinetic analyser (EKA) (Anton Paar KG, Graz, Austria). A dry fibre sample (*ca.* 2.5 g) was equilibrated in a 1 mM KCl supporting electrolyte solution by means of a single long time  $\zeta$ -potential measurement at 20 °C.

During the measurement, the electrolyte solution is forced through the packed fibre bed formed between two perforated Ag/AgCl electrodes in a cylindrical cell, which partially shears off the diffusive part of the electrochemical double layer giving rise to the streaming potential. The streaming potential is related to the  $\zeta$ -potential.<sup>9</sup> In order to exclude any overlaid effects due to swelling or extraction into the electrolyte solution,  $\zeta = f(\text{pH})$  was measured after  $\zeta = f(t)$ . The pH-dependence of the  $\zeta$ -potential is measured by changing the pH of the solution. The pH-value is varied in a range of  $3 < \text{pH} < 10$  by adding 0.1 M HCl or KOH. The theoretical background and further experimental details are reported elsewhere.<sup>9</sup>

Lignocellulosic fibres swell in water, causing a decay of  $\zeta = f(t)$  that can be described according to Kanamaru<sup>10</sup> by the following equation:

$$-\frac{d\zeta}{dt} = k(\zeta_t - \zeta_\infty) \quad (1)$$

which leads to:

$$-\ln \frac{\zeta_t - \zeta_\infty}{\zeta_0 - \zeta_\infty} = kt \quad (2)$$

where  $\zeta_t$  is a measured  $\zeta$ -potential value at time  $t$ ,  $k$  is the relative rate constant of the swelling process,  $\zeta_\infty$  is the  $\zeta$ -potential value which approaches the function  $\zeta = f(t)$  asymptotically and  $\zeta_0$  is the starting  $\zeta$ -potential value of the

dry material measured immediately after the fibres are contacted with the electrolyte solution.

### 2.5 Scanning electron microscopy

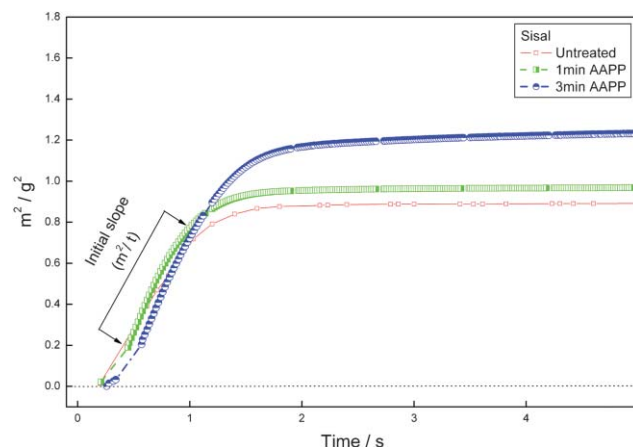
A JEOL-SM 5610LV was employed to observe the changes of the fibre surface morphology after exposure to AAPP treatment with an initial accelerating voltage of 15 kV. Prior to the examination, the samples were gold sputtered in an EMITECH K550 for 3 min to ensure good conductivity.

## 3.0 Results and discussion

The results reported here correspond to a series of optimised plasma treatment parameters obtained initially through empirical optimisation and later through Taguchi's design of experiments (DOE) methodology. The parameters investigated were: (a) distance between the plasma nozzle to the substrate, (b) treatment time and (c) effect of the feed gas pressure (oxygen, nitrogen and pressurised air were used as feed gases) on the critical surface tension of the lignocellulosic fibres investigated.

The distance between the fibres to be treated and the plasma nozzle was first optimised. In our system, distances smaller than 30 mm resulted in thermal degradation of the lignocellulosic fibres, leading to changes in colour and carbonisation of the fibres, whereas distances of 50 mm and 70 mm resulted only in minor changes of the wetting behaviour of the fibres. Treatment times of 1, 3, 15 and 25 min were investigated at fixed distances of 30 mm, 50 mm and 70 mm. However, it was found that treatment times exceeding 3 min resulted in a significant loss in the mechanical properties of the lignocellulosic fibres as measured according to ASTM D 3822-01.<sup>11</sup> Moreover, the feed gas composition used to create the plasma jet affected the wetting behaviour of the fibres. It was found that oxygen and nitrogen plasma lead to a reduction of the critical surface tension of the lignocellulosic fibres investigated, mainly due to its etching effect, which becomes more severe with prolonged treatment times. Therefore, we selected compressed air as the medium to generate the plasma and overcome, as far as possible, the negative impact of nitrogen and oxygen plasma on the lignocellulosic fibres. From the initial experimentation, it was concluded that the best parameters for AAPP treatment were 1 min and 3 min using atmospheric air as feed gas at a distance of 30 mm between the plasma nozzle and the fibres.

Atmospheric air pressure plasma (AAPP) provides the possibility of modifying the surface of any kind of lignocellulosic fibres in addition to removing contaminant substances attached to the surface in an environmentally sound manner. However, this has some limitations because lignocellulosic fibres undergo severe mass loss above 180 °C,<sup>12</sup> whereas the temperature of the plasma jet during AAPP treatment ranged from 140 °C to 180 °C measured by means of a thermocouple. Only abaca fibres showed a faint change in colour after AAPP treatment, possibly due to the thermal degradation of the fibres during the plasma, which dehydrated the fibres. Although no further degradation was observed, chemical and hence mechanical, degradation may have taken place.

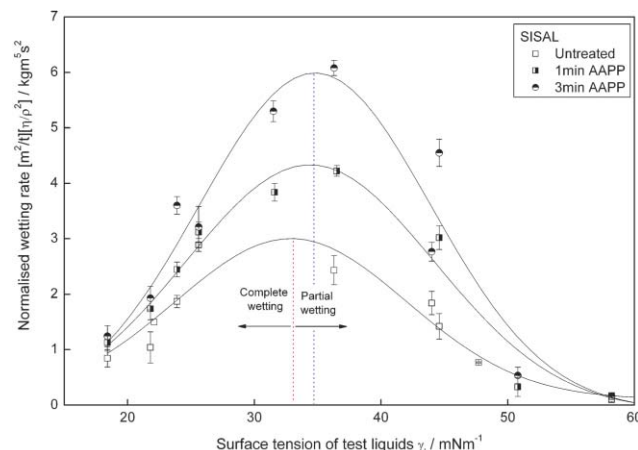


**Fig. 1** Typical weight rise curves of dimethyl sulfoxide (DMSO) into a packed sisal fibre bed. The initial slope of the function  $m^2 = f(t)$  is shown.

### 3.1 Wetting properties and fibre surface tension

Fig. 1 shows typical weight gain curves for the untreated, 1 min and 3 min AAPP-treated sisal fibres. The mass of test liquid imbibed into the packed bed of fibres increases with increased AAPP treatment time. The function  $m^2 = f(t)$  equals the wetting rate of the lignocellulosic fibres.

The study of fibre wettability has important implications in detergency, dyeing of textiles, coating processes and the design of fibre-reinforced composite systems, among other processes. The determination of the wetting behaviour of the lignocellulosic fibres using the capillary rise method may be affected by the swelling of the fibres when these are exposed to polar liquids. However, this process is not immediate as it is reported to take between 20 to 40 s.<sup>13</sup> As can be seen in Fig. 1, most measurements required less than 2 s to reach steady state. Fig. 2 shows a significant increase of the normalised wetting rate  $[m^2/t][\eta/\rho^2]$  of the AAPP treated sisal fibres with increased treatment time. The normalised wetting rate was obtained by multiplying the fibre wetting rate  $[m^2/t]$ , which is the initial slope of the function  $m = f(t)$ , with the factor containing the liquid properties. The critical solid–vapour surface tension  $\gamma_c$  of the lignocellulosic fibres can be estimated from the highest



**Fig. 2** Normalised wetting rate of untreated, 1 min and 3 min AAPP treated sisal fibres.

**Table 1** Critical surface tension  $\gamma_c$  of untreated, 1 min and 3 min AAPP treated lignocellulosic fibres.

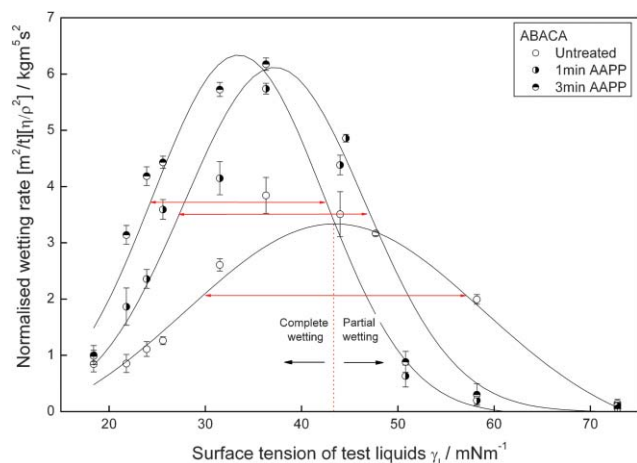
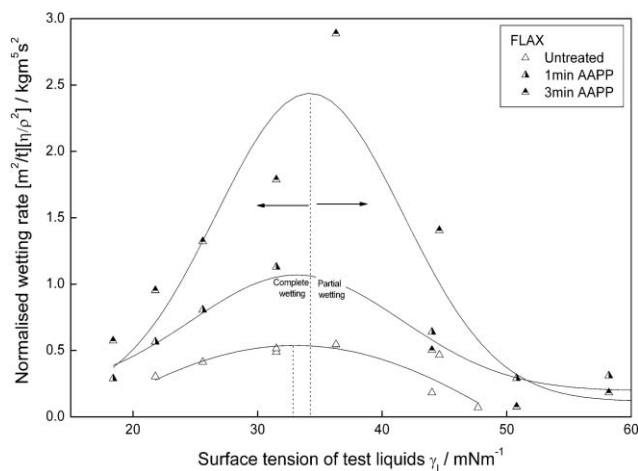
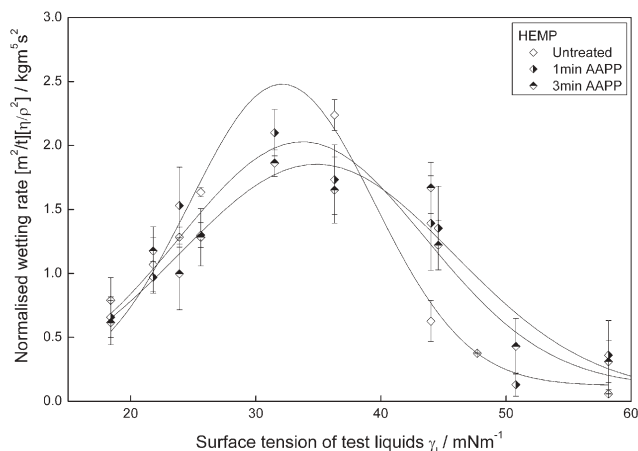
AAPP treatment time	Critical Surface Tension/ $\text{mN m}^{-1}$		
	Original	1 min	3 min
Abaca	$43.4 \pm 0.3$	$36.4 \pm 0.7$	$33.2 \pm 0.8$
Flax	$33.6 \pm 0.3$	$33.8 \pm 0.9$	$34.2 \pm 1.2$
Hemp	$31.0 \pm 0.2$	$33.7 \pm 0.8$	$34.8 \pm 0.8$
Sisal	$33.1 \pm 0.2$	$34.3 \pm 0.6$	$34.8 \pm 0.7$

point in each Gaussian fit to the normalised wetting rate, which equals  $C\gamma_1\cos\theta$ , as a function of the liquid surface tension  $\gamma_1$ .

Table 1 summarises the critical solid-vapour surface tension  $\gamma_c$  for the rest of the lignocellulosic fibres studied. Similar values in the range of  $35 \text{ mN m}^{-1}$  and  $51 \text{ mN m}^{-1}$  have been reported for untreated flax fibres<sup>8</sup> and pure cellulose.<sup>14</sup> A marginal increase in the value of  $\gamma_c$  can be seen for most the AAPP treated lignocellulosic fibres. The exception is abaca fibres, for which  $\gamma_c$  reduces progressively from approx.  $43 \text{ mN m}^{-1}$  (untreated fibres) to  $36 \text{ mN m}^{-1}$  and then to  $33 \text{ mN m}^{-1}$ , after 1 min and 3 min AAPP treatment, respectively. Despite the reduction in the critical surface tension of abaca fibres with longer AAPP treatment duration, the normalised wetting rate increases in the inverse direction, meaning that the abaca fibres absorb more liquid, particularly after 3 min of AAPP treatment. It should also be noted that the normalised wetting rate distribution, *i.e.* the half-width at half maximum, of plasma treated abaca fibres becomes narrower, which indicates that the fibres become more homogeneous so that the critical surface energy distribution narrows (Fig. 3).

Fig. 4 and 5 show a marginal increase in the normalised wetting rate of the untreated, 1 min and 3 min AAPP treated flax and hemp fibres, respectively. Both AAPP treatments resulted only in a marginal increase of the critical surface tension of these fibres, however the normalised wetting rate is much lower than for sisal and abaca fibres (Fig. 2 and 3), meaning that the AAPP treatment did not increase the liquid retention capabilities of flax and hemp fibres to the same extent as it occurred for sisal and abaca.

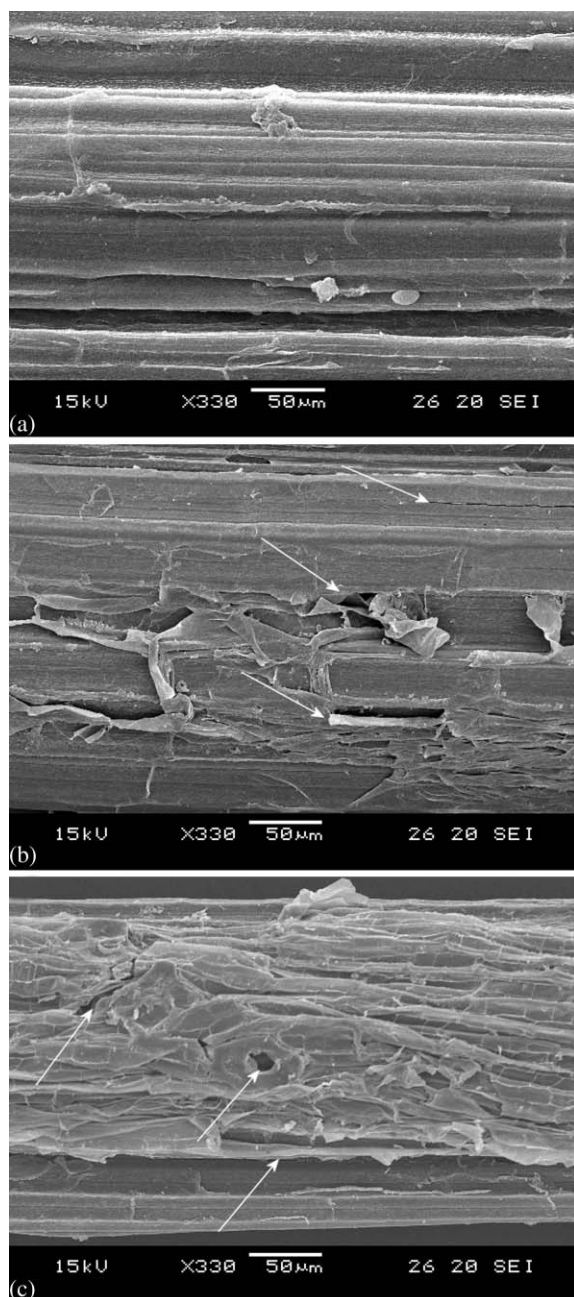
In the case of hemp fibres the normalised wetting rate (Fig. 5) shows the inverse trend to the rest of the fibres. The

**Fig. 3** Normalised wetting rate of the untreated, 1 min and 3 min AAPP treated abaca fibres.**Fig. 4** Normalised wetting rate of the untreated, 1 min and 3 min AAPP treated flax fibres.**Fig. 5** Normalised wetting rate of the untreated, 1 min and 3 min AAPP treated hemp fibres.

normalised wetting rate reduces with increasing AAPP treatment time, but at the same time, the critical surface tension  $\gamma_c$  increases marginally with longer treatment duration. Tentatively, this may be due to: (a) crosslinking of the surface of the hemp fibres which may have occurred during AAPP treatment, which consequently restricted the swelling of the fibres as the AAPP treatment time increased and (b) AAPP plasma treatments induced decomposition of hydrophobic compounds, which re-deposited on the fibre surface forming a denser hydrophobic protecting layer. In the case of abaca, flax and sisal fibres the increased wetting is due to an increase in the critical surface tension due to the modification of the surface chemistry through the introduction of various functional groups, most likely oxygen and nitrogen containing species,<sup>6†</sup> as well as the possible removal of non-cellulose substances.

† Examples may include: carboxyl ( $\text{R-COOH}$ ), peroxy ( $\text{R-OO-R}$ ), hydroperoxy ( $\text{R-OOH}$ ), amine ( $\text{R-NH}_2$ ) and nitroso ( $\text{R-N=O}$ ) groups. However, the direct quantification by X-ray photoelectron spectroscopy (XPS) is difficult due to the obvious similarity of the substrate and the AAPP modified fibres.

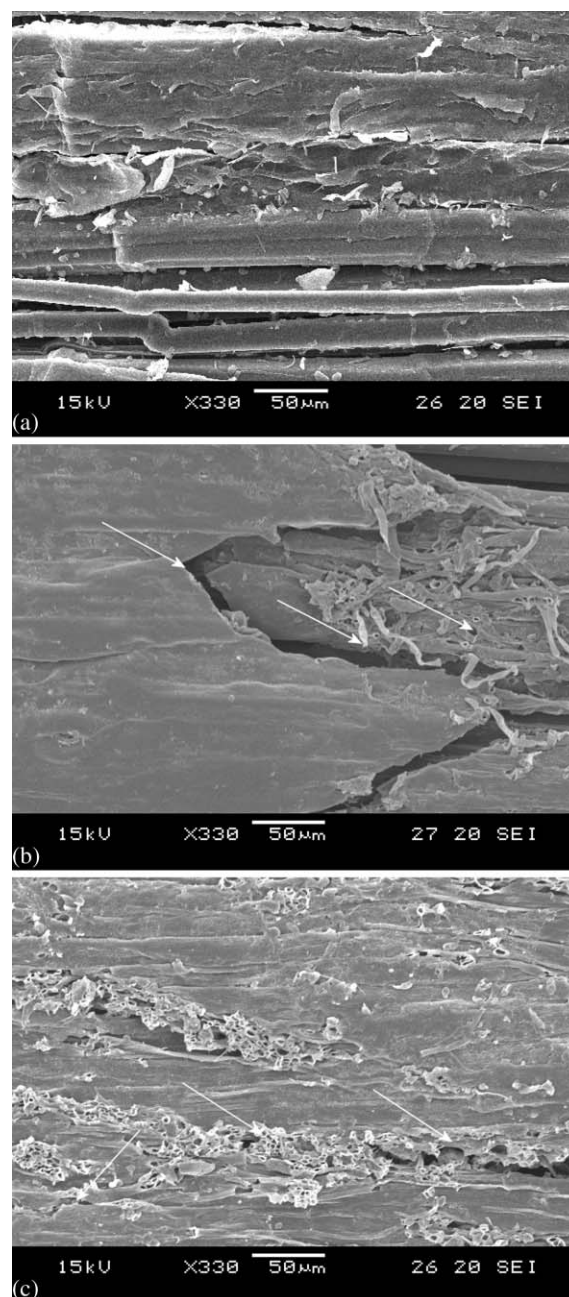




**Fig. 6** Surface morphology for the (a) untreated, (b) 1 min and (c) 3 min AAPP-treated abaca lignocellulosic fibres investigated. SEM magnification ( $\times 330$ ).

### 3.2 SEM analysis

Figs. 6–9 show the SEM micrographs of the surface for the (a) untreated, (b) 1 min and (c) 3 min AAPP-treated technical grade lignocellulosic fibres investigated. The untreated fibres (Figs. 6a–9a) are relatively more homogeneous than the surfaces of the AAPP-treated fibres. The deterioration of the morphology of all the fibres as the AAPP treatment time increased from 1 min to 3 min is obvious; after 1 min of treatment (Figs. 6b–9b), the fibres are etched, roughed and the corrugations are much deeper. After 3 min of AAPP treatment (Figs. 6c–9c), a large amount of fissures, pits and torn

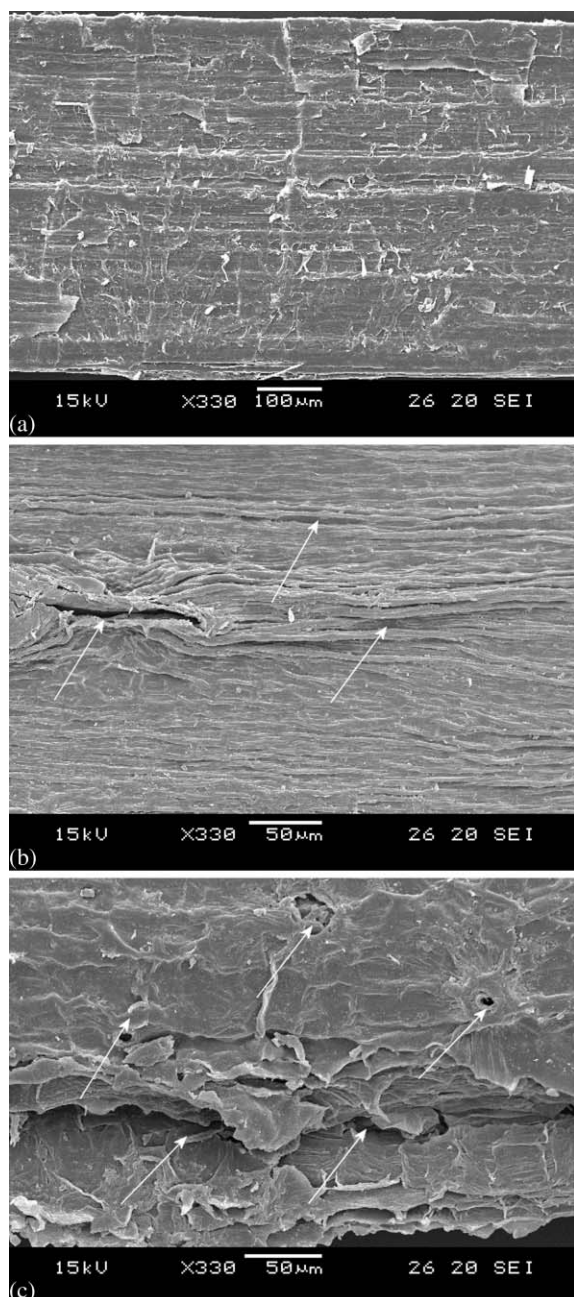


**Fig. 7** Surface morphology for the (a) untreated, (b) 1 min and (c) 3 min AAPP-treated flax lignocellulosic fibres investigated. SEM magnification ( $\times 330$ ).

microfibrils are evident because the longer treatment time intensifies the combined effect of etching and dehydrating of plasma. The etching effect of plasma, seem to have reduced the hydrophilic nature of hemp fibres, which is most likely due to the migration of hydrophobic compounds from the fibre bulk to the surface.

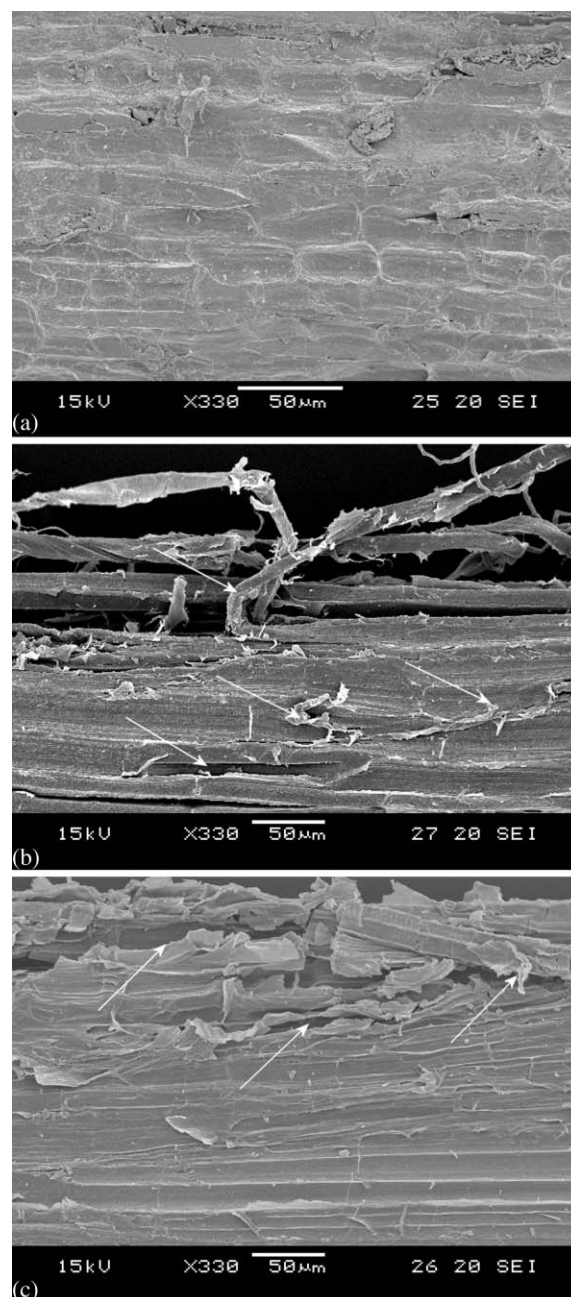
### 3.3 Time-dependent $\zeta$ -potential: swelling behaviour of the fibres

Fig. 10a–d show the time-dependent  $\zeta$ -potential for the untreated, 1 min and 3 min AAPP-treated fibres. Several factors have an effect on the decay of the  $\zeta$ -potential measured



**Fig. 8** Surface morphology for the (a) untreated, (b) 1 min and (c) 3 min AAPP-treated hemp lignocellulosic fibres investigated. SEM magnification ( $\times 330$ ).

as function of time for the untreated and AAPP-treated fibres, such as the chemical composition, polarity, porosity, swelling behaviour, macro- and microfibril structure of the lignocellulosic fibres.<sup>15</sup> All untreated fibres display initially a negative  $\zeta_0$ -value that increases asymptotically to a constant, but larger  $\zeta_\infty$ -value on different time scales, with the exception of flax fibres, whose initial value  $\zeta_0 = f(t)$  is positive and decreases with time to a much smaller but constant negative  $\zeta_\infty$ -value. Comparable trends with an initially positive  $\zeta_0$ -value have been previously reported for untreated lignocellulosic fibres, such as jute,<sup>16</sup> flax and cornhusk.<sup>17</sup> The initially positive  $\zeta_0$ -value of the untreated flax fibres is most likely due to the

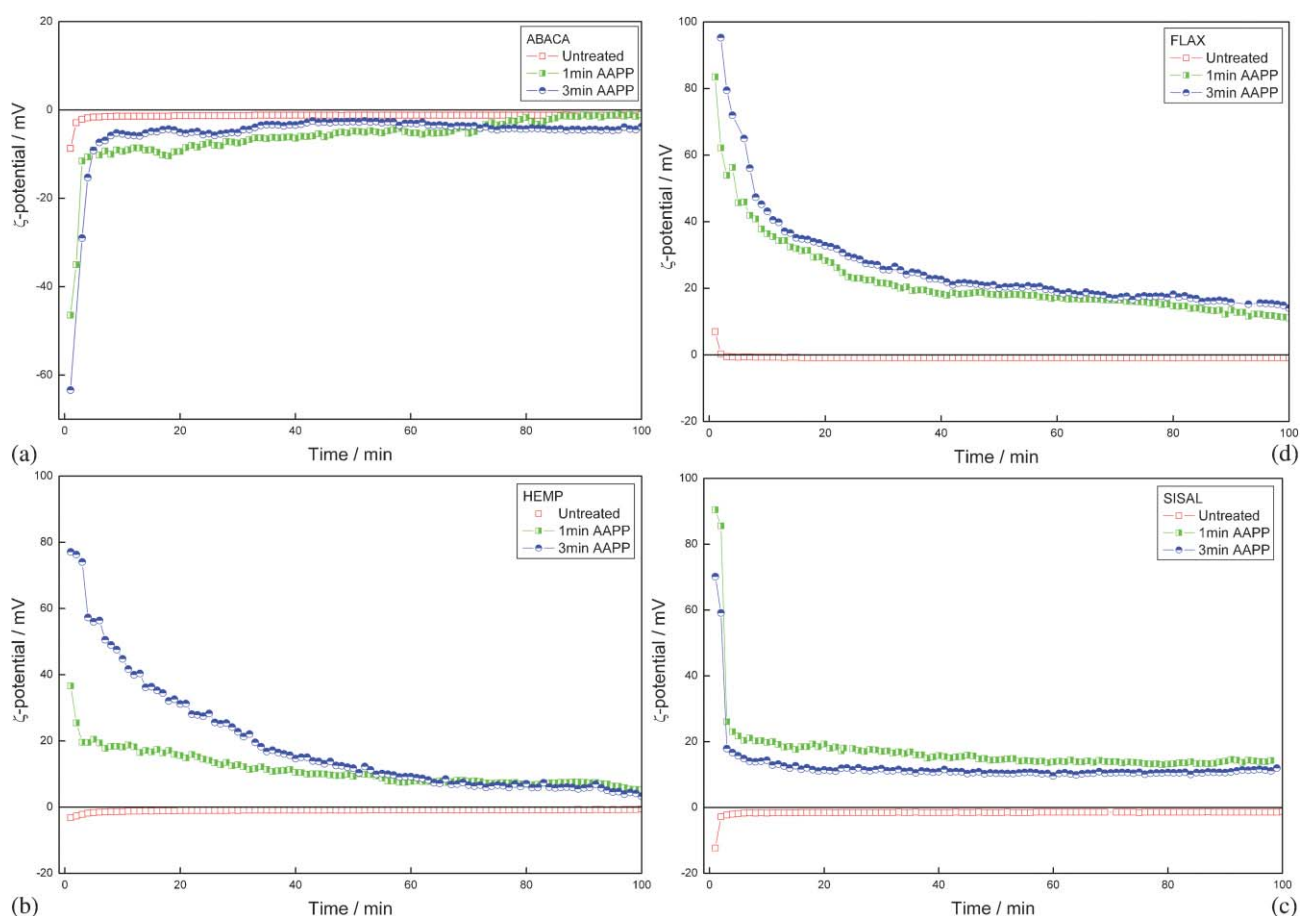


**Fig. 9** Surface morphology for the (a) untreated, (b) 1 min and (c) 3 min AAPP-treated sisal lignocellulosic fibres investigated. SEM magnification ( $\times 330$ ).

presence of amino acids and proteins such as glutamic acid ( $pK_a = 2.2, 4.2, 9.6$ ), hydroxyproline ( $pK_a = 1.92, 9.73$ ), glycine ( $pK_a = 2.34, 9.6$ ), proline ( $pK_a = 2.0, 10.6$ ) and glycoproteins<sup>18</sup> (for the  $pK_a$  values see ref. 19).

The decay in the modulus of the  $\zeta$ -potential as function of time is larger with prolonged AAPP treatment time, as shown in Fig. 10a–d. The change in  $\zeta = f(t)$  can be seen for the 1 min and 3 min AAPP-treated fibres. The  $\zeta$ -potential value of flax (Fig. 10b), hemp (Fig. 10c) and sisal (Fig. 10d) fibres decreases from a positive  $\zeta_0$ -value, rather than from a negative  $\zeta_0$  as for the untreated hemp and sisal fibres, and decreases asymptotically to a constant but smaller  $\zeta_\infty$ -value. In contrast, the





**Fig. 10** Time-dependent  $\zeta$ -potential for the untreated, 1 min and 3 min AAPP treated technical grade (a) abaca, (b) flax, (c) hemp and (d) sisal fibres.

abaca fibres (Fig. 10a) show a much more negative  $\zeta_0$ -value which increases asymptotically to a less negative  $\zeta_\infty$ -value. The larger positive  $\zeta_0$ -values of flax, hemp and sisal fibres after both AAPP treatments are due to the introduction of dissociable nitrogen-containing functional groups into the fibres after AAPP treatment. However, it is also possible that the apparent modification of the superstructure of the fibres leads to the exposure of amino acids and proteins naturally present in these fibres at the fibre/electrolyte interface. The amount exposed increases as function of the AAPP treatment duration. The formation of the electrochemical double layer depends strongly on the hydrophilicity of the surfaces, meaning that hydrophilic solid materials, like lignocellulosic fibres, will exhibit smaller  $\zeta$ -potential values due to their strong water uptake behaviour. This is because the adsorption of ions determine the  $\zeta$ -potential and occur in competition with the adsorption of water, but the concentration of the dissociable groups does not change,<sup>20</sup> therefore fewer ions can be adsorbed and the  $\zeta$ -value reduces. The re-adsorption of charged species into the electrochemical double layer and the removal of water-soluble ionic components (soluble metal salts making up the ash content)<sup>21</sup> might also affect the  $\zeta$ -potential.<sup>16,22</sup> It is known that multivalent ions particularly affect the formation of the electrochemical double layer and, therefore, the measured  $\zeta$ -potential. However, this effect is

expected to be rather small as the fibres swell in water and so cause a shift of the shear plane from the fibre surface into the liquid phase, which causes the reduction of the measured  $\zeta$ -potential.<sup>23</sup>

$\zeta$ -Potential measurements have been used in the past<sup>10</sup> to successfully verify the effectiveness of a surface modification treatment through the determination of any change in the surface charge of materials before and after treatment, as well as to determine any change in the water uptake behaviour ( $\Delta\zeta = (\zeta_0 - \zeta_\infty)/\zeta_0$ ) of the material at 100% relative humidity. The quotient  $(\zeta_0 - \zeta_\infty)/\zeta_0$  is directly proportional to the water adsorption of the material investigated at 100% relative humidity.<sup>15</sup> If indeed the surface of the fibres were modified after AAPP treatment and became more hydrophilic, they should be able to adsorb more water than the untreated fibres.

Table 2 shows the value and standard deviation of the  $\zeta_0$ ,  $\zeta_\infty$  and  $\Delta\zeta$  measured for the untreated, 1 min and 3 min AAPP-treated lignocellulosic fibres after both treatment times. The different magnitude in the  $\Delta\zeta$ -values reflects different degrees of hydrophilicity among the untreated fibres. Additionally, the  $\Delta\zeta$ -value of the fibres increases further with prolonged AAPP treatment time, except for hemp. It seems that the hydrophilic character of hemp reduces after exposure to AAPP. We also found a reduced liquid uptake for hemp fibres during the

**Table 2** Summary of the  $\zeta_0$ ,  $\zeta_\infty$  and  $\Delta\zeta$  and standard deviation of the untreated, 1 min and 3 min AAPP treated fibres

AAPP treatment time	Abaca			Flax			Hemp			Sisal		
	0 min	1 min	3 min	0 min	1 min	3 min	0 min	1 min	3 min	0 min	1 min	3 min
$\zeta_0$	-8.7	-46.6	-63.4	7.0	83.5	95.3	-3.2	36.5	77.1	-12.3	90.4	70.2
$\zeta_\infty$	-1.0	-1.0	-3.7	-0.9	11.1	14.1	-0.5	5.2	3.3	-1.2	14.2	12
$\Delta\zeta$	0.88	1.02	1.06	1.14	1.15	1.17	1.18	1.16	1.04	1.10	1.18	1.20

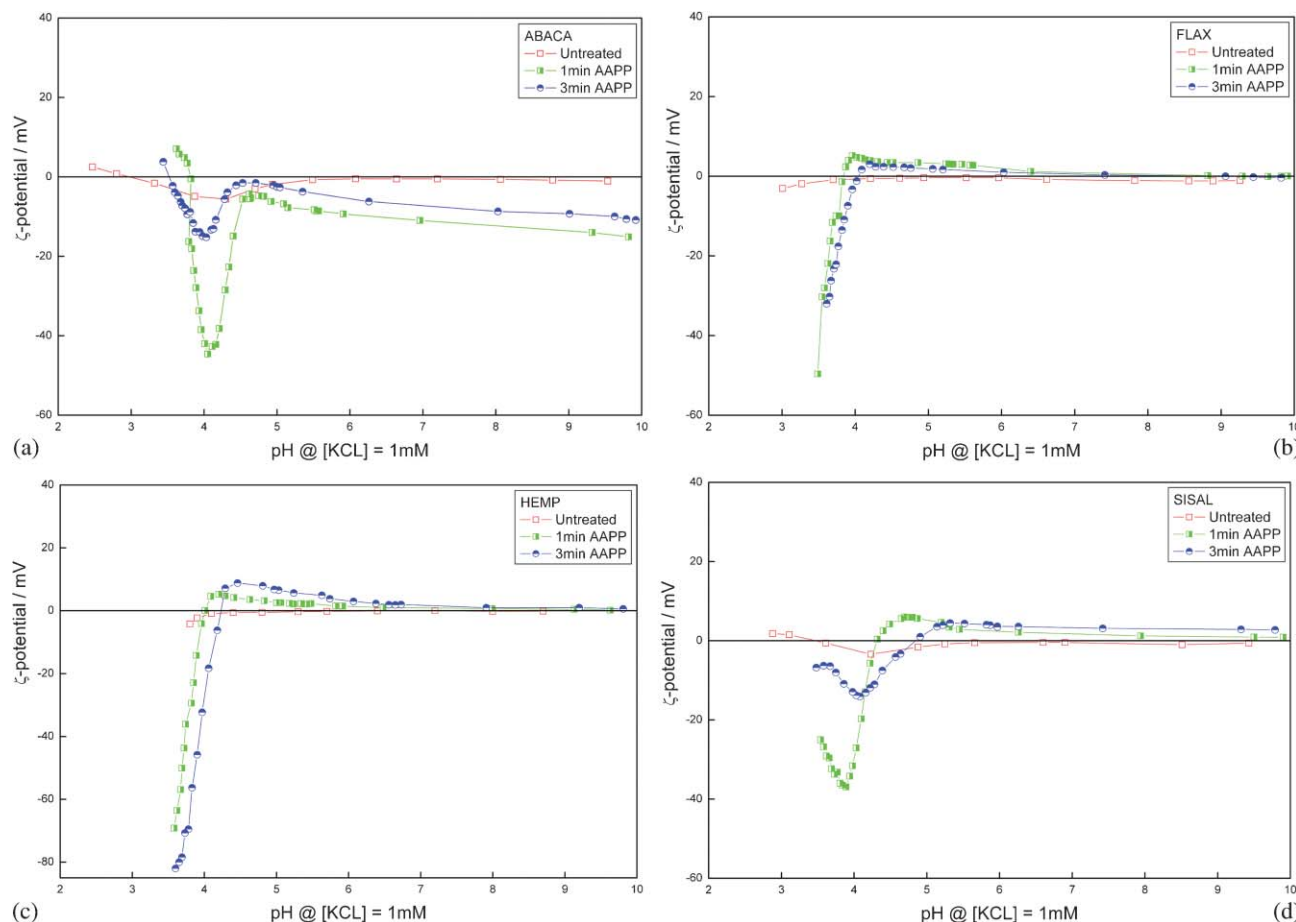
wetting measurements, shown in Fig. 5. Tentatively, the change in the structure of hemp fibres after AAPP treatment (Fig. 8a–c) seems to have been favourable for the formation of a denser hydrophobic protecting layer, possibly formed by linoleic and linolenic fatty acids,<sup>24</sup> as well as other fats, fatty alcohols and waxes.<sup>2</sup>

### 3.4 $\zeta$ -Potential: pH-dependent

Fig. 11a–d show the  $\zeta = f(\text{pH})$  measured for the untreated, 1 min and 3 min AAPP-treated lignocellulosic fibres. The electrochemical double layer that forms at the interface between the lignocellulosic fibres and the electrolyte solution is due to the dissociation of functional groups according to their  $\text{p}K_a$  values and the adsorption of ionic species. The small and negative  $\zeta_{\text{plateau}}$  in the more basic pH range of the

untreated fibres is also due to the dissociation of different acidic functional groups. The presence of functional groups in natural fibres is strongly associated to its chemical composition. Lignocellulosic fibres have a predominant presence of weak acids, e.g. R–OH, R–COOH, uronic acids and glutamic acid.<sup>25,26</sup>

In addition, ionic compounds like proteins and amino acids contain both acidic and basic groups<sup>27</sup> which produce a zwitterionic surface, thus the surface charge and  $\zeta$ -potential is pH-dependent.<sup>28,29</sup> It is likely that the zwitterionic compounds present in the lignocellulosic fibres investigated become more readily available at the interface of the electrolyte solution after AAPP treatment. The  $\zeta = f(\text{pH})$  changes drastically after exposure to AAPP at low acidic pH values, giving rise to a more negative  $\zeta$ -potential for all the lignocellulosic fibres investigated. This peak becomes more negative after extending



**Fig. 11** pH-dependent  $\zeta$ -potential for the untreated, 1 min and 3 min AAPP treated technical grade (a) abaca, (b) flax, (c) hemp and (d) sisal fibres.



the AAPP treatment time. A similar behaviour has been reported for other but untreated, lignocellulosic fibres including sisal,<sup>1</sup> jute<sup>16</sup> and flax.<sup>30</sup> This behaviour points to the tentative explanation that zwitterion compounds, which dissociate completely at excess HCl cause a preferential adsorption of Cl<sup>−</sup> anions on to the positive end of the hydroxyl dipole of cellulose.<sup>29,30</sup> Examples of zwitterion compounds in lignocellulosic fibres are carboxylic and amine surface groups. Bismarck *et al.*<sup>30</sup> also suggested a pH induced Cl<sup>−</sup> adsorption on positively charged surface sites.

An increased concentration of positively charged surface functional groups available at the AAPP-treated fibre/electrolyte interface is evident from the increasing  $\zeta_{\text{plateau}}$  compared with the  $\zeta_{\text{plateau}}$  of the untreated fibres. This is due to the air plasma functionalisation and/or the plasma induced change of the surface morphology, which resulted in an increased exposure and accessibility of zwitterionic functional compounds. The isoelectric point (iep), where the  $\zeta$ -potential is zero, could be determined only for untreated abaca and sisal fibres to be pH 3.0 and 3.4, respectively, because the swelling of the fibres causes a zero  $\zeta$ -potential value for the other untreated fibres. The low iep values of abaca and sisal are caused by the low  $pK_a$  values of the functional groups present, such as carboxyl groups ( $pK_a \approx 4.00$ )<sup>31,32</sup> and uronic acids ( $pK_a$  between 3.0 and 3.4).<sup>26,33</sup> In the case of abaca, the iep value increases after the exposure to AAPP from 3.0 to pH 3.5 after 1 min and 3.8 after 3 min exposure to AAPP, which confirms the reduction of the surface acidic character by introducing nitrogen containing functional groups. After exposure to AAPP the  $\zeta$ -potential is positive over a wide pH range for the other fibres, except for abaca; this points to the presence of nitrogen containing positively charged surface functional groups. In the case of 1 min AAPP treated fibres, the iep was determined to be 3.8 for flax, 4.0 for hemp and 4.3 for sisal fibres. After 3 min of AAPP treatment, the iep shifted towards even higher pH values, to 4.0 for flax, 4.2 for hemp and 4.8 for sisal fibres, which confirms the increased basic character of the AAPP treated fibres but also the acid induced change of the surface charge.

## 4.0 Conclusions

We studied the effects of atmospheric air pressure plasma (AAPP) treatment on the surface properties of abaca, flax, hemp and sisal fibres. Wettability measurements to determine the fibre surface tension and  $\zeta$ -potential measurements as a function of time and pH were performed in order to verify the effectiveness of the AAPP treatments. Untreated lignocellulosic fibres are inherently hydrophilic, as found by the small  $\zeta$ -potential equilibrium values ( $\zeta_{\infty}$ ) and  $\Delta\zeta$  measured in the decay of the  $\zeta$ -potential measured as a function of time. Prolonged exposure to AAPP causes the hydrophilic behaviour of abaca, flax and sisal fibres to increase. The exception are the hemp fibres. Tentatively, this may be due to: (a) crosslinking of the surface of hemp fibre may have occurred during AAPP treatment, which consequently restricted the swelling of hemp fibres as the AAPP treatment time increased and/or (b) AAPP plasma treatments induced decomposition of hydrophobic compounds of the fibre and re-deposition of an

apparently denser hydrophobic protecting layer. However, more research is necessary to find out the true cause of such behaviour.

The  $\zeta = f(t)$  reversal of the  $\zeta$ -sign is due to nitrogen-containing groups introduced by plasma or exposed by change in the surface morphology. The zwitterionic behaviour of the surface amine and carboxyl groups present in the lignocellulosic fibres modifies their surface charge and  $\zeta$ -potential as a function of pH, consequently having an effect on the sign and magnitude of the surface charge of this kind of natural fibres. Longer exposure to AAPP causes a shift of the  $\zeta$ -potential reversal to higher pH. Finally, the SEM micrographs of the surface morphology of the AAPP-treated fibres show damages the microfibril structure of the lignocellulosic fibres, which intensifies with prolonged treatment times.

## Acknowledgements

A. Baltazar-y-Jimenez gratefully is grateful to the Mexican Council on Science and Technology (CONACYT) for providing his scholarship. The authors are grateful to Wigglesworth & Co. (UK), Hemcore Ltd. (UK) and Heritage Arts & Crafts (the Philippines) for supplying the samples.

## References

- 1 A. Bismarck, A. K. Mohanty, I. Aranberri-Askargorta, S. Czaplá, M. Misra, G. Hinrichsen and J. Springer, *Green Chem.*, 2001, **3**, 100–107.
- 2 R. M. Rowell, J. S. Han and J. S. Rowell, in *Natural Polymers and Agro-fibres Bases Composites*, ed. E. Frollini, A. L. Leao and L. H. C. Mattoso, Embrapa Instrumentação Agropecuária, Sao Carlos - S.P., Brazil, 1st edn, 2000, pp. 115–134.
- 3 I. A. Tarchevsky and G. N. Marchenko, in *Cellulose: Biosynthesis and Structure*, ed. L. V. Backinowski and M. A. Chlenov, Springer, Berlin, 1991, pp. 9–31.
- 4 F. Munder, C. Füll and H. Hempel, in *Natural Fibres, Biopolymers and their Composites*, ed. A. K. Mohanty, M. Misra and L. T. Drzal, CRC Press, Boca Raton, 1st edn, 2005, pp. 109–140.
- 5 X. Yuan, K. Jayaraman and D. Bhattacharyya, *J. Adhes. Sci. Technol.*, 2002, **16**, 703–728.
- 6 A. Bismarck and J. Springer, in *Encyclopedia of Surface and Colloid Science*, ed. A. Hubbard, Marcel Dekker, New York, 1st edn., 2002, vol. 2, pp. 2471–2789.
- 7 R. B. Dodd and D. E. Akin, in *Natural Fibres, Biopolymers and their Composites*, ed. A. K. Mohanty, M. Misra and L. T. Drzal, CRC Press, Boca Raton, 1st edn, 2005, pp. 141–157.
- 8 I. Aranberri-Askargorta, T. Lampke and A. Bismarck, *J. Colloid Interface Sci.*, 2003, **263**, 580–589.
- 9 H. J. Jacobasch, F. Simon, C. Werner and C. Bellmann, *Tech. Mess.*, 1996, **63**, 447–452.
- 10 K. Kanamaru, *Kolloid-Z.*, 1960, **168**, 115–121.
- 11 A. Baltazar-y-Jimenez, M. Bistriz, E. Schulz and A. Bismarck, *Compos. Sci. Technol.*, 2007, DOI: 10.1016/j.compscitech.2007.04.028.
- 12 S. Kumar and I. Varma, *J. Macromol. Sci. Phys.*, 2006, **45**, 153–164.
- 13 S. Q. Shi and D. J. Gardner, *J. Adhes. Sci. Technol.*, 2000, **14**, 301–314.
- 14 J. M. van Hazendonk, J. C. van der Putten, J. T. F. Keurentjes and A. Prins, *Colloids Surf., A*, 1993, **81**, 251–261.
- 15 H.-J. Jacobasch, G. Bauböck and J. Schurz, *Colloid Polym. Sci.*, 1985, **263**, 3–24.
- 16 A. Bismarck, J. Springer, A. K. Mohanty, G. Hinrichsen and M. A. Khan, *Colloid Polym. Sci.*, 2000, **278**, 229–235.

- 17 A. Baltazar-y-Jimenez and A. Bismarck, *Cellulose*, 2007, **14**, 115–127.
- 18 C. Morvan, C. Andeme-Onzighi, R. Girault, D. S. Himmelsbach, A. Driouch and D. E. Akin, *Plant Physiol. Biochem.*, 2003, **41**, 935–944.
- 19 A. Albert and E. P. Serjeant, in *The Determination of Ionization Constants: a Laboratory Manual*, Chapman and Hall, New York, 3rd edn, 1984, pp. 166–174.
- 20 N. Kuehn, H.-J. Jacobasch and K. Lunkenheimer, *Acta Polym.*, 1986, **37**, 394–396.
- 21 A. Bismarck, I. Aranberri-Askargorta, J. Springer, T. Lampke, B. Wielage, A. Stamboulis, I. Shenderovich and H. H. Limbach, *Polym. Compos.*, 2002, **23**, 872–894.
- 22 K. Stana-Kleinschek and V. Ribitsch, *Colloids Surf., A*, 1998, **140**, 127–138.
- 23 V. Ribitsch, K. Stana-Kleinschek, T. Kreze and S. Strnad, *Macromol. Mater. Eng.*, 2001, **286**, 648–654.
- 24 B. D. Oomah, M. Bussan, D. V. Godfrey and J. C. G. Drover, *Food Chem.*, 2002, **76**, 33–43.
- 25 M. Östenson, H. Järund, G. Toriz and P. Gatenholm, *Cellulose*, 2006, **13**, 157–170.
- 26 D. Crônier, B. Monties and B. Chabbert, *J. Agric. Food Chem.*, 2005, **53**, 8279–8289.
- 27 R. J. Hunter, in *Foundations of Colloid Science Vol. 1*, ed. L. R. White, L. R. Fisher, N. Parker, R. M. Pashley, R. W. O'Brien, J. Ralston and F. Grieser, Oxford University Press, New York, 3rd edn, 1991, pp. 374–376.
- 28 H. M. Rendall and A. L. Smith, *J. Chem. Soc., Faraday Trans. 1*, 1978, **74**, 1179–1187.
- 29 A. Homola and R. O. James, *J. Colloid Interface Sci.*, 1977, **59**, 123–134.
- 30 G. L. Madan and S. K. Shrivastava, *Colloid Polym. Sci.*, 1976, **V254**, 476–480.
- 31 C. Morvan, M. Demarty and M. Thellier, *Plant Physiol.*, 1979, **63**, 1117–1122.
- 32 L. Bedouet, E. Denys, B. Courtois and J. Courtois, *Carbohydr. Polym.*, 2006, **65**, 165–173.
- 33 R. Narendra and Y. Yang, *Green Chem.*, 2005, **7**, 190.

# Find a SOLUTION

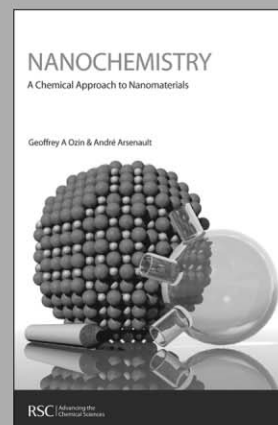
... with books from the RSC

**Choose from exciting textbooks, research level books or reference books in a wide range of subject areas, including:**

- Biological science
- Food and nutrition
- Materials and nanoscience
- Analytical and environmental sciences
- Organic, inorganic and physical chemistry

**Look out for 3 new series coming soon ...**

- RSC Nanoscience & Nanotechnology Series
- Issues in Toxicology
- RSC Biomolecular Sciences Series



**RSC** | Advancing the  
Chemical Sciences

[www.rsc.org/books](http://www.rsc.org/books)

# Rapid and clean synthesis of phthalimide derivatives in high-temperature, high-pressure H<sub>2</sub>O/EtOH mixtures

Joan Fraga-Dubreuil,<sup>\*a</sup> Gürbüz Çomak,<sup>ab</sup> Alasdair W. Taylor<sup>a</sup> and Martyn Poliakoff<sup>\*a</sup>

Received 22nd March 2007, Accepted 1st May 2007

First published as an Advance Article on the web 1st June 2007

DOI: 10.1039/b704405d

A variety of phthalimide derivatives have been synthesised effectively in high-temperature, high-pressure H<sub>2</sub>O/EtOH mixtures (HTHP-H<sub>2</sub>O/EtOH) as the solvent. This clean method is based on the condensation of *o*-phthalic acid and amines and affords phthalimide compounds as pure crystals in most cases, because of the dehydrating effect and change in solvation properties of H<sub>2</sub>O/EtOH at high pressures and temperatures. After conducting a series of model reactions, it was found that a mixture, 1/1 v/v H<sub>2</sub>O/EtOH, was appropriate for obtaining good yields combined with high purity of the phthalimides. Moderate to excellent yields were obtained depending on the nature of the amine. Aromatic amines generally afforded higher yields than aliphatic ones except for 3-hydroxypropylamine, where a yield up to 95% was obtained.

## Introduction

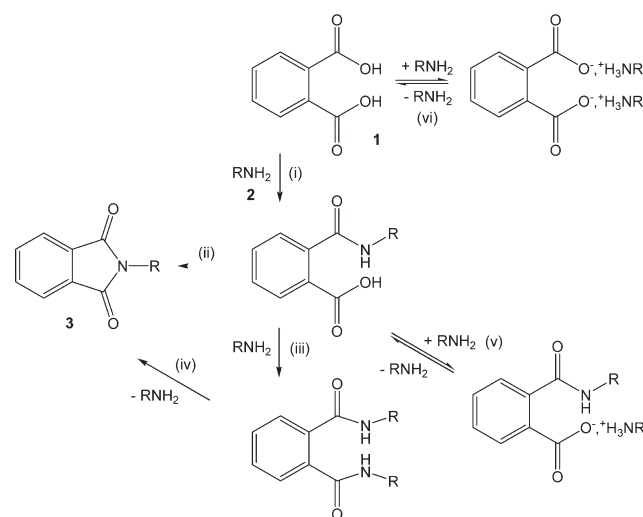
Phthalimide derivatives have been used extensively in synthetic chemistry, with a wide range of applications, particularly in biological chemistry. For example, properties such as anti-convulsant,<sup>1</sup> anti-inflammatory,<sup>2–4</sup> analgesic,<sup>5</sup> herbicidal<sup>6</sup> and insecticidal<sup>7</sup> have been reported. Typically, phthalimide derivatives are synthesised *via* the condensation of amines with phthalic anhydride in refluxing organic solvents. High boiling point solvents such as acetic acid,<sup>3,8,9</sup> DMF,<sup>10</sup> and dioxane<sup>11</sup> are commonly used. Synthesis in solvent-free conditions can be achieved by refluxing a mixture of phthalic anhydride with the amine<sup>1,2</sup> or by using a catalyst such as DABCO at room temperature.<sup>12</sup> There has also been work on using microwave irradiation as a heating method both in the presence<sup>13,14</sup> or absence<sup>15–17</sup> of organic solvents. Microwave-mediated and/or solventless syntheses give generally high yields of phthalimides within just a few minutes; however most of the traditional methods are not entirely satisfactory due to lengthy reaction times, the use of organic solvents or other auxiliary reagents.

In this paper, we propose an alternative, fast and clean method using high-temperature high-pressure water/ethanol as the solvent (HTHP-H<sub>2</sub>O/EtOH) to produce phthalimide derivatives from *o*-phthalic acid and amines as the reagents (Fig. 1).

The literature mentions very few examples of phthalimides synthesised in H<sub>2</sub>O<sup>18</sup> or EtOH.<sup>19,20</sup> Once again, anhydrides are the preferred starting materials, due to their higher reactivity compared to their corresponding acids and their higher solubility in organic solvents.<sup>21</sup> There are just a few reports of the use of *o*-phthalic acid as starting material,<sup>22,23</sup> with two steps sometimes being required to obtain the target phthalimide from phthalic acid derivatives.<sup>11,14</sup>

The preparation of anhydrides generally requires long reaction times in an organic solvent under reflux conditions,<sup>24</sup> and furthermore, anhydrides are known to undergo hydrolysis in hot water.<sup>25</sup> Therefore, we decided to study the reaction with *o*-phthalic acid as reactant instead. Our group has previously reported the continuous catalytic oxidation of *o*-xylene to *o*-phthalic acid in HTHP-H<sub>2</sub>O.<sup>26,27</sup>

Although several mechanisms have previously been proposed,<sup>8,28</sup> it is likely that the formation of the phthalimide proceeds in two steps (Fig. 1), starting with the nucleophilic attack of the amine on one of the carbonyl groups of the diacid, pathway (i), which releases the first molecule of water. Then, ring closure occurs leading to the formation of phthalimide together with a second molecule of water, pathway (ii). Other reactions can occur, such as bis-amidations, pathway (iii), possibly followed by an intramolecular deamination to give the final product, pathway (iv).<sup>29</sup> However, the acid–base neutralisation of the carboxylic acid



**Fig. 1** Possible reaction sequence for the formation of *N*-substituted phthalimides, **3**, in HTHP-H<sub>2</sub>O/EtOH.

<sup>a</sup>School of Chemistry, University of Nottingham, Nottingham, UK NG7 2RD. E-mail: Martyn.Poliakoff@nottingham.ac.uk

<sup>b</sup>Department of Chemistry, Faculty of Sciences & Arts, University of Çukurova, Adana, 01330, Turkey

could be problematic depending on the nature of the amine used, because the corresponding ammonium salts formed would prevent the amine from reacting further, pathways (v) and (vi).<sup>11</sup> This problem could be overcome in the HTHP-H<sub>2</sub>O environment because the acidity of *o*-phthalic acid is expected to decrease, thereby displacing the equilibrium towards the lefthand side.

Thus, there is scope for an efficient and rapid synthesis *via* the condensation reaction in Fig. 1, utilising HTHP-H<sub>2</sub>O as the solvent because this reaction produces H<sub>2</sub>O as a byproduct. Water is perhaps the cheapest, most readily available and innocuous solvent. It is not truly an “alternative” solvent, having been used in industry for a long time, but only relatively recently has its potential as a solvent for synthetic organic chemistry been explored. Reactions carried out in HTHP-H<sub>2</sub>O cover most major areas of organic synthesis, even reactions involving water-sensitive compounds.<sup>30,31</sup>

As the temperature of liquid water is increased, both the density and viscosity of the fluid fall and this has a large effect on its solvating properties. As the density decreases, H-bonding becomes less prevalent and water exists as a collection of dimers or monomers rather than an extended framework. This behaviour is reflected in the fall in the dielectric constant,  $\epsilon$ , from about 80 at room temperature to 27.5 at 250 °C and to 6 at the critical point.<sup>31</sup> Thus, near-critical water and supercritical water can act as non-polar solvents which dissolve organic compounds and gases that are insoluble under ambient conditions. Also, as the heated water cools, its organic solvating power decreases leading, to phase separation of solvent and solute.

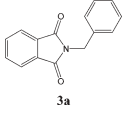
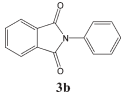
Condensation reactions have been achieved in HTHP-H<sub>2</sub>O, as it has shown, rather surprisingly, to be a good medium for dehydration reactions. The Fischer Indole synthesis, a staple of synthetic organic chemistry, has been achieved in a reasonable yield (67%) without additional acid at 222 °C.<sup>32</sup> In our laboratory, a range of benzimidazole compounds have also been synthesised in good yield in HTHP-H<sub>2</sub>O using a batch-type reactor by the condensation of 1,2-phenylenediamine and various carboxylic acids.<sup>33</sup> Interestingly, some of the benzimidazoles were isolated from the reaction mixture as pure crystalline products without the need for any work-up.

Most of the reported procedures for preparing phthalimides use a purification method *via* recrystallisation, particularly in EtOH or in water.<sup>1–3,12,15,16,17,22</sup> In addition, near-critical and supercritical EtOH have been suggested as interesting media both for chemical reactions and separations and also for replacing environmentally undesirable organic solvents.<sup>34</sup> Consequently, we decided to investigate the possibility of synthesis of phthalimide derivatives in H<sub>2</sub>O/EtOH mixtures as potential new “reaction/crystallisation” solvents in a high-temperature high-pressure batch reactor.

## Results and discussion

A series of experiments was performed in order to optimise the reaction conditions and particularly to investigate the role of the solvent used. The ratio of H<sub>2</sub>O/EtOH was varied using two model starting amines, aniline and benzylamine (Table 1). The results suggested that the reaction is very fast and is completed

**Table 1** Results obtained with *N*-phenylphthalimide and *N*-benzylphthalimide at different H<sub>2</sub>O/EtOH ratios after 5 min of heating

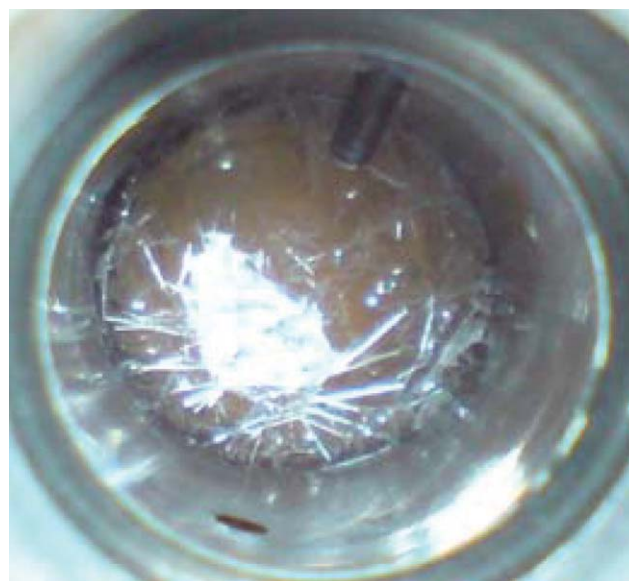
Phthalimide	$T_{\max}/^{\circ}\text{C}$	$p_{\max}/\text{psi}$	H <sub>2</sub> O/EtOH ratio (v/v)	Yield <sup>a</sup> (%)	Crystalline (Y/N)
 3a	263	1310	0/100	5	Y
	300	1560	50/50	77	Y
	303	1610	75/25	78	Y
	300	1640	90/10	80	N
	332	1700	100/0	94 <sup>b</sup>	N
 3b	274	1240	50/50	65	Y
	307	1515	75/25	59	Y
	311	1650	100/0	45	N

<sup>a</sup> Isolated yield of the phthalimide. <sup>b</sup> Product was extracted with Et<sub>2</sub>O.

within approximately 5 min plus the time the reactor takes to cool. We found that the ratio 1/1 v/v H<sub>2</sub>O/EtOH gave high purity crystals combined with good yields with both substrates (Fig. 2).

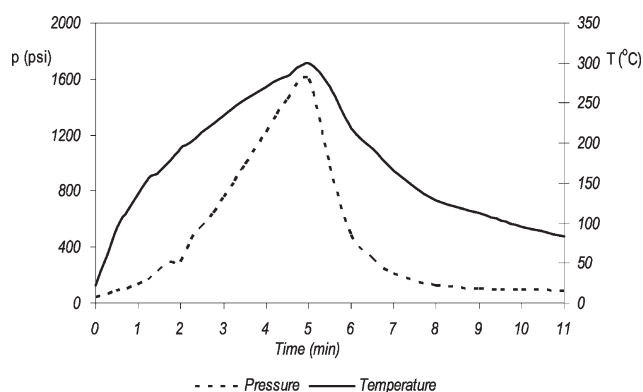
In order to check the viability of this method, the stability of the isolated *N*-benzylphthalimide, **3a** was also investigated by prolonged heating (20 min) at 360 °C and 3600 psi with the 1/1 v/v H<sub>2</sub>O/EtOH mixture. The compound appeared to be unaffected by the reaction conditions (neither hydrolysis nor esterification was observed) and was fully recovered.

From Table 1, it can be seen that the yield of the *N*-phenylphthalimide, **3b** decreased from 65 to 45% as the percentage of water was increased. With pure water, a non-crystalline product was obtained. In the case of benzylamine, there was no obvious difference in yields (*ca.* 80%) obtained with H<sub>2</sub>O/EtOH ratio, between 50/50 and 90/10. However, with a ratio of 90/10 H<sub>2</sub>O/EtOH or with pure water, the *N*-benzylphthalimide product was non-crystalline and had to be extracted with Et<sub>2</sub>O to isolate the product in good yield. This extraction afforded  $\leq 94\%$  yield of phthalimide. Analysis



**Fig. 2** Photo taken from the top of an opened autoclave showing *N*-benzylphthalimide as pure, white crystals at the bottom.





**Fig. 3**  $T/p$  profile of a typical “5 min” experiment using 5 mL of  $\text{H}_2\text{O}/\text{EtOH}$  mixture. It can be seen that a maximum pressure of 1600 psi ( $p_{\text{max}}$ ) and a temperature of 300 °C ( $T_{\text{max}}$ ) are obtained after 5 min heating. After quenching, the reactor was left to cool overnight.

of the solid by mass spectrometry indicated that it contained traces of the corresponding bis-amide (see pathway (iii), Fig. 1).

A reaction can often be improved by carrying it out under single rather than multi-phase conditions since the reactants interact better. However, according to the  $T/p$  profile of these experiments (Fig. 3) and the pressure-composition isotherms of  $\text{H}_2\text{O}/\text{EtOH}$  reported,<sup>35</sup> it is likely that our reaction mixtures are biphasic (gas and liquid) or close to the phase boundary for 50/50  $\text{H}_2\text{O}/\text{EtOH}$ , if the effects of the dissolved reactants/products are neglected.

By contrast, reactions in pure EtOH should be in a single phase ( $T_c = 241$  °C,  $p_c = 890.5$  psi), but the yield of *N*-benzyl phthalimide was very poor, only 5%. Although EtOH is a better solvent than  $\text{H}_2\text{O}$  for *o*-phthalic acid and most of the amines used in this work,<sup>36,37</sup> the presence of water appears to be important for the success of the reaction, possibly because  $\text{H}_2\text{O}/\text{EtOH}$  provides more rapid heat transfer than pure EtOH.

In Table 1, the  $T_{\text{max}}$  and  $p_{\text{max}}$  observed after 5 min increased with increasing proportion of water in the solvent. Also, in our previous work on the synthesis of benzimidazoles in a range of solvents including EtOH,<sup>33</sup> we found that the lower acidity

of the high-pressure high-temperature EtOH compared to  $\text{H}_2\text{O}$  was insufficient to catalyse this type of reaction. Many phthalimide derivatives have already been characterised crystallographically, for instance, *N*-phenylphthalimide<sup>38</sup> and *N*-benzylphthalimide.<sup>39</sup>

In the view of these results, it was decided to study this reaction with a variety of amines as substrates (aromatic, aliphatic and functionalised) with a 1/1 v/v  $\text{H}_2\text{O}/\text{EtOH}$  mixture or pure water as the solvent depending on the solubility of the products obtained (Table 2).

It can be seen that a range of phthalimides could be obtained after reaction times of only a few minutes in moderate to good yields depending on the substrate. Apart from the experiments using alkylamines (entries 10–12), the product could usually be isolated as pure crystals directly from the reaction mixture when 1/1 v/v  $\text{H}_2\text{O}/\text{EtOH}$  was used.

Clearly, this method cannot be used with substrates bearing functionalities, *e.g.* ester, cyano or ether groups that could react with  $\text{H}_2\text{O}$  under high-temperature, high-pressure conditions.<sup>30,31</sup> Halides are also problematic because they can undergo a nucleophilic substitution with  $\text{OH}^-$  from the dissociation of HTHP- $\text{H}_2\text{O}$ . This may explain why we obtained a lower yield (52%) with 4-bromoaniline as substrate (entry 2). The HBr released may have neutralised the amine, forming an unreactive ammonium salt. Also, 4-nitroaniline and 4-aminopyridine were unstable under these conditions (entries 5 and 6). In this reaction, GC analysis indicated the formation of a number of by-products including benzoic acid by decarboxylation of *o*-phthalic acid. The purification of the target product was found to be more difficult.

With 1,4-phenyldiene diamine, it was found that the selective mono-condensation of the diamine occurred with a yield of 83% *N*-(4-aminophenyl)phthalimide, **3f**. This is interesting because desymmetrisation was observed rather than the formation of the more expected phthalimide dimer. The preparation of this desymmetrised molecule has been reported previously but the route was far less straightforward than here.<sup>40</sup>

Unexpected results were obtained for amino acids (entries 7 to 9) because the isolated phthalimide products were all

**Table 2** Results obtained with different amines at different  $\text{H}_2\text{O}/\text{EtOH}$  ratio

Entry	Amine	Phthalimide product	$\text{H}_2\text{O}/\text{EtOH}$ v/v ratio	$T_{\text{max}}/\text{°C}$	$p_{\text{max}}/\text{psi}$	Time/min	Isolated phthalimide yield (%)	Crystalline (Y/N)	GC-RT/min <sup>a</sup>
1	4-hydroxyaniline	<b>3c</b>	1/1	312	2000	6	78	Y	— <sup>b</sup>
2	4-bromoaniline	<b>3d</b>	1/0	307	1930	6	51	N	15.8
3	2-(aminomethyl)pyridine	<b>3e</b>	1/1	380	4600	9	70	Y	16.2
4	<i>p</i> -phenylene diamine	<b>3f</b>	1/1	364	4010	10	83	Y	— <sup>b</sup>
5	4-nitroaniline	<b>3g</b>	1/1	364	4175	11	— <sup>c</sup>	N	15.8
6	4-aminopyridine	<b>3h</b>	1/1	374	3650	11	— <sup>c</sup>	N	16.3
7	4-aminobenzoic acid	<b>3b</b>	1/1	369	4790	9	64 <sup>d</sup>	Y	15.7
8	L-phenylalanine	<b>3i</b>	1/1	364	4245	10	86 <sup>d</sup>	Y	16.5
9	glycine	<b>3j</b>	1/1	359	4200	9	76 <sup>d</sup>	Y	11.4
10	<i>n</i> -butyl amine	<b>3k</b>	1/0	303	1335	6.5	62 <sup>e</sup>	N	13.3
11	allylamine	<b>3l</b>	1/0	374	3650	12	35 <sup>e</sup>	N	12.5
12	3-aminopropanol	<b>3m</b>	1/1	361	4600	8	95 <sup>f</sup>	N	14.2

<sup>a</sup> Phthalimides GC-retention times (see Experimental). <sup>b</sup> Not detected. <sup>c</sup> A complex mixture of products was obtained resulting from the decomposition of starting materials. <sup>d</sup> Yields of the corresponding pure decarboxylated phthalimide, *i.e.* in entry 7: *N*-phenylphthalimide, **3b**; entry 8: *N*-(2-ethylphenyl)phthalimide, **3i**; entry 9: *N*-methylphthalimide, **3j**. <sup>e</sup> Product isolated after extraction of the reaction mixture with  $\text{Et}_2\text{O}$ . <sup>f</sup> Yield calculated by GC with *N*-(3-hydroxypropyl)phthalimide as standard.

decarboxylated. Thus, 4-aminobenzoic acid, glycine and L-phenylalanine yielded selectively *N*-phenylphthalimide (64%), *N*-(2-ethylphenyl)phthalimide (86%) and *N*-methylphthalimide (76%), respectively. It is likely that the phthalimides, or more probably the amino acids, do not survive under our experimental conditions. Recent studies on the hydrothermal stability of amino acids indicate that temperatures greater than 250 °C are not favourable.<sup>41</sup> Although decarboxylation occurs, the use of amino acids with this method could be an interesting approach to synthesise phthalimides that could not be obtained *via* more traditional routes.

When butylamine or allylamine were used as substrates, pure H<sub>2</sub>O was used as the solvent because the products were soluble in 1/1 v/v H<sub>2</sub>O/EtOH. The resulting *N*-butyl and *N*-allylphthalimides were obtained as white powders, but GC analysis of the filtrate indicated that some of the product remained in the aqueous phase. Therefore, to achieve reasonable yields of the corresponding phthalimides, the aqueous solution was extracted with Et<sub>2</sub>O. In the case of allylamine, the yield was low (35%). This was probably due to polymerisation or degradation of the starting material. Better yields were obtained with butylamine (62%) and especially with 3-amino-propanol (95%).

## Conclusions

Although the method presented here cannot be applied universally, it provides a rapid and good-yielding synthesis of some potentially interesting phthalimide derivatives in HTHP-H<sub>2</sub>O/EtOH mixtures. This research has delivered a promising alternative approach compared to conventional methods. Water is the only by-product and there is no need for environmentally less benign organic solvents or any additional catalyst or reagents. Such a reaction has a low E-factor and high atom efficiency. A 1/1 v/v H<sub>2</sub>O/EtOH mixture shows promise as a “reaction/crystallisation” solvent, which gives a rapid and clean method for obtaining crystalline products sufficiently pure for further needs. It is likely that the method could be extended to aliphatic dicarboxylic acids, *e.g.* maleic acid, to increase the range of imides that can be synthesised in HTHP systems.

## Experimental

**Caution:** these reactions involve high pressures and must only be carried out in an apparatus with the appropriate pressure rating at the reaction temperature. A thorough safety assessment must be made.

All chemicals were obtained from Aldrich or Lancaster Synthesis. H<sub>2</sub>O was deionised and degassed (by boiling) prior to charging the vessel. All experiments were performed in a thick-walled, stainless steel (316SS) batch vessel reactor of 10 mL volume, developed at the University of Nottingham as previously described.<sup>33</sup> The apparatus incorporates design features to minimise the hazard of high pressure experiments, and no experiment was performed above the maximum pressure or temperature ratings. The pressure inside the vessel was generated autogenically by the amount of H<sub>2</sub>O/EtOH charged to the vessel and its temperature. In theory, it is

possible to obtain a desired pressure by adding an amount of H<sub>2</sub>O calculated by multiplying the vessel volume and the density (of H<sub>2</sub>O at the desired temperature). However, in practice the addition of organic compounds and EtOH usually results in a discrepancy between the calculated and actual pressures. The reactor has a maximum pressure rating of 60 MPa at 400 °C, and should not be charged with more than 6 mL of H<sub>2</sub>O.<sup>33</sup> It was found that using 5 mL of H<sub>2</sub>O (or H<sub>2</sub>O/EtOH) gave acceptable pressures. The reactor was fitted with an internal thermocouple which was connected to a temperature display, allowing real time in-situ monitoring of the temperature (see Fig. 3). During the course of an experiment, the temperature and pressures were recorded every 30 s. The reactor was placed in an aluminium pot surrounded by a heating jacket (200 W, Watlow<sup>TM</sup>) that allowed rapid heating from room temperature to supercritical conditions in ≤15 min. Cooling was achieved with a steady flow of H<sub>2</sub>O through a coil around a second pot, and the vessel could be returned to ambient conditions in 10–15 min.

A typical reaction procedure for the synthesis of phthalimides was as follows: into the thick-walled reactor (10 mL volume) were placed 332 mg *o*-phthalic acid (2 mmol), 2.5 mL of deionised, degassed H<sub>2</sub>O and 2.5 mL of EtOH. An equimolar amount of the desired amine was then added. The heater was pre-heated to 420 °C and the reactor was then heated for a specific length of time, rather than to a particular temperature. Once the reactor had been heated for the required time, it was placed in the cooling pot and allowed to return to ambient temperature and pressure. A typical temperature and pressure profile is given in Fig. 3. The solution was then left in the autoclave at room temperature for 24 h to allow crystals sufficient time to grow. The contents were then filtered and washed with either 1/1 v/v H<sub>2</sub>O/EtOH mixture or pure H<sub>2</sub>O. Resulting crystals were dried under vacuum for an appropriate amount of time.

Analysis was carried out using GC and <sup>1</sup>H NMR spectroscopy with a 300 MHz Bruker<sup>TM</sup> DPX300. Both the purity of the isolated phthalimides and the filtrate were analysed by GC using an Alltech EC<sup>TM</sup>-1 column (30 m and 0.32 mm i.d. polydimethylsiloxane stationary phase) on a Perkin-Elmer Autosystem GC with a flame ionisation detector (FID). He gas (12 psi) was the mobile phase and the injection volume was 1 µL. The initial temperature was 100 °C and isothermal conditions were maintained for the first 5 min and the temperature was then ramped at a rate of 20 °C min<sup>-1</sup> to 300 °C. Isothermal conditions were maintained for the final 5 min.

Melting points were recorded using a Gallenkamp melting point apparatus.

### *N*-Benzylphthalimide, 3a

Mp 112 °C (lit.,<sup>42</sup> 110–116 °C); δ<sub>H</sub> (300 MHz, acetone-*d*<sub>6</sub>) 4.85 (s, 2H, CH<sub>2</sub>N), 7.27–7.42 (m, 5H, ArH), 7.85–7.89 (m, 4H, ArH).

### *N*-Phenylphthalimide, 3b

Mp 205 °C (lit.,<sup>43</sup> 205 °C); δ<sub>H</sub> (300 MHz, acetone-*d*<sub>6</sub>) 7.45–7.56 (m, 5H, ArH), 7.92–8.99 (m, 5H, ArH).

***N*-(4-Hydroxyphenyl)phthalimide, 3c**

Mp 298 °C (lit.,<sup>44</sup> 294 °C);  $\delta_{\text{H}}$  (300 MHz, acetone- $d_6$ ) 6.98 (d, 2H, ArH), 7.31 (d, 2H, ArH), 7.89–7.96 (m, 4H, ArH), 8.70 (s, 1H, OH).

***N*-(4-Bromophenyl)phthalimide, 3d**

Mp 191 °C, possibly not pure (lit.,<sup>15</sup> 206 °C);  $\delta_{\text{H}}$  (300 MHz,  $\text{CDCl}_3$ ) 7.39 (d, 2H, ArH), 7.67 (d, 2H, ArH), 7.80–7.84 (m, 2H, ArH), 7.98–7.99 (m, 2H, ArH).

***N*-(2-Pyridylmethyl)phthalimide, 3e**

Mp 124 °C (lit.,<sup>3</sup> 124 °C);  $\delta_{\text{H}}$  (300 MHz,  $\text{CDCl}_3$ ) 5.04 (s, 2H,  $\text{CH}_2$ ), 7.18–7.28 (m, 1H, ArH), 7.30 (d, 1H, ArH), 7.65–7.68 (m, 1H, ArH), 7.70–7.73 (m, 2H, ArH), 7.74–7.75 (m, 2H, ArH), 7.89–7.90 (d, 1H, ArH).

***N*-(4-Aminophenyl)phthalimide, 3f**

Mp 244 °C (lit.,<sup>12</sup> 245 °C);  $\delta_{\text{H}}$  (300 MHz, acetone- $d_6$ ) 4.89 (broad s, 2H,  $\text{NH}_2$ ), 6.78 (d, 2H, ArH), 7.13 (d, 2H, ArH), 7.86–7.91 (m, 4H, ArH).

***N*-(2-Phenylethyl)phthalimide, 3i**

Mp 126 °C (lit.,<sup>45</sup> 128 °C);  $\delta_{\text{H}}$  (300 MHz,  $\text{CDCl}_3$ ) 3.01 (t, 2H,  $\text{CH}_2$ ), 3.94 (t, 2H,  $\text{CH}_2$ ), 7.28 (m, 5H, ArH), 7.71–7.73 (m, 2H, ArH), 7.84–7.86 (m, 2H, ArH).

***N*-Methylphthalimide, 3j**

Mp 132 °C (lit.,<sup>46</sup> 134 °C);  $\delta_{\text{H}}$  (300 MHz, acetone- $d_6$ ) 3.12 (s, 3H,  $\text{CH}_3$ ), 7.84 (s, 4H, ArH).

***N*-Butylphthalimide, 3k**

Mp 35 °C (lit.,<sup>47</sup> 35 °C);  $\delta_{\text{H}}$  (300 MHz, acetone- $d_6$ ) 0.96 (t, 3H,  $\text{CH}_3$ ), 1.31–1.44 (m, 2H,  $\text{CH}_2$ ), 1.62–1.77 (m, 2H,  $\text{CH}_2$ ), 3.69 (t, 2H,  $\text{NCH}_2$ ), 7.70–7.72 (m, 2H, ArH), 7.84–7.93 (m, 2H, ArH).

***N*-Allylphthalimide, 3l**

Mp 69 °C (lit.,<sup>48</sup> 69–71 °C);  $\delta_{\text{H}}$  (300 MHz, acetone- $d_6$ ) 4.30 (d, 2H,  $\text{NCH}_2$ ), 5.24 (d, 2H,  $\text{CH}_2$ ), 5.86–5.95 (m, 1H, CH), 7.72–7.77 (m, 2H, ArH), 7.84–7.89 (m, 2H, ArH).

***N*-(3-Hydroxypropyl)phthalimide, 3m**

Mp 74 °C (lit.,<sup>49</sup> 74–75 °C);  $\delta_{\text{H}}$  (300 MHz,  $\text{CDCl}_3$ ) 1.89–1.92 (quint, 2H,  $\text{CH}_2$ ), 3.63 (t, 2H,  $\text{CH}_2$ ), 3.74 (t, 1H, OH), 3.80–3.89 (t, 2H,  $\text{CH}_2\text{OH}$ ), 7.78–7.75 (m, 2H, ArH), 7.84–7.88 (m, 2H, ArH).

**Acknowledgements**

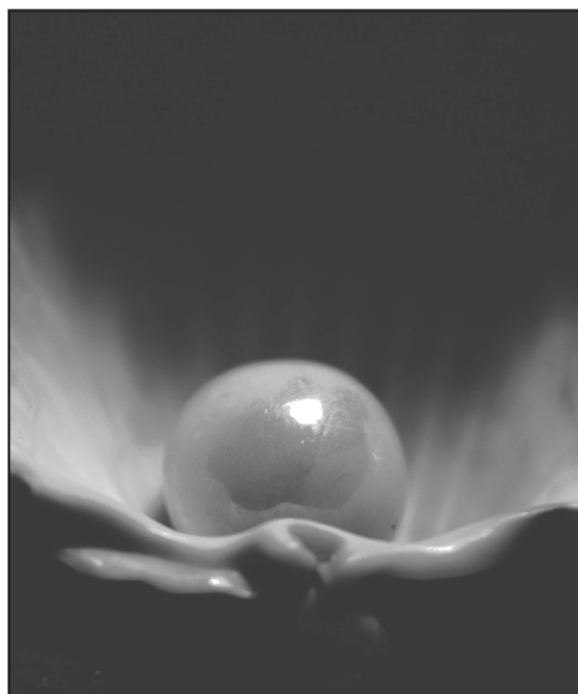
We thank Dr P. A. Hamley, Dr J. Ke and M. Thomas for help and advice. We thank the School of Chemistry of The University of Nottingham, the ERASMUS exchange programme and Prof. E. Sultan Giray for collaboration with the University of Çukurova, Adana, Turkey. We are also grateful to M. Guyler, R. Wilson and P. A. Fields from the workshops

in the School of Chemistry at The University of Nottingham for assistance on technical and engineering issues.

**References**

- 1 A. A. Abdel-Hafez, *Arch. Pharm. Res.*, 2004, **27**, 495.
- 2 L. M. Lima, P. Castro, A. L. Machado, C. A. M. Fraga, C. Lugnier, V. L. Gonçalves de Moraes and E. J. Barreiro, *Bioorg. Med. Chem.*, 2002, **10**, 3067.
- 3 X. Collin, J. Robert, G. Wielgosz, G. Le Baut, C. Bobin-Dubigeon, N. Grimaud and J. Petit, *Eur. J. Med. Chem.*, 2001, **36**, 639.
- 4 W. C. Groutas, L. S. Chong, R. Venkataraman, R. Kuang, J. B. Epp, N. Houser-Archfield, H. Huang and J. R. Hoidal, *Arch. Biochem. Biophys.*, 1996, **332**, 335.
- 5 R. Antunes, H. Buttista and R. M. Strivastuva, *Bioorg. Med. Chem. Lett.*, 1998, **8**, 3071.
- 6 S. Kawagushi and O. Ikeda, *Jpn. Pat. Appl.* JP2001328911, 2001.
- 7 K. Ebihara, T. Oora, M. Nakaya, S. Shiraishi and N. Yasui, *Jpn. Pat. Appl.* JP08245585, 1996.
- 8 C. J. Perry and Z. Parveen, *J. Chem. Soc., Perkin Trans. 2*, 2001, 512.
- 9 L. M. Lima, F. C. F. de Brito, S. D. de Souza, A. L. P. Miranda, C. R. Rodrigues, C. A. M. Fraga and E. J. Barreiro, *Bioorg. Med. Chem.*, 2002, **12**, 1533.
- 10 C. Zhang, Q. Ping, H. Zhang and J. Shen, *Eur. Polym. J.*, 2003, **39**, 1629.
- 11 R. W. Sinkeldam, M. H. C. J. van Houtem, G. Koeckelberghs, J. A. J. M. Vekemans and E. W. Meijer, *Org. Lett.*, 2006, **8**, 383.
- 12 M. M. Heravi, R. H. Shoar and L. Pedram, *J. Mol. Catal. A: Chem.*, 2005, **231**, 89.
- 13 K. Mogilaiah and G. R. Reddy, *Indian J. Chem., Sect. B: Org. Chem. Incl. Med. Chem.*, 2004, **43**, 882.
- 14 B. Martin, H. Sekljic and C. Chassaing, *Org. Lett.*, 2003, **5**, 1851.
- 15 H. Li, J. Zhang, Y. Zhau and T. Li, *Synth. Commun.*, 2002, **32**, 927.
- 16 T. Vidal, A. Petit, A. Loupy and R. N. Gedye, *Tetrahedron*, 2000, **56**, 5473.
- 17 H. N. Borah, R. C. Boruah and J. S. Sandhu, *J. Chem. Res. (S)*, 1998, S272.
- 18 E. Hoffmann and H. Schiff-Schenav, *J. Org. Chem.*, 1962, **27**, 4686.
- 19 N. Barooah, R. J. Sarna, A. S. Batsanov and J. B. Baruah, *J. Mol. Struct.*, 2006, **791**, 122.
- 20 J. B. Tingle and H. F. Rolker, *J. Am. Chem. Soc.*, 1908, **30**, 1882.
- 21 M. K. Gosh and K. L. Mittal, *Polyimides, fundamentals and application*, Marcel Dekker Inc., New York, 1996.
- 22 S. I. Zav'yalov, O. V. Dorofeeva, E. E. Rumyantseva, L. B. Kulikova, G. I. Ezhova, N. E. Kravchenko and A. G. Zavozin, *Pharm. Chem. J.*, 2002, **36**, 440.
- 23 A. A. Plenzha and S. E. Severin, *Izv. Akad. Nauk SSSR, Ser. Khim.*, 1966, **5–6**, 861.
- 24 D. V. Jacob, R. J. Kunnath and M. Lopez, *Res. J. Chem. Environ.*, 2006, **10**, 45.
- 25 W. C. Bell, K. S. Booksh and M. L. Myrick, *Anal. Chem.*, 1998, **70**, 332.
- 26 E. Garcia-Verdugo, J. Fraga-Dubreuil, P. A. Hamley, W. B. Thomas, K. Whiston and M. Poliakoff, *Green Chem.*, 2005, **7**, 294.
- 27 E. Garcia-Verdugo, E. Vernardou, W. B. Thomas, K. Whiston, W. Partenheimer, P. A. Hamley and M. Poliakoff, *Adv. Synth. Catal.*, 2004, **346**, 307.
- 28 J. W. Verbicky and L. Williams, Jr., *J. Org. Chem.*, 1981, **46**, 175.
- 29 D. V. Ramana, T. E. Yuvaraj and K. R. Reddy, *Indian J. Heterocycl. Chem.*, 2002, **12**, 103.
- 30 J. Fraga-Dubreuil and M. Poliakoff, *Pure Appl. Chem.*, 2006, **78**, 1971.
- 31 A. Kruse and E. Dinjus, *J. Supercrit. Fluids*, 2007, **39**, 362.
- 32 C. R. Strauss and R. W. Trainer, *Aust. J. Chem.*, 1998, **51**, 703.
- 33 L. M. Dudd, E. Vernardou, E. G. Verdugo, P. Licence, A. J. Blake, C. Wilson and M. Poliakoff, *Green Chem.*, 2003, **5**, 187.
- 34 (a) N. Karbass, V. Sans, E. Garcia-Verdugo, M. Isabel Burguete and V. Luis Santiago, *Chem. Commun.*, 2006, 3095; (b) R. E. N. Castro, G. J. Vidotti, A. F. Rubira and E. C. Muniz,

- J. Appl. Polym. Sci.*, 2006, **101**, 2009; (c) T. Nakagawa, H. Ozaki, T. Kamitanaka, H. Takagi, T. Matsuda, T. Kitamura and T. Harada, *J. Supercrit. Fluids*, 2003, **27**, 255; (d) J. Lu, E. C. Boughner, C. L. Liotta and C. A. Eckert, *Fluid Phase Equilib.*, 2002, **37**, 198.
- 35 (a) A. R. Bazaev, I. M. Abdulagatov, E. A. Bazaev and A. Abdurashidova, *J. Chem. Thermodyn.*, 2007, **39**, 385; (b) F. B. David and B. F. Dodge, *J. Chem. Eng. Data*, 1959, **4**, 107.
- 36 B. Ren, C. Hou, H. Chong, W. Li and H. Song, *J. Chem. Eng. Data*, 2006, **51**, 2022.
- 37 A. Apelblat, E. Manzurola and N. A. Balal, *J. Chem. Thermodyn.*, 2006, **38**, 565.
- 38 N. S. Magomedova, M. G. Neigauz, V. E. Zavodnik and V. K. Bel'skii, *Sov. Phys. Crystallogr.*, 1981, **26**, 475.
- 39 K. D. Warzecha, J. Lex and A. G. Griesbeck, *Acta Crystallogr., Sect. A: Found. Crystallogr.*, 2006, **62**, 2367.
- 40 K. Kownacki, L. Kaczmarek and A. Grabowska, *Chem. Phys. Lett.*, 1993, **210**, 373.
- 41 M. Ito, L. P. Gupta, H. Masuda and H. Kawahata, *Org. Geochem.*, 2006, **37**, 177.
- 42 *Handbook of Chemistry and Physics*, 47th edition, ed. R. C. Weast and S. M. Selby, The Chemical Rubber Co., Cleveland, OH, 1966, B-229.
- 43 R. G. R. Bacon and A. Karim, *J. Chem. Soc., Perkin Trans. 1*, 1973, **1**, 272.
- 44 M. L. Sherrill, F. L. Schaeffer and E. P. Shoyer, *J. Am. Chem. Soc.*, 1928, **50**, 474.
- 45 K. D. Warzecha, J. Lex, J. M. Neudoerfl and A. G. Griesbeck, *Acta Crystallogr., Sect. A: Found. Crystallogr.*, 2006, **62**, 1580.
- 46 M. V. Roux, P. Jimenez, M. A. Martin-Luengo, J. Z. Davalos, Z. Sun, R. S. Hosmane and J. F. Liebman, *J. Org. Chem.*, 1997, **62**, 2732.
- 47 N. S. Pawar, S. B. Attarde, D. S. Dalal, G. R. Sonar, U. R. Kapadi, D. G. Hundiware and P. P. Kumbhar, *J. Indian Council Chem.*, 2001, **18**, 29.
- 48 G. J. Hitchings, M. Helliwell and J. M. J. Vernon, *J. Chem. Soc., Perkin Trans. 1*, 1990, **1**, 83.
- 49 Y. Sato, H. Nakai, M. Wada, H. Ogiwara, T. Mizoguchi, Y. Migita, Y. Hatanaka and Y. Kanaoka, *Chem. Pharm. Bull.*, 1982, **30**, 1639.



## Looking for that **special** research paper from applied and technological aspects of the chemical sciences?

TRY this free news service:

### Chemical Technology

- highlights of newsworthy and significant advances in chemical technology from across RSC journals
- free online access
- updated daily
- free access to the original research paper from every online article
- also available as a free print supplement in selected RSC journals.\*

\*A separately issued print subscription is also available.

Registered Charity Number: 207890

RSCPublishing

[www.rsc.org/chemicaltechnology](http://www.rsc.org/chemicaltechnology)

22030683

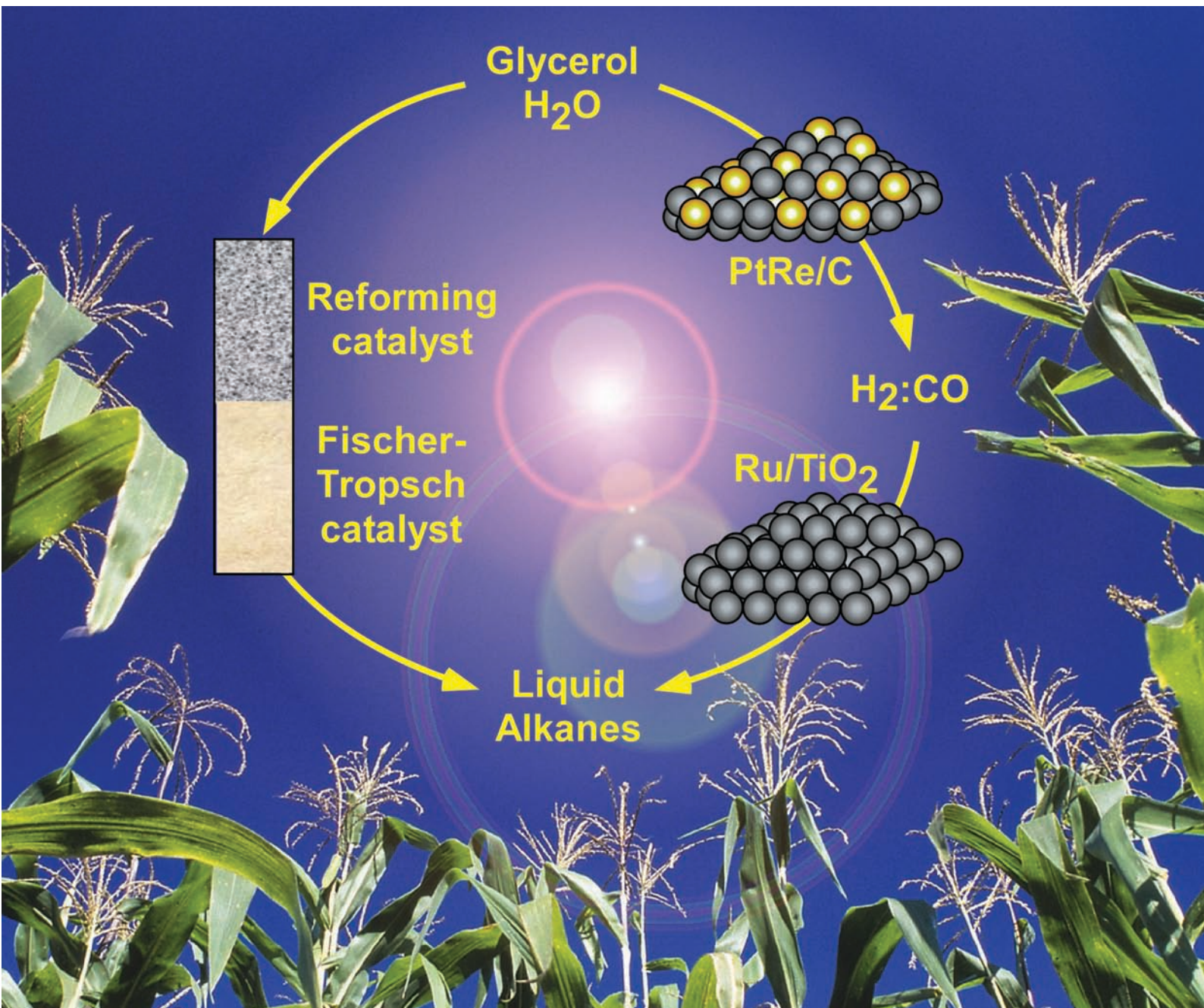


# Green Chemistry

Cutting-edge research for a greener sustainable future

[www.rsc.org/greenchem](http://www.rsc.org/greenchem)

Volume 9 | Number 10 | October 2007 | Pages 1029–1144



ISSN 1463-9262

Chen *et al.*  
Efficient and controlled  
polymerization of lactide

Simonetti *et al.*  
Coupling of glycerol processing with  
Fischer–Tropsch synthesis

Mack *et al.*  
Solvent-free method for the  
reduction of esters

Sheldrake and Schleck  
Dicationic molten salts as re-usable  
media for pyrolysis of cellulose



1463-9262(2007)9:10;1-T

RSC Publishing

# Coupling of glycerol processing with Fischer–Tropsch synthesis for production of liquid fuels

Dante A. Simonetti,<sup>a</sup> Jeppe Rass-Hansen,<sup>ab</sup> Edward L. Kunkes,<sup>a</sup> Ricardo R. Soares<sup>ac</sup> and James A. Dumesic<sup>\*a</sup>

Received 23rd March 2007, Accepted 4th June 2007

First published as an Advance Article on the web 22nd June 2007

DOI: 10.1039/b704476c

Liquid alkanes can be produced directly from glycerol by an integrated process involving catalytic conversion to H<sub>2</sub>/CO gas mixtures (synthesis gas) combined with Fischer–Tropsch synthesis. Synthesis gas can be produced at high rates and selectivities suitable for Fischer–Tropsch synthesis (H<sub>2</sub>/CO between 1.0 and 1.6) from concentrated glycerol feed solutions at low temperatures (548 K) and high pressures (1–17 bar) over a 10 wt% Pt–Re/C catalyst with an atomic Pt : Re ratio of 1 : 1. The primary oxygenated hydrocarbon intermediates formed during conversion of glycerol to synthesis gas are ethanol, acetone, and acetol. Fischer–Tropsch synthesis experiments at 548 K and 5 bar over a Ru-based catalyst reveal that water, ethanol, and acetone in the synthesis gas feed have only small effects, whereas acetol can participate in Fischer–Tropsch chain growth, forming pentanones, hexanones, and heptanones in the liquid organic effluent stream and increasing the selectivity to C<sub>5+</sub> alkanes by a factor of 2 (from 0.30 to 0.60). Catalytic conversion of glycerol and Fischer–Tropsch synthesis were coupled in a two-bed reactor system consisting of a Pt–Re/C catalyst bed followed by a Ru/TiO<sub>2</sub> catalyst bed. This combined process produced liquid alkanes with S<sub>C5+</sub> between 0.63 and 0.75 at 548 K and pressures between 5 and 17 bar, with more than 40% of the carbon in the products contained in the organic liquid phase at 17 bar. The aqueous liquid effluent from the integrated process contains between 5 and 15 wt% methanol, ethanol, and acetone, which can be separated from the water by distillation and used in the chemical industry or recycled for conversion to gaseous products. This integrated process has the potential to improve the economics of “green” Fischer–Tropsch synthesis by reducing capital costs and increasing thermal efficiency. Importantly, the coupling between glycerol conversion to synthesis gas and Fischer–Tropsch synthesis leads to synergies in the operations of these processes, such as (i) avoiding the highly endothermic and exothermic steps that would result from the separate operation of these processes and (ii) eliminating the need to condense water and oxygenated hydrocarbon byproducts between the catalyst beds.

## Introduction

Petroleum currently provides a significant fraction (~37%) of the world's energy.<sup>1</sup> In the United States, the total consumption of petroleum corresponds to about 7.5 billion barrels of oil equivalent each year ( $43 \times 10^{15}$  BTU), and almost 70% of this petroleum is consumed by the transportation sector. Indeed, more than 95% of the energy used by the transportation sector is provided by petroleum.<sup>2</sup> Because the proven reserves of petroleum are projected to be exhausted within the next half-century,<sup>2</sup> it is becoming important to develop alternative sources of transportation fuels. Biomass is an intriguing candidate in this respect because it is renewable, and the processing of biomass is CO<sub>2</sub> neutral.<sup>3</sup> Importantly, the amount of biomass grown annually in the U.S. is sufficient to

provide energy for approximately 70% of the transportation sector, provided that this biomass can be converted to clean-burning fuels having high energy densities, such as currently provided by petroleum. In particular, it is estimated that the U.S. could produce 1.3 billion dry tons of biomass per year without major changes in agricultural practices and still meet its food, feed, and export demands;<sup>4</sup> and this amount of biomass corresponds to approximately  $3.5 \times 10^9$  barrels of oil equivalent each year.

Biomass is comprised primarily of carbohydrates (e.g., starch and cellulose),<sup>3</sup> and one method to convert these compounds to liquid fuels is by fermentation to produce liquid alcohols, such as ethanol and butanol. The technology to convert grain-derived starches to ethanol by the combination of hydrolysis, fermentation, and distillation is well established,<sup>5,6</sup> and advances are being made in the cost-effective conversion of lignocellulosics to ethanol (e.g., through the development of new enzymes for cellulose hydrolysis).<sup>7–10</sup> The advantages of ethanol as a transportation fuel are that it is a liquid and it has a high octane number (i.e., research octane number of 130);<sup>11</sup> however, ethanol has the following disadvantages as a fuel: (i) it has a lower energy density compared

<sup>a</sup>Department of Chemical and Biological Engineering, University of Wisconsin, 1415 Engineering Drive, Madison, WI 53706, USA.

E-mail: dumesic@engr.wisc.edu; Fax: +1 608 262 5434

<sup>b</sup>Center for Sustainable and Green Chemistry, Technical University of Denmark, Department of Chemistry, DK-2800, Lyngby, Denmark

<sup>c</sup>Faculdade de Engenharia Química, Universidade Federal de Uberlândia, Av. João Naves de Ávila 2121, Uberlândia, MG 38408-100, Brasil



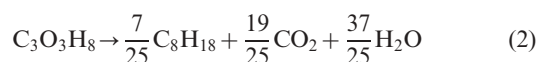
to petroleum (*i.e.*, approximately  $20 \times 10^3$  BTU  $l^{-1}$  for ethanol versus  $30 \times 10^3$  BTU  $l^{-1}$  for petroleum),<sup>12</sup> (ii) it is completely miscible with water, leading to significant absorption of water into the fuel, and (iii) it has a relatively low boiling point (346 K), leading to excessive evaporation at elevated temperatures. Importantly, the fermentation process used to produce bio-ethanol from carbohydrates leads to an aqueous solution containing only 5–10 wt% ethanol, and significant expenditure of energy is required to produce fuel-grade ethanol by distillation of this rather dilute aqueous solution.<sup>6,13</sup> Indeed, the overall energy balance for production of bio-ethanol is not very favorable, and it has been estimated that the amount of energy required to produce bio-ethanol is approximately equal to (or greater than) the energy-content of the ethanol produced.<sup>5,6,14,15</sup>

Long-chain alkanes comprise the vast majority of components in transportation fuels from petroleum (branched for gasoline and linear for diesel), and the conversion of renewable biomass resources to liquid alkanes thus represents an attractive processing option. For example, the liquid alkanes from such a conversion (i) can be distributed using infrastructure already employed for petroleum products, (ii) can be added to the existing petroleum pool for further processing, and (iii) can be combusted without alterations in existing engines. The production of liquid alkanes from biomass typically occurs by gasification of biomass to produce synthesis gas ( $H_2/CO$ ) followed by Fischer–Tropsch synthesis.<sup>16,17</sup> However, both conventional Fischer–Tropsch synthesis (*i.e.*, using coal or natural gas) and “green” Fischer–Tropsch synthesis (using biomass) have similar economic disadvantages, specifically, high capital and operating costs, of which greater than 50% stems from synthesis gas generation.<sup>18,19</sup> Also, Fischer–Tropsch synthesis processes suffer from low thermal efficiency.<sup>18,19</sup> Because of these limitations, liquid alkane production by Fischer–Tropsch synthesis becomes economically viable only at large scales.<sup>16–19</sup> Indeed, improvements in synthesis gas generation and thermal efficiency are necessary to improve the economics of Fischer–Tropsch synthesis processes.<sup>16,17,19</sup>

We have recently reported that glycerol can be converted to synthesis gas at high rates and selectivities at temperatures from 498 to 620 K according to eqn (1).<sup>20</sup>



This glycerol can be derived from fermentation of glucose,<sup>21</sup> from hydrogenolysis of sorbitol,<sup>22</sup> or as a waste product from the transesterification of plant oils and animal fats.<sup>23</sup> Operation at low temperatures provides the opportunity to couple this endothermic glycerol conversion with exothermic Fischer–Tropsch synthesis to produce liquid transportation fuels *via* the following integrated process:<sup>20</sup>



This integrated process can potentially improve the economics of “green” Fischer–Tropsch synthesis by reducing costs associated with synthesis gas production, for example, by eliminating the need for an  $O_2$ -blown auto-thermal reformer or biomass gasifier.<sup>16–20</sup> Also, our process presents the

opportunity for reducing the size of the Fischer–Tropsch synthesis reactor by producing an undiluted synthesis gas stream and for eliminating subsequent cleaning steps required for synthesis gas produced from biomass gasification.<sup>16–18,20</sup> A reduction in capital costs may result in reduced operation and maintenance costs as well.<sup>17</sup> Accordingly, our integrated process potentially allows for smaller scale Fischer–Tropsch synthesis plants to produce liquid fuels from biomass, which is an advantage for distributed biomass resources. In addition, the low temperature of our glycerol conversion process allows for potential thermal coupling with the Fischer–Tropsch synthesis reaction, thereby increasing thermal efficiency.<sup>20</sup> Furthermore, the coupling between these processes may lead to chemical synergies related to the presence of chemical species from both reactions in the same reactor. For example, the intermediates produced from glycerol conversion (*e.g.*, acetol) can enter the growing hydrocarbon chain on the Fischer–Tropsch catalyst sites. Fig. 1 shows a process schematic which illustrates this integrated process as well as potential end-uses for each of the three product phases. The gaseous product stream consisting of light alkanes can be combusted to produce heat and electricity while the oxygenated hydrocarbons in the aqueous phase effluent can be separated by distillation for use in the chemical industry. Importantly, the oil phase containing liquid alkanes can be upgraded to gasoline and diesel fuel.

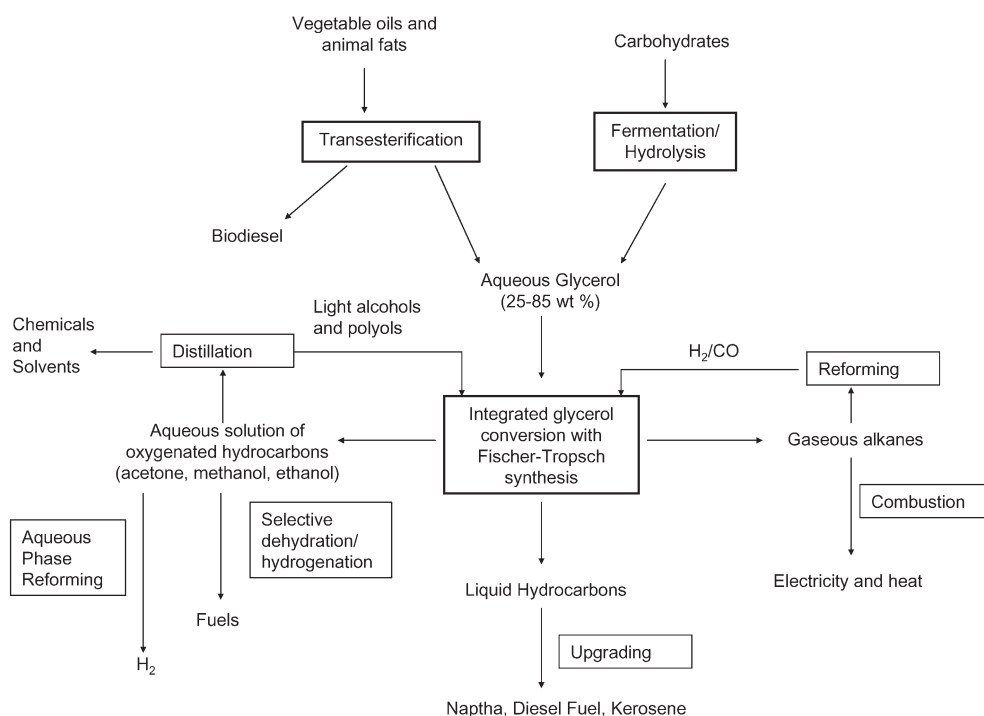
In this study, we demonstrate the formation of liquid fuels by the integration of glycerol conversion with Fischer–Tropsch synthesis. We conduct reaction kinetics studies at different pressures and glycerol feed concentrations to demonstrate that glycerol conversion produces synthesis gas suitable for Fischer–Tropsch synthesis at moderate pressures (*e.g.*, 17 bar) and using concentrated glycerol feeds (*e.g.*, 80 wt%). Furthermore, we conduct Fischer–Tropsch synthesis studies to investigate the effects of water and oxygenated hydrocarbons on the selectivity and activity of an Ru-based Fischer–Tropsch synthesis catalyst. Finally, we show that liquid alkanes can be produced directly from glycerol by conversion to synthesis gas combined with Fischer–Tropsch synthesis in a two-bed reactor system.

## Experimental

### Catalyst preparation and characterization

Glycerol conversion studies were carried out using a Pt–Re/C catalyst that was prepared by incipient wetness impregnation of carbon black (Vulcan XC-72) with an aqueous solution of  $H_2PtCl_6 \cdot 6H_2O$  (Sigma–Aldrich) and  $HReO_4$  (Strem Chemicals) to yield a catalyst with loadings of 5.1 wt% Pt and 4.9 wt% Re (atomic Pt : Re ratio of 1 : 1). The support was dried in air for 12 h at 373 K prior to impregnation, and 1.7 g of solution was used per gram of support. The catalyst was dried at 403 K for 12 h in air prior to activation. Several Ru/TiO<sub>2</sub> catalysts (1.0 wt% and 2.9 wt%) were prepared for Fischer–Tropsch synthesis according to the methods described by Iglesia *et al.*<sup>24</sup>

Prior to reaction kinetics studies or gas adsorption measurements (*i.e.*, CO and  $O_2$  chemisorption), the Pt–Re/C catalyst was reduced at 723 K (ramp rate of 0.5 K  $min^{-1}$ ) for 2 h in flowing  $H_2$  (140  $cm^3$ (NTP)  $min^{-1}$ ). The Ru/TiO<sub>2</sub>



**Fig. 1** Process pathway for production of liquid fuels from biomass by integrated glycerol conversion to synthesis gas and Fischer–Tropsch synthesis.

catalysts were reduced *in-situ* before reaction kinetics studies and gas adsorption measurements. The gas hourly space velocity (GHSV) was calculated for Fischer–Tropsch synthesis experiments using the total volumetric flowrate of gas (at standard conditions) to the reactor and a bed density of  $0.175 \text{ g cm}^{-3}$  (g catalyst per total bed volume) for Ru/TiO<sub>2</sub> catalyst diluted with an equal volume of crushed SiO<sub>2</sub> granules. The weight hourly space velocity (WHSV) was calculated for glycerol conversion experiments using the mass flowrate of glycerol into the reactor and the total mass of catalyst. The irreversible CO uptake of Pt–Re/C at 300 K was taken to be the number of catalytic sites ( $150 \mu\text{mol g}^{-1}$ ) and was measured using a standard gas adsorption apparatus described elsewhere.<sup>25</sup> This number of sites corresponds to a dispersion (molar CO : total metal ratio) of 29%. The dispersions of the Ru/TiO<sub>2</sub> catalysts were determined by chemisorption of O<sub>2</sub> at 195 K in a static chemisorption system.<sup>26</sup> Table 1 shows the properties of the Ru/TiO<sub>2</sub> catalysts, and these results are in agreement with similar catalysts studied by Iglesia *et al.*<sup>27</sup>

### Reaction kinetics measurements

The apparatus used to conduct reaction kinetics measurements for Pt–Re/C is described elsewhere.<sup>20</sup> Fresh catalyst was

loaded into a 12.7 mm (0.5 inch) outer diameter tubular stainless steel reactor with a wall thickness of 0.71 mm (0.028 inch). The catalyst bed was contained between an end plug of quartz wool (Alltech) and fused SiO<sub>2</sub> granules (–4 + 16 mesh; Sigma–Aldrich) which aid in vaporization of the liquid feed. The Pt–Re/C catalyst powder was mixed with an equal volume of SiO<sub>2</sub> granules to decrease the pressure drop across the catalyst bed. For experiments that combined glycerol conversion with Fischer–Tropsch synthesis, a bed of 1.0 wt% Ru/TiO<sub>2</sub> was mixed with an equal volume of crushed SiO<sub>2</sub> granules, and this bed was loaded downstream of the Pt–Re/C bed. The reactor was heated with a furnace consisting of a close fitting aluminum block heated externally by a well-insulated furnace (1450 W/115 V, Applied Test Systems series 3210). Type-K thermocouples (Omega) were attached to the outside of the reactor to measure reactor temperature, which was controlled with a series 16A type temperature controller (Dwyer Instruments). Fresh catalyst was reduced in flowing H<sub>2</sub>, as described previously. Mass-flow controllers (5850 Brooks Instruments) were used to control the flowrate of H<sub>2</sub>. An HPLC pump (Model 301, Alltech) was used to introduce the aqueous feed solution into a 6 inch needle with a point 5 style tip (Hamilton) soldered into a section of 3.2 mm (0.125 inch) outer diameter, stainless steel tubing, and this

**Table 1** Properties of Fischer–Tropsch catalysts

Ru loading (wt%)	BET surface area/m <sup>2</sup> g <sup>–1</sup>	Dispersion (O : Ru ratio)	Ru site density/10 <sup>16</sup> m <sup>–2</sup>	Average pellet radius/10 <sup>–4</sup> m	Average pore radius <sup>a</sup> /10 <sup>–10</sup> m	$\chi/10^{16} \text{ m}^{-1b}$
1.0	15	0.55	217	0.63	210	40
2.9	30	0.36	208	0.63	165	50

<sup>a</sup> Estimated from BET surface area measurement and values for similar catalysts studied by Iglesia, *et al.*<sup>27</sup> <sup>b</sup> Calculated as in ref. 27.



needle was positioned upstream of the Pt–Re/C catalyst bed. The liquid effluent was condensed in a gas-liquid separator and drained periodically for gas-chromatograph (GC) analysis (Agilent 6890 with a flame ionization detector (FID) and HP-Innowax column or Shimadzu GC-2010 with an FID detector and Rtx-5 column) and total organic carbon analysis (Shimadzu TOC-V CSH). Each effluent was tested for the presence of glycerol and other liquid byproducts. For runs that combined glycerol conversion with Fischer–Tropsch synthesis, the downstream system lines were heated to 373 K.

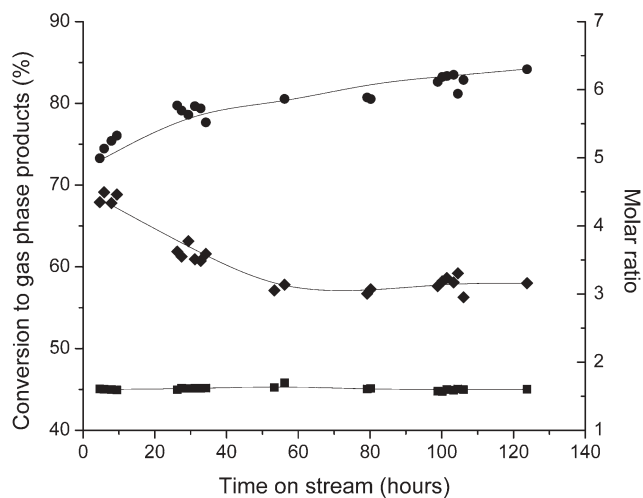
The effluent gas stream passed through a back-pressure regulator (GO Regulator, Model BP-60) which controlled the system pressure. The effluent gas was analyzed by gas chromatography:  $H_2$  with a Carle GC (series 8700) using a thermal conductivity detector (TCD), CO and  $CH_4$  using an HP 5890 GC with TCD and washed molecular sieve 5A 80/100 column (Alltech), and  $CO_2$  and light alkanes ( $C_2$ – $C_3$ ) using an HP 5890 GC with TCD and a Porapak QS 100/120 column (Alltech). All feed solutions were prepared by mixing glycerol (99.5%, ACS reagent, Sigma-Aldrich) with deionized water.

The apparatus used to conduct Fischer–Tropsch synthesis experiments is similar to the system used for reaction kinetics measurements of glycerol conversion over Pt–Re/C, except that the downstream lines from the reactor were heated to 373 K. The 2.9 wt% Ru/TiO<sub>2</sub> catalyst was mixed with an equal volume of crushed SiO<sub>2</sub> granules to help dissipate the heat generated by the exothermic Fischer–Tropsch reaction and loaded into a 12.7 mm (0.5 inch) outer diameter, stainless steel tubular reactor. The liquid phase products were collected in a gas-liquid separator and analyzed by GC (Shimadzu GC-2010 with an FID detector and Rtx-5 column). The effluent gas stream was analyzed for  $C_1$ – $C_{10}$  hydrocarbons with a Varian GC-MS (Saturn 3) using an FID detector and GS-Q capillary column.  $H_2$ , CO, and  $CO_2$  were analyzed using an HP 5890 GC with TCD and a Porapak QS 100/120 column (Alltech). Ultra-high purity CO and  $H_2$  (Linde) gases were mixed to give a synthesis gas feed with  $H_2 : CO \approx 2$ , and aqueous solutions of acetone, acetol, and ethanol were introduced into the reactor in a similar way as described above for glycerol conversion experiments.

## Results and discussion

### Glycerol conversion to synthesis gas

Fischer–Tropsch synthesis is typically operated at pressures between 5 and 20 bar,<sup>18</sup> and it is advantageous to carry out the conversion of glycerol to synthesis gas at these higher pressures to reduce compression costs. Accordingly, while our previous work investigated the performance of Pt–Re/C at atmospheric pressure,<sup>20</sup> in the present work we studied the production of synthesis gas at a pressure of 8.3 bar at 548 K over 10 wt% Pt–Re (atomic ratio 1 : 1)/C using a feed solution containing 30 wt% glycerol in water. Fig. 2 shows the conversion to gas phase products and the CO/ $CO_2$  and  $H_2$ /CO molar ratios for glycerol conditions at this elevated pressure. The total inlet flowrate of carbon (as glycerol) for this experiment was 833  $\mu\text{mol min}^{-1}$  (feed flowrate of 0.08  $\text{cm}^3 \text{min}^{-1}$ ), and the total conversion of glycerol was 90% (57% to gas phase products and 33% to liquid phase products). After a period of



**Fig. 2** Conversion to gas phase products (◆),  $CO/CO_2$  molar ratio (●), and  $H_2/CO$  molar ratio (■) for gas-phase processing of 30 wt% aqueous-glycerol feed at 548 K and 8.3 bar. Conversion to gas phase is calculated as (carbon atoms in gas phase product stream/total carbon into reactor as feed)  $\times 100$ . Reaction carried out using 0.08  $\text{cm}^3 \text{min}^{-1}$  of feed solution over 520 mg of catalyst (WHSV = 3.0  $\text{h}^{-1}$ ).

60 h, during which the conversion of glycerol to gas-phase products decreased from 68% to 57%, the catalyst showed excellent stability for an additional 60 h time on stream. The gas-phase effluent is comprised of synthesis gas with a  $H_2 : CO$  ratio equal to 1.6, which can be adjusted, if necessary, *via* the water-gas shift reaction to reach the stoichiometric 2 : 1 ratio appropriate for Fischer–Tropsch synthesis.<sup>20</sup> The balance of the gaseous products consists of  $CO_2$  ( $CO/CO_2$  molar ratio of 6) and light alkanes ( $C_1$ – $C_3$ , with a  $CO/\text{alkanes}$  carbon ratio of 10). At 548 K and 5 bar, the gas-phase product distribution and catalytic stability were similar, and the conversion to gas-phase products was 80%. The aqueous liquid effluent contained 15 wt% of oxygenated hydrocarbons (methanol, ethanol, *n*-propanol, ethylene glycol, 1,2 propanediol, acetone, and acetol), and the carbon balance closed to within 10% for this experiment.

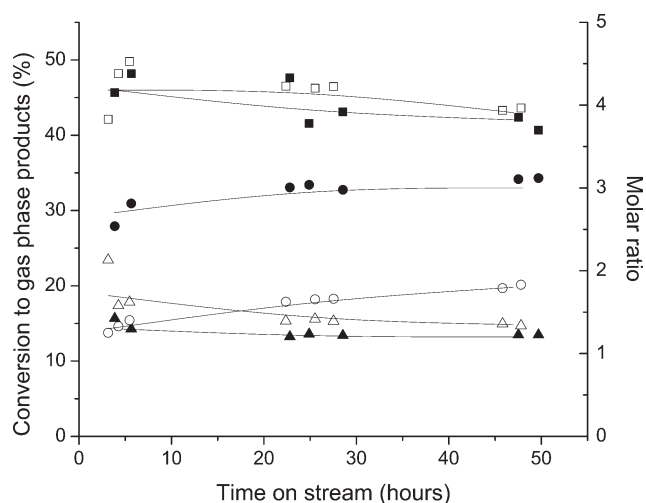
To couple the conversion of glycerol to synthesis gas with Fischer–Tropsch synthesis in a two-bed reactor system, it is necessary to expose the down-stream Fischer–Tropsch catalyst to water vapor from the aqueous glycerol feed. Iglesia *et al.* report that small amounts of water can, in fact, improve the performance of Co-based Fischer–Tropsch catalysts.<sup>28</sup> However, the highest water partial pressure in their study ( $P_{H_2O}/P_{CO} = 3$ ) was lower than that which results from conversion of a 30 wt% glycerol feed ( $P_{H_2O}/P_{CO} = 8$ ). Also, the studies by Iglesia *et al.* were conducted at higher total pressure (20 bar).<sup>28</sup> Therefore, it is advantageous to decrease the concentration of water in our system. Thus, we tested the Pt–Re/C catalyst for conversion of 50 wt% and 80 wt% glycerol solutions at pressures between 1 and 11 bar, and Table 2 shows the conversion to gas phase products as well as the  $H_2/CO$  and  $CO/CO_2$  molar ratios for these experiments. The conversion to gas phase products increases with decreasing concentration of glycerol in the feed at constant pressure and decreases with increasing pressure at constant feed

**Table 2** Performance of Pt–Re/C for conversion of concentrated solutions of glycerol in water to synthesis gas at various pressures. Reaction carried out over 1.0 g of catalyst at 548 K using  $\sim 0.04 \text{ cm}^3 \text{ min}^{-1}$  of feed (WHSV between 1.4 and  $1.7 \text{ h}^{-1}$ ). Conversion to gas phase products calculated as in Fig. 2

Feed concentration (wt%)	Pressure/bar	H <sub>2</sub> /CO	CO/CO <sub>2</sub>	Conversion to gas phase products (%)
80	1	1.4	23	86
50	1	1.6	11	96
80	5	1.2	13	56
50	5	1.5	7.8	76
80	11	1.0	5.0	44
50	11	1.4	2.7	55

concentration. The water gas shift activity increases at higher pressures and/or lower feed concentrations because of the increased partial pressure of H<sub>2</sub>O, as evidenced by the decrease in the CO : CO<sub>2</sub> ratio. These experiments were carried out at 548 K and pressures above the dew point for 50 wt% and 80 wt% glycerol feed solutions. Each condition tested showed stable operation for approximately 20 h time on stream, and there was only a 6% loss in activity after operation at 11 bar with 80 wt% glycerol feed. The liquid phase contained oxygenated hydrocarbon products similar to those for the conversion of a 30 wt% glycerol feed. Table 3 shows the carbon distributions for the conditions in Table 2. The primary gaseous carbon product is CO, while the aqueous liquid phase contains between 6 and 30 wt% oxygenated hydrocarbons when the conversion to gas phase products is less than 90%. The total conversion of glycerol was 100% for each condition.

The selectivity for production of C<sub>5+</sub> alkanes by Fischer–Tropsch synthesis typically increases at higher pressures. Therefore, we studied the conversion of glycerol to synthesis gas at 548 K for 11 and 17 bar, to test whether the Pt–Re/C catalyst would show good stability and selectivity at higher pressures with incomplete vaporization of the liquid feed. Fig. 3 shows the conversion to gas phase products and the H<sub>2</sub>/CO and CO/CO<sub>2</sub> molar ratios for 48 h time on stream. Lower CO/CO<sub>2</sub> ratios are observed at these higher pressures (as compared to glycerol conversion at 5 bar), indicating increased conversion of CO to CO<sub>2</sub> *via* water-gas shift. Furthermore, the conversion to gas phase products decreases (from 56% to 40%) when pressure increases to 11 or 17 bar. Thus, the Fischer–Tropsch catalyst in a two-bed system operating at 11 bar or



**Fig. 3** Conversion to gas phase products (squares), CO/CO<sub>2</sub> molar ratio (circles), and H<sub>2</sub>/CO molar ratio (triangles) for gas-phase processing of 80 wt% aqueous-glycerol feed at 548 K and 11 bar (closed symbols) and 17 bar (open symbols). Conversion to gas phase products calculated as in Fig. 2.

17 bar would be exposed to a large amount of oxygenated hydrocarbons from the aqueous-liquid effluent of the Pt–Re/C bed (*e.g.*, more than half of the carbon fed to the Pt–Re/C bed as glycerol). We note that the catalyst remains stable during this period of time at both pressures. The liquid phase product distributions at 11 and 17 bar contained 25 wt% and 29 wt% oxygenated hydrocarbons (methanol, ethanol, propanol, acetone, acetol, and propanediols), respectively.

The product distributions for the conversion of aqueous glycerol solutions at various pressures are consistent with the reaction scheme proposed by Cortright *et al.* for aqueous phase reforming of polyols, which consists of glycerol adsorption–dehydrogenation, C–C bond cleavage, and desorption of CO and H<sub>2</sub>.<sup>29</sup> Water-gas shift of adsorbed CO leads to CO<sub>2</sub> production, and cleavage of C–O as opposed to C–C bonds results in the formation of alkanes and alcohols.<sup>29</sup> We note that the methanol, ethanol, and acetone components in the aqueous effluent stream from the processing of glycerol are similar in concentration (5–30 wt%) to the aqueous ethanol stream produced by fermentation of glucose (*e.g.*, 5 wt%).<sup>6</sup> Thus, it may be advantageous to separate these valuable components from the effluent aqueous stream for use in the chemical industry (*e.g.*, as fuels or solvents).<sup>29</sup>

**Table 3** Carbon distribution for conversion of 50 wt% and 80 wt% solutions of glycerol in water to synthesis gas over Pt–Re/C at 548 K and various pressures. Reaction conditions as in Table 2

Feed concentration (wt%)	Pressure/bar	Total C <sub>in</sub> /μmol min <sup>-1</sup>	Total C <sub>out</sub> gas/μmol min <sup>-1</sup>	Mol% CO in gas products <sup>a</sup>	Total C <sub>out</sub> liquid <sup>b</sup> /μmol min <sup>-1</sup>	wt% oxygenates in aqueous effluent <sup>c</sup>	Error in C balance (%)
80	1	946	816	89	52	6.6	8
50	1	737	708	87	23	2.3	0.8
80	5	914	515	80	431	24	4
50	5	700	533	80	128	6.3	6
80	11	946	417	67	552	30	2
50	11	663	368	58	352	17	9

<sup>a</sup> Calculated as  $F_{\text{CO}}/F_{\text{total}} \times 100$ , where  $F_{\text{CO}}$  is the molar flowrate of carbon as CO and  $F_{\text{total}}$  is the total molar flowrate of carbon in gas products. <sup>b</sup> Determined by total organic carbon analysis of liquid effluent. <sup>c</sup> Calculated as total mass of methanol, ethanol, acetone, acetol, and propanediols per total mass of aqueous effluent.

**Table 4** Results of Fischer–Tropsch synthesis over 4 g of 2.9 wt% Ru/TiO<sub>2</sub> at 548 K. Reaction carried out using ~150 cm<sup>3</sup> min<sup>-1</sup> synthesis gas (H<sub>2</sub> : CO = 2)

Oxygenated feed molecule	$P_{\text{CO}}/\text{bar}$	$P_{\text{H}_2}/\text{bar}$	$P_{\text{H}_2\text{O}}/\text{bar}$	$P_{\text{oxygenate}}/\text{bar}$	Total $P/\text{bar}$	GHSV <sup>a</sup> /h <sup>-1</sup>	$X_{\text{CO}}^b$ (%)	Site time yield <sup>c</sup> /min <sup>-1</sup>	$S_{\text{C}_{5+}}^{d,e}$	$S_{\text{CH}_4}$	$S_{\text{C}_2-\text{C}_4}$	$\alpha_{\text{C}_3-\text{C}_{10}}^f$	$\alpha_{\text{C}_{11}-\text{C}_{30}}^g$
—	1.7	3.3	—	—	5	410	53	2.7	0.30	0.39	0.29	0.61	0.85
Water	1.7	3.5	2.9	—	8.1	630	55	2.8	0.32	0.41	0.29	0.61	0.84
Acetol–Water	1.8	3.5	2.6	0.2	8.1	630	30	1.5	0.60	0.24	0.17	0.80	0.79
Ethanol–Water	1.9	3.7	2.2	0.3	8.1	590	32	1.7	0.38	0.39	0.23	0.68	0.82
Acetone–Water	1.9	3.8	2.1	0.3	8.1	570	26	1.4	0.37	0.41	0.23	0.65	0.85

<sup>a</sup> Calculated as total volumetric flowrate into the reactor divided by total volume of the catalyst bed. <sup>b</sup> Conversion of CO is calculated as  $[(F_{\text{CO}})_{\text{in}} - (F_{\text{CO}})_{\text{out}}]/(F_{\text{CO}})_{\text{in}} \times 100$ , where  $F$  is the molar flowrate. <sup>c</sup> Defined as in ref. 27. <sup>d</sup> Selectivities calculated as  $S_{\text{C}_n\text{H}_x} = nF_{\text{C}_n\text{H}_x}/F_{\text{total}}$ , where  $n$  is the number of carbons in the hydrocarbon product  $\text{C}_n\text{H}_x$ ,  $F_{\text{C}_n\text{H}_x}$  is the molar flowrate of product  $\text{C}_n\text{H}_x$ , and  $F_{\text{total}}$  is the total molar flowrate of carbon in all Fischer–Tropsch hydrocarbon products. <sup>e</sup> Selectivities calculated on a CO<sub>2</sub> and oxygenated hydrocarbon free basis. <sup>f</sup> ASF chain growth probability for alkanes in the C<sub>3</sub>–C<sub>10</sub> range. <sup>g</sup> ASF chain growth probability for alkanes in the C<sub>11</sub>–C<sub>30</sub> range.

### Fischer–Tropsch synthesis

To achieve energy integration between the endothermic conversion of glycerol to synthesis gas and the exothermic conversion of synthesis gas to liquid alkanes, the temperature for the Fischer–Tropsch synthesis step must be comparable to (or higher than) that employed in the glycerol conversion step.<sup>20</sup> Also, the pressures at which both reactions are conducted must be similar to minimize compression costs. Furthermore, if the synthesis gas from the glycerol conversion step is fed directly to the Fischer–Tropsch catalyst, then this catalyst will be exposed to water and oxygenated hydrocarbon byproducts. Therefore, we conducted Fischer–Tropsch synthesis experiments at 548 K and a pressure of synthesis gas (H<sub>2</sub> : CO = 2) equal to 5 bar over 4 g of 2.9 wt% Ru/TiO<sub>2</sub> catalyst. In these experiments, the feed to the reactor was 150 cm<sup>3</sup> min<sup>-1</sup> of dry synthesis gas with co-feeds of water or aqueous solutions of acetol, ethanol, or acetone (the most abundant liquid phase products from glycerol conversion) to simulate the conditions of a two-bed reactor system processing an 80 wt% glycerol feed at 5 bar. We used a Ru-based Fischer–Tropsch catalyst, because a Co-based catalyst showed low activity during initial experiments, and Ru is a more active Fischer–Tropsch catalyst.<sup>30</sup> Additionally, the formation of inactive oxides at high partial pressures of water can cause Co-based Fischer–Tropsch catalysts to deactivate.<sup>18</sup>

Table 4 lists the conversion of CO, activity (as defined by the site time yield), and selectivities to CH<sub>4</sub>, C<sub>2</sub>–C<sub>4</sub>, and C<sub>5+</sub> hydrocarbons for these Fischer–Tropsch synthesis experiments. The conversion of CO is about 50% for Fischer–Tropsch synthesis with dry synthesis gas. The addition of water to the synthesis gas feed has a negligible effect. In particular, the conversion of CO, the activity, and the selectivities are similar to the values measured for the experiment

using dry synthesis gas. The CO conversion and the catalytic activity both decrease with the addition of oxygenated hydrocarbons to the synthesis gas. It is possible that adsorbed species from these molecules inhibit the Fischer–Tropsch reaction by blocking Ru sites for CO and H<sub>2</sub> adsorption. The selectivity to C<sub>5+</sub> hydrocarbons increases slightly (from 0.30 to 0.38) with the addition of ethanol and acetone to the synthesis gas, while the value of  $S_{\text{CH}_4}$  remains unchanged and the value of  $S_{\text{C}_2-\text{C}_4}$  decreases slightly. However, upon the addition of acetol to the synthesis gas, the C<sub>5+</sub> selectivity increases by a factor of two. This result indicates that acetol participates in Fischer–Tropsch chain growth. Indeed, acetol was the only oxygenated feed molecule to react upon addition to the synthesis gas stream during Fischer–Tropsch reaction. Specifically, while more than 90% of the ethanol and acetone feed molecules were recovered in the gaseous and aqueous liquid effluents, all of the acetol feed was converted to products, with 30% being converted to acetone, methanol, and ethanol in the aqueous product phase and 20% being converted to oxygenated species in the organic product phase (acetone, pentanones, hexanones, and heptanones). Another 10% of the acetol feed was converted to gaseous acetone. Therefore, 40% of the carbon fed to the reactor as acetol possibly entered into Fischer–Tropsch chain growth and was converted into liquid hydrocarbons.

The total carbon selectivities (Table 5) for these Fischer–Tropsch synthesis experiments exhibit similar trends as the Fischer–Tropsch selectivities in Table 4. The selectivities in Table 5 are based on the total amount of carbon in all of the products (*i.e.*, Fischer–Tropsch products as well as CO<sub>2</sub> and oxygenated hydrocarbons in the organic and aqueous liquid effluents). The addition of water to the synthesis gas feed increases the selectivity to CO<sub>2</sub> at the expense of

**Table 5** Total carbon selectivities for experiments in Table 4. Selectivities calculated as  $S_i = F_i/F_{\text{total}}$ , where  $F_i$  is the total flowrate of carbon in product  $i$ , and  $F_{\text{total}}$  is the total flowrate of carbon in all of the products

Oxygenated feed molecule	$S_{\text{CH}_4}$	$S_{\text{C}_2-\text{C}_4}$	$S_{\text{C}_{5+}}$	$S_{\text{CO}_2}$	$S_{\text{oxy aqueous}}^a$	$S_{\text{oxy organic}}^b$
—	0.35	0.27	0.29	0.09	—	—
Water	0.32	0.23	0.23	0.23	—	—
Acetol–Water <sup>c</sup>	0.16	0.11	0.40	0.05	0.16	0.06
Ethanol–Water	0.35	0.21	0.34	0.10	—	—
Acetone–Water	0.35	0.20	0.32	0.11	0.02	0.01

<sup>a</sup> Oxygenated hydrocarbon products (acetone, ethanol, and methanol) in aqueous liquid effluent. <sup>b</sup> Oxygenated hydrocarbon products (acetone, butanones, pentanones, hexanones, and heptanones) in organic liquid effluent. <sup>c</sup>  $S_{\text{gaseous acetone}}$  is 0.06.

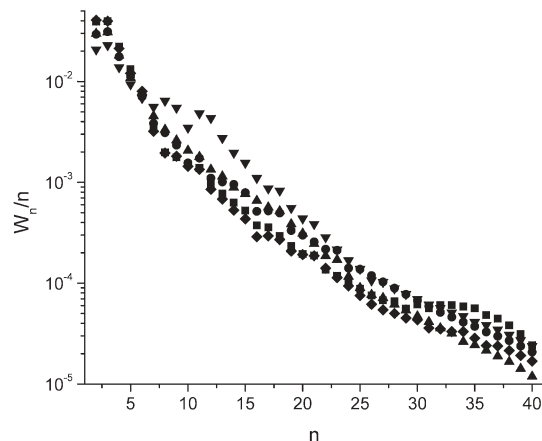
Fischer–Tropsch alkanes ( $C_1$ – $C_{5+}$ ), most likely by an increase in the rate of water-gas shift. We note that the  $CO_2$  selectivity for aqueous co-feeds of oxygenated molecules is similar to the value observed for the dry synthesis gas feed, even though the partial pressure of water is similar to that when water alone is co-fed. This result is possibly due to the lower activity of Ru/TiO<sub>2</sub> caused by site blocking, as explained previously. The selectivities in Table 5 show that the addition of aqueous solutions of ethanol or acetone to synthesis gas has a negligible effect on the product distribution, in agreement with the Fischer–Tropsch selectivities in Table 4. There is a slight increase in the value of  $S_{C_{5+}}$  and a corresponding decrease in the value of  $S_{C_2-C_4}$ , while  $S_{CH_4}$  is unchanged with the addition of ethanol and acetone to the synthesis gas feed. However, these total carbon selectivities confirm that the addition of acetol to the synthesis gas leads to a shift from light alkane products to heavier products. Light alkanes ( $C_1$ – $C_4$ ) account for more than 50% of the total carbon in the products for the dry synthesis gas experiment as well as experiments with water, ethanol, and acetone co-feeds. However, about 50% of the carbon in the products from the acetol co-feed experiment was contained in the  $C_{5+}$  hydrocarbons and oxygenated hydrocarbons in the organic liquid effluent. This increase in heavier products is accompanied by a more than two-fold decrease in selectivity to light alkanes. We note that the aqueous effluent from the acetol co-feed experiment is 6 wt% acetone, ethanol, and methanol, a solution suitable for further distillation.

In general, the product distribution of Fischer–Tropsch synthesis can be described by the Anderson–Schulz–Flory (ASF) chain growth model:

$$\frac{W_n}{n} = \alpha^{n-1} (1 - \alpha)^2 \quad (3)$$

where  $n$  is the hydrocarbon chain length,  $W_n$  is the weight fraction of hydrocarbon products of length  $n$ , and  $\alpha$  is the chain growth probability.<sup>18,31</sup> Eqn (3) assumes that chain growth probability is independent of  $n$ , and a semi-log plot of eqn (3) gives a straight line with a slope of  $\alpha$ .<sup>18,31</sup> However, the selectivity (and activity) of Fischer–Tropsch catalysts can be affected by transport limitations within the catalyst pellets, such that  $\alpha$  becomes dependent on chain length.<sup>27,28,31</sup> An increase in Ru site density or pellet radius leads to an increase in the  $C_{5+}$  selectivity caused by diffusion-enhanced readsorption of  $\alpha$ -olefins, which inhibits chain termination.<sup>31</sup> However, these diffusional limitations can become sufficiently severe that they inhibit CO diffusion within the pellet, resulting in a decrease in  $C_{5+}$  selectivity.<sup>31</sup> Iglesia *et al.* define a structural parameter ( $\chi$ ) to indicate the extent of these diffusion restrictions within a catalyst, and this parameter is dependent on catalyst pellet radius, pore size distribution, and the volumetric density of surface Ru atoms.<sup>31</sup>

For the 2.9 wt% Ru/TiO<sub>2</sub> catalyst used in this paper, the value of  $\chi$  is estimated to be  $50 \times 10^{16} \text{ m}^{-1}$ . This value is in agreement with values determined by Iglesia *et al.* for TiO<sub>2</sub>-supported Ru catalysts,<sup>27</sup> and it lies in the intermediate range, suggesting that transport limitations promote readsorption of  $\alpha$ -olefins but do not slow the diffusion of reactants into the catalyst pellets.<sup>31</sup> Indeed, catalysts with intermediate values of  $\chi$  lead to optimum  $C_{5+}$  selectivity.<sup>27,28,31</sup> Furthermore,



**Fig. 4** Molecular weight distributions for dry synthesis gas (■), and water (◆), acetone (●), ethanol (▲), and acetol (▼) co-feeds. Experimental conditions as in Table 4.

readsorption of olefins leads to deviation from ASF chain growth kinetics. As a hydrocarbon chain increases in length, diffusion through the catalyst pores becomes more difficult and the possibility for readsorption increases.<sup>27,28,31</sup> This effect increases the chain growth probability for longer hydrocarbon chains and results in curvature in the semi-log plot of the molecular weight distribution.<sup>27,28,31</sup> Fig. 4 shows semi-log plots for the five Fischer–Tropsch runs in Table 4, and these distributions begin to deviate from ASF kinetics at  $C_{10}$ – $C_{15}$ , in agreement with studies by Iglesia *et al.*<sup>27,28,31</sup> The deviation in the molecular weight distribution in the  $C_6$ – $C_{12}$  range for the experiment employing acetol co-feed is caused by increased formation of  $C_6$ – $C_{12}$  hydrocarbons from acetol entering into Fischer–Tropsch chain growth. Table 4 also shows values of  $\alpha$  for the  $C_3$ – $C_{10}$  and  $C_{11}$ – $C_{30}$  hydrocarbon ranges. The values of  $\alpha$  for  $C_{11}$ – $C_{30}$  are larger than those for  $C_3$ – $C_{10}$  for the dry synthesis gas experiment and the experiments with water, ethanol, and acetone co-feeds. Conversely, the two  $\alpha$  values for the acetol co-feed experiment are similar, resulting from an increase in the formation of  $C_6$ – $C_{12}$  alkanes during this run. We note that the olefin to paraffin ratios were low, consistent with the long bed residence times used in these studies (6–9 s).<sup>27</sup>

### Glycerol conversion combined with Fischer–Tropsch synthesis

Following our studies of glycerol conversion to synthesis gas and our studies of Fischer–Tropsch synthesis using synthesis gas streams containing water and oxygenated hydrocarbons (ethanol, acetone, acetol), we investigated the formation of liquid alkanes by the integration of glycerol conversion with Fischer–Tropsch synthesis. These experiments employed a two-bed catalyst system using 1.0 g of 10 wt% Pt–Re (1 : 1)/C followed by 1.7 g of 1.0 wt% Ru/TiO<sub>2</sub>, with an 80 wt% glycerol feed at 548 K and total pressures between 5 and 17 bar.

Table 6(A) shows the selectivities to  $C_{5+}$ ,  $CH_4$ , and  $C_2$ – $C_4$  alkanes for each of the combined experiments based solely on the alkane products from Fischer–Tropsch synthesis (*i.e.*, with the  $C_1$ – $C_3$  alkanes produced by the Pt–Re/C catalyst excluded). The selectivity for production of  $C_{5+}$  alkanes by Fischer–Tropsch synthesis typically increases at higher



**Table 6** Results from experiments for glycerol conversion combined with Fischer–Tropsch synthesis. (A) Selectivities to  $C_{5+}$ ,  $CH_4$ , and  $C_2$ – $C_4$  hydrocarbons over Ru/TiO<sub>2</sub>, calculated as in Table 4. (B) Total carbon selectivities, calculated as  $S_i = F_i/F_{\text{total}} \times 100$ , where  $F_i$  is the total flowrate of carbon in product  $i$ , and  $F_{\text{total}}$  is the total flowrate of carbon in all of the products. Reactions carried out at 548 K using  $\sim 0.04 \text{ cm}^3 \text{ min}^{-1}$  of 80 wt% glycerol feed (WHSV of glycerol over Pt–Re/C =  $1.7 \text{ h}^{-1}$ )

(A)	$P_{\text{tot}}/\text{bar}$	$S_{C_{5+}}$	$S_{CH_4}$	$S_{C_2-C_4}$	$\alpha_{C_3-C_{10}}^a$	$\alpha_{C_{11}-C_{30}}^b$
	5	0.63	0.15	0.21	0.85	0.75
	11	0.75	0.10	0.15	0.92	0.75
	17	0.70	0.12	0.18	0.92	0.71

(B)	$P_{\text{tot}}/\text{bar}$	$S_{\text{Alkanes}}^c$ (%)	$S_{CO_2}^d$ (%)	$S_{CO}^e$ (%)	$S_{\text{org-oxy}}^d$ (%)	$S_{\text{aq-oxy}}^e$ (%)
	5	31.9	15.2	37.3	1.7	13.9
	11	44.1	16.5	17.5	7.4	14.6
	17	55.2	23.1	1.3	9.1	11.2

<sup>a</sup> ASF chain growth probability for alkanes in the  $C_3$ – $C_{10}$  range.

<sup>b</sup> ASF chain growth probability for alkanes in the  $C_{11}$ – $C_{30}$  range.

<sup>c</sup> CO from glycerol. <sup>d</sup> Oxygenated hydrocarbon products (acetone, butanones, pentanones, hexanones, and heptanones) in organic liquid effluent. <sup>e</sup> Oxygenated hydrocarbon products (acetone, ethanol, and methanol) in aqueous liquid effluent.

pressures, and the results for the two-bed reactor system obey this trend. An increase in pressure from 5 to 11 bar results in an increase in the selectivity to  $C_{5+}$  hydrocarbons from 0.63 to 0.75; however, a further increase in pressure to 17 bar produces only a slight decrease in  $S_{C_{5+}}$  to 0.70. Importantly, the selectivity to  $C_{5+}$  hydrocarbons is almost three times higher than the total selectivity to  $CH_4$  and  $C_2$ – $C_4$  at 11 and 17 bar. Furthermore, the value of  $S_{C_{5+}}$  for the combined run at 5 bar is similar to the Fischer–Tropsch experiment with an acetol co-feed. This result indicates the participation of acetol in Fischer–Tropsch chain growth, thus increasing the selectivity to longer-chain hydrocarbons. Based on the production of CO from the glycerol conversion experiments discussed previously, the average conversion of CO across the Ru/TiO<sub>2</sub> bed was 28% and 42% for 5 and 11 bar, respectively, and the site time yield was  $1.3 \text{ min}^{-1}$  at both pressures. An increase in pressure to 17 bar results in an increase in the activity of the Fischer–Tropsch catalyst indicated by a higher average site-time yield ( $2.5 \text{ min}^{-1}$ ) and average conversion of CO (94%).

Table 6(B) shows the total carbon selectivities based on the total amount of carbon in all of the products. At 5 bar, the primary product from glycerol conversion was CO, with only 32% of the carbon being converted to alkanes; however, increasing the pressure to 11 and 17 bar shifts the carbon distribution toward  $C_1$ – $C_{5+}$  alkanes (*i.e.*,  $S_{\text{Alkanes}}$  increases to 42% and 51% at 11 bar and 17 bar, respectively). Also, the amount of carbon as oxygenates in the organic liquid effluent (acetone, pentanones, hexanones, and heptanones) increases by a factor of 5 with increasing pressure. This appearance of oxygenates in the organic liquid is similar to the Fischer–Tropsch experiment with an acetol co-feed described previously, and it further indicates the synergistic effects of acetol in the Fischer–Tropsch reaction. At 17 bar, the amount of carbon leaving the reactor as CO decreases by more than an order of magnitude, and the selectivity to alkanes increases compared to the run at 11 bar. However, the selectivity to  $C_{5+}$

**Table 7** Percentage of carbon contained in each product phase for experiments in Table 6 of glycerol conversion combined with Fischer–Tropsch synthesis

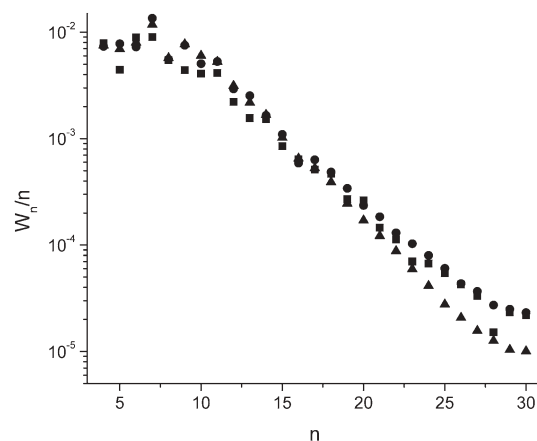
$P_{\text{tot}}/\text{bar}$	Gaseous <sup>a</sup>	Organic liquid <sup>b</sup>	Aqueous liquid <sup>c</sup>
5	71.6	14.6	13.9
11	54.3	31.1	14.6
17	50.5	38.2	11.2

<sup>a</sup> CO, CO<sub>2</sub>, and  $C_1$ – $C_9$  alkanes. <sup>b</sup>  $C_{5+}$  alkanes, acetone, butanones, pentanones, hexanones, and heptanones. <sup>c</sup> Methanol, ethanol, acetone, and *n*-propanol.

alkanes slightly decreases. This behavior results from both increased water-gas shift activity (indicated by higher  $S_{CO_2}$ ) as well as an increase in the rate of Fischer–Tropsch synthesis at higher pressures (as mentioned previously). The carbon distribution is shifted toward lighter alkane products (*i.e.*, increase in  $S_{\text{Alkanes}}$  without a corresponding increase in  $S_{C_{5+}}$ ).

Table 7 shows the percentage of carbon contained in the three products phases: gaseous (CO, CO<sub>2</sub>, and  $C_1$ – $C_9$  alkanes), organic liquid ( $C_{5+}$  alkanes, acetone, pentanones, hexanones, and heptanones), and aqueous liquid (acetone, methanol, and ethanol). We note that the percentage of carbon in the organic liquid-phase product was 43% at 17 bar, 35% at 11 bar, and 15% at 5 bar, with the percentage of carbon in gaseous products decreasing from 71% at 5 bar to approximately 50% at 11 and 17 bar. At 5 and 11 bar, 14% of the carbon is contained as oxygenated species in the aqueous effluent, and at 17 bar, this value slightly decreases to 10%. These aqueous liquid effluents contain between 5 wt% and 15 wt% methanol, ethanol, and acetone and are suitable for further distillation.

The value of  $\chi$  for the 1.0 wt% Ru/TiO<sub>2</sub> catalyst used in all the combined experiments was  $40 \times 10^{16} \text{ m}^{-1}$ , in agreement with results from Iglesia *et al.*<sup>27</sup> Fig. 5 shows the product molecular weight distributions for these experiments that combined glycerol conversion with Fischer–Tropsch synthesis, and these distributions exhibit similar deviations from ASF kinetics as the Fischer–Tropsch experiments described in the previous section, indicating  $\alpha$ -olefin readsorption effects. The intermediate value of  $\chi$  for this Ru/TiO<sub>2</sub> catalyst allows for optimum  $C_{5+}$  selectivity. Values of  $\alpha$  for the  $C_3$ – $C_{10}$  and



**Fig. 5** Molecular weight distributions for combined glycerol conversion with Fischer–Tropsch synthesis experiments at 548 K and 5 bar (■), 11 bar (●), and 17 bar (▲). Experimental conditions as in Table 6.

C<sub>11</sub>–C<sub>30</sub> hydrocarbon ranges are also shown in Table 6A. The values in the C<sub>3</sub>–C<sub>10</sub> range are high, most likely caused by the participation of oxygenates (acetol) in Fischer–Tropsch chain growth, increasing the production of C<sub>6</sub>–C<sub>12</sub> species. This result is similar to the acetol co-feed experiment in Table 4.

The C<sub>5+</sub> selectivity, selectivity to pentanones, hexanones, and heptanones in the organic liquid, and the conversion of CO for combined glycerol conversion with Fischer–Tropsch synthesis at 11 and 17 bar are all higher than those at 5 bar, despite the fact that synthesis gas production from glycerol is decreased at these elevated pressures. These results indicate that the more favorable Fischer–Tropsch conditions (*i.e.*, higher pressure) are more important to the integrated process than the synthesis gas production rate. Also, the H<sub>2</sub>/CO ratio varies between 1.0 and 1.5 for the conversion of glycerol to synthesis gas at pressures between 5 and 17 bar. However, the integrated runs at these pressures show good selectivities to C<sub>5+</sub> hydrocarbons. These results show that synthesis gas with a stoichiometric H<sub>2</sub>/CO ratio of 2 : 1 is not essential to the production of liquid alkanes *via* our integrated process. Furthermore, the Ru/TiO<sub>2</sub> catalyst is exposed to increasing amounts of oxygenated hydrocarbon byproducts at 11 and 17 bar; however, the selectivity to oxygenates in the aqueous liquid effluent at these pressures is similar to or lower than that of the aqueous effluent at 5 bar. This result indicates that the oxygenated hydrocarbon byproducts from glycerol react over the Ru/TiO<sub>2</sub> bed, most likely by entering into Fischer–Tropsch chain growth. Because the aqueous product distribution contains a wide array of oxygenated species, it is likely that other byproducts with similar functionality as acetol (*e.g.*, polyols, secondary alcohols, and hydroxyl-ketones) have a similar synergistic effect on Fischer–Tropsch synthesis. Importantly, these experiments demonstrate that liquid alkanes can be produced directly from glycerol in a two-bed reactor system using an integrated process.

### Potential industrial application

The integrated process presented in this paper has the potential to improve the economics of “green” Fischer–Tropsch synthesis. For example, previous studies investigating the optimum design of large scale “green” Fischer–Tropsch plants conclude that synthesis gas production and cleanup are critical steps in the entire process and have significant effects on the economics of producing liquid alkanes from biomass.<sup>16,17</sup> Studies by Hamelinck *et al.* and Tijmensen *et al.* show that capital costs account for more than 50% of the total costs of producing liquid alkanes from “green” Fischer–Tropsch synthesis, and of these capital costs nearly 50% result from biomass gasification (18–25%), oxygen production (12–15%) and synthesis gas processing and cleaning (10–18%).<sup>16,17</sup>

Typical gasifiers suitable for conventional “green” Fischer–Tropsch processes are circulated fluidized bed designs that can operate over a wide range of conditions.<sup>16,17</sup> For example, these gasifiers operate from atmospheric pressure to 30 bar using air or O<sub>2</sub> with exit temperatures of 1100–1240 K.<sup>17</sup> The major disadvantage of an air-blown gasifier operating at

atmospheric pressure is the increased cost for larger downstream equipment necessary to handle the synthesis gas diluted with N<sub>2</sub>.<sup>16,17</sup> Furthermore, dilution of synthesis gas with N<sub>2</sub> has negative effects on the C<sub>5+</sub> selectivity.<sup>17</sup> Pressurized gasifiers are more costly at small scale and are more difficult to maintain,<sup>17</sup> and the air separation plant required for O<sub>2</sub>-blown gasifiers is expensive, especially at small scales.<sup>16,17</sup> Another disadvantage of conventional biomass gasifiers is that the synthesis gas stream often contains contaminants (*e.g.*, HCN, NH<sub>3</sub>, H<sub>2</sub>S, COS, and HCl among others)<sup>17</sup> that must be removed to concentrations lower than 10–20 ppb each, with some requiring complete removal.<sup>17</sup> Typically, gas cleaning trains are comprised of five to seven different cleaning steps (*e.g.*, tar cracker, cyclone separator, bag filters, wet and/or dry scrubbers, and ZnO guard beds).<sup>16,17</sup> The integrated process presented in the present paper is advantageous over these conventional synthesis gas production methods in that our process produces an undiluted synthesis stream at the temperature, pressure, and purity appropriate for Fischer–Tropsch synthesis. In addition, our integrated process is advantageous over conventional gasifiers in that our process can produce synthesis gas with varying H<sub>2</sub>/CO compositions, thus eliminating the need for a water-gas shift reactor and allowing for the use of Fischer–Tropsch catalysts that operate at different H<sub>2</sub>/CO ratios.<sup>32–34</sup> Thus, capital costs and operating expenses can be reduced (by close to 50%) by eliminating the need for a biomass gasifier, large downstream equipment, and synthesis gas cleaning steps.

In addition to potential economic improvements, the different product streams of our integrated process each have potential end-uses, as illustrated in Fig. 1. In an industrial application, the gaseous product stream would contain primarily gaseous alkanes in the C<sub>1</sub>–C<sub>2</sub> range; however, some process studies show that recovering the C<sub>3</sub>–C<sub>4</sub> fractions from the gas stream is energy consuming and not economical.<sup>16</sup> Also, the gaseous products would contain unconverted H<sub>2</sub> and CO with some CO<sub>2</sub>. The most likely use for the gas alkanes in our process would be combustion to produce process heat and electricity (Fig. 1) with some of the unconverted H<sub>2</sub> and CO being recycled to the Fischer–Tropsch bed. However, these gaseous alkanes could be reformed to synthesis gas and recycled to the Fischer–Tropsch bed as well.<sup>16</sup> The organic liquid phase product contains primarily liquid hydrocarbons with a small amount of oxygenates (acetone, butanone, pentanone, hexanone, and heptanone). In some applications, the oxygenates could be hydrogenated to alcohols, which are excellent fuel additives. Alternatively, the oxygenates in the organic liquid could undergo hydrodeoxygenation to remove the oxygen and form saturated hydrocarbons.<sup>35</sup> If diesel fuel is the desired product, the C<sub>5</sub>–C<sub>9</sub> fraction would be separated, and the waxy C<sub>10+</sub> fraction would be hydrocracked to naphtha, kerosene, and diesel.<sup>16,17</sup> The aqueous liquid product stream contains oxygenated hydrocarbons (*e.g.*, ethanol, methanol, and acetone) at concentrations between 5–15 wt%. This aqueous solution is suitable for distillation with the oxygenated hydrocarbons either being recycled for further conversion to synthesis gas or being used as intermediates or solvents in the chemical industry. However, this aqueous solution could be converted to H<sub>2</sub> by aqueous phase

reforming<sup>29</sup> or upgraded to transportation fuels *via* selective dehydration/hydrogenation.<sup>36,37</sup>

## Conclusions

The production of synthesis gas from glycerol coupled with the conversion of synthesis gas to produce liquid fuels by Fischer–Tropsch synthesis is a net exothermic process with a heat of reaction that is 4% of the lower heating value of glycerol.<sup>20</sup> We show that conversion of glycerol over a Pt–Re/C catalyst produces a synthesis gas stream that is suitable for Fischer–Tropsch synthesis over a wide range of glycerol feed concentrations and at pressures up to 17 bar where incomplete vaporization of the glycerol feed occurs. Also, we have demonstrated that the oxygenated hydrocarbon byproducts in the synthesis gas stream from glycerol conversion (*e.g.*, ethanol, acetone, acetol) have positive effects on the Fischer–Tropsch synthesis step. In particular, water, ethanol and acetone have slightly positive effects, such as slightly increasing the selectivity to C<sub>5+</sub> hydrocarbons (S<sub>C5+</sub>); and, acetol can participate in Fischer–Tropsch chain growth, forming pentanones, hexanones, and heptanones in the liquid organic effluent stream. This synergistic participation of acetol (and, possibly, other oxygenates) in Fischer–Tropsch chain growth has beneficial effects with respect to integration of glycerol conversion with Fischer–Tropsch synthesis in a two-bed system, such as (i) eliminating the need to condense water and oxygenated hydrocarbon byproducts between the catalyst beds, (ii) allowing for operation at higher pressures (*i.e.*, 17 bar) where synthesis gas production over Pt–Re/C is decreased and the production of liquid byproducts is increased, and (iii) causing an increase in the selectivity to C<sub>5+</sub> hydrocarbons. Accordingly, glycerol conversion and Fischer–Tropsch synthesis can be carried out effectively (and perhaps synergistically) at the same conditions and in a two-bed reactor system, allowing the coupling between glycerol conversion and Fischer–Tropsch synthesis to be used for the production of liquid fuels from aqueous-glycerol solutions.

The integrated process presented in this paper is a simple, two step catalytic process that can be carried out at low temperature and moderate pressure and can effectively harness the energy from a renewable resource. Importantly, our process minimizes the amount of waste byproducts since each product phase is useful (Fig. 1). Therefore, this “green” process represents an energy efficient alternative for producing liquid transportation fuels from petroleum. Furthermore, it presents the opportunity for improving the economic viability of “green” Fischer–Tropsch synthesis by reducing costs associated with synthesis gas production and by improving the thermal efficiency of Fischer–Tropsch processes.

## Acknowledgements

This work was supported by the U.S. Department of Energy (DOE), Office of Basic Energy Sciences. R. R. Soares acknowledges a post-doctoral grant from CAPES. We thank Randy Cortright and Manos Mavrikakis for valuable discussions and collaborations throughout this project. We also thank Jennifer Ross for assistance in collecting reaction kinetics data.

## References

- 1 G. Alexander and G. Boyle, *Introducing Renewable Energy*, ed. G. Boyle, Oxford University Press, New York, 2004.
- 2 Energy Information Administration, U. S. Department of Energy, <http://www.eia.doe.gov/>.
- 3 D. L. Klass, *Biomass for Renewable Energy, Fuels, and Chemicals*, Academic Press, San Diego, 1998.
- 4 R. D. Perlack, L. L. Wright, A. F. Turhollow, R. L. Graham, B. J. Stokes and D. C. Erbach, *Biomass as Feedstock for a Bioenergy and Bioproducts Industry: The Technical Feasibility of a Billion-Ton Annual Supply*, United States Department of Energy, Oak Ridge National Laboratory, DOE/GO-102005-2135, 2005, 1–78.
- 5 A. E. Farrell, R. J. Plevin, B. T. Turner, A. D. Jones, M. O'Hare and D. M. Kammen, Ethanol can contribute to energy and environmental goals, *Science*, 2006, **311**, 506–508.
- 6 H. Shapouri, J. A. Duffield and M. Wang, *The Energy Balance of Corn Ethanol: An Update*, United States Department of Agriculture, Agricultural Economic Report No. 814, 2002, 1–15.
- 7 K. L. Kadam and J. D. McMillan, Availability of corn stover as a sustainable feedstock for bioethanol production, *Bioresour. Technol.*, 2003, **88**, 17–25.
- 8 J. D. McMillan, Bioethanol Production: Status and Prospects, *Renew. Energ.*, 1997, **10**, 295–302.
- 9 V. Senthilkumar and P. Gunasekaran, Bioethanol production from cellulosic substrates: engineered bacteria and process integration challenges, *J. Sci. Ind. Res. India*, 2005, **64**, 845–853.
- 10 P. O. Ward and A. Singh, Microbial technology for bioethanol production from agricultural and forestry wastes, in *Microbial Biotechnology in Agriculture and Aquaculture*, ed. R. C. Ramesh, Science Publishers, Inc., Enfield, NH, USA, 2005.
- 11 The European Fuel Oxygenates Association, <http://www.efoa.org/oxygen.html>.
- 12 Energy Efficiency and Renewable Energy, U.S. Department of Energy, <http://www.eere.energy.gov/>.
- 13 T. W. Patzek, Thermodynamics of the Corn-Ethanol Biofuel Cycle, *Crit. Rev. Plant Sci.*, 2004, **23**, 519–567.
- 14 T. Patzek and D. Pimentel, Thermodynamics of Energy Production from Biomass, *Crit. Rev. Plant Sci.*, 2005, **24**, 327–364.
- 15 D. Pimentel and T. W. Patzek, Ethanol Production Using Corn, Switchgrass, and Wood; Biodiesel Production Using Soybean and Sunflower, *Nat. Resour. Res.*, 2005, **14**, 65–76.
- 16 C. N. Hamelinck, A. P. C. Faaij, H. den Uil and H. Boerrigter, Production of FT transportation fuels from biomass; technical options, process analysis and optimisation, and development potential, *Energy*, 2004, **29**, 1743–1771.
- 17 M. J. A. Tijmensen, A. P. C. Faaij, C. N. Hamelinck and M. R. M. van Hardeveld, Exploration of the possibilities for production of Fischer Tropsch liquids and power via biomass gasification, *Biomass Bioenerg.*, 2002, **23**, 129–152.
- 18 C. H. Bartholomew and R. J. Farrauto, *Fundamentals of Industrial Catalytic Processes*, Wiley, Hoboken, NJ, USA, 2006.
- 19 P. L. Spath and D. C. Dayton, *Preliminary Screening–Technical and Economic Assessment of Synthesis Gas to Fuels and Chemicals with Emphasis on the Potential for Biomass-Derived Syngas*, United States Department of Energy, National Renewable Energy Laboratory, NREL/TP-510-34929, 2003, 1–142.
- 20 R. R. Soares, D. A. Simonetti and J. A. Dumesic, Glycerol as a Source for Fuels and Chemicals by Low-Temperature Catalytic Processing, *Angew. Chem., Int. Ed.*, 2006, **45**, 3982–3985.
- 21 C. S. Gong, J. X. Du, N. J. Cao and G. T. Tsao, Co-production of ethanol and glycerol, *Appl. Biochem. Biotechnol.*, 2000, **84–86**, 543–559.
- 22 T. A. Werpy, J. G. Frye, A. H. Zacher and D. J. Miller, PCT, Hydrogenolysis of 6-carbon sugars and other organic compounds, *World Pat. WO 03/035582 A1*, 2003.
- 23 J. Van Gerpen, Biodiesel processing and production, *Fuel Process. Technol.*, 2006, **86**, 1097–1107.
- 24 E. Iglesia, S. L. Soled and R. A. Fiato, Fischer–Tropsch Synthesis on Cobalt and Ruthenium – Metal Dispersion and Support Effects on Reaction-Rate and Selectivity, *J. Catal.*, 1992, **137**, 212–224.
- 25 B. E. Spiewak, J. Shen and J. A. Dumesic, Microcalorimetric Studies of CO and H<sub>2</sub> Adsorption on Nickel Powders Promoted with Potassium and Cesium, *J. Phys. Chem.*, 1995, **99**, 17640.

- 26 K. C. Taylor, Determination of Ruthenium Surface-Areas by Hydrogen and Oxygen Chemisorption, *J. Catal.*, 1975, **38**, 299–306.
- 27 E. Iglesia, S. C. Reyes and R. J. Madon, Transport-Enhanced Alpha-Olefin Readsorption Pathways in Ru-Catalyzed Hydrocarbon Synthesis, *J. Catal.*, 1991, **129**, 238–256.
- 28 E. Iglesia, Design, synthesis, and use of cobalt-based Fischer–Tropsch synthesis catalysts, *Appl. Catal. A*, 1997, **161**, 59–78.
- 29 R. D. Cortright, R. R. Davda and J. A. Dumesic, Hydrogen from catalytic reforming of biomass-derived hydrocarbons in liquid water, *Nature*, 2002, **418**, 964–967.
- 30 M. A. Vannice, The catalytic synthesis of hydrocarbons from H<sub>2</sub>/CO mixtures over the group VIII metals: I. The specific activities and product distributions of supported metals, *J. Catal.*, 1975, **37**, 449–461.
- 31 E. Iglesia, S. C. Reyes, R. J. Madon and S. L. Soled, Selectivity Control and Catalyst Design in the Fischer–Tropsch Synthesis – Sites, Pellets, and Reactors, *Adv. Catal.*, 1993, **39**, 221–302.
- 32 M. E. Dry, Chemical concepts used for engineering purposes, *Stud. Surf. Sci. Catal.*, 2004, **152**, 196–257.
- 33 M. E. Dry, FT catalysts, *Stud. Surf. Sci. Catal.*, 2004, **152**, 533–600.
- 34 M. E. Dry and A. P. Steynberg, Commercial FT process applications, *Stud. Surf. Sci. Catal.*, 2004, **152**, 406–481.
- 35 G. W. Huber, S. Iborra and A. Corma, Synthesis of transportation fuels from biomass: chemistry, catalysts, and engineering, *Chem. Rev.*, 2006, **106**, 4044–4098.
- 36 C. D. Chang, Hydrocarbons from methanol, *Catal. Rev. Sci. Eng.*, 1983, **25**, 1–118.
- 37 R. J. J. Nel and A. de Klerk, Fischer–Tropsch aqueous phase refining by catalytic alcohol dehydration, *Ind. Eng. Chem. Res.*, 2007, **46**, 3558–3565.



## Looking for that **special** chemical science research paper?

TRY this free news service:

### Chemical Science

- highlights of newsworthy and significant advances in chemical science from across RSC journals
- free online access
- updated daily
- free access to the original research paper from every online article
- also available as a free print supplement in selected RSC journals.\*

\*A separately issued print subscription is also available.

Registered Charity Number: 207890

RSCPublishing

[www.rsc.org/chemicalscience](http://www.rsc.org/chemicalscience)

22030682



# Synthesis of ionic liquids in micro-reactors—a process intensification study

Daniel A. Waterkamp,<sup>a</sup> Michael Heiland,<sup>a</sup> Michael Schlüter,<sup>a</sup> Janelle C. Sauvageau,<sup>a</sup> Tom Beyersdorff<sup>b</sup> and Jorg Thöming<sup>\*a</sup>

Received 23rd November 2006, Accepted 17th May 2007

First published as an Advance Article on the web 8th June 2007

DOI: 10.1039/b616882e

To date the manufacturing of ionic liquids on a large scale is limited by ineffective batch procedures employed for the alkylation step. Here we present a way to intensify the synthesis of 1-butyl-3-methylimidazolium bromide ([BMIM]Br) by using a continuously operating micro-reactor system. It consists of a microstructured mixer of 450  $\mu\text{m}$  channel width and reaction tubes with inner diameter ranging from 2 to 6 mm allowing a production rate of 9.3 kg [BMIM]Br per day. In this reactor system the strongly exothermic alkylation can be thermally controlled even at elevated temperatures leading to high reaction rates in a solvent-free modus. In spite of temperatures up to 85 °C the product purity achieved was above 99%. The degree of process intensification achieved results in a more than twentyfold increase of the space–time–yield compared to a conventional batch process. The measured conversion data could be modelled successfully using a second order reaction kinetic. With the generated kinetic parameters the time course of temperature and conversion was also simulated for batch synthesis. Based on these data the performance of the continuous micro-reactor and the conventional batch process was compared. The simulation shows the potential of process intensification as an improvement of space–time–yield in the range of two orders of magnitude.

## 1 Introduction

In general, ionic liquids are considered as green chemicals mainly because of their low vapour pressure which makes them attractive for green manufacturing processes. However, it has already been shown that despite the mentioned advantage of this group of compounds, there are also other hazardous risks like ecotoxicity which have to be taken into account for any assessment of chemical entities.<sup>1</sup> This means that a distinction has to be made between the species instead of just talking about the greenness of ionic liquids in general. Furthermore, for an assessment to be carried out, both processes involved, *i.e.*, the application as well as the manufacturing processes, have to be considered.

As it is known from the field of life cycle assessment, there are several factors which have a significant impact on the manufacturing process. Among them are the level of risk to operators and the neighbouring community, product yield and purity in addition to the residence time, which are all influenced by the size scale of the reactors employed. Micro-reactors have been demonstrated to show altered yield and selectivity as compared with conventional batch reactors through exploitation of the smallest scales.<sup>2</sup> Recently, it could be shown by one of the authors that despite laminar flow conditions, short diffusion lengths are achievable in micro-structured mixers,<sup>3</sup> which, together with small distances for

heat transfer, can be considered as the main reason for the process intensification potential in microreaction engineering.

Currently, the most widely used starting material for imidazolium-based ionic liquids are imidazolium halides (mostly bromides and chlorides) that are generally produced in batches as it is typically the case for ionic liquid synthesis.<sup>4–7</sup> For most of the exothermic reaction schemes, bench top glassware is limited in volume and temperature due to safety reasons and product quality demand. Furthermore, a solvent like 1,1,1-trichloromethane or THF is sometimes applied to dilute the reactants and thus keep the reactions under control.<sup>8,9</sup>

Both problems can be avoided by using micro-reactors. They offer the possibility of applying higher cooling temperatures due to high surface to volume ratios and short diffusion lengths and, by this means, enhance the reaction in terms of space–time–yield (STY). The second consequence of this is the advantage of allowing the alkylation to be performed in a solvent-free modus.

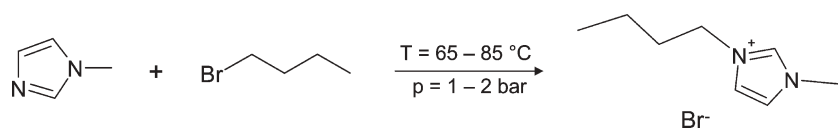
The aim of this study is to evaluate these projected advantages obtained through using a micro-reactor system consisting of a piston pump, a vortex mixer and a reaction tube. In contrast to a conventional batch synthesis, it will be shown from the investigation whether the possible increase in cooling temperature could improve the STY of the alkylation significantly at given product quality constraints without the risk of a runaway of temperature and, consequently, system pressure.

## 2 Materials and methods

As a representative of the reactions of interest, the butylation of methylimidazole, an example of a strongly exothermic

<sup>a</sup>University of Bremen, Centre for Environmental Research and Technology UFT, Leobener Straße, D28359, Bremen, Germany. E-mail: thoeming@uni-bremen.de; Fax: +49 (0) 421 218-8297; Tel: +49 (0) 421 218-2561

<sup>b</sup>IoLiTec GmbH & Co. KG, Ferdinand-Porsche-Straße 5/11, D 79211, Denzlingen, Germany



Scheme 1

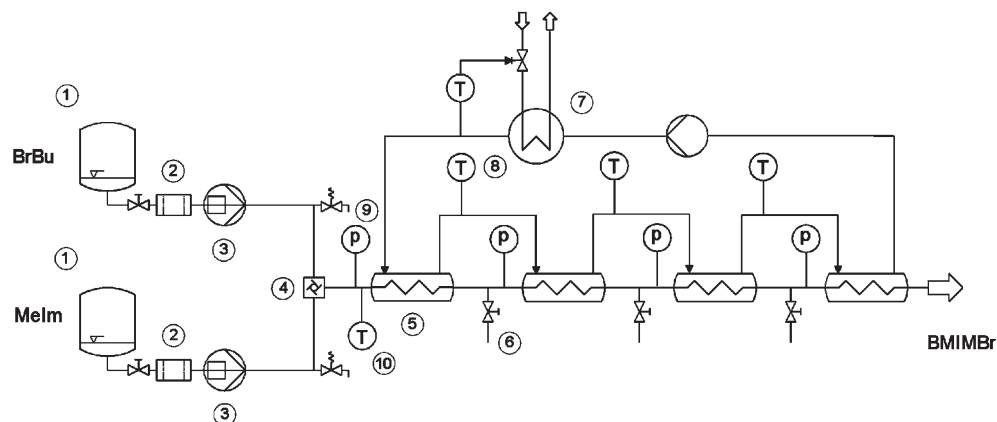


Fig. 1 Experimental set-up of the micro-reactor system for the continuous alkylation.

alkylation, was chosen. The formation of 1-butyl-3-methylimidazolium bromide ([BMIM]Br) by reaction of 1-methylimidazole (MeIm) and 1-bromobutane (BrBu) with a reaction enthalpy of  $-96 \text{ kJ mol}^{-1}$  can be described as shown in Scheme 1.

The reactants used for the synthesis of [BMIM]Br, MeIm and BrBu, are of  $>99\%$  purity, purchased from Acros Organics. As a reference for comparison, [BMIM]Br was obtained from Merck KG.

The experimental set-up is illustrated in Fig. 1. It consists of two pumps (3), a vortex-type micro-mixer of  $450 \mu\text{m}$  channel width (4) and a reaction tube with a total volume of  $306 \text{ mL}$  (5). The reaction tube is divided into four sections each of  $6 \text{ m}$  length. In order to ensure sufficient heat transfer based on the local surface area to volume ratio, the diameter of the tube in the first section,  $2 \text{ mm}$ , is smallest. This increases in sections two, three and four to  $3 \text{ mm}$ ,  $4 \text{ mm}$  and  $6 \text{ mm}$ , respectively. The entire system is made of either stainless steel or glass with PTFE applied as sealant.

The two pumps (3) draw the reactants from the storage tanks (1) separately. In the tubing, a  $7 \mu\text{m}$  mesh filter (2) is installed to prevent any particles from entering the pumps and the reaction line. The two liquid streams are then fed into the vortex-type micro-mixer ((4) in Fig. 1 and Fig. 2) where the reaction is initiated. After the mixing unit, the liquid enters the temperature regulated section of the reaction tube (5). After each section of the reaction tube, sample valves (6) are installed. The cooling/heating medium is water which circulates through the vessels and the thermostat (7) controls the temperature of the liquid stream to the defined value. To ensure isothermal conditions of the reaction tube, temperature gauges are installed in the cooling medium between the tempered sections (8). For measuring the inner temperature of the reaction tube a glass fibre with a Bragg grating is applied (10). The measuring principle, which is described elsewhere,<sup>10</sup> is based on a change of the refractive index by heat expansion

of the fibre core. In order to receive a temperature profile the fibre was located at different axial positions. For the monitoring of the reaction pressure, gauges (9) are installed in the reaction tube.

In this investigation IC-pumps were used although they are known for a residual pulsation to be detrimental to the effectiveness of the micro-mixer. Nonetheless, the pulsation effect was negligible with an analogous mixer set-up (1–4) as reported elsewhere.<sup>3</sup> In the experiments the total volume flow

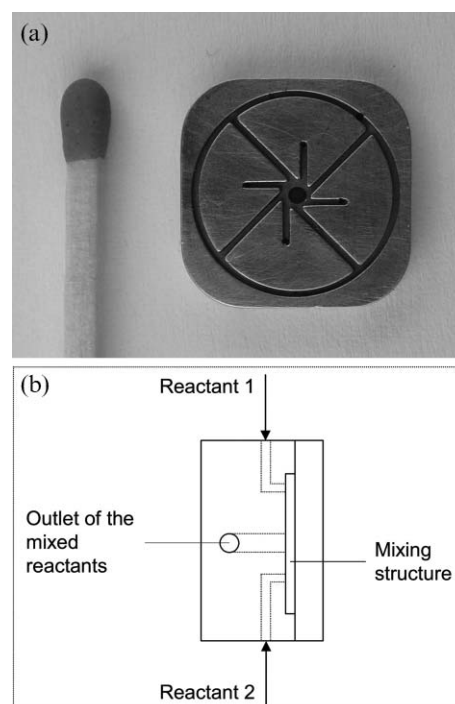


Fig. 2 Top view of the vortex-type micro-mixer (a) and side view of the working principle (b).

was constant at 480 mL h<sup>-1</sup> with a molar ratio of BrBu and MeIm of 1.2. In three experiments the temperature was maintained at 65, 75 and 85 °C. During the experiments we could observe a gauge pressure of up to 1 bar decreasing in flow direction.

Samples of approx. 5 mL are taken which are instantly quenched at  $T = -20$  °C, diluted and stored in 40 mL acetonitrile. For the determination of the conversion a HPLC-system of VWR-Hitachi was used in combination with a column from Waters (Atlantis HILIC Silica 5 µm, 4.6 × 150 mm). The concentration of [BMIM] and MeIm was determined using UV-absorption at 210 nm.

The final products were stored at 20 °C in closed glass bottles. For purity analysis, 1 g samples of these substances were treated for 30 min in a rotary evaporator operating at 50 °C and a pressure of 10 mbar. The product quality was then checked by NMR-analysis measuring the <sup>1</sup>H spectrum on a Bruker 200 MHz spectrometer using CDCl<sub>3</sub> with tetramethylsilane as the reference and by HPLC (HP Agilent 1100 series, column: Monochrome MS from Varian, RP18 5 µm, 3 × 150 mm) with a variable wavelength detector and a mass spectrometer (ESQUIRE-LC, ESI-Iontrap from Bruker). The eluent flow during HPLC measurements was 0.5 mL min<sup>-1</sup> and consisted of 70% acetonitrile and 30% 5 mmol L<sup>-1</sup> solution of ammonium acetate in 0.1 wt% acetic acid. Finally, the concentrations were determined again using UV-absorption at 210 nm.

### 3 Modelling

The theoretical model used to simulate the reaction is based on reaction kinetic, mass and compound balances in addition to heat transfer. Contrary to the model suggested by Große Böwing and Jess<sup>4</sup> but in accordance with the findings of Gainza<sup>11</sup> we assume that the reaction rate,  $r$ , can satisfactorily be described by a second order reaction kinetic of the form,

$$r = Ae^{\left(\frac{-E_a}{RT}\right)} c_{\text{MeIm}} c_{\text{BrBu}} \quad (1)$$

where  $R$  is the gas constant (J mol<sup>-1</sup> K<sup>-1</sup>),  $T$  the temperature (K),  $c$  the concentration (mol L<sup>-1</sup>),  $A$  the frequency factor (L mol<sup>-1</sup> s<sup>-1</sup>) and  $E_a$  the energy of activation (J mol<sup>-1</sup>). The last two parameters were determined using the Arrhenius equation that describes the temperature dependency of the reaction rate constant:

$$k_R(T) = Ae^{\left(\frac{-E_a}{RT}\right)} \quad (2)$$

In the linear form this equation can be written as

$$\ln(k_R(T)) = \ln(A) - \frac{E_a}{R} \times \frac{1}{T} \quad (3)$$

Furthermore, according to Levenspiel<sup>12</sup> the reaction rate constant of second-order kinetics can be obtained by plotting

$$y = \ln \frac{c_{\text{BrBu}} c_{\text{MeIm},0}}{c_{\text{BrBu},0} c_{\text{MeIm}}} \quad (4)$$

against the time  $t$  (s) at a specified temperature. The slope,  $s$ , of the regression line is represented by

$$s = (c_{\text{BrBu},0} - c_{\text{MeIm},0}) k_R(T) \quad (5)$$

From this equation the reaction rate constant can be obtained at given initial concentrations of BrBu and MeIm,  $c_{\text{BrBu},0}$  and  $c_{\text{MeIm},0}$  respectively. By plotting  $\ln(k(T))$  against  $1/T$  the frequency factor,  $A$ , and the activation energy,  $E_a$ , can be obtained. Assuming an ideal plug flow reactor the volume element dependence of the conversion  $X$  can be calculated using the following mole balances.

$$\frac{d\dot{n}_i}{dV} = -r(T) \quad \forall i \in \{\text{MeIm, BrBu}\} \quad (6)$$

The conversion of the limited reactant, the amine, is given as

$$dX = - \frac{d\dot{n}_{\text{MeIm}}}{\dot{n}_{\text{MeIm},0}} \quad (7)$$

and thus

$$\frac{dX}{dV} = \frac{r(T)}{\dot{n}_{\text{MeIm},0}} \quad (8)$$

where the left side of eqn (6) describes the change of mole flow in a cylindrical volume element of the reactor and  $r$  (mol s<sup>-1</sup> dm<sup>-3</sup>) is the reaction rate. The energy balance is given by the relation

$$\frac{dT}{dV} = \frac{ak(T_{\text{cool}} - T_{\text{reactor}}) + r(T)(-\Delta H_R)}{\sum (\dot{n}_i c_{pi})} \quad (9)$$

where  $a$  (dm<sup>-1</sup>) is the volume specific area of the inner wall of the tube reactor,  $k$  (W dm<sup>-2</sup> K<sup>-1</sup>) the heat transfer coefficient (between cooling agent and reactive mixture),  $T_{\text{cool}}$  (°C) is the temperature of the cooling agent,  $\Delta H_r$  (J mol<sup>-1</sup>) the enthalpy of reaction,  $\dot{n}_i$  (mol s<sup>-1</sup>) the mole flow of each compound, and  $c_{pi}$  (J mol<sup>-1</sup> K<sup>-1</sup>) the heat capacities of each compound. These coupled differential equations were solved using the ode45 solver for initial value problems of the software package MatLab.

The initial time dependent mole balances described by eqn (10) can be rewritten upon expansion and rearrangement of terms to conversion rate (eqn (11)), which was used to perform the simulation of the solvent-free batch synthesis in addition to eqn (12) for the temperature transients' description.

$$\frac{1}{V_{\text{reactor}}} \times \frac{dn_i}{dt} = -r(T) \quad \forall i \in \{\text{MeIm, BrBu}\} \quad (10)$$

$$\frac{dX}{dt} = \frac{r(T) V_{\text{reactor}}}{\dot{n}_{\text{MeIm},0}} \quad (11)$$

$$\frac{dT}{dt} = \frac{kA_s(T_{\text{cool}} - T_{\text{reactor}}) + V_{\text{reactor}} r(T)(-\Delta H_R)}{\sum (\dot{n}_i c_{pi})} \quad (12)$$

where  $dn_i/dt$  is the change of moles of the reactants and the product respectively,  $A_s$  (dm<sup>2</sup>) is the surface of the reactor (spherical shape) and  $\dot{n}_i$  (mol) is the amount of moles of each reactant.

The calculations were performed for a typical laboratory scale reactor volume of  $V_{\text{reactor}} = 4 \text{ L}$  and a heat transfer coefficient of  $k = 4 \text{ W dm}^{-2} \text{ K}^{-1}$ . The heat transfer coefficient was evaluated using similar chemical entities (triethylamine and chlorobutane) according to the standard procedure<sup>13</sup> for tube reactors.

Finally, the STY ( $\text{kg m}^{-3} \text{ h}$ ) can be calculated for the batch process (eqn (13)) and for continuous synthesis (eqn (14)) at a given conversion.

$$\text{STY} = \frac{m_{\text{product}}}{V_{\text{reactor}} \tau} \quad (13)$$

$$\text{STY} = \frac{\dot{m}_{\text{product}}}{V_{\text{reactor}}} \quad (14)$$

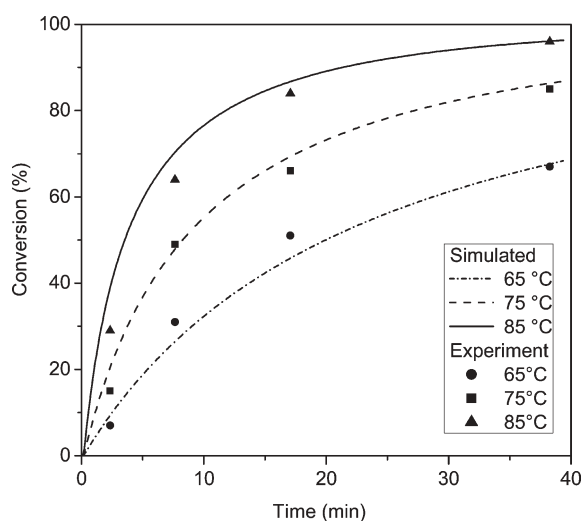
Referring to the product [BMIM]Br,  $m_{\text{product}}$  (kg) and  $\dot{m}_{\text{product}}$  ( $\text{kg s}^{-1}$ ) are the mass and mass flow, respectively, and  $\tau$  (s) is the residence time.

## 4 Results and discussion

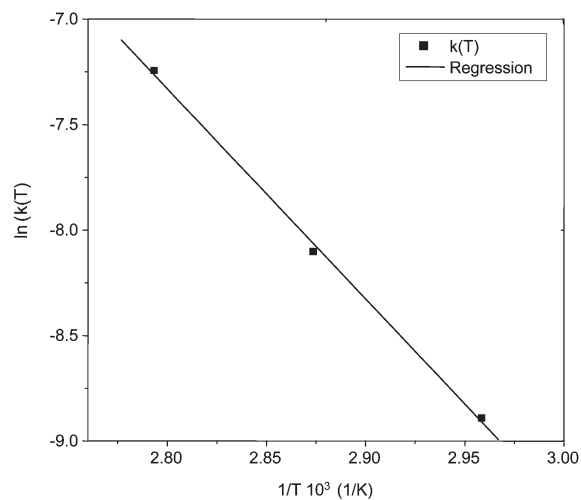
Both the synthesis in the micro-reactor and the simulated batch reaction were performed in the solvent-free mode to demonstrate the comparative performance clearly. The conversion data obtained from the continuous alkylation in the micro-reactor at three different temperatures (Fig. 3) are used in three steps.

### 4.1 Determination of kinetic constants

Firstly, the experimental data were used to determine the kinetic parameters  $k(T)$  and  $E_a$ : The rate constants at the three set temperatures (65, 75 and 85 °C) were evaluated through graphical analysis by applying eqn (4) and eqn (5). From the linear regression carried out on the Arrhenius plot (Fig. 4) based on eqn (3) the kinetic parameters obtained are as follows: frequency factor  $A = 8.51 \times 10^8 \text{ L mol}^{-1} \text{ s}^{-1}$  and energy of activation  $E_a = 82.818 \text{ kJ mol}^{-1}$ .



**Fig. 3** Conversions measured during continuous synthesis versus simulated transients at three temperature levels (65, 75 and 85 °C).

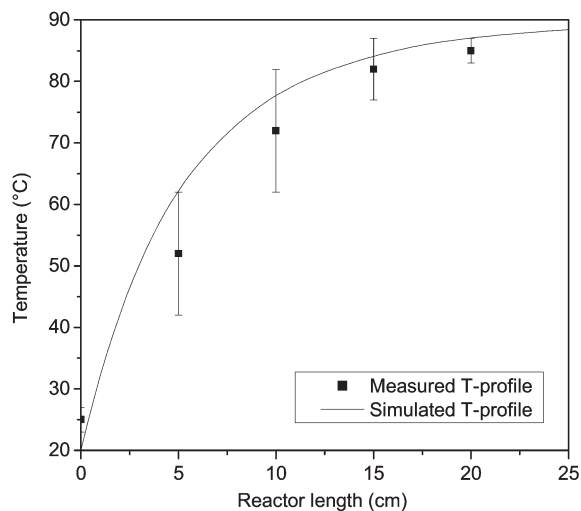


**Fig. 4** Arrhenius plot based on the experimental conversion data from IL-synthesis in the micro-reactor from which the best fit of the  $k_r(T_i)$ -values was determined according to Levenspiel.<sup>12</sup> The presented line yields the regression  $\ln(k(T)) = -9961.3 \times 1/T + 20.562$ ;  $R^2 = 0.9983$ .

### 4.2 Continuous synthesis

In a second step, the kinetic parameters were introduced to the model for simulating the course of conversion (eqn (8)). Comparing the simulated and measured values (Fig. 3) a satisfying correlation can be demonstrated. It can be seen clearly that, as expected, the conversion rate rises with increasing wall temperature.

It can further be shown that temperature measurements showed a good agreement with the simulated values. The data illustrated in Fig. 5 were obtained from measurements with the glass fibre placed along the reaction tube in the entrance zone of the reactor where the reactants have to be heated to the final reaction temperature. In this figure, the data were plotted on the same plane as the simulated temperature profile resulting



**Fig. 5** Comparison of simulated temperature transients with the temperature profile measured inside the first section of the reaction tube; wall temperature: 85 °C.



from theoretical calculation executing the reactors model that includes the determined kinetic parameters and the independently computed heat transfer coefficient  $k = 4 \text{ W dm}^{-2} \text{ K}^{-1}$ .

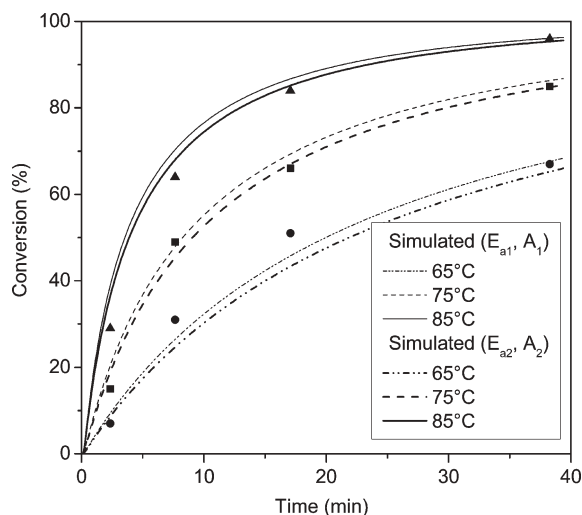
From Fig. 5, it can be noted that the simulated temperature curve tends to have a steeper slope. This was expected as the model does not include axial thermal conductivity that would otherwise smoothen the temperature profiles. This implies that an overestimation of the hot spots is likely when varying the wall temperature to identify runaway temperatures. The variation of the measured temperature values decreases with increasing reactor length which could be linked to an inhomogeneous liquid flow in the entrance region of the reactor tube.

It should be noted that isothermal conditions were assumed for the kinetic analysis. Nevertheless, as demonstrated in Fig. 5, simulation results and measurements show a short heating zone. To evaluate the error that could have resulted from the isothermal assumption, a second kinetic analysis was carried out.

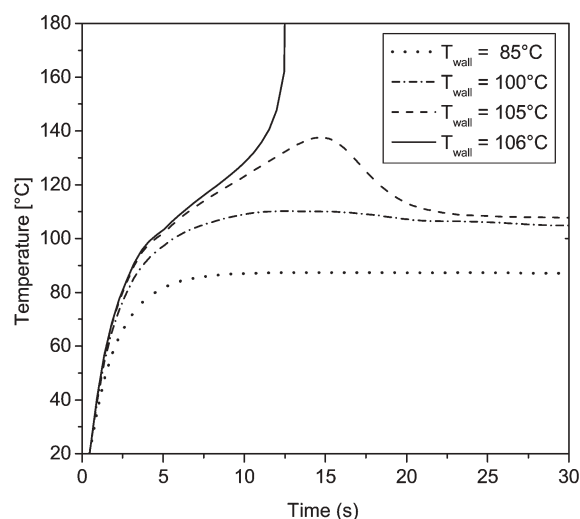
In this second analysis, the residence time was reduced by the time taken for heating the reaction media to the desired temperature level. From this procedure the new set of kinetic parameters obtained are  $E_{a2} = 82.830 \text{ kJ mol}^{-1}$  and  $A_2 = 7.82 \times 10^8 \text{ L mol}^{-1} \text{ s}^{-1}$ .

In Fig. 6 the simulated conversion curves for both sets of kinetic data are presented. They clearly demonstrate that at temperatures above  $70^\circ\text{C}$  the new parameters give a better fit. For this reason the second kinetic data set was applied in the following to calculate the maximum wall temperature.

As in any reaction system the micro-reactor is expected to be limited by a maximum wall temperature as shown in Fig. 7. At a certain temperature, depending on the geometry and therefore the surface area to volume ratio, the heat produced by the reaction can not be sufficiently removed through the reactor wall, consequently leading to a temperature increase. Through possible auto-acceleration effects influenced by such



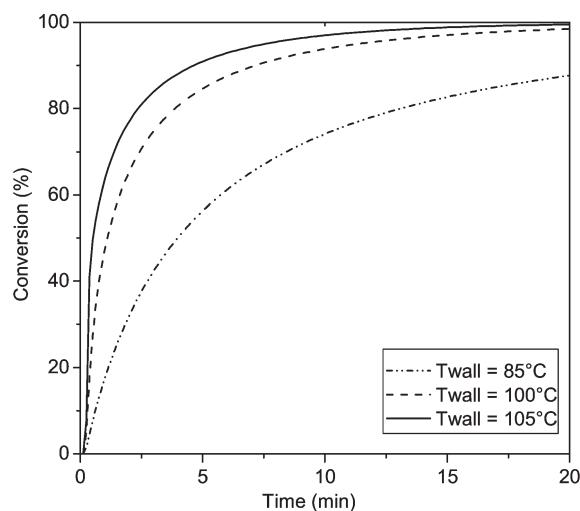
**Fig. 6** Comparison of simulated conversion transients obtained with kinetic data set 1 and 2. Experimental conversion data are taken from Fig. 3.



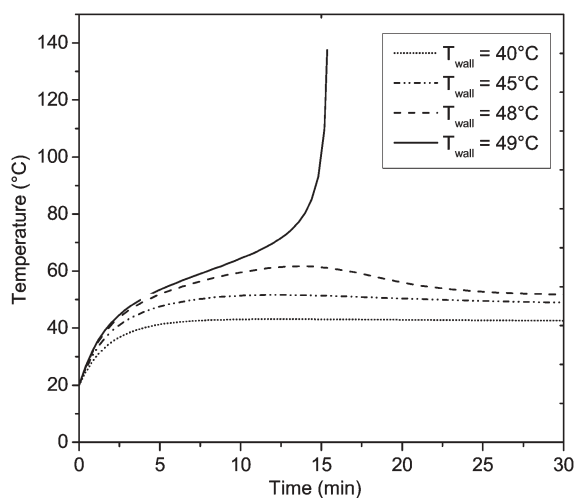
**Fig. 7** Temperature transients inside the micro-reactor during ionic liquid synthesis at different wall temperatures.

local temperature increases, the reaction could get out of control resulting in thermal runaway behaviour. High temperature peaks of up to a few hundred  $^\circ\text{C}$  could appear, which could in turn affect the product quality through decomposition, and concurrently reduce process safety. With the developed reactor model the maximum wall temperature can be estimated at which the synthesis can be operated safely avoiding a runaway of the reaction (Fig. 7). In the experimental reactor, a small diameter was used in the first section where the reaction rate is fastest. This enables an enhanced local heat flux not only due to the high surface area to volume ratios realised but also the existing smaller diffusion lengths.

In the experiment, a conversion of 95% could be obtained after 38 min at  $85^\circ\text{C}$  (Fig. 3). To reach 97% conversion the reaction time has to be extended to 48 min. The residence time demand can be reduced down to 10 min (Fig. 8) with a



**Fig. 8** Simulated conversion of the reaction according to Scheme 1 and eqn (8) in the micro-reactor at different wall temperatures.



**Fig. 9** Simulation of temperature transients in batch synthesis according to eqn (12) based on kinetic data set 2 as received from eqn (3). For wall temperatures above 48 °C a runaway of the fluid temperature cannot be avoided. Case study reactor volume: 4 L; heat transfer coefficient  $k$ : 400 W m<sup>-2</sup> K<sup>-1</sup>.

temperature increase of 20 K reaching the simulated limiting temperature of 105 °C (Fig. 7). With respect to the production of [BMIM]Br at a 97% conversion these two process alternatives at 85 °C and 105 °C lead to STYs of 1.27 kg h<sup>-1</sup> L<sup>-1</sup> and 6.1 kg h<sup>-1</sup> L<sup>-1</sup>, respectively.

### 4.3 Comparison with batch synthesis

In contrast to the micro-reactor, the batch reactor is limited by a low maximum wall temperature of 48 °C. Above this value, a runaway of the reaction temperature (Fig. 9) and the system pressure cannot be avoided. At the maximum wall temperature of 48 °C for the batch synthesis a conversion of 97% can be expected after approximately 19 h according to eqn (11). With the total volume of 4 L and with respect to [BMIM]Br, a STY of 0.054 kg h<sup>-1</sup> L<sup>-1</sup> reactor volume is obtained.

Though the experiments for the continuous [BMIM]Br-synthesis in the micro-reactor at 85 °C exhibit a 24 × greater STY than the batch synthesis, even an improvement of factor 100 seems to be applicable at higher wall temperatures of  $T_{\text{wall}} = 105$  °C as shown by the simulation.

For large scale batch synthesis of [BMIM]Br, it has to be noted, that for security reasons, it is advisable to perform the reaction in a solvent, while adding one reactant slowly. In this case even higher process intensification can be expected by using micro-reactor technology.

### 4.4 Evaluation of product quality

The [BMIM]Br products synthesized at 65 °C and at 75 °C were yellowish high viscous liquids. The analysis by HPLC MS showed excellent quality comparable with the same compound produced by Merck KG.

Traces of impurities could only be detected in the product synthesized at 85 °C, which was crystalline with a pale yellow

colour. Most probably the MS-signals found in this product were caused by 1-ethyl-3-methylimidazolium at a retention time of 6.14 min and 1-pentyl-3-methylimidazolium cations at a retention time of 8.7 min since the charge specific masses  $m/z$  were 111.2 and 153.1 respectively. Nevertheless these compounds were negligible as they both appeared at less than 0.1% of the main product peak value.

By <sup>1</sup>H-NMR no impurities could be detected except for some traces of 1-bromobutane in the sample synthesized at 65 °C. This is possibly due to some residues of the alkylating reactant 1-bromobutane that could not be removed totally by evaporation. The chemical shifts  $\delta_{\text{H}}$  noted were: 0.95 (t, CH<sub>3</sub>), 1.29 (m, CH<sub>2</sub>), 1.91 (m, CH<sub>2</sub>), 4.13 (s, N-CH<sub>3</sub>), 4.35 (t, N-CH<sub>2</sub>), 7.55 (d, NCH), 7.67 (d, NCH), 10.30 (s, N(H)CN). 1-Methylimidazole was not found in any of the samples. We suppose that storing the reaction mixture for several days at 20 °C from the time of sampling at conversions of 70–95% to the moment of purity analysis allowed the mixtures to slowly complete the conversion.

## 5 Concluding remarks

This investigation has pointed out the potential of micro-reactors for a continuous production of imidazolium-based ionic liquids at high efficiency without any additional solvent needed to control the reaction. The findings illustrate the significance of high specific surface area of the reaction system to carry away heat resulting from strongly exothermic reactions. It is therefore imperative for further optimization of the micro-reactor to adjust the surface to volume ratio with respect to the desired reaction temperature. This could in turn lead to hundredfold STYs compared to those of conventional batch systems, which are much more strictly limited by temperature.

The product purity received was above 99%. However, some traces of impurities could be detected at the highest temperature investigated. Additional experiments performed at temperatures above 100 °C and gauge pressures above 2 bar would allow one to understand whether there is a correlation between temperature, residence time and impurities.

With the micro-reactor investigated, the process intensification potential has been revealed and, concurrently, the chances for increased sustainability in ionic liquid manufacturing.

## Acknowledgements

The authors would like to thank Peter Behrend, Anja Müller, Melenke Stolle, and Stefan Stolte for their assistance in performing the experiments as well as Prof. Dr Bernd Jastorff from the University of Bremen, for helpful discussions. We also thank our partners Dr Natalie Salk, Dr Thorsten Plaggenborg and Torben Seemann from Fraunhofer IFAM, Bremen, for providing us with the micro-mixers, Dr Christoph v. Kopylow and Berthold Müller for providing the glass fibre-based temperature measurement system, Philip Jaeger from Eurotechnica GmbH, Bargteheide, for manufacturing the mini-plant and Dr Thomas Schubert from IoLiTec, as well as Dr Guntram Koller and Dr Welz Biermann from Merck KG for a fruitful cooperation. The financial support of this

investigation (project No. 16SV1970) by VDI/VDE-IT within the “BMBF Förderschwerpunkt Mikrosystemtechnik” is gratefully acknowledged.

## References

- 1 B. Jastorff, R. Störmann, J. Ranke, K. Mölter, F. Stock, B. Oberheitmann, W. Hoffmann, J. Hoffmann, M. Nüchter, B. Ondruschka and J. Filser, *Green Chem.*, 2003, **5**, 136–142.
- 2 S. J. Haswell and P. Watts, *Green Chem.*, 2003, **5**, 240.
- 3 M. Hoffmann, M. Schlüter and N. Rübiger, *Chem. Eng. Sci.*, 2006, **61**, 2968–2976.
- 4 A. Große Böwing and A. Jess, *Green Chem.*, 2005, **7**, 230–235.
- 5 A. Große Böwing, A. Jess and P. Wasserscheid, *Chem. Ing. Tech.*, 2005, **77**(9), 1430–1439.
- 6 K. M. Chan, N.-H. Chang and M. R. Grimmet, *Aust. J. Chem.*, 1977, **30**, 2005–2013.
- 7 J. S. Wilkes, J. A. Levisky, R. A. Wilson and C. L. Hussey, *Inorg. Chem.*, 1982, **21**, 1263–1264.
- 8 P. Bonhôte, A.-P. Dias, N. Papageorgiou, K. Kalyanasundaram and M. Grätzel, *Inorg. Chem.*, 1996, **35**, 1168–1178.
- 9 S. V. Dzyuba and R. A. Bartsch, *Chem. Commun.*, 2001, 1466–1467.
- 10 *German Pat.*, 10 2004 031 324 A1 2006.01.19.
- 11 A. H. Gainza, *Int. J. Chem. Kinet.*, 2006, **36**(9), 500A–509A.
- 12 O. Levenspiel, *Chemical Reaction Engineering*, John Wiley & Sons, 3rd edn, 1999.
- 13 VDI-Wärmeatlas, 10. Auflage, Springer-Verlag, Berlin, Heidelberg, 2006.

# STOP!

searching...

**Save valuable time searching for that elusive piece of vital chemical information.**

Let us do it for you at the Library and Information Centre of the RSC.

**We are your chemical information support, providing:**

- Chemical enquiry helpdesk
- Remote access chemical information resources
- Speedy response
- Expert chemical information specialist staff

Tap into the foremost source of chemical knowledge in Europe and send your enquiries to

**library@rsc.org**

RSC Publishing

**www.rsc.org/library**

12120515

# Bisoxazoline-functionalised enantioselective monolithic mini-flow-reactors: development of efficient processes from batch to flow conditions†‡

M. Isabel Burguete,<sup>a</sup> Alfonso Cornejo,<sup>b</sup> Eduardo García-Verdugo,<sup>\*a</sup> Juan García,<sup>c</sup> Maria José Gil,<sup>b</sup> Santiago V. Luis,<sup>\*a</sup> Victor Martínez-Merino,<sup>b</sup> Jose Antonio Mayoral<sup>d</sup> and Maia Sokolova<sup>a</sup>

Received 23rd March 2007, Accepted 24th May 2007

First published as an Advance Article on the web 13th June 2007

DOI: 10.1039/b704465h

Monolithic polymers functionalised with BOX-Cu moieties can be applied for the cyclopropanation reaction under batch and flow conditions using either conventional or supercritical solvents.

## Introduction

Development of supported enantioselective catalysts having the advantage of being easily separated and reused and showing a potential for practical applications is an important goal nowadays.<sup>1,2</sup> Nevertheless, data from the literature show that results with supported systems are often different from those expected from solution studies. Thus, even experienced organic chemists consider the support as a black box, assuming the idea that enantioselective immobilised systems are usually less efficient in terms of activity and selectivity than the homogeneous ones. Fortunately, an appropriate design can lead to heterogeneous catalysts with similar or improved efficiencies relative to those of the homogeneous ones.<sup>3,4</sup>

Bisoxazoline-copper complexes (BOX-Cu) and related species show a large number of applications in enantioselective catalysis.<sup>5</sup> Accordingly, many efforts have been directed towards making these species heterogeneous.<sup>6–9</sup> Such efforts are a clear example of how the immobilisation of a homogeneous catalyst to a suitable support is a very tricky task. Indeed, completely different results are achieved depending on the immobilisation methodology and with the characteristics and properties of the support used.<sup>6</sup> The morphology of the support and the type of immobilization contribute to the performance of the final catalyst as it controls both the accessibility and nature of the microenvironment of the active centers.<sup>3</sup>

Supported catalysts allow for their easy separation and reuse, being ideal to develop continuous flow processes based on fix-bed reactors. Continuous flow processes are really attractive from an industrial perspective. They offer a number

of potential advantages over existing batch techniques.<sup>10</sup> Although some interesting approaches were recently reported for continuous asymmetric processes using either organic or inorganic supports, the applicability of these approaches is sometimes limited.<sup>11</sup> Furthermore, to the above mentioned difficulties to develop efficient supported catalysts, additional factors should be considered in order to design an efficient heterogeneous catalytic continuous flow process. Catalysts packed as random catalytic fix-bed reactors lead to stagnation zones, hot-spot formation and long residence times distribution, resulting in low process efficiency.<sup>10,12</sup>

Here we report our results using BOX-Cu functionalised polymeric monoliths under batch and flow conditions. It is possible to implement the separation and long-term stability of the catalyst and to achieve a good space-time yield and enantioselectivity of the benchmark reaction under study. We show not only the importance of the polymeric matrix, but also the key role of the proper adjustment of experimental conditions either for the batch or flow reactions that allow for a fine tuning of the overall process. Catalysts based on monolithic polymers can be used to develop efficient continuous asymmetric reactions, solving some of the drawbacks found for random packed catalytic reactors.

## Experimental

**Safety note:** some of the experiments described in this paper involve the use of relatively high pressures and require equipment with the appropriate pressure rating. It is the responsibility of individual researchers to verify that their particular apparatus meets the necessary safety requirements.

The monomer 2,2'-[2-(4-vinylphenyl)-1-(4-vinylbenzyl)ethylidene]bis-[(4S)-4-phenyl-4,5-dihydro-2-oxazole] (**3**) was synthesized as previously reported in ref. 9. Styrene (VB), divinylbenzene (DVB, 80% grade) and ethyl diazoacetate (EDA) were purchased from Aldrich and used without further purification. The cyclopropanes used for analytical determinations have been synthesized as previously reported.<sup>9</sup>

## Preparation of monolithic mini-flow-reactors

Monoliths were molded into a glass or a stainless-steel column (15 cm × ¼ inch) using a solution of 0.01 g of azobisisobutyronitrile (AIBN) and **3** (0.1 mol) in styrene (0.7 mol), and

<sup>a</sup>Dpt. of Inorganic and Organic Chemistry, Universidad Jaume I, Avda. Sos Baynat s/n, 12071, Castellón, Spain. E-mail: luiss@gio.uji.es; Fax: +34 964 72 82 14; Tel: +34 964 72 82 39

<sup>b</sup>Dpt. of Organic Chemistry, Instituto de Ciencia de Materiales de Aragón, Facultad de Ciencias, Universidad de Zaragoza-C.S.I.C., E-50009, Zaragoza, Spain. Fax: +34 976 76 20 77; Tel: +34 976 76 22 72

<sup>c</sup>Dtp. de Ingeniería Química y Tecnología del Medio Ambiente, Facultad de Ciencias, Universidad de Valladolid, Prado de la Magdalena 47011 Valladolid, Spain. Fax: +34 983 42 30 13; Tel: +34 983 42 31 74

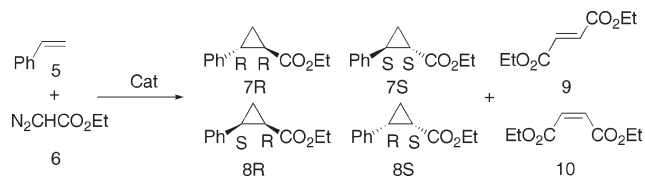
<sup>d</sup>Dpt. of Applied Chemistry, Universidad Pública de Navarra, Edificio los acebos. Campus Arrosadia, 31006, Pamplona, Spain. Fax: +34 948 16 96 06; Tel: +34 948 16 95 95

† Dedicated to Professor M. Poliakov for his 60th birthday.

‡ Electronic supplementary information (ESI) available: Detailed kinetic information. See DOI: 10.1039/b704465h



divinylbenzene (80% w/w, 0.2 mol), using toluene (0.25 g), and 1-dodecanol (1.25 g) as the porogens. The polymerisation mixture was stirred and purged with nitrogen for 3 min and poured into the mould. The polymerisation was allowed to proceed for 24 h at 70 °C. THF was used to remove the porogenic solvents and any other soluble compounds after the polymerisation reaction.



**Scheme 1** Benchmark cyclopropanation reaction.

### Cyclopropanation under batch conditions

To a solution of EDA (0.5 M) and VB (2 M) in  $\text{CH}_2\text{Cl}_2$  (25 mL) was added PhGli-BOX-Cu(OTf)<sub>2</sub> (0.4 mol%) as the catalyst. The reaction was monitored by HPLC by taking 10  $\mu\text{L}$  aliquots, which were diluted in 1 mL solution of  $\text{CH}_3\text{CN}$  containing ethyl benzoate (1 mg  $\text{mL}^{-1}$ ) as the internal standard. HPLC conditions: C18 column  $\text{CH}_3\text{CN} : \text{H}_2\text{O}$  60 : 40 (0.1% v/v TFA); 30 °C; flow rate: 1  $\text{mL min}^{-1}$ ; 3.3 min (EDA), 4.4 min (ethyl maleate), 7.4 min (ethyl fumarate), 11.4 min (ethyl benzoate, internal standard), 14.1 min (cyclopropane, *cis*), 16.6 min (styrene), 19.4 min (cyclopropane, *trans*). An assay of enantiomeric purity was performed by gas chromatography with a Cyclodex-B column: 30 m  $\times$  0.25 mm  $\times$  0.25  $\mu\text{m}$ , FID detector; helium as carrier gas, 20 p.s.i.; injector temperature: 230 °C; detector temperature: 250 °C; oven temperature program: 125 °C isotherm. Retention times: (1*S*,2*R*)-cyclopropane **14S**, 28.3 min; (1*R*,2*S*)-cyclopropane **14R**, 29.1 min; (1*R*,2*R*)-cyclopropane **13R**, 33.9 min; (1*S*,2*S*)-cyclopropane **13S**, 34.3 min.

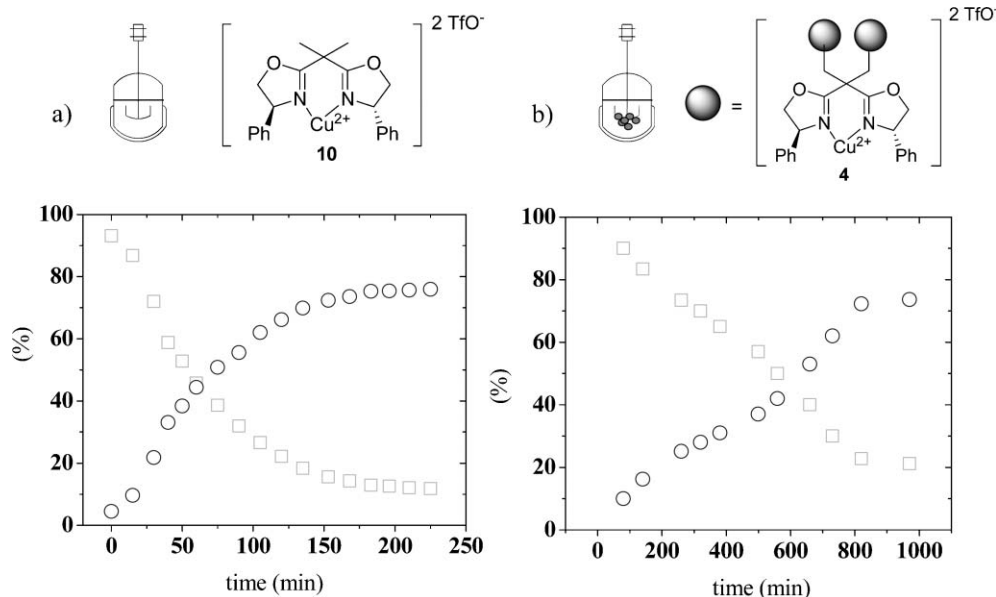
### Cyclopropanation under continuous flow conditions

A fresh reaction mixture of styrene (2.0 M) and ethyl diazoacetate (0.5 M) in anhydrous degassed methylene chloride was pumped through the monolithic column at different flow-rates using an HPLC pump. Samples were taken every 30 or 60 min and analyzed by HPLC and GC. Experiments were started when product streams were

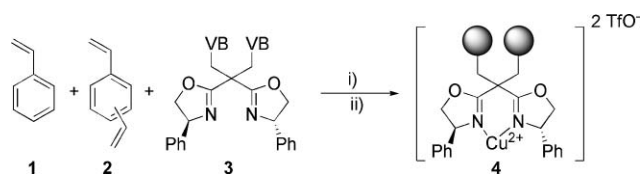
stabilized after the initiation period (*ca.* 1 h). For the solventless reaction the solution was prepared without the addition of methylene chloride (1.78 M EDA in VB : EDA). For supercritical fluid (SCF) runs, the SCF was pressurised and delivered by a Peltier cooled pump running in constant flow mode, the organic substrates (4 : 1 VB : EDA, 1.78 M EDA in VB : EDA) being delivered at a constant rate *via* a standard HPLC pump. All feed streams were mixed (dynamic mixer) before being passed through the catalytic bed. Products were collected after a single stage depressurisation of the fluid mixture by an electronic backpressure regulator.

### Results and discussion

The benchmark reaction selected for the present study was the cyclopropanation reaction between styrene (VB) and ethyl diazoacetate (EDA) (Scheme 1). First, the reaction was performed under batch conditions with the homogeneous copper complex (0.4 mol% PhGli-BOX-Cu(OTf)<sub>2</sub> **10** as the homogeneous catalyst) with a solution of EDA (0.5 M) and of VB (2 M) in  $\text{CH}_2\text{Cl}_2$ . Fig. 1 shows the evolution of the reaction with time. After two hours of reaction, *ca.* of 85% of conversion of EDA was achieved. The cyclopropane (CP) yield (**7** + **8**) was around 75% with a 70 : 30 *trans* : *cis* ratio (TON 96 g CP per g Cu; TOF 31.4 (g CP per g Cu)  $\text{h}^{-1}$ ). The enantioselectivity of the reaction was constant for the aliquots evaluated, being 58% ee for the *trans* isomer and 45% ee for the *cis*.



**Fig. 1** Batch cyclopropanation reaction between **5** and **6**. (□) % EDA conversion; (○) % yield (**7** + **8**). (a) Homogeneous catalysed process. (b) Heterogeneous catalysed process.



**Scheme 2** (i) **1** : **2** : **3** 70 : 20 : 10, % mol; mixture of monomers : toluene : 1-dodecanol 40 : 10 : 50, % weight; 70 °C, 1% AIBN; 24 h. (ii) Cu(OTf)<sub>2</sub>/MeOH.

The supported catalyst was prepared by polymerisation of the chiral monomer (**3**) with styrene (**1**) and divinylbenzene (**2**) in the presence of the porogenic mixture (Scheme 2). The mixture was placed within a glass tube that acts as a mold. After the polymerization process was completed, the glass tube was broken, and the monolith was sliced into disks of the required thickness. The polymeric monoliths, when the reaction is performed in a batch process, can be removed as a single piece. The monolith was mechanically stable, greatly facilitating its manipulation and, therefore, the catalyst can be easily reused. The monolithic polymer showed a bisoxazoline loading of 0.66 meq g<sup>-1</sup>, as determined by elemental analysis. However, only a limited amount of bisoxazoline moieties were loaded with copper (32% of the functional sites, 0.21 meq of Cu per g by ICP-MS). Most likely this reflects that some chiral moieties are located in highly cross linked regions and have a reduced accessibility or cannot adopt the proper conformation to form the corresponding chelate complexes.

It is important to mention that the supported catalyst is prepared by polymerization of the corresponding di-vinyl chiral monomer (**3**). Therefore, the chiral moieties are almost randomly distributed throughout the polymeric matrix and the polymer itself may become chiral, to some extent, creating many different chiral microenvironments. The exact micro-environment distribution depends on a complex series of factors, such as solvents, polarity of monomers, kinetics of polymerization of each monomer, *etc.*<sup>3</sup> In some cases, chiral moieties will become part of the linear chain (probably with un-reacted alkene left), in other cases it will be incorporated as cross linkers. On the other hand, the cross linking degree is one of the main factors affecting the accessibility of functional sites

in the polymer. Therefore, diffusion has a tremendous impact not only on Cu loading but also on the reaction outcome. Indeed, when the benchmark reaction was performed with the polymeric catalytic disc (0.4 mol% of Cu, 0.5 M of EDA and 2 M VB, see graph in Fig. 1b) the kinetics of the reaction was slower than that observed for the homogeneous catalysed reaction. The activity of the catalyst for the heterogeneous batch process was around 5 fold slower than that for the homogeneous one. Thus, reaction periods longer than 16 hours were needed to yield to the same conversion degree (*ca.* 78% EDA conversion, TOF 5.8 (g CP per g Cu) h<sup>-1</sup>). Remarkably, the catalyst showed a good asymmetric induction, with an ee of 62% for the *trans* isomers and a 56% ee for the *cis*, which are slightly better than those observed for the homogeneous catalysed process (58% ee for *trans*, 45% ee *cis*). However, the regioselectivity was slightly lower with a *trans* : *cis* ratio of 59 : 41.

In order to design a continuous process, we prepared the monolithic materials with the required functionality within a mini-flow reactor. The preparation of the monolithic reactor was carried out by thermally induced bulk polymerization of the chiral monomers and co-monomers into a stainless steel column (15 cm × ¼ inch) having the same composition than the monolith used for the batch experiments. The corresponding Cu-bisoxazoline complex was prepared by recirculation through the column of a solution of Cu(OTf)<sub>2</sub> in MeOH for 24 h. After this period the column was washed with MeOH to eliminate any non-complexed copper.

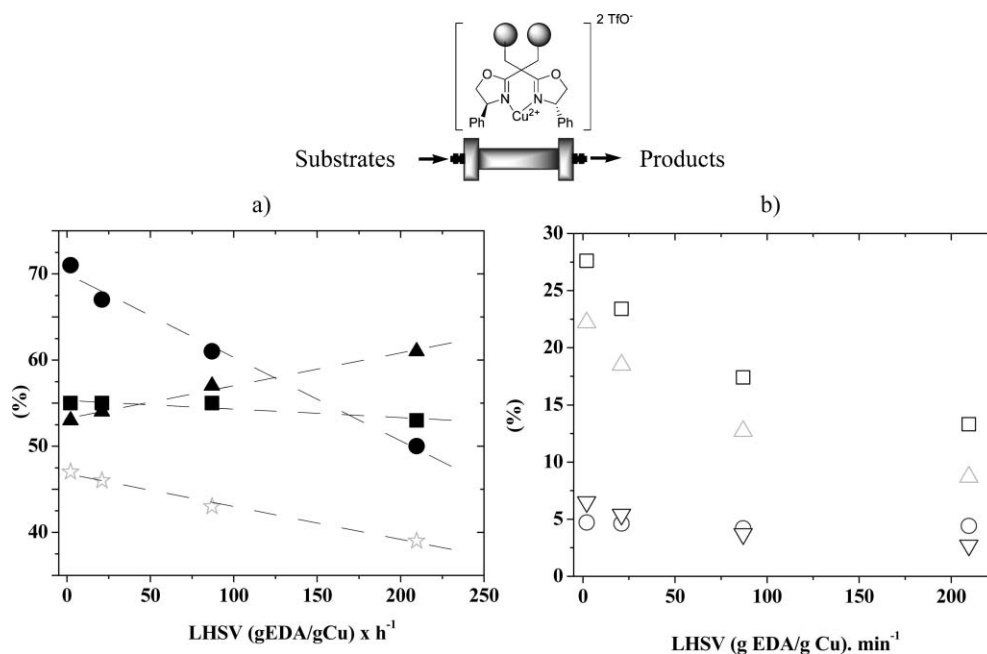
A solution of EDA and VB (0.5 M EDA and 2 M VB) in CH<sub>2</sub>Cl<sub>2</sub> was continuously pumped at different flow rates through the monolithic mini-flow-reactor to investigate the effect of the residence time of the reagents within the catalyst bed. Aliquots taken at regular time intervals at the outlet of the reactor were analyzed for the cyclopropanes (**7** and **8**) content. Some results are gathered in Table 1.

As expected, the conversion depends on the flow rates (Table 1). An increase of the flow rate (from 2 to 200 μL min<sup>-1</sup>) led to a decrease of cyclopropane yield (from 61% to 29%) and EDA conversion (from 100% to 46%), which is consistent with a reduction in the residence time in the reactor and hence a decrease in the reaction time. Quantitative conversion of EDA

**Table 1** Results for the cyclopropanation reaction in a monolithic mini-flow reactor<sup>a</sup>

Entry	Flow/ μL min <sup>-1</sup>	Residence time/min <sup>b</sup>	(g EDA per g Cu <sup>2+</sup> ) h <sup>-1</sup>	Conversion (% EDA) <sup>c</sup>	Yield (%) ( <b>7</b> + <b>8</b> ) <sup>d</sup>	Chemoselectivity <sup>e</sup> (%)	TON/g CP g Cu <sup>-1</sup> <sup>f</sup>
1	2	350.0	2.1	100	61	76	7.5
2	20	35.0	21.0	86	52	75	6.4
3	83	8.4	87.0	63	38	75	4.6
4	200	3.5	209.6	46	29	77	3.5
5 <sup>g</sup>	—	—	—	87	75	92	96 <sup>h</sup>
6 <sup>i</sup>	—	—	—	78	72	87	93 <sup>h</sup>
7 <sup>j</sup>	20	35	76	74	44	75	19.5
8 <sup>k</sup>	1100	0.64	296	100	63	76	2.0

<sup>a</sup> The reaction was carried out at rt using a solution of EDA (0.5 M) and VB (2 M) in CH<sub>2</sub>Cl<sub>2</sub>. All figures are average numbers of aliquots, determined every 30 or 60 min by means of GLC analysis with a Cyclodex-B column. 0.4 g of monolithic catalyst. <sup>b</sup> Residence time = ( $V_R \times \rho_{\text{solvent, reactor}} / (F_R \times \rho_{\text{solvent, STP}})$ ), where  $V_R$  = reactor volume (cm<sup>3</sup>),  $\rho_{\text{solvent, reactor}}$  = solvent density at process  $T$  and  $P$  (g cm<sup>-3</sup>);  $\rho_{\text{solvent, STP}}$  = solvent density at standard  $T$  and  $P$  (g cm<sup>-3</sup>);  $F_R$  = flow rate (cm<sup>3</sup> min<sup>-1</sup>); volume reactor 700 μL. <sup>13</sup> <sup>c</sup> % EDA = (mmol CP (**7** + **8**) + mmol ethyl fumarate + mmol ethyl maleate)/mmol EDA × 100. <sup>d</sup> % yield = mmol CP (**7** + **8**)/mmol EDA × 100. <sup>e</sup> Chemoselectivity % = mmol CP (**7** + **8**)/(mmol CP (**7** + **8**) + mmol ethyl fumarate + mmol ethyl maleate) × 100. <sup>f</sup> TON per catalytic cycle or bed volume. <sup>g</sup> Homogeneous complex, batch process. <sup>h</sup> TON for the batch processes. <sup>i</sup> Heterogeneous catalyst **4**, batch process. <sup>j</sup> solventless, 1.78 M EDA in VB. <sup>k</sup>  $F_{\text{scO2}} = 1 \text{ cm}^3 \text{ min}^{-1}$ ,  $F_{\text{organic}} = 0.1 \text{ cm}^3 \text{ min}^{-1}$ , 1.78 M EDA in VB,  $P = 8 \text{ MPa}$ ,  $T = 40 \text{ °C}$ .



**Fig. 2** Continuous cyclopropanation reaction between **5** and **6** in CH<sub>2</sub>Cl<sub>2</sub>. (a) (●) % ee *trans* vs LHSV; (■) % ee *cis* vs. LHSV; (▲) % *trans* vs. LHSV; (☆) % *cis* vs. LHSV; (b) % each cyclopropane vs. LHSV, (□) % **7R**, (○) % **7S**, (△) % **8R**, (▽) % **8S**.

was achieved for the longest residence time (2 μL min<sup>-1</sup>) (for more details see the ESI†).

By pumping a 0.5 M EDA solution at different flow rates, we are not only changing the residence time but also the actual EDA/Cu ratio. These variations of the amount of EDA pumped per gram of catalyst and per hour (g EDA × g<sup>-1</sup> Cu<sup>2+</sup> × h<sup>-1</sup>, LHSV (linear hour space velocity), Fig. 2) have a remarkable effect on the observed ee values. Thus, an increase in the LHSV led to lower ee values for the *trans* isomer (from 71% ee to 50% ee for the two LHSV limits considered). Nevertheless, the enantioselectivity for the *cis* isomers remained almost constant at 55% ee for the different LHSV considered. Furthermore, the *trans* : *cis* selectivity increased with the LHSV.

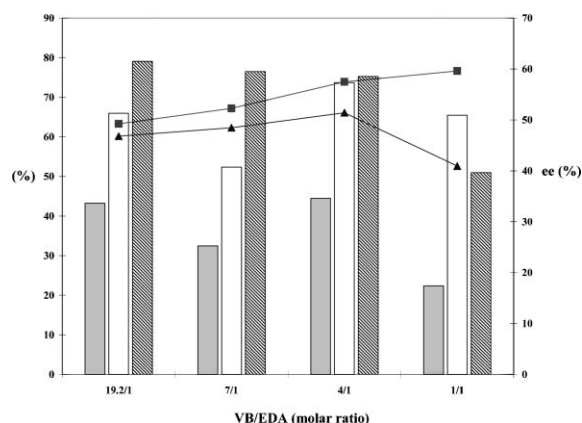
An explanation for these results can be found when the variations on the individual yields for each cyclopropane (**7R**, **7S**, **8R** and **8S**) with the LHSV were analysed (see Fig. 2b).<sup>13</sup> The concentration of the compound **7S** was almost constant for the different conditions assayed, while the other three cyclopropanes showed a similar variation profile, decreasing with the increase in LHSV. The enantiomeric excess for the *cis* isomer (**8R** and **8S**), which is a relation between both of them, was almost constant, with both enantiomers showing a similar variation with LHSV. However, the formation of **7R** strongly decreased with LHSV, while **7S** remained constant for the different LHSV values. Thus, the ee decreased with the LHSV.

Our monolithic mini-flow reactor system based on Cu-bisoxazoline in a continuous flow set-up offers advantages and disadvantages with respect to the batch reactions using either heterogeneous or homogeneous catalysts. In the continuous flow system, the enantioselectivity of the reaction improves for both stereoisomers compared to the homogeneous batch system. The improvement was significant: from 51% ee up to 71% ee (*trans*) and from 40% ee up to 55% ee

(*cis*). For the heterogeneous batch system, the ee values increased only for the *trans* isomer (from 62% ee to 71% ee), showing similar ee for the *cis* isomer (56% ee vs. 55% ee) under continuous flow conditions. However, the continuous process was less chemoselective than the batch ones. The higher EDA/Cu ratios in the continuous process seems to lead to higher formation of fumarates and maleates.

The use of CH<sub>2</sub>Cl<sub>2</sub> as the solvent for this reaction is an important drawback from an environmental point of view. In this regard, the continuous set-up based on monolithic mini-flow catalytic reactors allowed us to perform the reaction under solventless conditions. Thus, the reaction was carried out at rt by pumping, at 0.02 mL min<sup>-1</sup>, different VB/EDA solutions with molar ratios ranging from 19.2 : 1 to 1 : 1. Under solventless conditions, the flow allowed us to keep a high VB/EDA ratio at the active site throughout the process. As seen in Fig. 3, an increase in chemoselectivity is always detected for high VB/EDA ratios. Best results (Fig. 3) were obtained for a VB/EDA molar ratio 4 : 1. The enantioselectivities of both *trans* and *cis* isomers were similar to those found for the reaction in CH<sub>2</sub>Cl<sub>2</sub> for a similar residence time (57% ee for the *trans* isomer and 51% ee for the *cis*); so that the overall efficiency of the process was not reduced. As a matter of fact, the final productivity of our system experienced a three fold increase (from 11 (g of CP per g of Cu<sup>2+</sup>) × h<sup>-1</sup> to 33 (g of CP per g of Cu<sup>2+</sup>) × h<sup>-1</sup> for the solventless process, Table 1).

The use of a solvent to efficiently overcome diffusional limitations in our polymeric monoliths should produce a great improvement to the overall efficiency. This was dramatically exemplified with the use of supercritical fluids (SCFs) that intrinsically favour diffusion on complex solid geometries with diffusional limitations.<sup>14</sup> Thus, the reactions were carried out at 40 °C and 8 MPa by pumping 0.1 mL min<sup>-1</sup> of a solution of VB/EDA (4 : 1, 1.78 M of EDA) and 1.0 mL min<sup>-1</sup> of CO<sub>2</sub>,



**Fig. 3** Solventless continuous cyclopropanation reaction between **5** and **6**: grey bars: % yield; white bars: % conv. EDA; line bars: % chemoselectivity; (—■—) % ee (*trans*); (—▲—) % ee (*cis*).

affording a 63% yield of cyclopropanes and good selectivities (*trans* : *cis* ratio 53 : 47; 59% ee for *trans* and 44% ee for *cis* isomer). It is important to note that for the  $\text{scCO}_2$  process a temperature of 40 °C is required, but room temperature was used with conventional or solventless conditions. This can account for the slight decrease in enantioselectivity detected.

The stability of the monolithic catalyst was also evaluated. For the continuous set-up, no noticeable changes were observed in both product yield and enantioselectivity after *ca.* 5 hours of continuous use for the conditions assayed (DCM, solventless and  $\text{scCO}_2$ ). Metal analysis of the solution by ICP-MS showed levels of leached total metals <1 ppm. A significant improvement in the productivity was found going from conventional to supercritical conditions with the same reactor (from 55 (g of CP per g of  $\text{Cu}^{2+}$ ) to 937 (g of CP per g of  $\text{Cu}^{2+}$ ) for *ca.* 5 hours of continuous use).

Although, during the last decade, SCFs have been increasingly explored for performing a variety of enantioselective catalytic reactions, most examples involve batch reactors.<sup>15,16</sup> There are only a few antecedents of continuous asymmetric synthesis in SCFs.<sup>17</sup> The high productivity values, along with the long-term stability of the catalytic system described here, open the possibility for practical applications of the systems based on the chiral catalysts supported onto monolithic mini-flow reactors and SCFs. Indeed, we have found a similar high productivity trend for these types of fix-bed reactors for the Heck reaction catalysed by Pd in  $\text{ncEtOH}^{8d}$  and also for enzymatic reactions in  $\text{scCO}_2$ .<sup>18</sup>

## Conclusions

In conclusion, the monolithic mini-flow-reactors presented here show a high potential for practical applications in enantioselective catalytic reactions. Our results demonstrate that immobilisation of the catalyst can produce positive effects after the appropriate design of the whole set of experimental conditions. Thus, the monolithic systems under flow conditions provided an increase in enantioselectivities of *ca.* 20% relative to those for the homogenous batch process.

Additionally, the use of  $\text{scCO}_2$  as a solvent creates a much more efficient and environmentally friendly process. Using

$\text{scCO}_2$  the productivity can be maximised with a 16–17 fold increase relative to the flow reaction in DCM. Furthermore, the use of  $\text{scCO}_2$  provides not only environmental advantages, but also allows process intensification. Thus, productivities of interest for fine chemicals preparation of 186 g of CP per g of  $\text{Cu}^{2+} \text{ h}^{-1}$  can be achieved with a small reactor (700  $\mu\text{L}$ ), making the application of the new technologies considered here economically viable.

Further improvements, in particular regarding to the enantioselectivity, are in progress through chemical and morphological optimisation of the present systems and by taking advantage of the tuneable properties of the supercritical solvents.

## Acknowledgements


Financial support has been provided by MEC and Fundació Bancaixa-UJI (projects CTQ2005-08016-003 and P11B2004-13). E. García-Verdugo thanks MEC for a personal grant (Ramon y Cajal program) and M. Sokolova is greatly thankful to the EU (Marie Curie program) for personal financial support.

## References

- (a) R. Noyori, *Asymmetric Catalysis in Organic Synthesis*, Wiley, New York, 1994; (b) *Comprehensive Asymmetric Catalysis*, ed. E. N. Jacobsen, A. Pfaltz, and H. Yamamoto, Springer-Verlag, Berlin-Heidelberg, 1999; (c) *Asymmetric Catalysis on Industrial Scale*, ed. H. U. Blaser and E. Schmidt, Wiley-VCH: Weinheim, 2004.
- (a) See thematic issue: Recoverable Catalysts and Reagents, *Chem. Rev.*, ed. J. A. Gladysz, 2002, **102**; (b) S. Brase, F. Lauterwasser and R. E. Ziegert, *Adv. Synth. Catal.*, 2003, **345**, 869.
- (a) P. Hodge, *Chem. Soc. Rev.*, 1997, **26**, 417; (b) D. C. Sherrington, *Chem. Commun.*, 1998, 2275; (c) B. Altava, M. I. Burguete, E. García-Verdugo, S. V. Luis and M. J. Vicent, *React. Funct. Polym.*, 2001, **48**, 25.
- (a) B. Altava, M. I. Burguete, J. M. Fraile, J. I. García, S. V. Luis, J. A. Mayoral and M. J. Vicent, *Angew. Chem., Int. Ed.*, 2000, **39**, 1503; (b) Q.-H. Fan, R. Wang and A. S. C. Chan, *Biorg. Med. Chem. Lett.*, 2002, **12**, 1867.
- (a) A. K. Ghosh, M. Packiarajan and J. Cappiello, *Tetrahedron: Asymmetry*, 1998, **9**, 1; (b) F. Fache, E. Schulz, M. L. Tommasino and M. Lemaire, *Chem. Rev.*, 2000, **100**, 2159; (c) E. Schulz, *Chiral Diazaligands for Asymmetric Synthesis*, in *Topics in Organometallic Chemistry*, ed. M. Lemaire and P. Mangeney, vol. 15; Springer, Berlin, 2005, p. 93.
- D. Rechavi and M. Lemaire, *Chem. Rev.*, 2002, **102**, 3467.
- (a) A. Mandoli, S. Orlandi, D. Pini and P. Salvadori, *Chem. Commun.*, 2003, 2466; (b) A. Weissberg and M. Portnoy, *Chem. Commun.*, 2003, 1538; (c) S. Lundgren, S. Lutsenko, C. Jönsson and C. Moberg, *Org. Lett.*, 2003, **5**, 3663; (d) A. Mandoli, S. Orlandi, D. Pini and P. Salvadori, *Tetrahedron: Asymmetry*, 2004, **15**, 3233; (e) J. G. Knight and P. E. Belcher, *Tetrahedron: Asymmetry*, 2005, **16**, 1415.
- (a) A. Lee, W. Kim, J. Lee, T. Hyeon and B. M. Kim, *Tetrahedron: Asymmetry*, 2004, **15**, 2595; (b) K. Aoki, T. Shimada and T. Hayashi, *Tetrahedron: Asymmetry*, 2004, **15**, 1771; (c) D. Rechavi, B. Albela, B. Laurent and M. Lemaire, *Tetrahedron*, 2005, **61**, 6976; (d) T. M. Lancaster, S. S. Lee and J. Y. Ying, *Chem. Commun.*, 2005, 3577.
- (a) M. I. Burguete, J. M. Fraile, J. I. García, E. García-Verdugo, S. V. Luis and J. A. Mayoral, *Org. Lett.*, 2000, **2**, 3905; (b) M. I. Burguete, J. M. Fraile, J. I. García, E. García-Verdugo, C. I. Herrerías, S. V. Luis and J. A. Mayoral, *J. Org. Chem.*, 2001, **66**, 8893.
- (a) P. Hodge, *Curr. Opin. Chem. Biol.*, 2003, **7**, 362; (b) U. Jas and A. Kirschning, *Chem.-Eur. J.*, 2003, **9**, 5708; (c) A. Kirschning,



- U. Jas and G. Kunz, *Chemistry in flow-new continuous flow reactors in organic synthesis*, in: *Innovation and Perspectives in Solid Phase Synthesis and Combinatorial Libraries*, ed. R. Epton, MPG Books Ltd., Cornwall, UK, 2004; (d) P. Hodge, *Ind. Eng. Chem. Res.*, 2005, **44**, 8542; (e) N. Karbass, V. Sans, E. García-Verdugo, M. I. Burguete and S. V. Luis, *Chem. Commun.*, 2006, 3095.
- 11 (a) P. Hodge, D. W. L. Sung and P. W. Stratford, *J. Chem. Soc., Perkin Trans. 1*, 1999, 2335; (b) D. W. L. Sung, P. L. Hodge and P. W. Stratford, *J. Chem. Soc., Perkin Trans. 1*, 1999, 1463; (c) D. A. Annis and E. N. Jacobsen, *J. Am. Chem. Soc.*, 1999, **121**, 4147; (d) M. I. Burguete, E. García-Verdugo, M. J. Vicent, S. V. Luis, H. N. Pennemann, N. G. Keyserling and J. Martens, *Org. Lett.*, 2002, **4**, 3947; (e) B. Altava, M. I. Burguete, E. García-Verdugo, S. V. Luis and M. J. Vicent, *Green Chem.*, 2006, **8**, 717.
- 12 A. Cybulski and J. A. Moulijn, *Structured Catalysts and Reactors*, Marcel Dekker, 1998.
- 13 Residence time was calculated according to standard literature: O. Levenspiel, *Chemical Reaction Engineering*, Wiley, New York, 3rd edn, 1998. More detailed information about the kinetics of the reaction can be found in the supplementary material.
- 14 (a) A. Baiker, *Chem. Rev.*, 1999, **99**, 453; (b) E. J. Beckman, *J. Supercrit. Fluids*, 2004, **28**, 121.
- 15 (a) W. Leitner, *Acc. Chem. Res.*, 2002, **35**, 746; (b) D. Prajapati and M. Gohain, *Tetrahedron*, 2004, **60**, 815; (c) P. G. Jessop, *J. Supercrit. Fluids*, 2006, **38**, 211.
- 16 For asymmetric cyclopropanation in SCFs see: (a) D. C. Wynne and P. G. Jessop, *Angew. Chem., Int. Ed.*, 1999, **38**, 1143; (b) D. C. Wynne, M. M. Olmstead and P. G. Jessop, *J. Am. Chem. Soc.*, 2000, **122**, 7638; (c) C. M. Rayner, *Org. Process Res. Dev.*, 2007, **11**, 121.
- 17 (a) M. T. Reetz, W. Wiesenhofer, G. Francio and W. Leitner, *Chem. Commun.*, 2002, 992; (b) P. B. Webb and D. J. Cole-Hamilton, *Chem. Commun.*, 2004, 612; (c) M. Solonas, A. Pfaltz, P. G. Cozzi and W. Leitner, *J. Am. Chem. Soc.*, 2004, **126**, 16142; (d) P. Stephenson, P. Licence, S. K. Ross and M. Poliakoff, *Green Chem.*, 2004, **6**, 521; (e) H. R. Hobbs, B. Kondor, P. Stephenson, R. A. Sheldon, N. R. Thomas and M. Poliakoff, *Green Chem.*, 2006, **8**, 816; (f) P. Stephenson, B. Kondor, P. Licence, K. Scovell, S. K. Ross and M. Poliakoff, *Adv. Synth. Catal.*, 2006, **348**, 1605.
- 18 P. Lozano, E. García-Verdugo, R. Piamtongkam, N. Karbass, T. De Diego, M. I. Burguete, S. V. Luis and L. Iborra, *Adv. Synth. Catal.*, 2007, 0000.

	<p><b>Comments received from just a few of the thousands of satisfied RSC authors and referees who have used ReSource - the online portal helping you through every step of the publication process.</b></p>
	<p><b>'I wish the others were as easy to use.'</b></p>
<p><b>'ReSource is the best online submission system of any publisher.'</b></p>	<p><b>authors</b> benefit from a user-friendly electronic submission process, manuscript tracking facilities, online proof collection, free pdf reprints, and can review all aspects of their publishing history</p> <p><b>referees</b> can download articles, submit reports, monitor the outcome of reviewed manuscripts, and check and update their personal profile</p> <p><b>NEW!! We have added a number of enhancements to ReSource, to improve your publishing experience even further.</b></p> <p>New features include:</p> <ul style="list-style-type: none"> <li>● the facility for authors to save manuscript submissions at key stages in the process (handy for those juggling a hectic research schedule)</li> <li>● checklists and support notes (with useful hints, tips and reminders)</li> <li>● and a fresh new look (so that you can more easily see what you have done and need to do next)</li> </ul> <p><b>Go online today and find out more.</b></p>

**RSC Publishing**

**www.rsc.org/resource**

# Halide-free highly-pure imidazolium triflate ionic liquids: Preparation and use in palladium-catalysed allylic alkylation†

Loïc Leclercq, Isabelle Suisse, Guy Nowogrocki and Francine Agbossou-Niedercorn\*

Received 28th February 2007, Accepted 24th May 2007

First published as an Advance Article on the web 13th June 2007

DOI: 10.1039/b703096g

The reaction of three oxygenated heterocycles (tetrahydrofuran, tetrahydropyran, 1,4-dioxane) with trifluoromethane sulfonic anhydride in the presence of the non-nucleophilic base poly(4-vinylpyridine) affords alkyltriflates quantitatively *via* ring opening. The alkyltriflates react with *N*-alkylimidazoles providing the bis-imidazolium bis-triflate salts in high yields. Hydroxymethyl substituted oxygenated heterocycles are converted into imidazolium triflate salts without opening of the heterocycle. Two imidazolium salts were characterized by X-ray crystallographic structure determination. The halide free ionic liquids were applied successfully as solvents in the palladium catalysed allylic alkylation. A co-crystal of **15** and tetrabutylammonium triflate has also been characterized by X-ray crystallographic structure analysis.

## Introduction

The potential of ionic liquids (ILs) to replace environmentally harmful solvents has become an active and exiting area of research<sup>1</sup> even if their toxicity and biodegradability are not yet completely determined.<sup>1f</sup> ILs have been particularly studied as new media for catalysis.<sup>1,2</sup> The most widely studied IL cations are currently non-symmetrical 1,3-dialkylimidazolium ions.<sup>1,3,4</sup> On the basis of the anion, which has an important influence on their properties, *N,N'*-dialkylimidazolium ionic liquids can be classified into four groups<sup>5</sup> *i.e.* (a) systems based on relatively hygroscopic anions like [Cl<sup>−</sup>], [AlCl<sub>4</sub><sup>−</sup>], (b) stable systems based on anions such as [CF<sub>3</sub>SO<sub>3</sub><sup>−</sup>] (= [OTf]), [(CF<sub>3</sub>SO<sub>2</sub>)N<sup>−</sup>] (= [NTf<sub>2</sub>]), (c) systems based on water reactive anions that can generate HF by hydrolysis *e.g.* [PF<sub>6</sub><sup>−</sup>] and [BF<sub>4</sub><sup>−</sup>], and (d) systems based on alkylsulfates<sup>6</sup> and alkyl-sulfonates.<sup>7,8</sup> Currently, 1,3-dialkylimidazolium cations associated with fluorous anions like [PF<sub>6</sub><sup>−</sup>] and [BF<sub>4</sub><sup>−</sup>] are the most studied. 1,3-Dialkylimidazolium cations coupled with anions such as [OTf] and [NTf<sub>2</sub>] form ILs that are much more stable towards the above mentioned side reactions.<sup>5,9</sup> In addition, the increased anion size, the more diffuse charge, and the decrease in hydrogen bonding, properties associated with such anions, contribute to the lower viscosities of the corresponding 1,3-dialkylimidazolium ILs.<sup>5</sup> They are also characterised by low melting points and high conductivities.

To prepare 1,3-substituted imidazolium ILs with fluorous anions, three methods have been used. The first one involves alkylation of an *N*-substituted imidazole with an alkyl halide (chloride or bromide) followed by an anion metathesis reaction carried out either in the presence of the appropriate acids (*i.e.* HPF<sub>6</sub>, HBF<sub>4</sub>, HOTf)<sup>10–12</sup> or their salts (*e.g.* NaPF<sub>6</sub>,

AgPF<sub>6</sub>, NaBF<sub>4</sub>, LiNTf<sub>2</sub>).<sup>11–13</sup> Unfortunately, the ILs prepared by this method can be contaminated by halide ions that may react with solute materials. The presence of halide contamination can thus be critical in catalysis and may lead to a catalyst poisoning and deactivation<sup>1d,14</sup> and also change the physical properties of the IL.<sup>11</sup> The second efficient method involves an imidazole alkylation by alkyltriflates.<sup>9,15</sup> For example, a hydroxyester was transformed into its triflate derivative in the presence of triflic anhydride and 2,6-lutidine. The intermediate triflate reacted further with 1-methylimidazole producing the triflate imidazolium salt.<sup>15</sup> Even if this method has been applied successfully, some limitations exist. The use of pyridine type bases in a non-aqueous reaction mixture (anhydrous dichloromethane, for example) results in the production of a mixture of the expected alkyl triflate and pyridinium triflate salts. The separation of this pyridinium salt from the product is not easy to perform. This methodology presents another drawback due to the extreme electrophilicity of alkyl triflates, which can react with the base pyridine.<sup>16,17</sup> A third method of preparation of halide-free imidazolium ILs has been reported very recently by Dupont.<sup>8</sup> Alkanesulfonate anions were substituted by a series of other anions (BF<sub>4</sub><sup>−</sup>, PF<sub>6</sub><sup>−</sup>, OTf<sup>−</sup>...) through reaction of *N,N'*-dialkylimidazolium alkanesulfonate species with the desired anion salt or corresponding acid.

We became interested in developing organometallic catalysis in ionic liquids and sought to prepare new halide free IL for specific applications.<sup>18</sup> Here, we report on the synthesis and characterization of new triflate imidazolium salts and on their use in palladium catalysed allylic alkylation.

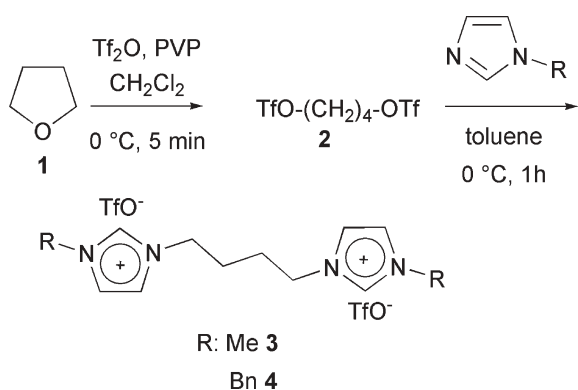
## Results and discussion

### Synthesis and characterization of imidazolium salts

Our synthesis strategy is based on (1) the use of oxygen heterocycles as starting material to introduce new substituents on the imidazolium cations<sup>19</sup> and (2) on the use of poly(4-vinylpyridine) (PVP) as the base, which presents the advantage of expeditious purification by filtration.

Unité Catalyse et Chimie du Solide UMR CNRS 8181, ENSCL (CHIMIE), BT C7, BP 90108, 59652, Villeneuve d'Ascq Cedex, France. E-mail: francine.agbossou@enscl-lille.fr; Fax: +33 3 20 43 65 85 Tel 33 3 20 43 49 27

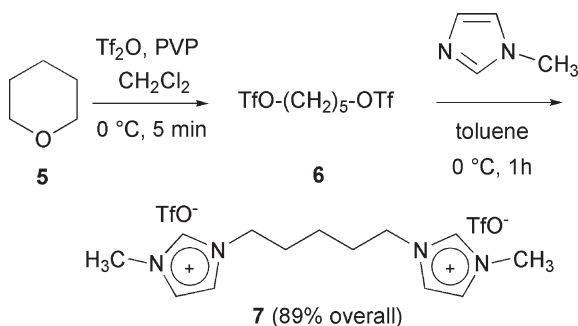
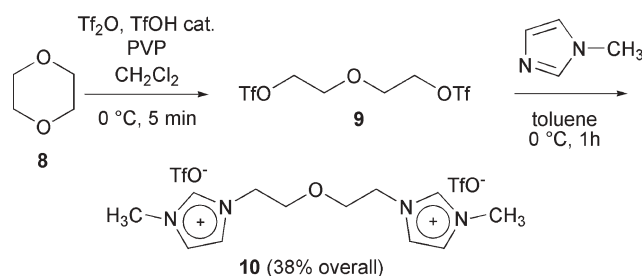
† Electronic supplementary information (ESI) available: Cation coordination environment and view of the molecular arrangement in compound **16**. See DOI: 10.1039/b703096g

Scheme 1 Synthesis of bis-imidazolium salts **3** and **4**.

We first reacted tetrahydrofuran (**1**) with triflic anhydride in the presence of PVP in dichloromethane at 0 °C (Scheme 1).<sup>20</sup> With the aid of PVP, the reaction took place in a very short time (5 min) and the diester **2** was isolated quantitatively by filtration. Two factors can likely account for the high yield observed in the formation of **2**. The first one is the limitation of the base alkylation process (at 0 °C, the alkylation is sufficiently slow to be a negligible side-reaction)<sup>16</sup> and the second one is the easy opening of the oxygen heterocycles for thermodynamic reasons (see below). After work up, and because of the moderate stability of dialkyltriflates,<sup>16</sup> **2** was reacted directly with commercial *N*-substituted imidazoles in anhydrous toluene at 0 °C providing the bis-imidazolium salts **3** and **4** in overall 91 and 94% yield, respectively. Tetrahydropyran **5** was similarly converted into the diester **6** and further into the salt **7** in 89% yield (Scheme 2).

The bis-imidazolium salts **3** and **4** precipitated in toluene and, after filtration were isolated in high overall yield and purity. No precipitation of the bis-imidazolium salt **7** occurred in toluene. Nevertheless, after one night standing at room temperature, a layer of IL **7** appeared beneath the toluene phase and could be easily isolated. The same reaction was carried out with 1,4-dioxane **8**. However, the presence of a catalytic amount of triflic acid (*ca.* 20 mol%) was necessary to observe the opening of the heterocycle (Scheme 3). Then, the intermediate diester **9** was reacted with *N*-methylimidazole. The bis-imidazolium salt **10** formed a separate phase and, after separation, was isolated with a moderate non-optimised yield of 38% but with a high purity.

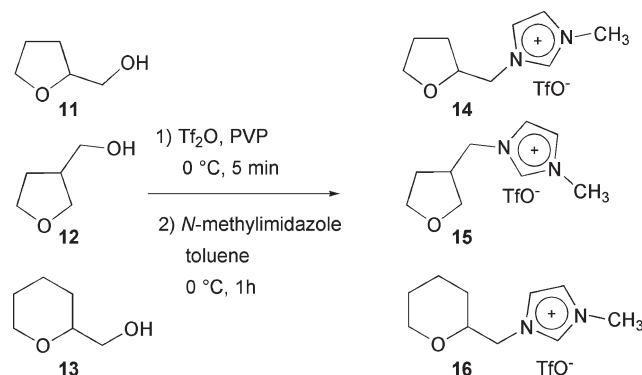
We performed DFT calculations (B3LYP, 6-31g\*) to compare the energies of formation of the intermediate triflic

Scheme 2 Synthesis of the bis-imidazolium salt **7**.Scheme 3 Synthesis of the bis-imidazolium salt **10**.

esters **2**, **6**, and **9** by ring opening of the heterocycles. The enthalpy change ( $\Delta H$ ) is negative,  $-20$ ,  $-15$ , and  $-15$  kcal mol<sup>-1</sup>, respectively for **2**, **6**, and **9**. Thus, the necessity of an acid catalysis to convert **8** into **9** is most probably related to a higher activation energy than that required while going from **1** to **2** and from **5** to **6**. The modest yield into salt **10** can then be explained by a low conversion of **8** into **9** placed in our reaction conditions at 0 °C compared to the quantitative conversion of **1** and **5** into **2** and **6**, respectively.<sup>21</sup>

Next, we reacted similarly the hydroxymethyl heterocyclic derivatives tetrahydro-2-furanmethanol **11**, tetrahydro-3-furanmethanol **12**, and tetrahydropyran-2-methanol **13** (Scheme 4).<sup>17</sup> This time, no opening of the heterocycle was observed, even in the presence of triflic acid, and only the primary alcohol end reacted producing **14**, **15**, and **16**, respectively, after reaction of the intermediate triflate esters with *N*-methylimidazole in 82 and 83% yield, respectively. The  $\Delta H$  of formation of **14**, **15**, and **16** calculated by DFT is  $-10$ ,  $-9$ , and  $-11$  kcal mol<sup>-1</sup>, respectively. If an opening of the heterocycle is taken into consideration for the calculation,  $\Delta H$  becomes slightly positive. Thus, we are probably not observing any ring opening as the reaction is carried out at 0 °C over one hour in order to avoid pyridine alkylation with the intermediate alkyl triflates.<sup>22</sup>

All new imidazolium salts have been characterized by <sup>1</sup>H and <sup>13</sup>C NMR, and elemental analysis. Solid compounds could be characterized by X-ray crystallographic structure determination. Salts **7**, **10**, **14**, and **15** are true room temperature ionic liquids whereas **3**, **4**, and **16** are high temperature ionic liquids (mp 71.2, 111.7, and 85.1 °C, respectively) (Table 1). A crystallization of **3** was carried out efficiently while using another IL as the solvent. A mixture of 1/3 of **3** and 2/3 (v/v) of 1-butyl-3-methyl-imidazolium triflate was warmed until

Scheme 4 Synthesis of the imidazolium salts **14**, **15**, and **16**.

**Table 1** Imidazolium salts synthesized

Salt	Structure	Yield(%)	mp/°C
3		91	71.2
4		94	111.7
7		89	—
10		38	—
14		82	—
15		83	—
16		92	85.1

homogeneity and then left at room temperature allowing small crystals suitable for single-X-ray crystallographic structure determination to grow in the IL mixture (Fig. 1). For **16**, the crystallization was carried out in toluene (Fig. 2).

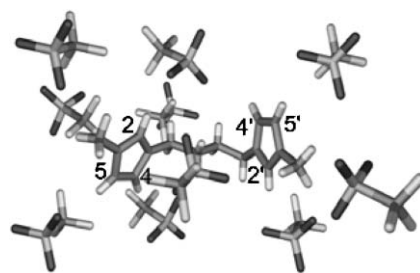
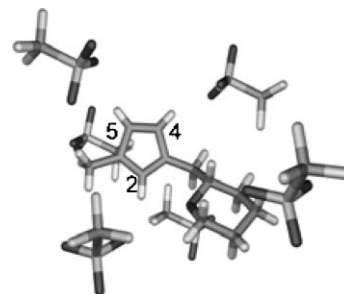
Crystal structures of **3** and **16**<sup>23,24</sup> ‡ reveal the supramolecular polymeric organization already observed for other ILs.<sup>25,26</sup> In the crystal lattice, the ions of **3** and **16** are organized as channels of imidazolium rings in which triflate anions are accommodated as ribbons (see ESI†). The layers of cations and anions are connected by hydrogen bonds.<sup>25,26</sup> For compound **3**, a bis-imidazolium unit is surrounded closely by ten triflate anions. Six of the latter interact directly with the imidazolium cations through hydrogen bonds (Fig. 1, Table 2).

‡ CCDC reference numbers 290114, 290115, 621900. For crystallographic data in CIF or other electronic format see DOI: 10.1039/b703096g

**Table 2** Distances (Å) and angles (°) of C–H···O hydrogen bonds in **3**<sup>a</sup> (see ref. 23)

	C···H	H···O	C···O	C–H···O	Symmetry operators for O
C <sub>2</sub> –H <sub>2</sub> ···O <sub>5</sub>	0.95(3)	2.23(3)	3.166(4)	169(2)	1 – x, 1 – y, 2 – z
C <sub>5</sub> –H <sub>5</sub> ···O <sub>1</sub>	0.95(2)	2.32(2)	3.257(6)	169(2)	–x, –y, –z
C <sub>2</sub> –H <sub>2</sub> ···O <sub>3</sub>	0.90(3)	2.33(3)	3.198(3)	161(2)	–x, 1 – y, 2 – z
C <sub>5</sub> –H <sub>5</sub> ···O <sub>3</sub>	0.95(3)	2.45(3)	3.377(3)	165(2)	1 – x, 1 – y, 2 – z
C <sub>2</sub> –H <sub>2</sub> ···O <sub>1</sub>	0.90(3)	2.63(2)	3.276(6)	129(2)	–x, 1 – y, 2 – z
C <sub>7</sub> –H <sub>7</sub> ···O <sub>6</sub>	0.95(2)	2.62(3)	3.388(4)	138(2)	1 – x, 1 – y, 2 – z
C <sub>9</sub> –H <sub>9A</sub> ···O <sub>4</sub>	0.92(2)	2.63(2)	3.227(3)	123(1)	–x, 1 – y, 2 – z
C <sub>8</sub> –H <sub>8B</sub> ···O <sub>4</sub>	0.99(2)	2.69(2)	3.243(4)	116(1)	–x, 1 – y, 2 – z

<sup>a</sup> Only H···O that have significant interactions are given.

**Fig. 1** The cation coordination environment in **3** obtained by X-ray diffraction structure analysis.<sup>23</sup>**Fig. 2** The cation coordination environment in **16** obtained by X-ray diffraction structure analysis.<sup>24</sup>

For **16**, six triflate anions are in close proximity with the imidazolium cation, four having direct interactions with the latter (Fig. 2, Table 3). For **3** and **16**, C–H···O hydrogen bonds are noticed between protons of the imidazolium cations and oxygens of the triflate anions. In **16**, the interaction between H(2) and the oxygen atom of the tetrahydropyran cycle (H···O:  $d = 2.634$  Å and C–H···X:  $96.46^\circ$ ) is most probably unavoidable due to steric congestion rather than weak hydrogen-bonding.<sup>27</sup> The shortest distances (strongest hydrogen bonds) are measured for the most acidic hydrogens H(2) (H(2)···O:  $d = 2.231$  Å) and H(2') (H(2')···O:  $d = 2.332$  Å) in **3** and H(2) (H(2)···O:  $d = 2.393$  Å) in **16**. The other hydrogen bonds involve H(4), H(4'), H(5), and H(5') hydrogens of the imidazolium rings (H···O:  $2.321$  Å  $< d < 2.937$  Å) for **3** and H(4) and H(5) (H···O:  $2.441$  Å  $< d < 2.508$  Å) for **16**.<sup>23a</sup> The intermolecular interactions between the triflate oxygens and the imidazolium hydrogens possess properties of weak to moderate hydrogen bonds (H···O:  $d > 2.2$  Å;  $130^\circ < \text{C–H} \cdots \text{O} < 170^\circ$ ).<sup>28</sup> In **3**, intermolecular C–H···π hydrogen bonds have been found between the C–H of the *N*-methyl group of one imidazolium cation with that of a



**Table 3** Distances (Å) and angles (°) of C–H···O hydrogen bonds in **16**<sup>a</sup> (see ref. 24)

	C···H	H···O	C···O	C–H···O	Symmetry operators for O
C <sub>2</sub> –H <sub>2</sub> ···O <sub>1</sub>	0.91(2)	2.51(2)	3.166(2)	142(2)	1 + x, y, z
C <sub>5</sub> –H <sub>5</sub> ···O <sub>3</sub>	0.91(2)	2.44(2)	3.299(2)	158(2)	1.5 – x, 0.5 + y, 0.5 – z
C <sub>4</sub> –H <sub>4</sub> ···O <sub>2</sub>	0.92(2)	2.51(2)	3.357(4)	154(2)	0.5 + x, 1.5 – y, 0.5 + z
C <sub>6</sub> –H <sub>6A</sub> ···O <sub>2</sub>	1.00(2)	2.49(2)	3.407(2)	152(2)	1.5 – x, y – 0.5, 0.5 – z
C <sub>12</sub> –H <sub>12</sub> ···O <sub>2</sub>	0.95(3)	2.57(2)	3.445(2)	153(2)	1.5 – x, 0.5 + y, 0.5 – z
C <sub>12</sub> –H <sub>12</sub> ···O <sub>3</sub>	0.97(2)	2.53(2)	3.463(7)	163(2)	1.5 + x, 1.5 – y, 0.5 + z
C <sub>9</sub> –H <sub>9B</sub> ···O <sub>3</sub>	1.00(2)	2.75(2)	3.469(3)	129(1)	1 – x, 1 – y, –z
C <sub>5</sub> –H <sub>5</sub> ···O <sub>1</sub>	0.91(2)	2.96(2)	3.499(2)	120(1)	1.5 – x, 0.5 + y, 0.5 – z

<sup>a</sup> Only H···O that have significant interactions are given.

neighbouring imidazolium unit (C–H···π, *d* = 2.9 Å).<sup>29</sup> As space between layers of imidazolium cations is between 5.8 and 10.9 Å, no π–π stacking is observed (the standard π–π stacking distance is approximately 3.5 Å).

### Palladium catalysed allylic alkylation in imidazolium triflate ionic liquids

Next, the new imidazolium triflate ionic liquids **7**, **10**, **14**, and **15** were applied in the Tsuji–Trost reaction (Scheme 5, Table 4).<sup>30,31</sup> The alkylation of (*rac*)-(*E*)-1,3-diphenyl-3-acetoxyprop-1-ene by dimethyl malonate was catalysed by palladium species generated *in situ* through reaction of Pd(OAc)<sub>2</sub> with triphenylphosphine (TPP).<sup>32</sup> The base tetrabutyl ammonium acetate forms a homogeneous solution with the ionic liquids. If the palladium species Pd(OAc)<sub>2</sub> is introduced in the IL without phosphine, palladium black is observed and no catalytic reaction is taking place. We compared experiments carried out in the bis-imidazolium dichloride **17** (run 1),<sup>33</sup> in IL **7** alone (run 2), and in **7** in the presence of NaCl (4 mol% *vs.* Pd(OAc)<sub>2</sub> 2 mol%) (run 3). The low reaction rates observed for runs 1 and 3 compared to run 2 indicate that the palladium catalysed allylic alkylation is inhibited by chloride ions. This can be likely due to chloride coordination to palladium<sup>34,35</sup> producing catalytic intermediates with different properties. This would affect the coordination of the allyl substrate and the oxidative addition steps and consequently the overall kinetic of the process.

In the halide free ILs **7**, **10**, **14**, and **15**, within 12 h, the conversions were 62, 64, 75, and 71%, respectively (runs 2, 4, 5, and 6). These catalytic results can be compared with those reported by Xiao for the same reaction while using K<sub>2</sub>CO<sub>3</sub> as the base in an ionic liquid.<sup>31a</sup> Here the catalytic process is slightly less efficient. If one compares the *pK<sub>a</sub>* values, in DMSO, of acetate (12.3),<sup>36</sup> diethyl malonate (16.4, which should be close to dimethylmalonate),<sup>36</sup> and dialkylimidazolium cations (24),<sup>37</sup> one should not expect any deprotonation of either the malonate or the imidazolium. Yet, the allylation process is occurring. There is probably a deprotonating

**Scheme 5** Palladium catalysed allylic alkylation reaction.

equilibrium involving the acetate and malonate species generating the requested nucleophile. The latter adds then to the “Pd(PPh<sub>3</sub>)<sub>2</sub>(allyl)” intermediate produced by addition of the allyl acetate substrate to the “Pd(PPh<sub>3</sub>)<sub>2</sub>” key species providing the alkylation product.

The structure of the imidazolium influences slightly the kinetic of the catalytic process. Thus, the tetrahydrofuran substituted IL **14** (run 5) and **15** (run 6) allow a slightly higher conversion than the bis-imidazolium ditriflate salts **7** (run 2) and **10** (run 4). A better solubility of the reactants in the IL **14** and **15** can be considered. When THF was added to **7** (25% v/v) (run 7 *vs.* 2), a small conversion increase was

**Table 4** Allylic alkylation in different ionic liquids as solvent<sup>a</sup>

Run	Ionic liquid	IL structure	Conversion (%) <sup>b</sup>
1	<b>17</b>		0.5
2	<b>7</b>		62
3 <sup>c</sup>	<b>7</b>	“	1
4	<b>10</b>		64
5	<b>14</b>		75
	<b>15</b>		71
7 <sup>d</sup>	<b>7</b>		73
8 <sup>d</sup>	<b>14</b>		53

<sup>a</sup> Pd(OAc)<sub>2</sub> = 2 mol%; Ligand = 8 mol%; Ionic liquid = 2 mL; *n*Bu<sub>4</sub>NOAc = 2 mmol; *trans*-1,3-diphenyl-3-acetoxy-prop-1-ene = 1 mmol; dimethylmalonate = 1.5 mmol; 50 °C; 12 h. <sup>b</sup> Determined by <sup>1</sup>H NMR. <sup>c</sup> NaCl 4 mol% *vs.* Pd. <sup>d</sup> THF 25% v/v.



**Fig. 3** Co-crystal of imidazolium/tetrabutylammonium triflate **18** obtained by X-ray diffraction analysis after catalysis with salt **15**.<sup>38</sup>

obtained which can also be correlated to the solubility of the reagents. On the contrary, a THF addition to **14** (run 8) induced a decrease of the conversion compared to the run performed in the IL **15** alone (run 6). We were able to recycle the catalyst within ionic liquids **7**, **10**, **14**, and **15** four times without any loss of activity.

At the end of the reaction carried out in IL **15**, a solid formed that could be recrystallised while using 1-butyl-3-methyl-imidazolium triflate as the solvent. The crystalline solid **18** is an ionic co-crystal of **15** and tetrabutyl ammonium triflate.<sup>38</sup> The latter is formed during catalysis by anion metathesis between **15** and tetrabutyl ammonium acetate. The dissolution of molecules in an IL occurs with disruption of the hydrogen bond network which can generate nanostructures with polar and non-polar regions where inclusion-type compounds can be formed.<sup>39</sup> Here, ionic and hydrogen bonding interactions coexist in the mixture (Fig. 3, Table 5). We observe moderate hydrogen interactions principally between imidazolium rings and triflate ions that form a cage around the tetrabutylammonium cation.

## Conclusions

In summary, we have developed a new efficient synthesis of highly pure halide free triflate based imidazolium salts while introducing original substituents onto the imidazolium unit. The method developed is very useful to avoid a metathesis

**Table 5** Distances (Å) and angles (°) of C–H⋯O hydrogen bonds in **18**<sup>a</sup>(see ref. 38)

	C⋯H	H⋯O	C⋯O	C–H⋯O	Symmetry operators for O
C <sub>1</sub> –H <sub>1</sub> ⋯O <sub>5</sub>	0.93	2.28(3)	2.957(4)	129(2)	<i>x</i> , <i>y</i> , <i>z</i>
C <sub>4</sub> –H <sub>4A</sub> ⋯O <sub>4</sub>	0.93	2.40(3)	3.134(4)	137(2)	<i>x</i> , 1 + <i>y</i> , <i>z</i>
C <sub>1</sub> –H <sub>1</sub> ⋯O <sub>3</sub>	0.93	2.82(3)	3.163(4)	103(2)	<i>x</i> , <i>y</i> , <i>z</i>
C <sub>4</sub> –H <sub>4B</sub> ⋯O <sub>3</sub>	0.97	2.61(3)	3.174(5)	117(2)	<i>x</i> , <i>y</i> , <i>z</i>
C <sub>9</sub> –H <sub>9A</sub> ⋯O <sub>1</sub>	0.96	2.47(3)	3.344(4)	151(2)	<i>x</i> + 1, <i>y</i> , <i>z</i>
C <sub>2</sub> –H <sub>2</sub> ⋯O <sub>4</sub>	0.93	2.78(3)	3.404(5)	125(2)	<i>x</i> , 1 + <i>y</i> , <i>z</i>
C <sub>2</sub> –H <sub>2</sub> ⋯O <sub>6</sub>	0.93	2.51(3)	3.426(3)	168(2)	<i>x</i> , 1 + <i>y</i> , <i>z</i>
C <sub>18</sub> –H <sub>18B</sub> ⋯O <sub>2</sub>	0.97	2.32(2)	3.275(3)	169(2)	<i>x</i> , <i>y</i> – 1, <i>z</i>
C <sub>18</sub> –H <sub>18A</sub> ⋯O <sub>6</sub>	0.97	2.37(3)	3.323(4)	166(2)	<i>x</i> – 1, <i>y</i> , <i>z</i>
C <sub>10</sub> –H <sub>10A</sub> ⋯O <sub>1</sub>	0.97	2.38(2)	3.335(3)	175(2)	<i>x</i> , <i>y</i> , <i>z</i>
C <sub>14</sub> –H <sub>14B</sub> ⋯O <sub>4</sub>	0.97	2.57(3)	3.359(5)	138(2)	<i>x</i> , <i>y</i> , <i>z</i>

<sup>a</sup> Only H⋯O that have significant interactions are given.

process and consequently any contamination by halides. This procedure can be general for the preparation of a variety of triflate imidazolium salts. The new ionic liquids can be conveniently used as solvents in palladium catalysed reaction like the Tsuji–Trost C–C bond forming reaction. The use of halide free triflate imidazolium ionic liquids in palladium-catalysed reactions will be reported in due course.

## Experimental section

### Materials

D<sub>2</sub>O (99.95% isotopic purity), CDCl<sub>3</sub>, and [D<sub>6</sub>] acetone were obtained from Euriso-top. Trifluoromethanesulfonic anhydride was freshly prepared prior to use by distillation of a 1 : 1 w/w mixture of trifluoromethanesulfonic acid and phosphorus pentoxide.<sup>40</sup> *N*-Methylimidazole was freshly distilled over KOH. (*rac*)-(*E*)-1,3-Diphenyl-3-acetoxyprop-1-ene was prepared by acylation of the appropriate alcohol with Ac<sub>2</sub>O in dichloromethane under DMAP catalysis.<sup>41</sup> All other chemicals were purchased from Acros, Aldrich, Fluka or Strem and used without further purification. Solvents were distilled under positive pressure of dry nitrogen before use and dried by standard methods: dichloromethane from CaH<sub>2</sub> and toluene from Na/Hg amalgam. All reactions were carried out in oven-dried glassware under nitrogen, using standard Schlenk and vacuum line techniques. The <sup>1</sup>H and <sup>13</sup>C spectra were recorded at room temperature on an Advance 300 Bruker spectrometer, at 300.13 and 75.49 MHz, respectively. Chemical shifts are given in ppm units (δ) relative to tetramethylsilane (TMS), for <sup>1</sup>H and <sup>13</sup>C. <sup>13</sup>C NMR triflate anion signals are not reported. Elemental analysis was performed by “Service Central d’Analyse du CNRS”. X-Ray diffraction analysis was performed on a Bruker SMART CCD.

### 3-Methyl-1-[4-(1-methylimidazolium-3-yl)butyl]-imidazolium ditriflate (**3**)

Under nitrogen, a Schlenk tube equipped with a magnetic stir bar was charged with THF (0.43 g, 6 mmol), dichloromethane (20 mL) and poly(4-vinylpyridine) (3 g, 10.6 mmol). After cooling to 0 °C, trifluoromethanesulfonic anhydride (2.0 g, 7.1 mmol) was added dropwise. At the end of the addition, the reaction mixture was stirred for 1 min at room temperature. The reaction mixture was filtered through a sintered glass funnel and the solid washed with 5 mL of dichloromethane. The filtrate was washed with saturated NaHCO<sub>3</sub>, dried over MgSO<sub>4</sub>, and concentrated under vacuum to give the bis-triflate quantitatively as a white solid. This solid was dissolved in anhydrous toluene (10 mL) under a nitrogen atmosphere and the solution was cooled to 0 °C. *N*-Methylimidazole (6.18 g, 75.2 mmol) was added and the resulting solution was stirred for an hour during which time the imidazolium salt precipitated. After filtration, the salt was dried overnight at 120 °C in vacuum (2.83 g, 91%). Mp 71.2 °C. <sup>1</sup>H NMR ([D<sub>6</sub>] acetone, 300.13 MHz) δ 2.89 (m, 4H, N–CH<sub>2</sub>–CH<sub>2</sub>), 4.04 (s, 6H, CH<sub>3</sub>–N), 4.45 (t, 4H, N–CH<sub>2</sub>–CH<sub>2</sub>), 7.71 (s, 2H, CH=CH), 7.79 (s, 2H, CH=CH), 9.10 (s, 2H, N–CH=N). <sup>13</sup>C NMR ([D<sub>6</sub>] acetone, 75.49 MHz) δ 27.38 (N–CH<sub>2</sub>–CH<sub>2</sub>), 36.64 (CH<sub>3</sub>–N), 49.63 (N–CH<sub>2</sub>–CH<sub>2</sub>), 123.47 (CH=CH), 127.78 (CH=CH),

138.52 (N–CH=N). Anal. calcd for  $C_{14}H_{20}N_4F_6O_6S_2$ : C, 32.43; H, 3.89; N, 10.81. Found: C, 32.54; H, 3.91; N, 10.84.

### 3-Benzyl-1-[4-(1-benzylimidazolium-3-yl)butyl]-imidazolium ditriflate (4)

This compound was prepared following the procedure used to prepare **3**. **4** was obtained in 94% yield. Mp 111.7 °C.  $^1H$  NMR ( $[D_6]$  Acetone, 300.13 MHz)  $\delta$  2.04 (m, 2H, N–CH<sub>2</sub>–CH<sub>2</sub>), 4.47 (m, 2H, N–CH<sub>2</sub>–CH<sub>2</sub>), 5.57 (s, 2H, N–CH<sub>2</sub>–Ph), 7.43–7.45 (m, 5H, CH<sub>aro</sub>), 7.77 (s, 1H, CH=CH), 7.83 (s, 1H, CH=CH), 9.29 (s, 1H, N–CH=N).  $^{13}C$  NMR ( $[D_6]$  Acetone, 75.49 MHz)  $\delta$  27.38 (N–CH<sub>2</sub>–CH<sub>2</sub>), 49.84 (N–CH<sub>2</sub>–CH<sub>2</sub>), 53.73 (N–CH<sub>2</sub>–Ph), 123.55 (CH=CH), 123.96 (CH=CH), 129.64 (CH<sub>meta</sub>), 129.94 (CH<sub>para</sub>), 130.05 (CH<sub>ortho</sub>), 135.27 (CH<sub>aro</sub>), 137.28 (N–CH=N). Anal. calcd for  $C_{26}H_{28}N_4F_6O_6S_2$ : C, 46.56; H, 4.21; N, 8.35. Found: C, 46.39; H, 4.22; N, 8.40.

### 3-Methyl-1-[5-(1-methylimidazolium-3-yl)pentyl]-imidazolium ditriflate (7)

This compound was prepared following the procedure used to prepare **3**. **7** was isolated in 89% yield.  $^1H$  NMR ( $[D_6]$  acetone, 300.13 MHz)  $\delta$  1.41 (m, 2H, N–CH<sub>2</sub>–CH<sub>2</sub>–CH<sub>2</sub>), 1.97 (m, 2H, N–CH<sub>2</sub>–CH<sub>2</sub>–CH<sub>2</sub>), 3.98 (s, 6H, CH<sub>3</sub>–N), 4.30 (t, 4H, N–CH<sub>2</sub>–CH<sub>2</sub>), 7.68 (s, 2H, CH=CH), 7.76 (s, 2H, CH=CH), 9.05 (s, 2H, N–CH=N).  $^{13}C$  NMR ( $[D_6]$  acetone, 75.49 MHz)  $\delta$  23.08 (N–CH<sub>2</sub>–CH<sub>2</sub>–CH<sub>2</sub>), 33.42 (N–CH<sub>2</sub>–CH<sub>2</sub>–CH<sub>2</sub>), 36.57 (CH<sub>3</sub>–N), 49.88 (N–CH<sub>2</sub>–CH<sub>2</sub>), 123.35 (CH=CH), 124.67 (CH=CH), 138.98 (N–CH=N). Anal. calcd for  $C_{15}H_{22}N_4F_6O_6S_2$ : C, 33.84; H, 4.16; N, 10.62. Found: C, 33.78; H, 4.32; N, 10.67.

### 3-Methyl-1-[2-[2-(1-methylimidazolium-3-yl)ethoxy]ethyl]-imidazolium ditriflate (10)

This compound was prepared following the procedure used to prepare **3** except that triflic acid was introduced (20 mol%) along with the substrate before cooling. **10** was isolated in 38% yield.  $^1H$  NMR (acetone- $d_6$ , 300.13 MHz)  $\delta$  2.07 (m, 2H, CH<sub>2</sub>–CH<sub>2</sub>–O), 4.03 (s, 3H, CH<sub>3</sub>–N), 4.55 (m, 2H, N–CH<sub>2</sub>–CH<sub>2</sub>), 7.70 (s, 1H, CH=CH), 7.73 (s, 1H, CH=CH), 9.08 (s, 1H, N–CH=N).  $^{13}C$  NMR ( $[D_6]$  acetone, 75.49 MHz)  $\delta$  32.28 (CH<sub>2</sub>–CH<sub>2</sub>–O), 35.61 (CH<sub>3</sub>–N), 49.24 (N–CH<sub>2</sub>–CH<sub>2</sub>), 122.95 (CH=CH), 123.40 (CH=CH), 137.12 (N–CH=N). Anal. calcd for  $C_{14}H_{20}N_4F_6O_7S_2$ : C, 31.46; H, 3.78; N, 10.48. Found: C, 31.51; H, 3.79; N, 10.52.

### 1-Methyl-3-(tetrahydrofuran-2-ylmethyl)-imidazolium triflate (14)

This compound was prepared following the procedure used to prepare **3**. **14** was isolated in 82% yield.  $^1H$  NMR (CDCl<sub>3</sub>, 300.13 MHz)  $\delta$  1.57 (m, 1H, CH<sub>2</sub>–CH–O), 1.91 (m, 2H, O–CH<sub>2</sub>–CH<sub>2</sub>), 2.14 (m, 1H, CH<sub>2</sub>–CH–O), 3.76–3.92 (m, 2H, O–CH<sub>2</sub>–CH<sub>2</sub>), 3.93 (s, 3H, N–CH<sub>3</sub>), 4.14 (m, 2H, N–CH<sub>2</sub>–CH), 4.40 (m, 1H, O–CH–CH<sub>2</sub>), 7.41 (s, 1H, CH=CH), 7.52 (s, 1H, CH=CH), 9.03 (s, 1H, N–CH=N).  $^{13}C$  NMR (CDCl<sub>3</sub>, 75.49 MHz)  $\delta$  25.53 (O–CH<sub>2</sub>–CH<sub>2</sub>), 28.51 (CH<sub>2</sub>–CH–O), 33.30 (N–CH<sub>3</sub>), 36.24 (N–CH<sub>2</sub>–CH), 53.28 (O–CH<sub>2</sub>–CH<sub>2</sub>), 68.40 (O–CH–CH<sub>2</sub>), 123.17 (CH=CH), 123.29 (CH=CH), 136.94

(N–CH=N). Anal. calcd for  $C_{10}H_{15}N_2F_3O_4S$ : C, 37.97; H, 4.78; N, 8.86. Found: C, 37.81; H, 4.72; N, 8.80.

### 1-Methyl-3-(tetrahydrofuran-3-ylmethyl)-imidazolium triflate (15)

This compound was prepared following the procedure used to prepare **3**. **15** was isolated in 83% yield.  $^1H$  NMR (acetone- $d_6$ , 300.13 MHz)  $\delta$  1.79 (m, 1H, CHH'–CH<sub>2</sub>–O), 2.23 (m, 1H, N–CH<sub>2</sub>–CH), 2.88 (m, 1H, CHH'–CH<sub>2</sub>–O), 3.51 (m, 2H, O–CH<sub>2</sub>–CH), 3.85 (s, 3H, N–CH<sub>3</sub>), 3.95 (m, 2H, O–CH<sub>2</sub>–CH<sub>2</sub>), 4.06 (m, 2H, N–CH<sub>2</sub>–CH), 7.27 (s, 1H, CH=CH), 7.52 (s, 1H, CH=CH), 9.07 (s, 1H, N–CH=N).  $^{13}C$  NMR (CDCl<sub>3</sub>, 75.49 MHz)  $\delta$  34.4 (O–CH<sub>2</sub>–CH<sub>2</sub>), 37.8 (CH–CH<sub>2</sub>–O), 40.2 (N–CH<sub>3</sub>), 55.6 (N–CH<sub>2</sub>–CH), 65.7 (O–CH<sub>2</sub>–CH), 74.6 (O–CH<sub>2</sub>–CH<sub>2</sub>), 117.1 (CH=CH), 121.1 (CH=CH), 136.7 (N–CH=N). Anal. calcd for  $C_{10}H_{15}N_2F_3O_4S$ : C, 37.97; H, 4.78; N, 8.86. Found: C, 37.97; H, 4.78; N, 8.79.

### 1-Methyl-3-(tetrahydro-2H-pyran-2-ylmethyl)-imidazolium triflate (16)

This compound was prepared following the procedure used to prepare **3**. **16** was isolated in 92% yield. Mp 85.1 °C.  $^1H$  NMR ( $[D_6]$  acetone, 300.13 MHz)  $\delta$  (ppm) 1.26 (m, 1H, CH<sub>2</sub>–CH–O), 1.51 (m, 3H, CH<sub>2</sub>–CH–O and CH<sub>2</sub>–CH<sub>2</sub>–CH<sub>2</sub>–), 1.73 (m, 2H, CH<sub>2</sub>–CH<sub>2</sub>–O), 3.38 (m, 1H, CH<sub>2</sub>–CH<sub>2</sub>–O), 3.73 (m, 1H, CH<sub>2</sub>–CH<sub>2</sub>–O), 3.94 (m, 1H, CH<sub>2</sub>–CH–O), 4.08 (s, 3H, N–CH<sub>3</sub>), 4.22 (m, 1H, N–CH<sub>2</sub>–CH), 4.44 (m, 1H, N–CH<sub>2</sub>–CH), 7.70 (m, 1H, CH=CH), 7.71 (m, 1H, CH=CH), 9.02 (s, 1H, N–CH=N).  $^{13}C$  NMR ( $[D_6]$  Acetone, 75.49 MHz)  $\delta$  23.38 (CH<sub>2</sub>–CH<sub>2</sub>–CH<sub>2</sub>), 26.31 (CH<sub>2</sub>–CH<sub>2</sub>–O), 29.02 (CH<sub>2</sub>–CH–O), 36.60 (N–CH<sub>3</sub>), 54.73 (CH<sub>2</sub>–CH<sub>2</sub>–O), 68.76 (CH<sub>2</sub>–CH–O), 76.20 (CH–CH<sub>2</sub>–N), 124.24 (CH=CH), 124.28 (CH=CH), 138.13 (N–CH=N). Anal. calcd for  $C_{11}H_{17}N_2F_3O_4S$ : C, 40.00; H, 5.19; N, 8.48. Found: C, 40.34; H, 5.20; N, 8.49.

### General allylic alkylation procedure

A Schlenk tube was charged with the IL (2 mL), followed by Pd(OAc)<sub>2</sub> (4.5 mg, 2 mol%), PPh<sub>3</sub> (21.0 mg, 8 mol%), and *n*Bu<sub>4</sub>NOAc (603.0 mg, 2 mmol). After repeated degassing and flushing with nitrogen, the mixture was heated to 50 °C during 20 min. Then, after cooling, 1,3-diphenylpropenylacetate (252.0 mg, 1 mmol) and dimethylmalonate (198.2 mg, 1.5 mmol) were added and the mixture stirred at 50 °C for 12 h. The product was extracted with hexane and the organic layer was washed twice with water and dried over MgSO<sub>4</sub>. The conversion was determined by  $^1H$  NMR. The mass balance was > 95% for each catalytic experiment.

### Acknowledgements

This work was supported by the CNRS and the Ministère de la Recherche (grant to L. L.). We are most grateful to Prof. Jean-François Paul for calculations and stimulating discussions.

### References

- (a) J. S. Wilkes, *Green Chem.*, 2002, **4**, 73–80; (b) T. Welton, *Chem. Rev.*, 1999, **99**, 2071–2083; (c) J. D. Holbrey and K. R. Seddon,



- Clean Products and Processes*, 1999, **1**, 223–236; (d) M. J. Earle and K. R. Seddon, *Pure Appl. Chem.*, 2000, **72**, 1391–1398; (e) H. Olivier-Bourbigou, *J. Mol. Cat. A: Chem.*, 2002, **182**, 419–437; (f) J. S. Wilkes, *J. Mol. Cat. A: Chem.*, 2004, **214**, 11–17.
- 2 (a) P. Wasserscheid and W. Keim, *Angew. Chem. Int. Ed.*, 2000, **39**, 3772–3789; (b) J. Dupont, R. F. de Souza and P. A. Z. Suarez, *Chem. Rev.*, 2002, **102**, 3667–3692; (c) R. Sheldon, *Chem. Commun.*, 2001, 2399–2407; (d) C. M. Gordon, *Appl. Cat. A: Gen.*, 2001, **222**, 101–107; (e) D. Zhao, M. Wu, Y. Kou and E. Min, *Catal. Today*, 2002, **74**, 157–189; (f) C. C. Tzschucke, C. Market, W. Bannwarth, S. Roller, A. Hebel and R. Haag, *Angew. Chem. Int. Ed.*, 2002, **41**, 3964–4000.
- 3 First report on an imidazolium IL, see: J. S. Wilkes, J. A. Levisky, R. A. Wilson and C. L. Hussey, *Inorg. Chem.*, 1982, **21**, 1263–1264.
- 4 R. Hagiwara and Y. Ito, *J. Fluorine Chem.*, 2000, **105**, 221–227.
- 5 C. Chiappe and D. Pieraccini, *J. Phys. Org. Chem.*, 2005, **18**, 275–297.
- 6 J. D. Holbrey, W. M. Reichert, R. P. Swatloski, G. A. Broker, W. R. Pitner, K. R. Seddon and R. D. Rogers, *Green Chem.*, 2002, **4**, 407–413.
- 7 L. Brinchi, R. Germani and G. Savelli, *Tetrahedron Lett.*, 2003, **44**, 2027–2029.
- 8 C. C. Cassol, G. Ebeling, B. Ferrera and J. Dupont, *Adv. Synth. Catal.*, 2006, **348**, 243–248.
- 9 P. Bonhôte, A.-P. Dias, N. Papageorgiou, K. Kalyanasundaram and M. Grätzel, *Inorg. Chem.*, 1996, **35**, 1168–1178.
- 10 J. D. Holbrey, A. E. Visser, S. K. Spear, W. M. Reichert, R. P. Swatloski, G. A. Broker and R. D. Rogers, *Green Chem.*, 2003, **5**, 129–135.
- 11 K. R. Seddon, A. Stark and M. J. Torres, *Pure Appl. Chem.*, 2000, **72**, 2275–2287.
- 12 J. G. Huddleston, H. D. Willauer, R. P. Swatloski, A. E. Visser and R. D. Rogers, *Chem. Commun.*, 1998, 1765–1766.
- 13 (a) P. A. Z. Suarez, J. E. L. Dullius, S. Einloft, R. F. De Souza and J. Dupont, *Polyhedron*, 1996, **15**, 1217–1219; (b) J. S. Wilkes and M. J. Zaworotko, *J. Chem. Soc., Chem. Commun.*, 1992, 965–967.
- 14 (a) Y. Chauvin and H. Olivier-Bourbigou, *Chem.-Tech.*, 1995, **30**; (b) P. J. Dyson, D. J. Ellis, D. G. Parker and T. Welton, *Chem. Commun.*, 1999, 25–26; (c) C. Daguenet and P. J. Dyson, *Organometallics*, 2004, **23**, 6080–6083; (d) P. J. Dyson, *Trans. Met. Chem.*, 2002, **27**, 353–358; (e) V. Gallo, P. Mastroianni, C. F. Nobile, G. Romanazzi and G. P. Suranna, *Dalton Trans.*, 2002, 4339–4342; (f) M. A. Klingshirn, G. A. Broker, J. D. Holbrey, K. H. Shaughnessy and R. D. Rogers, *Chem. Commun.*, 2002, 1394–1395; (g) D. L. Davies, S. K. Kandola and R. K. Patel, *Tetrahedron: Asymmetry*, 2004, **15**, 77–80.
- 15 J. J. Jodry and K. Mikami, *Tetrahedron Lett.*, 2004, **45**, 4429–4431.
- 16 S. A. Ross, M. Piété and B. Meunier, *J. Chem. Soc., Perkin Trans.*, 2000, 571–574.
- 17 M. G. Ambrose and R. W. Binkley, *J. Org. Chem.*, 1983, **48**, 674–677.
- 18 Z. Fei, T. J. Geldbach, D. Zjao and P. J. Dyson, *Chem. Eur. J.*, 2006, **12**, 2122–2130.
- 19 Examples of ether-substituted imidazolium ionic liquids, see: (a) L. C. Branco, J. N. Rosa, J. J. Moueua Ramos and C. A. M. Afonso, *Chem. Eur. J.*, 2002, **8**, 3671–3677; (b) B. A. DaSilveira Neto, L. S. Santos, F. M. Nachtigall, M. N. Eberlin and J. Dupont, *Angew. Chem. Int. Ed.*, 2006, **45**, 7251–7254.
- 20 (a) E. Lindner, G. Von Au and H. J. Eberle, *Chem. Ber.*, 1981, **114**, 810–813; (b) R. Chen, A. Schlossman, E. Breuer, G. Hägele, C. Tillmann, J. M. Van Gelder and G. Colomb, *Heteroat. Chem.*, 2000, **11**, 470–479.
- 21 All heterocyclic substrates were reacted at 0 °C during 5 min with triflic anhydride. This does not exclude that a higher yield into the intermediate triflic diester **9** could be obtained during prolonged reaction times, but with a risk of exhaustive PVP alkylation.
- 22 No reaction is observed when 2-methyltetrahydrofuran was placed in our reaction conditions (triflic anhydride, triflic acid (20 mol%), PVP, 0 °C, 5 min).
- 23 Crystal data of **3**:  $C_{14}H_{20}F_6N_4O_6S_2$ ,  $M = 518.46$ , triclinic,  $a = 8.6516(15)$ ,  $b = 10.1699(17)$ ,  $c = 12.195(2)$ ,  $\alpha = 87.354(3)$ ,  $\beta = 85.474(3)$ ,  $\gamma = 83.360(3)$ ,  $V = 1061.7 \text{ \AA}^3$ ,  $T = 100 \text{ K}$ , space group:  $P-1$ ,  $Z = 2$ , 8258 reflections measured, 4396 independent reflections,  $R1 = 0.0341$ ,  $Rw = 0.0890$ , CCDC 290115.
- 24 Crystal data of **16**:  $C_{11}H_{17}F_3N_2O_4S$ ,  $M = 330.33$ , monoclinic,  $a = 8.5166(14)$ ,  $b = 10.8790(18)$ ,  $c = 16.006(3)$ ,  $\beta = 103.000(3)$ ,  $V = 1445.0 \text{ \AA}^3$ ,  $T = 100 \text{ K}$ , space group:  $P2(1)/n$ ,  $Z = 4$ , 11172 reflections measured, 3237 independent reflections,  $R1 = 0.0350$ ,  $Rw = 0.0933$ , CCDC 290114.
- 25 For crystal structures see: (a) C. M. Gordon, J. D. Holbrey, A. R. Kennedy and K. R. Seddon, *J. Mater. Chem.*, 1998, **8**, 267–2636; (b) J. Dupont, P. A. Z. Suarez, R. F. de Souza, R. A. Burrow and J. P. Kintzinger, *Chem. Eur. J.*, 2000, **6**, 2377–2381; (c) J. van den Broeke, M. Stam, M. Lutz, H. Kooijman, A. L. Spek, B.-J. Deelman and G. van Koten, *Eur. J. Inorg. Chem.*, 2003, 2798–2811; (d) J. D. Holbrey, W. M. Reichert, J. S. Nieuwenhuyzen, R. Seddon and R. D. Rogers, *Chem. Commun.*, 2003, 1636–1637; (e) S. Saha, S. Hayashi and H. Hamaguchi, *Chem. Lett.*, 2003, **32**, 740–741; (f) A. Downard, M. J. Earle, C. Hardacre, S. E. J. McMath, M. Nieuwenhuyzen and S. Teat, *J. Chem. Mater.*, 2004, **16**, 43–48; (g) J. D. Holbrey, W. M. Reichert and R. D. Rogers, *Dalton Trans.*, 2004, **15**, 2267–2271; (h) D. G. Golovanov, K. A. Lyssenko, M. Y. Antipin, Y. S. Vygoskii, E. I. Lozinskaya and A. S. Shaplov, *CrystEngComm*, 2005, **7**, 53–56.
- 26 (a) J. Dupont, *J. Braz. Chem. Soc.*, 2004, **15**, 341–350; (b) C. S. Consorti, P. A. Z. Suarez, R. F. de Souza, R. A. Burrow, D. H. Farrar, A. J. Lough, W. Loh, L. H. M. Da Silva and J. Dupont, *J. Phys. Chem. B.*, 2005, **109**, 4341–4349; (c) F. C. Gozzo, L. S. Santos, R. Austi, C. S. Consorti, J. Dupont and M. N. Eberlin, *Chem. Eur. J.*, 2004, **10**, 6187–6193.
- 27 (a) G. R. Desiraju, *Acc. Chem. Res.*, 1996, **29**, 441–449; (b) T. Steiner and G. R. Desiraju, *Chem. Commun.*, 1998, 891–892.
- 28 G. A. Jeffrey, *An Introduction to hydrogen bonding*, Oxford University Press, Oxford, 1997.
- 29 J. F. Malone, C. M. Murray, M. H. Charlton, R. Docherty and A. J. Lavery, *J. Chem. Soc., Faraday Trans.*, 1997, **93**, 3429–3436.
- 30 B. M. Trost, *Acc. Chem. Res.*, 1980, **13**, 385–393.
- 31 For palladium catalysed allylic alkylation in ionic liquids, see: (a) W. Chen, L. Xu, C. Chatterton and J. Xiao, *Chem. Commun.*, 1999, 1247–1248; (b) J. Ross, W. Chen, L. Xu and J. Xiao, *Organometallics*, 2001, **20**, 138–142; (c) J. Ross and J. Xiao, *Chem. Eur. J.*, 2003, **9**, 4900–4906; (d) S. Toma, B. Gotov, I. Kmentová and E. Solčaniová, *Green Chem.*, 2000, **2**, 149–151; (e) C. de Bellefon, E. Pollet and P. Grenouillet, *J. Mol. Cat. A: Chem.*, 1999, **145**, 121–126; (f) I. Kmentová, B. Gotov, E. Solčaniová and S. Toma, *Green Chem.*, 2002, **4**, 103–106.
- 32 C. Amatore, E. Carré, A. Jutand and M. A. M'Barki, *Organometallics*, 1995, **14**, 1818–1826.
- 33 The 3-methyl-1-[5-(1-methylimidazolium-3-yl)pentyl]-imidazolium dichloride was synthesized under microwave, in a high pressure tube, with 1,5-dichloropentane and N-methylimidazole. For experimental details see: (a) R. S. Varma and V. V. Namboodiri, *Pure Appl. Chem.*, 2001, **73**, 1309–1313; (b) R. S. Varma and V. V. Namboodiri, *Chem. Commun.*, 2001, 643–644.
- 34 C. Amatore, M. Azzabi and A. Jutand, *J. Am. Chem. Soc.*, 1991, **113**, 8375–8384.
- 35 Preparation of 1-alkyl-3-methylimidazolium tetrachloropalladate(II) salts, see for example: (a) J. E. L. Dullius, P. A. Z. Suarez, S. Einloft, R. F. De Souza, J. Dupont, J. Fischer and A. De Cian, *Organometallics*, 1998, **17**, 815–819; (b) C. Hardacre, J. D. Holbrey, P. B. McCormac, S. E. J. McMath, M. Nieuwenhuyzen and K. R. Seddon, *J. Mater. Chem.*, 2001, **11**, 346–350.
- 36 F. G. Bordwell, *Acc. Chem. Res.*, 1988, **21**, 456–463.
- 37 R. W. Alder, P. R. Allen and S. J. Williams, *J. Chem. Soc., Chem. Commun.*, 1995, 1267–1268.
- 38 Co-crystal data:  $C_{27}H_{51}F_9N_3O_7S_2$ ,  $M = 707.83$ , triclinic,  $a = 9.5883(13)$ ,  $b = 9.7729(13)$ ,  $c = 19.198(3)$ ,  $\alpha = 85.627(2)$ ,  $\beta = 88.693(2)$ ,  $\gamma = 88.563(2)$ ,  $V = 1792.7 \text{ \AA}^3$ ,  $T = 100 \text{ K}$ , space group:  $P-1$ ,  $Z = 2$ , 14089 reflections measured, 7772 independent reflections,  $R1 = 0.0578$ ,  $Rw = 0.1722$ , CCDC 621900.
- 39 J. D. Holbrey, W. M. Reichert, M. Nieuwenhuyzen, O. Sheppard, C. Hardacre and R. D. Rogers, *Chem. Commun.*, 2003, 476–477.
- 40 P. J. Stang and T. E. Dueber, *Org. Synth. Coll. Vol. VI*, 1988, **VI**, 757–761.
- 41 T. Hayashi, A. Yamamoto, Y. Ito, E. Nishiok, H. Miura and K. Yanagi, *J. Am. Chem. Soc.*, 1989, **111**, 6301–6311.



# Heterogeneous vanadium catalysts for racemization and chemoenzymatic dynamic kinetic resolution of benzylic alcohols

S. Wuyts, J. Wahlen, P. A. Jacobs\* and D. E. De Vos

Received 5th January 2007, Accepted 16th May 2007

First published as an Advance Article on the web 14th June 2007

DOI: 10.1039/b700187h

Cheap and readily available oxovanadium compounds such as vanadyl sulfate ( $\text{VOSO}_4$ ) and vanadium oxide ( $\text{V}_2\text{O}_5$ ) catalyze the racemization of benzylic alcohols in the absence of any additives (*e.g.*, bases or hydrogen mediators) or co-catalysts. The reaction occurs at 80 °C in *n*-octane as the solvent and does not require anhydrous or oxygen-free conditions. Experiments clearly demonstrated that  $\text{VOSO}_4$  is a reusable and truly heterogeneous racemization catalyst. Insight into the reaction mechanism was obtained from  $^{18}\text{O}$ -labeling experiments, which showed that the formation of carbenium ion intermediates is a key step. The V-catalyzed racemization was combined with a lipase-catalyzed kinetic resolution to give a chemoenzymatic dynamic kinetic resolution of benzylic alcohols. The dynamic kinetic resolution (DKR) proceeds in one pot and does not need additives or specifically designed acyl donors. Under optimized conditions, the DKR process yields the corresponding esters in good chemical yield (>90%) and high optical purity (>99% ee).

## 1. Introduction

Enantiomerically pure alcohols and esters are key components for asymmetric synthesis. An attractive route for their preparation is dynamic kinetic resolution (DKR), which combines the kinetic resolution (*e.g.*, enzyme-catalyzed KR) of a racemic mixture of alcohols with the *in situ* racemization of the slow-reacting enantiomer.<sup>1</sup> DKR provides optically enriched esters in up to quantitative yields, whereas the maximum yield in conventional KR is limited to 50%. Generally, racemization requires relatively harsh thermal or strongly acidic or basic conditions,<sup>2</sup> which are incompatible with a stereoselective one-pot transformation. On the other hand, various transition metal complexes of rhodium, iridium and ruthenium are known to catalyze the racemization of optically active alcohols under mild conditions.<sup>3</sup> The racemization proceeds *via* a hydrogen transfer pathway involving dehydrogenation of the chiral alcohol and re-addition of hydrogen to the intermediate ketone. Unfortunately, only a few of these metals (mainly Ru-based complexes) are compatible with an *in situ* enzymatic reaction.<sup>4</sup> Frequently encountered obstacles are the interference of the metal with the enzyme, resulting in poor KR, or inhibition of the racemization reaction by the enzyme. Moreover, additives required for the chemical or enzymatic reaction, or the acyl donor and the byproducts produced upon acylation can also affect the racemization or the kinetic resolution. Therefore, the search for new racemization catalysts continues to be an important research topic. In this respect, recyclable catalysts are of particular interest.<sup>4h,5,6</sup> Recent advances in aerobic alcohol

oxidation catalyzed by oxovanadium species prompted us to investigate the potential of vanadium as a catalyst for the racemization of secondary alcohols.<sup>7,8</sup> Herein we report on the racemization and chemoenzymatic DKR of benzylic alcohols using heterogeneous vanadium catalysts.

## 2. Experimental

### 2.1 Materials and product analysis

All materials were obtained from commercial sources and were used without purification.  $\text{H}_2^{18}\text{O}$  ( $^{18}\text{O}$  content > 95%) was obtained from Fluka. Lipase B (CALB) from *Candida antarctica* adsorbed on a macroporous acrylic resin was purchased from Sigma (Novozym 435). Vanadyl sulfate ( $\text{VOSO}_4 \cdot 5\text{H}_2\text{O}$ ) was obtained from Merck or Acros and gave nearly identical results. Powder X-ray diffraction, XRD, (Siemens D5000 $\text{m}^{\text{atic}}$  diffractometer with Ni-filtered Cu  $\text{K}\alpha$  radiation) showed that the diffraction pattern of commercial  $\text{VOSO}_4 \cdot 5\text{H}_2\text{O}$  corresponds with the XRD data reported for the mineral species minasragrite.<sup>9</sup> According to scanning electron microscopy (Philips XL30 FEG microscope), the majority of the crystals had a rod-like shape, with dimensions of 20–50  $\mu\text{m}$  in length and 10–20  $\mu\text{m}$  in width.

Yields and enantiomeric purities of substrates and reaction products were determined using an HP 6890 gas chromatograph (Chirasil-DEX CB fused silica WCOT column, 25 m  $\times$  0.32 mm  $\times$  0.25  $\mu\text{m}$ ) and a flame-ionization detector. Nitrogen was used as the carrier gas. Yields were determined using the internal standard (*i.e.*, tetradecane) method and individual calibration factors to correct for the detector response. GC–MS analyses were performed on an Agilent 6890N GC (He carrier gas, HP-5MS column, 30 m  $\times$  0.25 mm  $\times$  0.25  $\mu\text{m}$ ) coupled to an Agilent 5973 Network Mass Selective Detector (electron impact ionization at 70 eV).

Centre for Surface Chemistry and Catalysis, Katholieke Universiteit Leuven, Kasteelpark Arenberg 23 Box 2461, 3001, Leuven, Belgium.  
E-mail: pierre.jacobs@biw.kuleuven.be; Fax: +32 1632 1998;  
Tel: +32 1632 1610

Reference compounds were prepared by established synthetic procedures. Enantiopure octanoyl esters were obtained by the lipase-catalyzed esterification of racemic phenylalkanols with vinyl octanoate. Racemic esters were prepared by the direct acylation of the corresponding racemic alcohols with octanoic acid in the presence of *N,N'*-dicyclohexylcarbodiimide and 4-(dimethylamino)pyridine.<sup>10</sup>

## 2.2 Reaction procedures

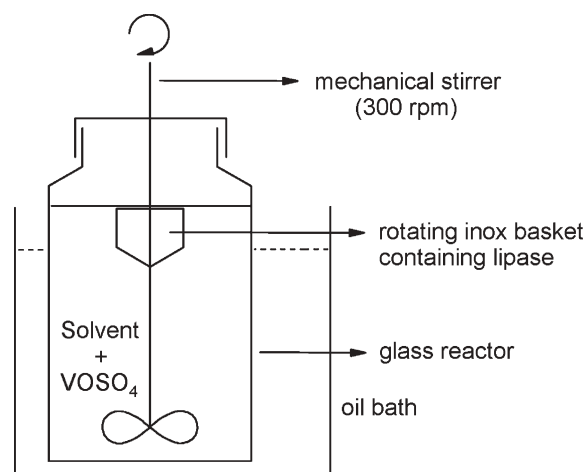
**Standard racemization reaction.** Racemization reactions were performed at 80 °C in a well-stirred (500 rpm) glass vial containing 10 mL of the solvent, 0.5 mmol (*S*)-1-phenylethanol (*S*)-**1a** (ee > 99%) and 0.25 mmol tetradecane as an internal GC standard. After introduction of all reaction components, 0.1 g of the vanadium catalyst was added. When the reaction was performed under an inert atmosphere instead of under air, the mixture was carefully flushed with nitrogen gas prior to reaction.

**Heterogeneity test and catalyst reuse.** In order to check the heterogeneous nature of the observed catalysis, a conventional filtrate test was performed.<sup>11</sup> Using  $\text{VOSO}_4 \cdot 5\text{H}_2\text{O}$  as the catalyst, a standard racemization reaction was carried out, and at a low degree of racemization, half of the hot catalyst suspension was filtered (0.45  $\mu\text{m}$ ), and the reaction progress in the clear filtrate and in the catalyst suspension (both at 80 °C) was further monitored by chiral GC analysis.

**Determination of the oxygen isotopic composition of 1-phenylethanol.** In order to study the mechanism of the vanadium-catalyzed racemization of 1-phenylethanol, the reaction was carried out in the presence of a small amount of  $^{18}\text{O}$ -enriched water. The reaction was performed at 80 °C in a glass vial containing 5 mL of *n*-octane, 0.125 mmol (*S*)-1-phenylethanol (*S*)-**1a** (ee > 99%) and 0.05 g  $\text{VOSO}_4 \cdot n\text{H}_2\text{O}$  (pre-dried for 3 h at 60 °C). Finally, 0.01 g of  $^{18}\text{O}$ -enriched water ( $^{18}\text{O}$  content > 95%) was added to the reaction mixture.

The evolution of the enantiomeric excess was monitored by chiral GC analysis and the oxygen isotopic composition of 1-phenylethanol **1a** was determined by GC–MS. The alcohol isomers were not resolved from one another on the achiral GC–MS column. The  $^{16}\text{O}$  and  $^{18}\text{O}$  composition of **1a** was deduced from the comparison of the relative abundances of the ion fragments at mass/charge ratios of 122 (reflecting the  $^{16}\text{O}$  content) and 124 (reflecting the  $^{18}\text{O}$  content).<sup>12</sup> The oxygen isotopic composition calculated from the mass spectral fragments 107 and 109 was nearly identical. These fragments correspond to the parent ion (122/124) and a  $\text{C}_7\text{H}_7\text{O}$  fragment (107/109) resulting from the loss of a methyl group ( $\text{M}^+ - 15$ ).

**Standard DKR reaction.** DKR reactions were performed in a 100 mL glass reactor equipped with a blade stirrer rotating at 300 rpm (Scheme 1). A conical basket made of inox gauze was mounted on the shaft of the stirrer. The basket was filled with 0.11 g of immobilized lipase and the reactor was loaded with 100 mL of the solvent (*n*-octane or toluene) and 1.27 mmol racemic 1-phenylethanol (*rac*-**1a**). Finally, 0.2 g of  $\text{VOSO}_4 \cdot 5\text{H}_2\text{O}$  was added and the reactor was closed and heated to



Scheme 1 DKR reaction setup.

80 °C. Once the reaction temperature was reached, 2 equivalents (equiv.) of vinyl octanoate (2.54 mmol) were added and the reaction progress was monitored by chiral GC analysis. After 2.25 h, another 2 equivalents of vinyl octanoate were added.

## 3. Results and discussion

Employing *n*-octane as the solvent at 80 °C, several vanadium compounds were screened for their activity in the racemization of (*S*)-1-phenylethanol (ee > 99%) (**1a**). Reactions were carried out under a nitrogen atmosphere to prevent the net oxidation of the alcohol. After 1.5 h, the enantiomeric excess (ee) and the alcohol yield were determined by chiral GC analysis (Table 1). Among the various vanadium catalysts examined,  $\text{V}_2\text{O}_4$  and  $\text{VOSO}_4 \cdot 5\text{H}_2\text{O}$  showed the highest activity for the racemization of (*S*)-**1a**, giving **1a** in 15–2% ee and 82–96% yield, respectively. When the reaction was performed under an air atmosphere, a similar reaction rate was observed and importantly, no oxidation products (*i.e.*, acetophenone) were detected (Entry 4). Surprisingly,  $\text{VO}(\text{acac})_2$  (acac = acetylacetonate) and  $\text{V}_2\text{O}_5$ , two commonly used (pre)catalysts for oxovanadium-catalyzed transformations,<sup>7</sup> showed almost no activity in the racemization of (*S*)-**1a** (Entry 6 and 7).

Table 1 Vanadium-catalyzed racemization of (*S*)-1-phenylethanol<sup>a</sup>

Entry	Catalyst	ee <sup>b</sup> (%)	Yield <sup>b</sup> (%)
1	$\text{V}(\text{acac})_3$	99	99
2	$\text{V}_2\text{O}_3$	90	82
3	$\text{VOSO}_4 \cdot 5\text{H}_2\text{O}$	2	96
4 <sup>c</sup>	$\text{VOSO}_4 \cdot 5\text{H}_2\text{O}$	2	94
5 <sup>d</sup>	$\text{V}_2\text{O}_4$	15	82
6	$\text{VO}(\text{acac})_2$	99	98
7	$\text{V}_2\text{O}_5$	98	94
8	$\text{NaVO}_3$	99	99

<sup>a</sup> (*S*)-**1a** (0.50 mmol), tetradecane (0.25 mmol) and V catalyst (0.1 g) in octane (10 mL) were stirred for 1.5 h at 80 °C under  $\text{N}_2$ .

<sup>b</sup> Alcohol yield and ee determined by chiral GC analysis. <sup>c</sup> Air atmosphere. <sup>d</sup> 60 °C.

Vanadyl sulfate was selected for further investigation regarding reaction conditions, substrate scope and reaction mechanisms. Toluene and *n*-octane were the preferred solvents with respect to the rate of racemization and alcohol yield. With 1,4-dioxane or *N,N*-dimethylformamide as the solvent, very little racemization was observed. To verify whether the observed catalysis is due to solid  $\text{VOSO}_4$  or to leached vanadium species, the racemization of (*S*)-**1a** was carried out under standard conditions. After 1 h (ee = 41%), half of the reaction mixture was filtered at 80 °C, and both the clear filtrate and the remaining catalyst suspension were further stirred at 80 °C. No further racemization of (*S*)-**1a** was observed in the filtrate, not even after prolonged reaction times, whereas the reaction proceeded smoothly in the catalyst suspension (Fig. 1). This experiment clearly shows the complete absence of any catalytically active vanadium species in solution. To demonstrate the recyclability of the catalyst, a standard racemization reaction was carried out, and at the end of the reaction the solid  $\text{VOSO}_4$  was recovered by centrifugation and was washed with octane. The catalyst along with replenished reagents and solvent was reused twice without any loss of the original catalytic activity (Fig. 2). Product yields (not shown) remained equally high over the three runs. For the second and third run, a slight increase of the reaction rate is observed. Scanning electron microscopy revealed a partial fragmentation of the original particles upon vigorous stirring of the catalyst under reaction conditions. The reduced crystal size might explain the enhanced racemization rate in the subsequent runs with the same catalyst. Similarly, milling of the catalyst with a ball mill reduced the crystal size and produced slightly more active catalysts.

Various enantiopure alcohols could be racemized using  $\text{VOSO}_4$  in octane (Table 2). Halogen substituents (*e.g.*, Br) on the aromatic ring are tolerated (Entry 2). Initial kinetics showed that the racemization of (*S*)-1-(4-bromophenyl)ethanol, which contains an electron-withdrawing substituent, proceeded 3.5 times more slowly than the racemization of (*S*)-**1a**. When the methyl group in the benzylic position is replaced by an ethyl group, the racemization proceeded as

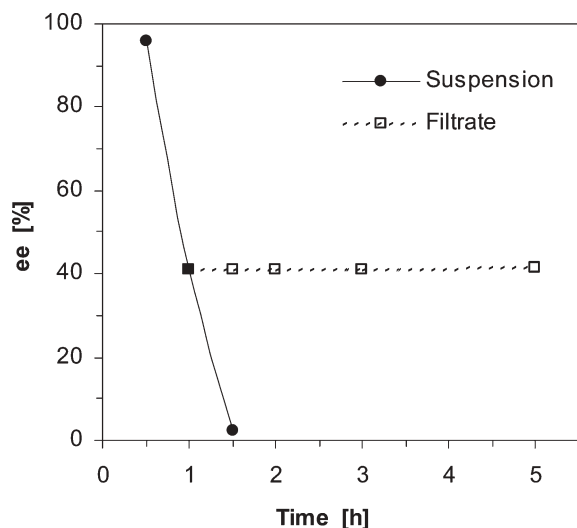


Fig. 1 Filtrate test for  $\text{VOSO}_4$  in the racemization of (*S*)-**1a**.

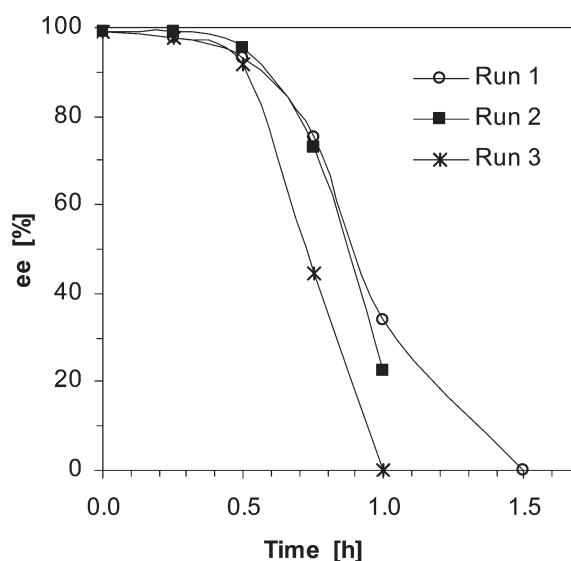


Fig. 2 Reuse of  $\text{VOSO}_4$  in the racemization of (*S*)-**1a**.

well, but at a slightly lower rate (Entry 4). The introduction of small functional groups next to the alcohol is tolerated, as demonstrated in the reaction of the  $\beta$ -chloro-substituted alcohol (Entry 5). The racemization of (*S*)-1-indanol proceeded efficiently at room temperature (Entry 6). Racemization of aliphatic alcohols such as (*R*)-2-octanol did not occur, not even after prolonged reaction times or at higher temperatures (Entry 7).

Regarding the mechanism of the V-catalyzed racemization, we first considered redox pathways involving cleavage of the  $\alpha$ -CH bond. Possible routes may involve hydride or

Table 2 Racemization of secondary alcohols with vanadyl sulfate<sup>a</sup>

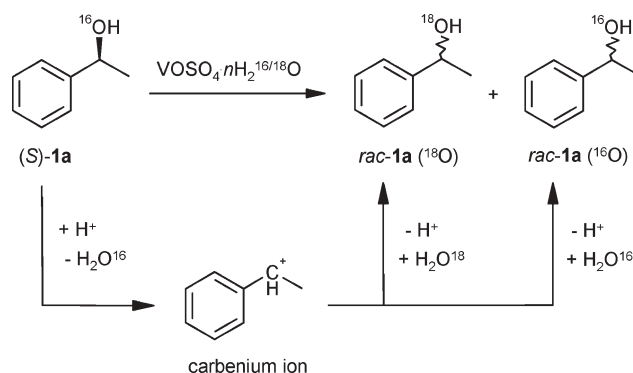
Entry	Substrate	<i>T</i> /°C	Time/h	ee (%)	Yield (%)
1		80	1.5	6	95
2		80	2.5	12	96
3		60	6.5	48	96
4		80	3.5	5	88
5		80	5.0	39	97
6		25	3.5	3	98
7		100	24	99	95

<sup>a</sup> Alcohol (0.25 mmol), tetradecane (0.125 mmol) and  $\text{VOSO}_4 \cdot 5\text{H}_2\text{O}$  (0.05 g) in octane (10 mL) were stirred under air.

hydrogen-atom abstraction with intermediate formation of a ketone or an  $\alpha$ -hydroxy carbon radical, respectively. During the racemization of (*S*)-**1a** with  $\text{VOSO}_4$  under air, no traces of ketone were observed, and addition of acetophenone (1 equivalent relative to (*S*)-**1a**) did not result in a rate enhancement. This suggests that the racemization does not proceed *via* a hydrogen transfer pathway.<sup>3c</sup> Addition of radical inhibitors like 2,6-di-*tert*-butylphenol did not affect the reaction rate nor the alcohol yield.<sup>13</sup> Moreover, optically active esters are not racemized by the  $\text{VOSO}_4$  catalyst. Both observations disfavor a radical pathway. Alternatively, chiral alcohols such as **1a** may be racemized *via* protonation, water loss, and formation of an  $\text{sp}^2$  carbenium ion, which is planar and prochiral. Subsequent addition of water to the carbocation occurs stereorandomly leading to racemization.<sup>6,12,14,15</sup>

Direct evidence for the involvement of acid catalysis was obtained by studying the racemization of (*S*)-**1a** in the presence of  $\text{VOSO}_4 \cdot n^{16/18}\text{H}_2\text{O}$  containing  $^{18}\text{O}$ -enriched hydration water (~40%  $^{18}\text{O}$  enrichment). For a reaction proceeding through carbocation intermediates,  $^{18}\text{O}$  exchange between water and (*S*)-**1a** will occur during racemization. Mass spectrometric analysis of **1a** indicated that the hydroxyl oxygen atom was 35%  $^{18}\text{O}$ -labeled at 8% ee (Fig. 3). The high level of  $^{18}\text{O}$  incorporation proves that carbenium ion formation is the key step (Scheme 2).<sup>12,14</sup> This acid-catalyzed mechanism is supported by the observation that the addition of bases such as sodium carbonate or *N,N*-diisopropylethylamine inhibits the catalyst. In addition, under suboptimal conditions, the racemization of (*S*)-**1a** is accompanied with the formation of side products uniquely indicative of carbenium ion intermediates. Thus, prolonged heating of (*S*)-**1a** with  $\text{VOSO}_4$  yields, besides *rac*-**1a**, styrene and bis( $\alpha$ -methylbenzyl)ether. These products are similar to those of other acid-catalyzed reactions of secondary alcohols.<sup>16</sup>

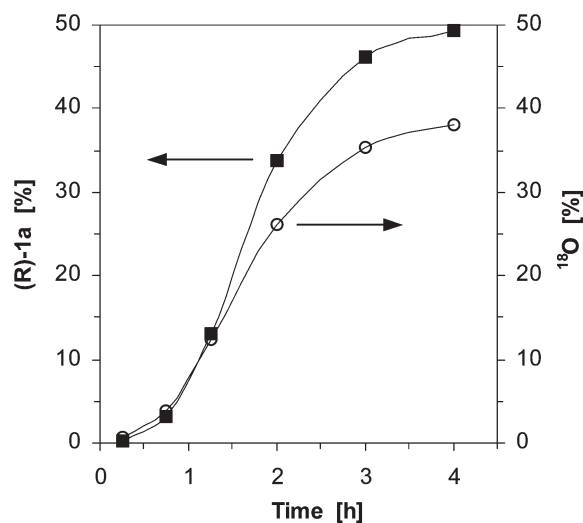
As shown in Fig. 2, the racemization catalyzed by  $\text{VOSO}_4 \cdot 5\text{H}_2\text{O}$  is characterized by a specific decay of the enantiomeric excess: a slow linear decrease is followed by a



**Scheme 2**  $^{18}\text{O}$  incorporation during the vanadium-catalyzed racemization of (*S*)-**1a**.

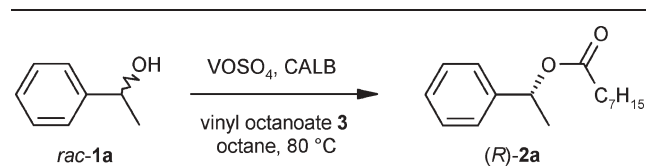
steep decay of the ee. This induction period is shorter at higher reaction temperatures and the same induction period is still present when the catalyst is reused or when the catalyst is subjected to consecutive heating/cooling cycles. At this time, we assume that the induction period is due to the presence of water on the catalyst surface. This is consistent with all observations, particularly regarding the relationship between pretreatment and activity. An increased temperature likely causes desorption of water from the surface of the catalyst. As the Brønsted acidity of inorganic metal sulfates is considered to result from polarized water molecules bonded to the metal cation, it is clear that the hydration degree will strongly affect the number and the strength of the acid sites.<sup>15</sup> The induction period probably is the result of the gradual formation of stronger acid sites upon water desorption, as is also observed for cation-containing zeolites upon dehydration.

Having established the potential of vanadium as a racemization catalyst,  $\text{VOSO}_4$  was combined with an immobilized *Candida antarctica* lipase B (CALB) to effect the chemoenzymatic DKR of racemic **1a**. CALB was the preferred lipase as it tolerates a wide range of acyl donors and shows a high enantioselectivity in the acylation of benzylic alcohols.<sup>17</sup> Importantly,  $\text{VOSO}_4$  itself does not catalyze the esterification. The DKR was carried out in one pot, although it was found necessary to physically separate the immobilized lipase and the solid vanadyl sulfate. This was achieved by isolating CALB in a porous inox basket which was suspended in a 100 mL glass reactor containing the  $\text{VOSO}_4$  crystals (Scheme 1). Preliminary experiments showed that an appropriate acyl donor is required. Commonly used esters like vinyl or isopropenyl acetate resulted in some inhibition of the racemization, but with vinyl octanoate **3** as the acyl donor,  $\text{VOSO}_4$  retained its original activity and selectivity, and a successful DKR of *rac*-**1a** could be achieved. (*R*)-1-Phenylethyl octanoate (**2a**) was obtained in good chemical yield and in high enantiomeric purity using the appropriate amount of  $\text{VOSO}_4$  (Table 3, Entry 2). Lowering the amount of  $\text{VOSO}_4$  resulted in an insufficient racemization rate, which is translated into a lower ester yield and ee (Entry 1). Using toluene as the solvent instead of octane, a comparable yield was obtained after 3.5 h, but the ee of **2a** decreased considerably (Entry 4). In order to obtain the ester in even higher enantiomeric purities, the total amount of acyl donor **3** was reduced to 2 equivalents relative



**Fig. 3** Racemization of (*S*)-**1a** catalyzed by  $\text{VOSO}_4 \cdot n\text{H}_2^{16/18}\text{O}$ : formation of (*R*)-**1a** (chiral GC analysis) and isotopic composition of *rac*-**1a** based on the 122/124 ion fragments (GC–MS).



**Table 3** DKR of *rac*-**1a** using vanadyl sulfate and lipase CALB<sup>a</sup>

Entry	VOSO <sub>4</sub> /g	<b>3</b> <sup>b</sup> (equiv.)	Time/h	Yield <sup>c</sup> (%)	ee <sup>c</sup> (%)
1	0.1	4	4.5	67	82
2	0.2	4	3.5	94	95
3	0.5	4	4.5	78	90
4 <sup>d</sup>	0.2	4	3.5	93	76
5	0.2	2	3.5	93	99

<sup>a</sup> *rac*-**1a** (1.27 mmol), vinyl octanoate **3**, VOSO<sub>4</sub>·5H<sub>2</sub>O and lipase B (0.11 g) in octane (100 mL) were stirred (300 rpm) at 80 °C. <sup>b</sup> The total amount of **3** was added in two equal portions at 0 and 2.25 h. <sup>c</sup> Ester yield and ester ee determined by chiral GC analysis. <sup>d</sup> 100 mL of toluene.

to **1a**. This resulted in an identical yield of **2a** but the ee increased to 99% (Entry 5).

## Conclusions

In conclusion, oxovanadium compounds catalyze the racemization of benzylic alcohols without the need for additives or inert conditions. Vanadyl sulfate is a reusable and truly heterogeneous racemization catalyst that can be combined with a resolving lipase for the DKR of racemic benzylic alcohols.

## Acknowledgements

S. W. and J. W. thank K. U. Leuven and FWO–Vlaanderen for fellowships. This work was supported by the Belgian Government (IAP project on Supramolecular Chemistry and Catalysis).

## References

- (a) F. F. Huerta, A. B. E. Minidis and J.-E. Bäckvall, *Chem. Soc. Rev.*, 2001, **30**, 321; (b) M.-J. Kim, Y. Ahn and J. Park, *Curr. Opin. Biotechnol.*, 2002, **13**, 578; (c) O. Pàmies and J.-E. Bäckvall, *Chem. Rev.*, 2003, **103**, 3247.
- E. J. Ebberts, G. J. A. Ariaans, J. P. M. Houbiers, A. Bruggink and B. Zwanenburg, *Tetrahedron*, 1997, **53**, 9417.
- (a) P. M. Dinh, J. A. Howarth, A. R. Hudnott, J. M. J. Williams and W. Harris, *Tetrahedron Lett.*, 1996, **37**, 7623; (b) J. H. Koh, H. M. Jeong and J. Park, *Tetrahedron Lett.*, 1998, **39**, 5545; (c) O. Pàmies and J.-E. Bäckvall, *Chem.-Eur. J.*, 2001, **7**, 5052.
- (a) A. L. E. Larsson, B. A. Persson and J.-E. Bäckvall, *Angew. Chem., Int. Ed.*, 1997, **36**, 1211; (b) B. A. Persson, A. L. E. Larsson, M. Le Ray and J.-E. Bäckvall, *J. Am. Chem. Soc.*, 1999, **121**, 1645; (c) M.-J. Kim, Y. K. Choi, M. Y. Choi, M. J. Kim and J. Park, *J. Org. Chem.*, 2001, **66**, 4736; (d) A. Dijkman, J. M. Elzinga, Y.-X. Li, I. W. C. E. Arends and R. A. Sheldon, *Tetrahedron: Asymmetry*, 2002, **13**, 879; (e) J. H. Choi, Y. H. Kim, S. H. Nam, S. T. Shin, M.-J. Kim and J. Park, *Angew. Chem., Int. Ed.*, 2002, **41**, 2373; (f) B. Martín-Matute, M. Edin, K. Bogár and J.-E. Bäckvall, *Angew. Chem., Int. Ed.*, 2004, **43**, 6535; (g) B. Martín-Matute, M. Edin, K. Bogár, F. B. Kaynak and J.-E. Bäckvall, *J. Am. Chem. Soc.*, 2005, **127**, 8817; (h) N. Kim, S.-B. Ko, M. S. Kwon, M.-J. Kim and J. Park, *Org. Lett.*, 2005, **7**, 4523.
- (a) S. Wuyts, D. E. De Vos, F. Verpoort, D. Depla, R. De Gryse and P. A. Jacobs, *J. Catal.*, 2003, **219**, 417; (b) W. H. Kim, R. Karvembu and J. Park, *Bull. Korean Chem. Soc.*, 2004, **25**, 931; (c) A. Zsigmond, A. Kecskemeti, K. Bogar, F. Notheisz and E. Mernyak, *Catal. Commun.*, 2005, **6**, 520; (d) K. Yamaguchi, T. Koike, M. Kotani, M. Matsushita, S. Shinachi and N. Mizuno, *Chem.-Eur. J.*, 2005, **11**, 6574.
- (a) S. Wuyts, K. De Temmerman, D. De Vos and P. Jacobs, *Chem. Commun.*, 2003, 1928; (b) D. Klomp, T. Maschmeyer, U. Hanefeld and P. A. Peters, *Chem.-Eur. J.*, 2004, **10**, 2088; (c) S. Wuyts, K. De Temmerman, D. E. De Vos and P. A. Jacobs, *Chem.-Eur. J.*, 2005, **11**, 386; (d) P. Lozano, T. De Diego, M. Larnicol, M. Vaultier and J. L. Iborra, *Biotechnol. Lett.*, 2006, **28**, 1559; (e) Y. Zhu, K.-L. Fow, G.-K. Chuah and S. Jaenicke, *Chem.-Eur. J.*, 2007, **13**, 541.
- Oxovanadium-catalyzed aerobic oxidation of alcohols: (a) M. Kirihaara, Y. Ochiai, S. Takizawa, H. Takahata and H. Nemoto, *Chem. Commun.*, 1999, 1387; (b) Y. Maeda, N. Kakiuchi, S. Matsumura, T. Nishimura, T. Kawamura and S. Uemura, *J. Org. Chem.*, 2002, **67**, 6718; (c) S. Velusamy and T. Punniyamurthy, *Org. Lett.*, 2004, **6**, 217; (d) A. T. Radosevich, C. Musich and F. D. Toste, *J. Am. Chem. Soc.*, 2005, **127**, 1090; (e) S.-S. Weng, M.-W. Shen, J.-Q. Kao, Y. S. Munot and C.-T. Chen, *Proc. Natl. Acad. Sci. U. S. A.*, 2006, **103**, 3522.
- During this work, the use of Lewis-acid oxovanadium complexes for the DKR of allylic alcohols was reported. The racemization proceeds via a [3,3]sigmatropic rearrangement and is applicable to a limited number of allylic alcohols: S. Akai, K. Tanimoto, Y. Kanao, M. Egi, T. Yamamoto and Y. Kita, *Angew. Chem., Int. Ed.*, 2006, **45**, 2592.
- M. L. Smith and J. Marinenko, *Am. Mineral.*, 1973, **58**, 531.
- A. Rauf and H. Parveen, *Eur. J. Lipid Sci. Technol.*, 2004, **106**, 97.
- R. A. Sheldon, M. Wallau, I. W. C. E. Arends and U. Schuchardt, *Acc. Chem. Res.*, 1998, **31**, 485.
- M. V. Merritt, D. B. Anderson, K. A. Basu, I.-W. Chang, H.-J. Cheon, N. E. Mukundan, C. A. Flannery, A. Y. Kim, A. Vaishampayan and D. A. Yens, *J. Am. Chem. Soc.*, 1994, **116**, 5551.
- For V-catalyzed alcohol oxidation with a radical mechanism, see: V. Conte, F. Di Furia and G. Modena, *J. Org. Chem.*, 1988, **53**, 1665.
- E. Grunwald, A. Heller and F. S. Klein, *J. Chem. Soc.*, 1957, 2604.
- Inorganic metal (e.g., Cu or Al) sulfates are used as catalysts in the dehydration of alcohols. For example, see: (a) R. V. Hoffman, R. D. Bishop, P. M. Fitch and R. Hardenstein, *J. Org. Chem.*, 1980, **45**, 917; (b) T. Nishiguchi and C. Kamio, *J. Chem. Soc., Perkin Trans. 1*, 1989, 707; (c) E. J. Eisenbraun, K. W. Payne and J. S. Bymaster, *Org. Prep. Proced. Int.*, 2000, **32**, 557. However, in comparison with VOSO<sub>4</sub>, these metal sulfates showed no or very low activity, or low selectivity in the racemization of (*S*)-**1a**.
- For example, see: B. S. Kwak and T. J. Kim, *Appl. Catal., A*, 1999, **188**, 99.
- A. Ghanem and H. Y. Aboul-Enein, *Tetrahedron: Asymmetry*, 2004, **15**, 3331.

# A microwave approach to the selective synthesis of $\omega$ -laurolactam

Tomas D. Conesa,<sup>a</sup> Juan M. Campelo,<sup>a</sup> James H. Clark,<sup>b</sup> Rafael Luque,<sup>\*b</sup> Duncan J. Macquarrie<sup>b</sup> and Antonio A. Romero<sup>\*a</sup>

Received 18th April 2007, Accepted 25th May 2007

First published as an Advance Article on the web 15th June 2007

DOI: 10.1039/b705881k

The Beckmann rearrangement of cyclododecanone oxime, the monomer for the production of Nylon 12, was successfully accomplished using a wide range of micro-mesoporous catalysts, under microwave conditions, affording the selective production of  $\omega$ -laurolactam in high conversions after a short period of time (typically 5 min).

## Introduction

Microwave technology has been the subject of extensive studies during the past few years<sup>1</sup> and many reports have appeared dealing with several applications of microwave-assisted synthesis as an interdisciplinary research field.<sup>2</sup> This novel and cleaner reaction tool relies on the power of microwaves to reduce the reaction times and energy consumption together with an increase in yields and selectivity in some cases.<sup>3</sup>

The Beckmann rearrangement of cyclic oximes is a well-known reaction in which the cyclic lactam is produced, usually selectively and in high yields, in the presence of solid acids.<sup>4</sup> Interestingly, only a few research highlights dealing with the rearrangement of the cyclododecanone oxime (Cdox) have been reported so far.<sup>5</sup>  $\omega$ -Laurolactam ( $\omega$ -l) is the monomer for the production of Nylon 12 which has several interesting applications in the automotive industry, medicine, sport and manufacture of food packaging articles. Its commercial production in the liquid phase (*ca.* 50 000 t year<sup>-1</sup> worldwide)<sup>6</sup> is energy consuming and co-produces a substantial amount of ammonium sulfate as waste. Furthermore, the majority of the  $\omega$ -l preparation methods have been reported in the patent literature and have described liquid phase Beckmann rearrangements involving mineral acid catalysts<sup>7</sup> and anhydrides of organic sulfonic acids.<sup>8</sup> Only very few were performed using solid acid catalysts.<sup>5-9</sup> In order to overcome the problems related with mineral acids and energy intensive processing, a combination of microwave-assisted chemistry and heterogeneous catalysis could potentially be the key to cleaner and safer methodologies. The synthesis, characterisation and catalytic application of micro- and mesoporous materials has been a major research topic in our groups for a long time.<sup>10</sup>

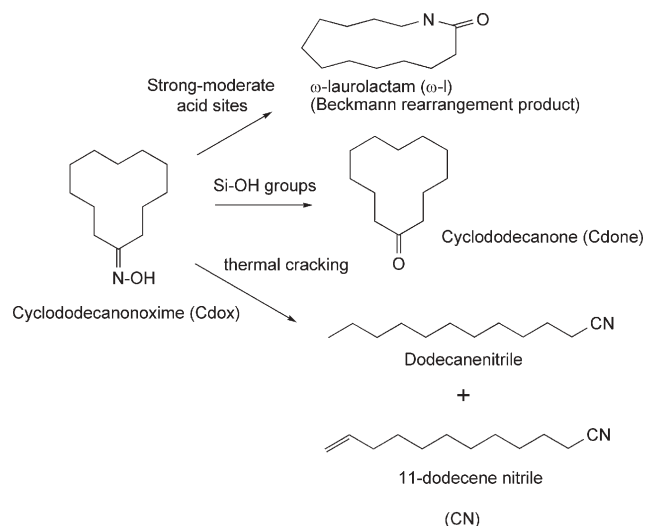
We have recently developed a wide range of acidic micro- and mesoporous materials that have proven to be highly active and selective in different acid catalysed reactions, including the Beckmann rearrangement of cyclohexanone oxime.<sup>11</sup> A combination of weak (Lewis) and strong (Brønsted) acid sites

has been shown to be critical in order to achieve highly active and selective materials in the reaction.

Here, we report for the first time the highly selective production of  $\omega$ -l in a short reaction time *via* microwave heating in the presence of porous solid acids.

## Results and discussion

A series of micro-mesoporous materials including mesoporous aluminosilicates, silicoaluminophosphates and microporous commercial zeolites were screened (see Experimental). The presence of strong Brønsted acid sites in the materials was found to be critical in order to attain highly active catalysts as we will discuss later. Firstly, the different parameters involved in microwave assisted reactions that could potentially affect the performance of the solid acids in the Cdox rearrangement were explored in order to optimise the conversion and selectivity to  $\omega$ -l. The initial microwave reaction conditions were: 20 mg Cdox, 20 mg catalyst, 130 °C, 15 min. Chlorobenzene (PhCl) was employed as solvent in the reaction due to the good results obtained with this solvent in previous work<sup>5a</sup> as well as the good solubility of the cyclic oxime in PhCl. Cyclododecanone (Cdone) was the only by-product found but dodecanenitrile and 11-dodecenitrile (CN) (Scheme 1) were not detected in the reaction mixture.



**Scheme 1** Product distribution in the Beckmann rearrangement of Cdox.

<sup>a</sup>Departamento de Química Orgánica, Universidad de Córdoba, Campus de Rabanales, Ctra Nnal IV Km 396, Edificio Marie Curie, Córdoba, Spain. E-mail: qo1rorea@uco.es

<sup>b</sup>Green Chemistry Centre of Excellence, Department of Chemistry, The University of York, York, UK. E-mail: rla3@york.ac.uk; Fax: +44 1904 432705; Tel: +44 1904 432568

**Table 1** Effect of microwave power on the catalytic performance [total conversion ( $X_T$ ) and selectivities to  $\omega$ -1 ( $S_{\omega-1}$ ) and Cdone ( $S_{\text{Cdone}}$ )] of AlB-2 and Al-SBA-15(20) in the Beckmann rearrangement of Cdox under microwave irradiation<sup>a</sup>

Entry	Catalyst	Power/W	$X_T$ (mol%)	$S_{\omega-1}$ (mol%)	$S_{\text{Cdone}}$ (mol%)
1	AlB-2	200	29	94	6
2		225	35	96	4
3		250	40	95	5
4		275	49	98	2
5	Al-SBA-15(20)	200	44	91	9
6		225	49	95	5
7		250	55	98	2
8		275	73	99	1

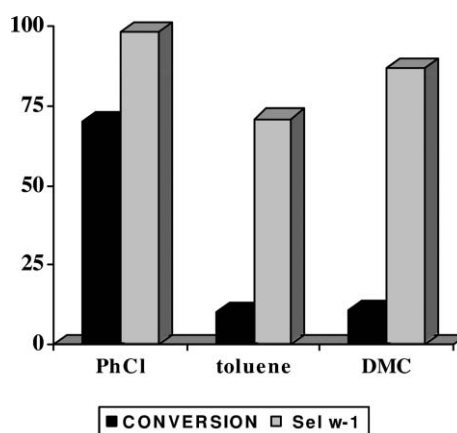
<sup>a</sup> Reaction conditions: 20 mg Cdox, 3 mL PhCl, 20 mg catalyst, 130 °C, 15 min.

### Effect of the microwave power

The microwave power had a notable effect on reaction rates as shown in Table 1 for the particular case of AlB-2 and Al-SBA-15, respectively. A power increase of 75 W (from 200 to 275 W) almost doubled the conversion and also slightly increased the selectivity to  $\omega$ -1. A similar trend was found for all the solid acids screened in the reaction.  $\beta$ -25 zeolite provided the best conversion values in the reaction ( $\sim 80\%$  at 275 W, not shown) but in any case comparable to that of Al-SBA-15 (Table 1, entry 8).

### Effect of the solvent

From a green chemistry standpoint, PhCl is not the greenest solvent for our reaction, so in an attempt to completely or partially replace the PhCl with a more environmentally compatible solvent, several solvents were screened in the Beckmann rearrangement of Cdox. The effect of some of these solvents in the catalytic performance of the Al-SBA-15(20) is illustrated in Fig. 1. The extraordinary effect in both conversion and selectivity to  $\omega$ -1 when employing toluene and dimethyl carbonate (DMC) instead of PhCl is notable. Moreover, water-miscible solvents (*i.e.* methanol, ethanol, *etc.*) were also screened as a potential PhCl replacement. Very poor conversion values ( $<10\%$  using ethanol under Fig. 1 reaction conditions) were found. This could be due to the poor solubility of the oxime and/or products in the alcohol. However, the partial replacement of PhCl for toluene gives promising results (*i.e.* 57% conversion and 87% selectivity to  $\omega$ -1 were found using a fluorinated AlB-2 material under the standard reaction conditions with a 1 : 2 w/w PhCl : toluene mixture).



**Fig. 1** Solvent effect in the activity and selectivity of Al-SBA-15(20) in the Beckmann rearrangement of Cdox under microwave irradiation (reaction conditions: 20 mg Cdox, 3 mL solvent, 275 W, 130 °C, 20 mg cat.).

Even more interesting results were found in a solventless environment. 20 mg Cdox together with the catalyst (20 mg) were placed in a microwave tube and microwaved under similar reaction conditions (see Experimental). Data is summarised in Table 2. Surprisingly,  $\beta$ -25 zeolite provided very low conversion values whereas Al/MCM-41 and Al-SBA-15 materials gave the best results of all the materials screened (entries 2, 3, 5 and 6). In terms of selectivity, a decrease in selectivity to  $\omega$ -1 in the solventless reactions compared to the PhCl ones was found. Cdone was found as the major by-product coming from the transformation of Cdox over Si-OH groups. The lower activity of  $\beta$ -25 compared to the mesoporous materials may be due to the pore size constraints of the zeolite framework (*ca.* 1.2 nm) that may retain the oxime and/or product formed inside it under solventless conditions, compared to the mesoporous Al-MCM-41(20) (*ca.* 2.3 nm) and specially Al-SBA-15(20) (*ca.* 5.1 nm). A significant increase in conversion was also found increasing either the temperature from 130 to 180 °C (Table 2, entries 3 and 5) or the quantity of catalyst (entry 6) at the expense of the  $\omega$ -1 selectivity. Higher quantities of Cdone, dodecanenitrile and CN as by-products when increasing the temperature were also observed.

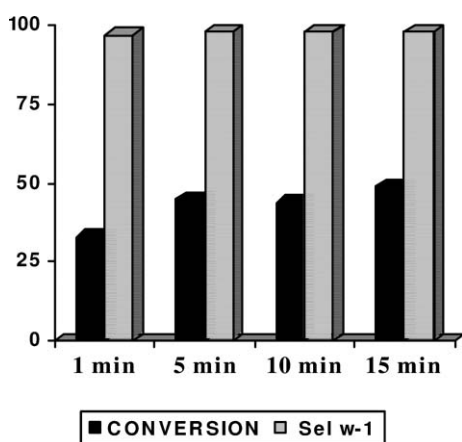
### Effect of the time of reaction

After optimisation of the power and the solvent employed in the Beckmann rearrangement, the time of reaction was the next parameter to be optimised. Interestingly, the conversion

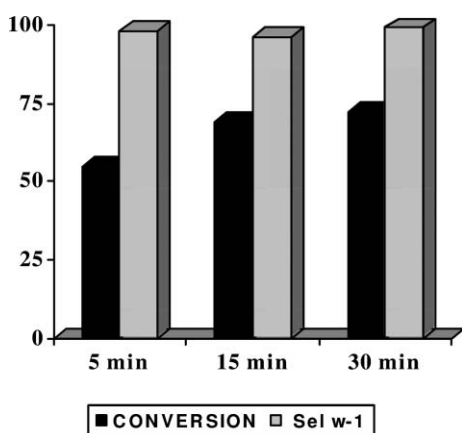
**Table 2** Catalytic performance [total conversion ( $X_T$ ) and selectivities to  $\omega$ -1 ( $S_{\omega-1}$ ), Cdone ( $S_{\text{Cdone}}$ ) and CN ( $S_{\text{CN}}$ )] of different micro-mesoporous materials in the Beckmann rearrangement of Cdox under microwave irradiation and in the absence of solvent<sup>a</sup>

Entry	Catalyst	$X_T$ (mol%)	$S_{\omega-1}$ (mol%)	$S_{\text{Cdone}}$ (mol%)	$S_{\text{CN}}$ (mol%)
1	AlB-2	33	75	25	—
2	Al-MCM-41(20)	54	86	14	—
3	Al-SBA-15(20)	57	87	13	—
4	Commercial $\beta$ -25	10	87	13	—
5	Al-SBA-15(20) <sup>b</sup>	82	78	19	3
6	Al-SBA-15(20) <sup>c</sup>	88	79	21	—

<sup>a</sup> Reaction conditions: 20 mg Cdox, 20 mg catalyst, 275 W, 130 °C, 15 min. <sup>b</sup> 180 °C. <sup>c</sup> 130 °C, 40 mg catalyst.



**Fig. 2** Effect of time of reaction on the activity and selectivity of AlB-2 employed as catalyst in the Beckmann rearrangement of Cdox under microwave irradiation (reaction conditions: 20 mg Cdox, 3 mL PhCl, 275 W, 130 °C, 20 mg cat.).



**Fig. 3** Effect of time of reaction on the activity and selectivity of Al-SBA-15(20) employed as catalyst in the Beckmann rearrangement of Cdox under microwave irradiation (reaction conditions: 20 mg Cdox, 3 mL PhCl, 275 W, 130 °C, 20 mg cat.).

did not significantly increase after reaction times longer than 5 min (Fig. 2 and 3) and a good conversion [over 33% for all materials] was found after only 1 min of reaction. Selectivity to ω-1 (>95% in all cases) remained unchanged with time of reaction.

#### Effect of the catalyst quantity

As expected, the quantity of solid acid used in the reaction increased the conversion of Cdox in the systems (Tables 3

**Table 3** Effect of the quantity of catalyst in the catalytic performance [total conversion ( $X_T$ ) and selectivities to ω-1 ( $S_{\omega-1}$ ) and Cdone ( $S_{Cdone}$ )] of Al-B-2 in the Beckmann rearrangement of Cdox under microwave irradiation<sup>a</sup>

Entry	Cat. quantity/mg	$X_T$ (mol%)	$S_{\omega-1}$ (mol%)	$S_{Cdone}$ (mol%)
1	10	30	98	2
2	20	49	98	2
3	30	65	97	3
4	40	73	97	3

<sup>a</sup> Reaction conditions: 20 mg Cdox, 3 mL PhCl, 275 W, 130 °C, 15 min.

**Table 4** Effect of the quantity of catalyst in the catalytic performance [total conversion ( $X_T$ ) and selectivities to ω-1 ( $S_{\omega-1}$ ) and Cdone ( $S_{Cdone}$ )] of Al-SBA-15(20) in the Beckmann rearrangement of Cdox under microwave irradiation<sup>a</sup>

Entry	Cat. quantity/mg	$X_T$ (mol%)	$S_{\omega-1}$ (mol%)	$S_{Cdone}$ (mol%)
1	10	38	98	2
2	20	73	99	1
3	30	85	98	2
4	40	94	97	3

<sup>a</sup> Reaction conditions: 20 mg Cdox, 3 mL PhCl, 275 W, 130 °C, 15 min.

and 4), with an increase in the quantity of catalyst added. Significantly, the conversion did not appreciably change for Al-SBA-15(20) at quantities higher than 35 mg (91%), but it almost doubled when the catalyst amount was increased from 10 to 20 mg (Table 4, entries 1 and 2). The selectivity remained almost unchanged with an increase of the amount of catalyst. A similar trend was found for all materials tested in the Beckmann rearrangement of Cdox (AlB-2 example in Table 3).

#### Effect of the reaction temperature

Reactions carried out at different temperatures employing some examples of the materials screened in the reaction are included in Table 5.

Temperature was not found to be one of the critical parameters for the reaction (Table 5). Selectivities to ω-1 remained unchanged and the mesoporous materials, including Al-MCM-41(20) and Al-SBA-15(20) had activities comparable to that of the microporous β-25 zeolite.

#### Effect of the quantity of oxime

Further experiments were performed with increasing quantities of Cdox. Results are summarised in Table 6. Results demonstrated an increase in the catalyst efficiency, in terms of ω-1

**Table 5** Effect of the reaction temperature in the catalytic performance [total conversion ( $X_T$ ) and selectivities to ω-1 ( $S_{\omega-1}$ ) and Cdone ( $S_{Cdone}$ )] of various micro-mesoporous materials in the Beckmann rearrangement of Cdox under microwave irradiation<sup>a</sup>

Entry	Catalyst	130 °C			180 °C		
		$X_T$ (mol%)	$S_{\omega-1}$ (mol%)	$S_{Cdone}$ (mol%)	$X_T$ (mol%)	$S_{\omega-1}$ (mol%)	$S_{Cdone}$ (mol%)
1	AlB-2	49	98	2	55	98	2
2	Al-MCM-41(20)	61	97	3	72	97	3
3	Al-SBA-15(20)	73	99	1	83	98	2
4	β-25	68	>99	—	76	>99	—

<sup>a</sup> Reaction conditions: 20 mg Cdox, 3 mL PhCl, 275 W, 15 min, 20 mg cat.



**Table 6** Effect of the quantity of oxime in the catalytic performance [total conversion ( $X_T$ ) and selectivities to  $\omega$ -1 ( $S_{\omega-1}$ ) and Cdone ( $S_{Cdone}$ )] of Al-MCM-41(20) material in the Beckmann rearrangement of Cdox under microwave irradiation<sup>a</sup>

Entry	Oxime Quantity/mg	$X_T$ (mol%)	$S_{\omega-1}$ (mol%)	$S_{Cdone}$ (mol%)
1	20	61	97	3
2	50	50	94	6
3	100	39	95	5

<sup>a</sup> Reaction conditions: 3 mL PhCl, 275 W, 130 °C, 15 min, 20 mg cat.

produced, with increasing quantities of Cdox in the Beckmann rearrangement. In all cases, selectivities to  $\omega$ -1 were preserved. The production of  $\omega$ -1 was three times higher when the quantity of oxime was increased from 20 mg (12 mg  $\omega$ -1 formed) to 100 mg (39 mg  $\omega$ -1 produced) for the Al-MCM-41(20) material. Moreover, in the particular case of 100 mg of Cdox, a longer reaction time will probably lead to a better lactam yield. In this regard, further studies are ongoing to examine the feasibility of the solventless system.

### Optimised parameters and results

Tables 7 and 8 summarise the main optimised results of the microwave assisted Beckmann rearrangement of Cdox using various solid acids with both PhCl as solvent or a solventless system. Surface acidity data, using pyridine (py) and 2,6-dimethylpyridine (dmpy) as probe molecules have also been included. In general, the solid acids afforded the  $\omega$ -1 in high yields and selectivity in a short reaction time, with the exception of the B-MCM-41 and B-SBA-15 that exhibited a poor performance in the reaction due to their low surface acidity (Table 7, entries 3 and 4). Medium to strong acid sites

are prerequisite for the reaction. However, in terms of selectivity to  $\omega$ -1, the strong Brønsted acidity present in zeolitic materials does not seem to make a significant difference. Al-MCM-41(20) and Al-SBA-15(20) (Table 7, entries 5 and 6) exhibited catalytic activities and selectivities comparable to those of commercial microporous materials (*i.e.*  $\beta$ -zeolite) after microwave heating for 5 min.

A greener solventless system was successfully used as shown in Table 8. Al-MCM-41 and especially Al-SBA-15 provided extremely good results compared to those of microporous commercial zeolitic materials despite their lower acidities. However, selectivity was found to be significantly reduced in the solventless system. The transformation of Cdox to Cdone is more important in the presence of an organic solvent such as PhCl or toluene.

Finally, the solids were filtered after the reaction and the liquid filtrate was tested in another reaction cycle. No conversion was detected in the filtrate when returned to reaction conditions, confirming the truly heterogeneous behaviour of our solid acids.

### Experimental

Al-MCM-41(Si/Al ratio 20), B-MCM-41 (Si/B ratio 20), AlB-MCM-41 (AlB-2, AlB-2F Si/Al + B and Al/B ratios, 20 and 2, respectively) and SiAlP [(SiO<sub>2</sub> + Al<sub>2</sub>O<sub>3</sub>)/AlPO<sub>4</sub> ratio 4.5] materials have been synthesized as previously reported.<sup>10a,12</sup> Fluorinated AlB-2 material was obtained from AlB-2 material after treatment with a 0.1 M NH<sub>4</sub>F solution for 34 h.<sup>11b</sup> Al- and B-SBA-15 (Si/Al and Si/B ratio 20) were prepared according to a previously reported methodology by Yue *et al.*<sup>12</sup> and Eswaramoorti and Dalai,<sup>13</sup> respectively. Commercial  $\beta$ -25

**Table 7** Optimised catalytic performance of different micro-mesoporous materials in the Beckmann rearrangement of Cdox under microwave irradiation using PhCl as solvent<sup>a</sup>

Entry	Catalyst	$X_T$ (mol%)	$S_{\omega-1}$ (mol%)	$S_{Cdone}$ (mol%)	Surface acidity (300 °C)/ $\mu\text{mol g}^{-1}$	
					py	dmpy
1	Blank	— <sup>b</sup>	—	—	— <sup>c</sup>	— <sup>c</sup>
2	AlB-2	65	93	7	196	85
3	B-MCM-41	<15	88	12	— <sup>c</sup>	— <sup>c</sup>
4	B-SBA-15(20)	<15	>99	—	— <sup>c</sup>	— <sup>c</sup>
5	Al-MCM-41(20)	94	94	6	170	92
6	Al-SBA-15(20)	90	96	4	174	98
7	SiAlP-4.5	79	96	4	93	76
8	Commercial $\beta$ -25	97	>95	<5	216	190
9	Commercial ZSM-5	20	>99	—	239	217

<sup>a</sup> Dodecanenitrile and CN were not detected; reaction conditions: 20 mg Cdox, 3 mL PhCl, 40 mg catalyst, 275 W, 180 °C, 5 min. <sup>b</sup> No reaction. <sup>c</sup> No adsorption of the probe molecule at this temperature.**Table 8** Optimised catalytic performance of different micro-mesoporous materials in the Beckmann rearrangement of Cdox under microwave irradiation in a solventless system<sup>a</sup>

Entry	Catalyst	$X_T$ (mol%)	$S_{\omega-1}$ (mol%)	$S_{Cdone}$ (mol%)	$S_{CN}$ (mol%)
1	Blank	— <sup>b</sup>	—	—	—
2	Al-MCM-41 (20)	80	81	19	—
3	Al-SBA-15 (20)	95	84	12	4
4	Commercial $\beta$ -25	54	80	20	—
5	Commercial ZSM-5	<15	79	21	—

<sup>a</sup> Reaction conditions: 20 mg Cdox, 40 mg catalyst, 275 W, 180 °C, 5 min. <sup>b</sup> No reaction. <sup>c</sup> No adsorption of the probe molecule at this temperature.

zeolite (SiO<sub>2</sub>/Al<sub>2</sub>O<sub>3</sub> ratio 25) and ZSM-5(30) (SiO<sub>2</sub>/Al<sub>2</sub>O<sub>3</sub> ratio 30) were purchased from Zeolyst Int. Cdox was prepared according to a literature reported procedure.<sup>14</sup> Microwave experiments were carried out in a CEM-DISCOVER model with PC control and monitored by sampling aliquots of reaction mixture that were subsequently analysed by GC/GC-MS using a HP5890 series II gas chromatograph fitted with a capillary column and an FID detector. Reaction products were ω-1 and Cdone. For the solventless reactions, Cdox and the catalyst were added to a microwave tube, microwaved under different reaction conditions and then the solid mixture containing the reaction products was extracted with PhCl (3 mL) and subsequently analysed by GC as described before.

## Conclusions

The main aim of this research was to demonstrate the applicability of microwave heating to relatively complicated acid catalysed reactions, in particular the Beckmann rearrangement of Cdox, commonly performed under conventional heating. The solid acids screened in the reaction were found to be extremely active and selective in the production of ω-1 in a short period of time (typically 5 min). The microwave power, the solvent and the quantity of catalyst employed in the process proved to be the most critical parameters with optimised conditions using 275 W power and 40 mg of catalyst in both PhCl and solventless systems. Of note were the results obtained in the solventless system with Al-MCM-41 and especially Al-SBA-15 that prove the reaction can take place in the absence of solvent, giving quantitative conversions to the cyclic lactam.

## References

- (a) D. M. P. Mingos and D. R. Baghurst, *Chem. Soc. Rev.*, 1991, **20**, 1; (b) S. A. Galema, *Chem. Soc. Rev.*, 1997, **26**, 233; (c) C. Gabriel, S. Gabriel, E. H. Grant, B. S. J. Halstead and D. M. P. Mingos, *Chem. Soc. Rev.*, 1998, **27**, 213; (d) R. S. Varma, *Green Chem.*, 1999, **1**, 43; (e) M. Larhed, Ch. Moberg and A. Hallberg, *Acc. Chem. Res.*, 2002, **35**, 717; (f) R. Trotzki, M. Nüchter and B. Ondruschka, *Green Chem.*, 2003, **5**, 285.
- M. Nüchter, B. Ondruschka, W. Bonrath and A. Gum, *Green Chem.*, 2004, **6**, 128.
- M. J. Gronnow, R. J. White, J. H. Clark and D. J. Macquarrie, *Org. Process Res. Dev.*, 2005, **9**, 516.
- (a) D. Mao, Q. Chen and G. Lu, *Appl. Catal., A*, 2003, **244**, 273; (b) R. Maheswari, K. Shanthi, T. Sivakumar and S. Narayanan, *Appl. Catal., A*, 2003, **248**, 291; (c) L. Forni, G. Fornasari, G. Giordano, C. Lucarelli, A. Katovic, F. Trifiro, C. Perri and J. B. Nagy, *Phys. Chem. Chem. Phys.*, 2004, **6**, 1842.
- (a) M. A. Camblor, A. Corma, H. Garcia, V. Semmer-Herléndan and S. Valencia, *J. Catal.*, 1998, **177**, 267; (b) N. Kuroda, J. Kawai and H. Shimomura, *EP Pat.*, 1 329 448 A1, 2003; (c) A. Corma, S. Iborra and M.-I. Rodriguez, *WO Pat.*, 2004037785 A1, 2004; (d) S. Yamamoto, A. Haruta and Y. Fukuda, *Jpn. Pat.*, 2005022977, 2005.
- United Nations Environment Programme Publications. <http://www.chem.unep.ch/irptc/sids/OECD/SIDS/947046.pdf>.
- (a) J. C. Michel and P. Patin, *US Pat.*, 4 211 700, 1980; (b) J. Ollivier, *EP Pat.*, 0 798 290 A1, 1997; (c) J. Ollivier, *US Pat.*, 5 719 316, 1998; (d) J. Ollivier and D. Drutel, *WO Pat.*, 9 901 424, 1999.
- M. Hans and V. Heinz-Werner, *US Pat.*, 4 689 412, 1987.
- (a) K.-U. Otto, S. Hans-Helmut and K. Hermann, *US Pat.*, 3 586 668, 1971; (b) L. Garcia and M. Del Pino, *ES Pat.*, 2 048 098, 1994; (c) S. Yamamoto, A. Haruta and Y. Fukuda, *Jpn. Pat.*, 2005023014, 2005.
- (a) J. M. Campelo, R. M. León, D. Luna, J. M. Marinas and A. A. Romero, *Stud. Surf. Sci. Catal.*, 2002, **142**, 1299; (b) J. H. Clark, *Acc. Chem. Res.*, 2002, **35**, 791; (c) J. M. Campelo, M. Jaraba, D. Luna, R. Luque, J. M. Marinas, A. A. Romero, J. A. Navio and M. Macias, *Chem. Mater.*, 2003, **15**, 3352; (d) J. M. Campelo, D. Luna, R. Luque, J. M. Marinas, A. A. Romero, J. J. Calvino and M. P. Rodriguez-Luque, *J. Catal.*, 2005, **230**, 327; (e) R. Luque, J. M. Campelo, D. Luna, J. M. Marinas and A. A. Romero, *Microporous Mesoporous Mater.*, 2005, **84**, 11; (f) R. Luque, J. M. Campelo, T. D. Conesa, D. Luna, J. M. Marinas and A. A. Romero, *New J. Chem.*, 2006, **30**, 1228; (g) V. Budarin, J. H. Clark, J. J. E. Hardy, R. Luque, K. Milkowski, S. J. Tavener and A. J. Wilson, *Angew. Chem., Int. Ed.*, 2006, **45**, 3782; (h) V. Budarin, J. H. Clark, R. Luque and D. J. Macquarrie, *Chem. Commun.*, 2007, 634.
- (a) T. D. Conesa, J. M. Hidalgo, R. Luque, J. M. Campelo and A. A. Romero, *Appl. Catal., A*, 2006, **299**, 224; (b) T. D. Conesa, J. M. Campelo, D. Luna, J. M. Marinas and A. A. Romero, *Appl. Catal., B*, 2007, **70**, 567; (c) T. D. Conesa, R. Mokaya, J. M. Campelo and A. A. Romero, *Chem. Commun.*, 2006, 1839.
- Y. Yue, A. Gedeon, J. L. Bonardet, N. Melosh, J. B. D'Espinose and J. Fraissard, *Chem. Commun.*, 1999, 1967.
- I. Eswaramoorthi and A. K. Dalai, *Microporous Mesoporous Mater.*, 2006, **93**, 1.
- J. Fontán and A. Martín, *La Caracterización de Compuestos Orgánicos*, ed. S. M. McElvain, Aguilar, Madrid, 1968, p. 193.

# Mild oxidation of styrene and its derivatives catalyzed by ionic manganese porphyrin embedded in a similar structured ionic liquid

Ye Liu, Hong-Jiao Zhang, Yong Lu,\* Yue-Qin Cai and Xiu-Li Liu

Received 10th April 2007, Accepted 30th May 2007

First published as an Advance Article on the web 18th June 2007

DOI: 10.1039/b705356h

Without the auxiliary involvement of axial ligands and organic solvents, the ionic manganese porphyrin (**1c**) with a pyridinium tag embedded in a pyridinium based ionic liquid, [BPy][BF<sub>4</sub>], efficiently catalyzed the oxidation of styrene and its derivatives under mild conditions, affording high activity/oxide selectivity and good stability even after 5 recycling uses.

## Introduction

Various oxidations such as epoxidation of olefins and hydroxylation of hydrocarbons with oxygen donors (iodosylarenes, alkylhydroperoxides, hydrogen peroxide, hypochlorites, periodates *etc.*) have been catalyzed by metalloporphyrins as model catalysts of cytochrome P450 in homogeneous organic media, in which the axial ligands like imidazole or pyridine (derivatives) are required necessarily to activate and stabilize active metal porphyrin species.<sup>1–5</sup> Anyway, the intermolecular self-aggregation due to  $\pi$ – $\pi$  stacking and the propensity to oxidation led to deactivation, destruction and difficult recovery of metalloporphyrin in such systems. In order to solve these problems, many heterogeneous methods have been developed to improve metalloporphyrin dispersion, stability and recovery.<sup>6–8</sup>

Ambient ionic liquids (ILs) are not only environmentally benign solvents with unique physical properties such as non-volatility, non flammability, and thermal stability, but are also mobile and flexible “carriers” of functional units (such as metal complexes, ligands) through the formation of covalent bonds.<sup>9,10</sup> For example, to avoid metal catalyst leaching out of IL system, efforts have been made to enhance the solubility/miscibility of the metal catalysts through grafting electron-donor ligands into ILs which can coordinate with metal centers,<sup>11</sup> or incorporating imidazolium or pyridinium tags into a metal complex.<sup>12</sup> Herein, we report the oxidation of styrene and its derivatives with iodosylbenzene (PhIO) oxidant catalyzed by Mn porphyrin with a pyridinium tag (**1c**) which was embedded in an ambient IL of *N*-butyl-pyridinium tetrafluoroborate ([BPy][BF<sub>4</sub>]) (Scheme 1).<sup>13</sup> Without auxiliary involvement of the axial ligand and the volatile organic solvent, such a built-up ionic Mn porphyrin in [BPy][BF<sub>4</sub>] exhibited high catalytic activity and much improved stability. The considerations of combining metalloporphyrins and ILs together were highlighted by the following points besides the advantage of IL as solvent. (1) By introducing pyridinium cations and PF<sub>6</sub><sup>–</sup> anions into the skeleton of metalloporphyrin, the conventional neutral metalloporphyrin could be regarded as a functional

group which was grafted into the IL; (2) pyridine (derivatives) could act as the axial ligands for metalloporphyrins. ILs based on the pyridinium (or imidazolium) structure might play the role of axial ligands to replace the conventional ones; (3) the common IL based on pyridinium with conjugated features could interact with the super-conjugated porphyrin through  $\pi$ – $\pi$  interactions; (4) The strong electron-withdrawing effect of the pyridinium cation in metalloporphyrin could decrease the electron density of porphyrino ring.

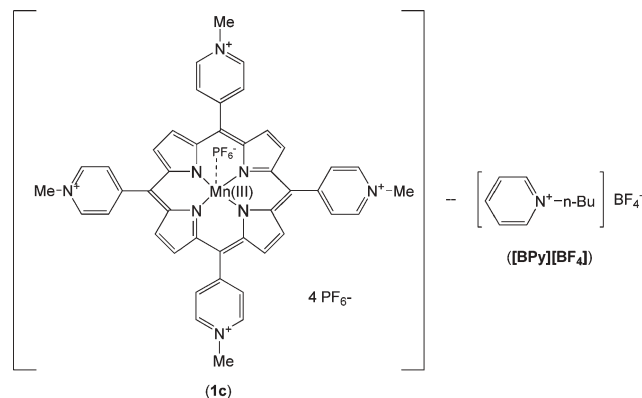
## Experimental

### Measurement and analysis

The <sup>1</sup>H NMR (500 MHz, 298 K) spectra were recorded on a Bruker Avance 500 spectrometer. The elemental analyses were performed by the Analytical Center in ECNU. The UV-Vis spectra were recorded on a Cary 100 spectrophotometer. GC analyses were performed by SHIMADZU-14B chromatography equipped with a HP-1 capillary column (30 m × 0.25 mm × 0.25  $\mu$ m). GC-MS analyses were recorded on an Agilent 6890 instrument equipped with Agilent 5973 mass selective detector.

### Synthesis

**Synthesis of manganese tetrakis-(*N*-methyl-4-pyridinium)-porphyrin hexafluorophosphate {[Mn<sup>III</sup>T(*N*-Me-4-Py)P][PF<sub>6</sub>]<sub>5</sub>, **1c**}. In a N<sub>2</sub> atmosphere, a mixture of salicylic acid (4.0 g, 28 mmol) and pyridine-4-carbaldehyde (6.4 g, 60 mmol**



**Scheme 1** Multi-component IL system: **1c** embedded in [BPy][BF<sub>4</sub>].

Shanghai Key Laboratory of Green Chemistry and Chemical Processes, Chemistry Department of East China Normal University, Shanghai 200062, P. R. China. E-mail: ylu@chem.ecnu.edu.cn; Fax: 86 21 62233424; Tel: 86 21 62232078

dissolved in refluxed 500 mL *o*-xylene) was added to pyrrole (4.0 g, 60 mmol) dropwise over 40 min. After refluxing for another 2.5 h, the reaction mixture was cooled to room temperature and poured into 30 mL methanol to stand overnight. The resultant black precipitates were washed with methanol until the shining purple solids were obtained as tetrakis(4-pyridyl)-porphyrin {[H<sub>2</sub>T(4-Py)P], **1a**} with a yield of 32 wt%. <sup>1</sup>H NMR (**1a**, CDCl<sub>3</sub>): δ = 9.1 (d, 8H, pyridyl, *CHNCH*), 8.9 (s, 8H, pyrrolyl, β-*H*), 8.2 (d, 8H, pyridyl, *CHCCH*), −2.9 (s, 2H, 2*NH*) ppm. UV-Vis (**1a**): λ<sub>max</sub> = 417 (s, Soret band), 513 (w, Q band), 547 (w, Q band), 588 (w, Q band), 644 (w, Q band) nm. Elemental analysis found (calculated) for C<sub>40</sub>H<sub>26</sub>N<sub>8</sub> (**1a**): C 77.61 (77.67), H 4.12 (4.21), N 18.20 (18.12).

In a N<sub>2</sub> atmosphere, while the solution of **1a** (1.5 g, 2.5 mmol) in 100 mL DMF was heated to 100 °C, MeI (2.8 g, 20 mmol) was added. After refluxing for 1 h, the reaction mixture was cooled to room temperature and recrystallized with diethyl ether, yielding red-brown solid tetrakis(*N*-methyl-4-pyridinium)-porphyrin iodide {[H<sub>2</sub>T(*N*-Me-4-Py)P][I]<sub>4</sub>, **1b**} (yield: 82%). If **1b** dissolved in deionized water was treated directly with NH<sub>4</sub>PF<sub>6</sub> aqueous solution, the shining dark-purple solids of tetrakis(*N*-methyl-4-pyridinium)-porphyrin hexafluorophosphate [H<sub>2</sub>T(*N*-Me-4-Py)P][PF<sub>6</sub>]<sub>4</sub> (**1b'**) were obtained after washing with water with a yield of 95%. <sup>1</sup>H NMR (**1b'**, CDCl<sub>3</sub>): δ = 9.5 (d, 8H, pyridinium, *CHN<sup>+</sup>CH*), 9.2 (d, 8H, pyrrolyl, β-*H*), 9.0 (d, 8H, pyridinium, *CHCCH*), 4.7 (s, 12H, N<sup>+</sup>CH<sub>3</sub>), −3.1 (s, 2H, 2*NH*) ppm. UV-Vis (**1b'**): λ<sub>max</sub> = 422 (s, Soret band), 517 (w, Q band), 550 (w, Q band), 590 (w, Q band), 644 (w, Q band) nm. Elemental analysis found (calculated) for C<sub>44</sub>H<sub>38</sub>N<sub>8</sub>P<sub>4</sub>F<sub>24</sub> (**1b'**): C 41.83 (41.97), H 3.11 (3.02), N 8.79 (8.90).

The mixture of 0.83 g [H<sub>2</sub>T(*N*-Me-4-Py)P][I]<sub>4</sub> (**1b**, 0.7 mmol) and 1.97 g Mn(OAc)<sub>2</sub>·6H<sub>2</sub>O (7 mmol) in 100 mL acetic acid was heated at 80 °C for 6 h. After removal of the solvent *in vacuo*, the residues left were recrystallized with methanol/diethyl ether to yield the dark-purple solids as [Mn<sup>III</sup>T(*N*-Me-4-Py)P][I]<sub>5-x</sub>[OAc]<sub>x</sub> (*x* = 0–5), which was dissolved in deionized water, and then treated with excess NH<sub>4</sub>PF<sub>6</sub> aqueous solution. The purple-red solids precipitated readily. By washing with deionized water and methanol, the purple solids of manganese tetrakis(*N*-methyl-4-pyridinium)-porphyrin hexafluorophosphate {[Mn<sup>III</sup>T(*N*-Me-4-Py)P][PF<sub>6</sub>]<sub>5</sub>, **1c**} were obtained with a yield of 86%. Due to the influence of the <sup>55</sup>Mn quadrupolar nucleus and the paramagnetism of Mn<sup>III</sup> porphyrin **1c**, the signals in the <sup>1</sup>H NMR of **1c** were broadened to flatness. UV-Vis (**1c**): λ<sub>max</sub> = 463 (s, Soret band), 537 (w, Q band), 581 (w, Q band), 627 (w, Q band) nm.

**Synthesis of manganese tetrakis-(4-pyridyl)-porphyrin** {[Mn<sup>III</sup>T(4-Py)P], **2b**}. The solution of 0.5 g **1a** (0.8 mmol) in 100 mL acetic acid was added with 1.9 g Mn(OAc)<sub>2</sub>·6H<sub>2</sub>O (6.8 mmol). After refluxing overnight, the residues obtained were washed with deionized water, yielding dark-purple solids with a yield of 92%. UV-Vis (**2b**): λ<sub>max</sub> = 471 (s, Soret band), 568 (w, Q band), 603 (w, Q band) nm.

#### General procedures for oxidation of styrene and its derivatives

In open air, 2 mL [BPy][BF<sub>4</sub>] was mixed with [Mn<sup>III</sup>T(4-*N*-Me-Py)P][PF<sub>6</sub>]<sub>5</sub> (**1c**) and 400 μmol styrene or its derivative

(analytical grade reagent used as received), yielding a totally homogeneous light-purple solution in which 600 μmol PhIO was added afterwards to take up the oxidation at the appointed temperature. After completion of the reaction, diethyl ether was used to extract the organic compounds including reactants and products (2 mL × 3). The conversions were based on GC analyses with 1-dodecane as the internal standard. The selectivities of products were based on GC analyses with the normalization method. The product structures were further confirmed by GC-mass analyses.

The ionic liquid phase left was dried *in vacuo* to remove traces of diethyl ether and used without further treatment for the next run. In every run, due to the stoichiometric consumption of PhIO oxidant, it was added (400 μmol) additionally besides the substrates.

## Results and discussion

The application of ionic metalloporphyrin **1c** to catalyze styrene oxidation was inspired by the basic concept of functionalization of ILs. By modification of the conventional neutral manganese porphyrin of [Mn<sup>III</sup>T(4-Py)P] (**2b**) with a pyridinium tag and a PF<sub>6</sub><sup>−</sup> anion, the obtained metalloporphyrin could be regarded as a porphyrin-functionalized IL, although it was surely in solid state without the feature of melting point <100 °C. In our work, the selection of PF<sub>6</sub><sup>−</sup> as the anion was because of its hydrophobicity, facilitating the purification work-up in the synthetic process (by precipitation of **1c** directly from the aqueous phase as described in the Experimental). In consideration of more similar components, originally we were supposed to use [BPy][PF<sub>6</sub>] as the matched solvent for **1c**. However, [BPy][PF<sub>6</sub>] in solid state at room temperature was not suitable to be a solvent, and then [BPy][BF<sub>4</sub>] was on top of the list. Fortunately, **1c** was readily miscible in [BPy][BF<sub>4</sub>] due to the ionic nature and their similar skeletons, building up the multi-component IL system which was composed of four types of ion {[Mn<sup>III</sup>T(*N*-Me-4-Py)P]<sup>5+</sup>, [BPy]<sup>+</sup>, [PF<sub>6</sub>]<sup>−</sup>, [BF<sub>4</sub>]<sup>−</sup>} (Scheme 1). The oxidation of styrene catalyzed by **1c** and the conventional neutral **2b** in [BPy][BF<sub>4</sub>] and a volatile organic solvent, respectively, is indicated in Table 1. In open air, with ionic **1c** embedded in [BPy][BF<sub>4</sub>] as the catalytic system, the oxidation of styrene was readily carried out in the homogeneous phase. Under mild reaction conditions (30 °C) and no auxiliary involvement of the other axial ligand, the isoelectronic products of styrene oxide and phenylacetaldehyde were obtained in a yield of 86% and 10% respectively, without C=C bond cleavage (No. 1). The use of pyridine as an axial ligand deteriorated the catalytic activity badly (No. 2, 4), implying that the ionic liquid of [BPy][BF<sub>4</sub>] could behave as the preferred axial ligand and the solvent dually. The relatively stronger coordination of pyridine to **1c** did not give rise to the formation and stability of the active species Mn(V)=O.<sup>5,14</sup> On the other hand, the miscibility/high solubility between **1c**, styrene and solvent played an important role for oxidation efficiency (No. 1–6). The excellent match of **1c** and [BPy][BF<sub>4</sub>] in terms of ionic nature, structural skeleton and miscibility did conquer the limitation of mass transfer, favoring the catalytic activity. The high efficiency of **1c** in [BPy][BF<sub>4</sub>] can also be seen in Table 2. Even when the



**Table 1** Comparison of **1c** and **2b** in IL and organic solvent respectively for oxidation of styrene<sup>a</sup>

No.	Catalyst	Solvent	Axial ligand	Conversion (%)	Selectivity (%)		
					Styrene oxide	Phenylacetaldehyde	Benzaldehyde
1	<b>1c</b> <sup>b</sup>	[BPy][BF <sub>4</sub> ]	—	96	90	10	0
2	<b>1c</b> <sup>b</sup>	[BPy][BF <sub>4</sub> ]	Pyridine	74	80	20	0
3	<b>1c</b> <sup>b</sup>	CH <sub>3</sub> CN <sup>d</sup>	—	91	80	20	0
4	<b>1c</b> <sup>b</sup>	CH <sub>3</sub> CN <sup>d</sup>	Pyridine	71	74	26	0
5	<b>1c</b> <sup>c</sup>	CH <sub>2</sub> Cl <sub>2</sub> <sup>d</sup>	—	16	44	36	20
6	<b>1c</b> <sup>c</sup>	CH <sub>2</sub> Cl <sub>2</sub> <sup>d</sup>	Pyridine	32	70	20	10
7	<b>2b</b> <sup>b</sup>	[BPy][BF <sub>4</sub> ]	—	48	73	27	0
8	<b>2b</b> <sup>b</sup>	[BPy][BF <sub>4</sub> ]	Pyridine	95	69	31	0
9	<b>2b</b> <sup>b</sup>	CH <sub>3</sub> CN <sup>d</sup>	—	97	86	14	0
10	<b>2b</b> <sup>b</sup>	CH <sub>3</sub> CN <sup>d</sup>	Pyridine	98	77	23	0
11	<b>2b</b> <sup>b</sup>	CH <sub>2</sub> Cl <sub>2</sub> <sup>d</sup>	—	26	73	20	7
12	<b>2b</b> <sup>b</sup>	CH <sub>2</sub> Cl <sub>2</sub> <sup>d</sup>	Pyridine	52	84	10	6

<sup>a</sup> Catalyst 0.4 mol% (1.6 μmol); substrate 400 μmol; pyridine 130 μmol; PhIO 600 μmol; solvent 2 mL; reaction temperature 30 °C; reaction time 1 h. <sup>b</sup> Homogeneous reaction system. <sup>c</sup> Inhomogeneous reaction system. <sup>d</sup> CH<sub>3</sub>CN and CH<sub>2</sub>Cl<sub>2</sub> were distilled with CaO before use.

**Table 2** Effect of the concentration of ionic porphyrin **1c** in [BPy][BF<sub>4</sub>] on oxidation of styrene<sup>a</sup>

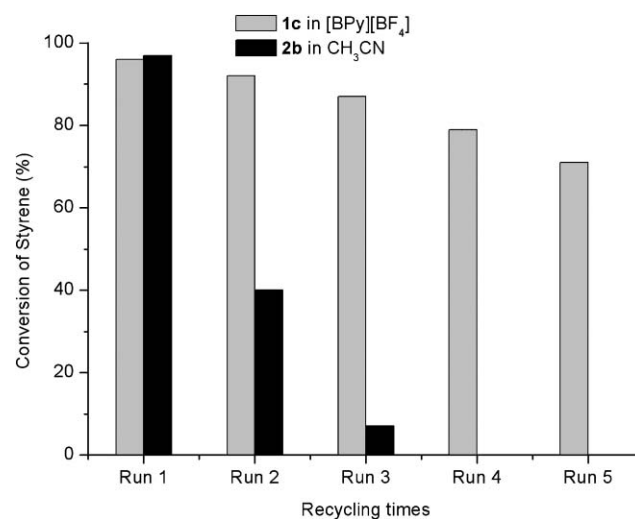
Concentration of <b>1c</b> (mol%) <sup>d</sup>	Conversion of styrene (%) <sup>b</sup>	Turnover Rate/h <sup>-1</sup>	Selectivity (%) <sup>c</sup>		
			Styrene oxide	Benzaldehyde	Phenylacetaldehyde
0.005 (50 ppm)	41	8200	91	0	9
0.025 (250 ppm)	60	2400	90	0	10
0.05 (500 ppm)	88	1760	91	0	9
0.1 (1000 ppm)	95	950	90	0	10
0.4 (4000 ppm)	97	243	90	0	10
0.8	98	123	91	0	9
1.2	97	81	90	0	10

<sup>a</sup> Styrene 400 μmol; PhIO 600 μmol; [BPy][BF<sub>4</sub>] 2 mL; reaction time 1 h; temperature 30 °C. <sup>b</sup> Based on GC analysis with 1-dodecane as an internal standard. <sup>c</sup> Based on GC analysis according to the normalization method. <sup>d</sup> Based on ratio of **1c** to styrene.

concentration of catalyst **1c** was decreased to 0.005 mol%, a styrene conversion of 41% was obtained with turnover rate of 8200 h<sup>-1</sup>. Whereas catalyzed by the conventional neutral Mn porphyrin of **2b**, the effective oxidation of styrene necessarily required the participation of axial ligands (pyridine or CH<sub>3</sub>CN). The catalytic performance was strongly dependent on the selection of axial ligands and solvents.

As shown in Table 1, the catalytic performance of fresh **1c** in [BPy][BF<sub>4</sub>] (Table 1, No. 1) and fresh **2b** in CH<sub>3</sub>CN (Table 1, No. 9) were competitive in terms of activity and selectivity. In order to compare the stability of the **1c**-[BPy][BF<sub>4</sub>] system to the conventional neutral porphyrin **2b** in CH<sub>3</sub>CN, recycling uses of them were carried out (Fig. 1), which presented a great difference in activity and recyclability. In the system **1c**-[BPy][BF<sub>4</sub>], after five runs the conversion of styrene maintained at 71%, the product distribution varied dramatically from original styrene oxide to complete phenyl acet-aldehyde in 5th run (Table 3). The UV-Vis analysis proved that after five recycling uses, **1c** was still present with a characteristic Soret peak at 465 nm, although degradation of **1c** coming from the oxidative destruction of porphyrino ring was also observed. Whereas, for the system **2b**-CH<sub>3</sub>CN, only after three runs did the catalyst **2b** break down completely with total loss of activity and without any appearance of a Soret peak in the UV-Vis profile. Meanwhile, the color of the reaction solution faded from red-purple to light-yellow rapidly, also indicating the complete degradation of the conjugated porphyrino ring.

The results in Table 3 show that during the recycling uses of **1c**-[BPy][BF<sub>4</sub>], the selectivity to styrene oxide and phenyl-acetaldehyde nearly overturned completely in 1st run and 5th run. In order to clarify the derivation of the various oxidized products, the purchased (±)-styrene oxide (Johnson Matthey, 98%) was used to replace styrene in the fresh **1c**-[BPy][BF<sub>4</sub>] system and the used one, respectively (Table 4). It was found that there was not any conversion of (±)-styrene oxide to

**Fig. 1** Comparison of the recycling uses of **1c** in [BPy][BF<sub>4</sub>] (Table 1, No. 1) and **2b** in CH<sub>3</sub>CN (Table 1, No. 9) for the oxidation of styrene.

**Table 3** Recycling uses of **1c**-[BPy][BF<sub>4</sub>] for oxidation of styrene<sup>a</sup>

Run	Conversion (%) <sup>b</sup>	Selectivity (%) <sup>c</sup>		
		Styrene oxide	Phenyl acetaldehyde	Benzaldehyde
1	96	90	10	0
2	92	90	10	0
3	87	60	40	0
4	79	17	82	1
5	71	0	99	1

<sup>a</sup> **1c** 0.4 mol% (1.6 μmol); styrene 400 μmol; [BPy][BF<sub>4</sub>] 2 mL; reaction temperature 30 °C; reaction time 1 h; PhIO (400 μmol), which was added per pass. <sup>b</sup> Based on GC analysis with 1-dodecane as an internal standard. <sup>c</sup> Based on GC analysis according to the normalization method.

**Table 4** The isomerization of purchased (±)-styrene oxide in **1c**-[BPy][BF<sub>4</sub>] system

Catalyst	Conversion of styrene oxide	Percentage of styrene oxide and phenylacetaldehyde (%) <sup>c</sup>	
		Styrene oxide	Phenylacetaldehyde
None	0	98	2
Fresh <b>1c</b> <sup>a</sup>	0	98	2
1st use <b>1c</b> <sup>b</sup>	0	97	3
2nd use <b>1c</b> <sup>b</sup>	0	98	2

<sup>a</sup> **1c** 0.4 mol% (styrene oxide 400 μmol); PhIO 600 μmol; [BPy][BF<sub>4</sub>] 2 mL; reaction temperature 30 °C; reaction time 1 h. <sup>b</sup> The used **1c**-[BPy][BF<sub>4</sub>] was the leftover obtained from the oxidation of styrene after removal of the organic compounds by extraction with diethyl ether. <sup>c</sup> Based on GC analysis.

phenylacetaldehyde in any case, ruling out the possibility of the subsequent isomerization of styrene oxide to phenylacetaldehyde. The formation of phenylacetaldehyde did undergo different reaction routes that could be catalyzed by other active Mn porphyrin species induced from the active Mn(V)-oxo derivative. Supposedly, the formation of phenylacetaldehyde may result from the induced Mn(IV)-oxo intermediate. And the gradual accumulation of this Mn(IV)-oxo species in the recycling uses gave rise to the formation of phenylacetaldehyde. This viewpoint could be supported by the research in ref. 15a, where the mechanism of Mn porphyrin catalyzed-oxidation of alkenes was discussed. It was claimed that the derivation of Mn(V)=O species (coming from **1c** precursor) to different Mn(III, IV, V)-oxo species would lead to epoxide or rearranged products independently. Among which, Mn(IV)-oxo species were targeted to the rearranged product through a radical mechanism, giving rise to an increased amount of aldehyde relative to the oxide.

On the other hand, the influence of water content on the catalytic performance of the **1c**-[BPy][BF<sub>4</sub>] system was investigated in Table 5 (the molar ratio of H<sub>2</sub>O/[BPy][BF<sub>4</sub>] was ca. 0.3–1). It was indicated absolutely that the presence of water in the **1c**-[BPy][BF<sub>4</sub>] system led to decreased activities, which resulted from the sluggish formation of the active Mn(V)=O species with the influence of H<sub>2</sub>O as an axial ligand, but not from the breakdown of porphyrin **1c** by the intervention of H<sub>2</sub>O. Since the reaction time was extended, the excellent conversions could still be obtained as shown in Table 5. Upon the completion of the reaction, the obvious Soret band of **1c** at 465 nm in the presence of water (No. 4, reaction for 3 h) was even stronger than that without water (No. 1, reaction for 1 h), suggesting the surprisingly improved oxidation tolerance for **1c**. Whereas, the hydrolysis of BF<sub>4</sub><sup>−</sup> or PF<sub>6</sub><sup>−</sup> within the **1c**-[BPy][BF<sub>4</sub>] system in the presence of water (possibly leading to the formation of HF, and then the breakdown of porphyrino ring) could not be observed herein, implying the more innocent nature of pyridinium based ILs than that of imidazolium based ILs with a relatively higher reactivity propensity for hydrolysis and hydrogen bond interactions.<sup>16–20</sup>

Hence, it was considered that the gradual degradation of **1c** (accompanied by the loss of the Soret band) was mainly ascribed to oxidation breakdown caused by active oxygen donation from excess PhIO, but with no relation to the influence of water. The decreased catalytic activity of **1c** could be due to the degradation of the porphyrino ring or the sluggish formation of the active Mn(V)=O species. And the derivation of Mn(V)=O species to other Mn(III, IV, V)-oxo species was responsible for the changed selective distribution of the oxygenated products.

Another advantage of the **1c**-[BPy][BF<sub>4</sub>] system was the facile separation of the metalloporphyrin catalyst from the organic products. Upon completion of the reaction, the homogeneous solution was extracted by diethyl ether, leaving behind the light-purple IL phase which could be reused directly for next run. The leaching of Mn into the organic phase was beyond the limit of ICP (inductive coupled plasma emission spectrometer) detection (<0.01 μg g<sup>−1</sup>).

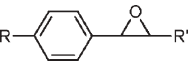
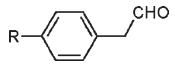
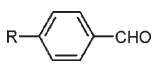
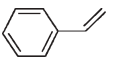
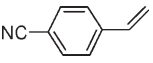
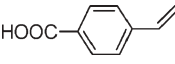
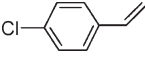
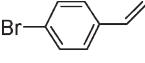
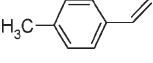
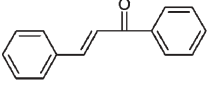
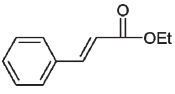
These obtained results suggest that the deactivation of **1c**-[BPy][BF<sub>4</sub>] resulted from the destruction (self-aggregation and oxidation degradation) of the metalloporphyrin being suppressed dramatically as we expected through entailing the neutral Mn porphyrin with the pyridinium tag and the PF<sub>6</sub><sup>−</sup> anion. Due to the common ionic nature, the similar conjugated features, and the repulsive force between the positive charges or the negative charges, the π–π interaction between **1c** and

**Table 5** The influence of water on the catalytic performance of the **1c**-[BPy][BF<sub>4</sub>] system for oxidation of styrene<sup>a</sup>

No.	Solvent	Conversion (%)	Selectivity (%)	
			Styrene oxide	Phenylacetaldehyde
1	[BPy][BF <sub>4</sub> ]	95	90	10
2	[BPy][BF <sub>4</sub> ] + 5 mmol H <sub>2</sub> O	85	93	7
3	[BPy][BF <sub>4</sub> ] + 10 mmol H <sub>2</sub> O	76	91	9
4	[BPy][BF <sub>4</sub> ] + 15 mmol H <sub>2</sub> O	70 (95, 3 h) <sup>b</sup>	92 (81, 3 h) <sup>b</sup>	8 (19, 3 h) <sup>b</sup>

<sup>a</sup> **1c** 0.4 mol% (substrate 400 μmol); PhIO 600 μmol; [BPy][BF<sub>4</sub>] 2 mL; reaction temperature 30 °C; reaction time 1 h. <sup>b</sup> Conversion and selectivity obtained at extended time (3 h) is indicated in parentheses.

**Table 6** Oxidation of styrene and its derivatives catalyzed by **1c**-[BPyl][BF<sub>4</sub>]<sup>a</sup>

No.	Catalyst	Conversion (%) <sup>b</sup>	Selectivity (%) <sup>c</sup>		
					
1		96 (1 h) <sup>d</sup>	90	10	0
2		97 (3 h) <sup>d</sup>	100	0	0
3		98 (3 h) <sup>d</sup>	100	0	0
4		95 (4 h) <sup>d</sup>	57	35	9
5		91 (4 h) <sup>d</sup>	65	29	6
6		91 (2 h) <sup>d</sup>	57	40	4
7		96 (4 h) <sup>d</sup>	100	0	0
8		71 (4 h) <sup>d</sup>	100	0	0

<sup>a</sup> **1c** 1.6 μmol (0.4 mol%); substrate 400 μmol; PhIO 600 μmol; pyridine 130 μmol; [BPyl][BF<sub>4</sub>] 2 mL; reaction temperature 30 °C. <sup>b</sup> Based on GC analysis with 1-dodecane as an internal standard. <sup>c</sup> Based on GC analysis according to the normalization method. <sup>d</sup> Reaction time is indicated in parentheses.

[BPyl][BF<sub>4</sub>] counteracted the  $\pi$ - $\pi$  stacking of the porphyrin itself, which favored the stability and dispersion of **1c** in [BPyl][BF<sub>4</sub>]. On the other hand, the pyridinium cations in **1c** made the electron density at the *meso*-carbons decrease, able to improve the oxidation tolerance of the metalloporphyrin.<sup>5</sup> Meanwhile [BPyl][BF<sub>4</sub>] not only acted as the ideal solvent for **1c** and the conjugated substrates, but also played the role of axial ligand to **1c** like pyridine derivative, favoring stability and activation of the active oxomanganese(v) porphyrin species.<sup>5,15</sup>

The generality of **1c**-[BPyl][BF<sub>4</sub>] to the substrates was demonstrated in Table 6, in which a wide array of styrene derivatives with different electronic and steric effects was selected. With the electron-withdrawing group in the *para*-position of styrene, the selectivities for the oxides were remarkable (100%). If the substituting groups possess an electron-donor nature (-Cl, -Br, -CH<sub>3</sub>), the increased electron density at the  $\alpha$ -C of styrene could easily lead to the subsequent oxidation of benzaldehyde through the bond cleavage at  $\alpha$ -C and  $\beta$ -C of styrene. While for the substrates (entry 8, 9) with internal C=C bonds, epoxides were the only products, implicating the facile access of the substrate to the oxomanganese (v) porphyrin domain.<sup>13</sup> For the olefins with saturated alkyl groups, such as 1-hexene, 1-chloropropene, cyclohexene *etc.*, poor conversions were observed because of the severe mass transfer limitation, mainly ascribed to the immiscibility of such substrates with the conjugated catalytic system of **1c**-[BPyl][BF<sub>4</sub>].

## Conclusions

In summary, the ionic Mn porphyrin **1c** embedded in the ambient IL of [BPyl][BF<sub>4</sub>] has been developed as an efficient and recyclable catalytic system for the oxidation of styrene and its derivatives compared to the conventional neutral **2b**. The good activity and the improved stability of **1c** in [BPyl][BF<sub>4</sub>] were dependent on a number of factors that included the dual roles of [BPyl][BF<sub>4</sub>] as the axial ligand and the solvent, the decreased electron density at the *meso*-carbon of porphyrin **1c**, and the suppressed  $\pi$ - $\pi$  stacking of the porphyrin itself due to the ionic nature and the similar conjugated feature between **1c** and [BPyl][BF<sub>4</sub>].<sup>†</sup>

## Acknowledgements

The National Natural Science Foundation of China (No. 20673039, 20533010, 20590366) and the Science & Technology Commission of Shanghai Municipality (No. 06JC14023) are gratefully acknowledged for financial support.

<sup>†</sup> [BPyl][BF<sub>4</sub>] was prepared according to standard procedures by metathesis of [BPyl]Cl with NaBF<sub>4</sub> in CH<sub>3</sub>CN, followed by filtration, removal of the solvent on a rotatory evaporator, and extraction by CH<sub>2</sub>Cl<sub>2</sub>. The obtained solution was then treated with active carbon and a 5 Å molecular sieve respectively, yielding a viscous liquid after finally drying in high vacuum.

## References

- 1 B. Meunier, *Chem. Rev.*, 1992, **92**, 1411.
- 2 D. Mansuy and P. Bottioni, *Cytochrome P450 Model Systems in Metalloporphyrins in Catalytic Oxidations*, ed. R. A. Sheldon, Marcel Dekker, New York, 1994, p. 99.
- 3 T. Lai, F. Chan, P. So, D. Ma, K. Wong and C. Che, *Dalton Trans.*, 2006, **40**, 4845.
- 4 K. A. Srinivas, A. Kumar and S. M. S. Chauhan, *Chem. Commun.*, 2002, 2456.
- 5 E. Rose, B. Andrioletti, S. Zrig and M. Quelquejeu-Ethève, *Chem. Soc. Rev.*, 2005, **34**, 573.
- 6 F. Bedioui, *Coord. Chem. Rev.*, 1995, **144**, 39.
- 7 C. Gilmartin and J. R. L. Smith, *J. Chem. Soc., Perkin Trans. 2*, 1995, 243.
- 8 (a) J. Zhang and C. Che, *Org. Lett.*, 2002, **4**, 1911; (b) C. Liu, W. Yu, S. Li and C. Che, *J. Org. Chem.*, 1998, **63**, 7364.
- 9 F. Alonso, I. P. Beletskaya and M. Yus, *Tetrahedron*, 2005, **61**, 11771.
- 10 J. Dupont, R. F. de Souza and P. A. Z. Suarez, *Chem. Rev.*, 2002, **102**, 3667.
- 11 (a) C. Vallée, Y. Chauvin, J.-M. Basset, C. C. Santini and J.-C. Galland, *Adv. Synth. Catal.*, 2005, **347**, 1835; (b) C. Yang, H. M. Lee and S. P. Nolan, *Org. Lett.*, 2001, **3**, 1511; (c) F. Favre, H. Olivier-Bourbigou, D. Commereuc and L. Saussine, *Chem. Commun.*, 2001, 1360.
- 12 (a) S. B. Park and H. Alper, *Org. Lett.*, 2003, **5**, 3209; (b) J.-C. Xiao, B. Twamley and J. M. Shreeve, *Org. Lett.*, 2004, **6**, 3845; (c) P. Wasserscheid, C. M. Gordon, C. Hilgers, M. J. Muldoon and I. R. Dunkin, *Chem. Commun.*, 2001, 1186.
- 13 D. Behar, P. Neta and S. Carl, *J. Phys. Chem. A*, 2002, **106**, 3139.
- 14 C. G. Oliveri, N. C. Gianneschi, S. T. Nguyen, C. A. Mirkin, C. L. Stem and M. Pink, *J. Am. Chem. Soc.*, 2006, **128**, 16286.
- 15 (a) R. D. Arasasingham, G. X. He and T. C. Bruice, *J. Am. Chem. Soc.*, 1993, **115**, 7985; (b) J. T. Groves and M. K. Stem, *J. Am. Chem. Soc.*, 1988, **110**, 8628.
- 16 R. P. Swatloski, J. D. Holbrey and R. D. Rogers, *Green Chem.*, 2005, **5**, 361.
- 17 G. A. Baker and S. N. Baker, *Aust. J. Chem.*, 2005, **58**, 174.
- 18 S. Chowdhury, R. S. Mohan and J. L. Scott, *Tetrahedron*, 2007, **63**, 2363.
- 19 K. Dong, S. Zhang, D. Wang and X. Yao, *J. Phys. Chem. A*, 2006, **110**, 9775.
- 20 E. A. Turner, C. C. Pye and R. D. Singer, *J. Phys. Chem. A*, 2003, **107**, 2277.

## Textbooks from the RSC

The RSC publishes a wide selection of textbooks for chemical science students. From the bestselling *Crime Scene to Court*, 2nd edition to groundbreaking books such as *Nanochemistry: A Chemical Approach to Nanomaterials*, to primers on individual topics from our successful *Tutorial Chemistry Texts* series, we can cater for all of your study needs.

Find out more at [www.rsc.org/books](http://www.rsc.org/books)

Lecturers can request inspection copies – please contact [sales@rsc.org](mailto:sales@rsc.org) for further information.



Registered Charity No. 207890

RSCPublishing

[www.rsc.org/books](http://www.rsc.org/books)



# A facile approach towards enantiomerically pure masked $\beta$ -amino alcohols†

Pankaj Gupta, Bhahwal Ali Shah, Rajinder Parshad, Ghulam Nabi Qazi and Subhash Chandra Taneja\*

Received 25th January 2007, Accepted 30th May 2007

First published as an Advance Article on the web 20th June 2007

DOI: 10.1039/b701192j

$\beta$ -Amino alcohols are bioactive molecules, used also as catalysts in asymmetric C–C bond formation. While asymmetric synthesis has been the preferred route for their preparation, there was always been a need to develop a facile methodology involving environmentally friendly transformations. Masked amines in the form of phthalimide alcohols, prepared *via* a fast coupling reaction in an ionic liquid as a reusable reaction media together with reduction and an efficient biocatalytic resolution, offer a green methodology for enantiomerically pure products (ee > 99%, 50 g L<sup>-1</sup>).

The  $\beta$ -amino alcohol structural motif is found in a wide variety of biologically active alkaloids and peptides.<sup>1</sup> They have recently been used as intermediates for the synthesis of 1-phenyl-2-[(2-phenyl-1-alkylethyl)amino] ethanol derivatives **1**, a new and important class of anti-diabetic agent<sup>2</sup> and (*R*)-denopamine **2** (Fig. 1), a potent orally active  $\beta$ 1 receptor agonist used in the treatment of heart failure.<sup>3</sup> The catalytic use of chiral  $\beta$ -amino alcohols during the addition of dialkylzinc to prochiral aldehydes<sup>4</sup> and in the Henry reaction<sup>5</sup> provided an efficient procedure for asymmetric C–C bond construction. Their importance is also well recognized in asymmetric catalysis as many chiral auxiliaries and ligands comprise this vital subunit.<sup>6</sup> Consequently, construction of the  $\beta$ -amino alcohol structural motif has been an important target for organic chemists.<sup>7,8</sup>

The asymmetric hydrogenation of prochiral amino ketones is regarded as one of the important methods for the preparation of chiral amino alcohols. For example Lei *et al.* recently used ruthenium complexes as efficient catalysts for the asymmetric hydrogenation of amino ketones.<sup>8a</sup> They reported enantioselective hydrogenation of  $\alpha$ -phthalimido ketones to corresponding masked primary amino alcohols of general formula as given in Fig. 2.

An alternative route to optically active  $\beta$ -amino alcohols involved ring opening of racemic terminal epoxides catalysed by chiral complexes.<sup>9</sup> However, due to the use of metal

complexes at elevated temperature during asymmetric catalytic hydrogenations,<sup>8</sup> there was always a need to develop alternative synthetic methods in combination with biocatalytic transformations, thus providing a more environment friendly route to their preparation. The importance of biocatalytic methods for the preparation of optically active compounds is now well recognized.<sup>10,11</sup> In the present study, we envisaged developing a green and facile chemo-enzymatic route for the preparation of biologically important chiral masked amino alcohols of general chemical structure as shown in Fig. 2 with high enantiopurity from a readily synthesizable racemic precursor. The strategy involved the development of a highly efficient method of preparation of masked amines through the formation of *N*-phthalimide derivatives, as free amino functions generally cause inhibition of lipases.

Additional advantages of tagging a phthalimide subunit are the facilitation of their separation and detection by liquid chromatography during the course of enzymatic hydrolysis, miscibility with organic solvents of medium polarity and easy maneuvering of the free hydroxy group. Our attempts were initiated with the preparation of  $\alpha$ -phthalimido ketones *via* coupling of  $\alpha$ -bromo ketones and potassium phthalimide in DMF by a reported method.<sup>8a</sup> However, the preparation required longer duration (~12 h) and in our hands the final yield varied between 70–85%. Therefore, the strategy envisaged firstly developing a highly efficient method of preparation of  $\alpha$ -phthalimido ketones. The improved methodology involved the coupling of bromoketones with potassium phthalimide in an ionic liquid [1-butyl-3-methylimidazolium tetrafluoroborate]. In this method the coupling reaction was completed within 10–15 min of stirring at room temperature (Scheme 1), the product **2** was easily extracted in THF in almost quantitative yield, and the ionic liquid could be reused (5 times without loss of activity) for the reaction. The coupling reaction thus demonstrated the importance of ionic liquids as reusable and

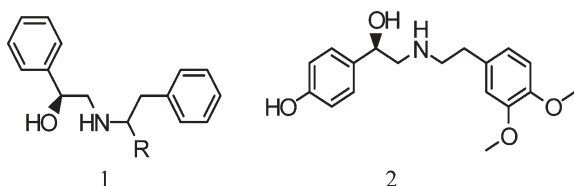


Fig. 1 1-Phenyl-2-[(2-phenyl-1-alkylethyl)amino] ethanol derivatives **1** and (*R*)-denopamine **2**.

Indian Institute of Integrative Medicine (CSIR), Canal Road, Jammu Tawi, 180001, India. E-mail: sc\_taneja@yahoo.co.in; Fax: +91 191 2569017/2569333; Tel: +91 191 2569000-06

† Electronic supplementary information (ESI) available: Spectra of novel compounds and HPLC profiles of all the resolved compounds. See DOI: 10.1039/b701192j

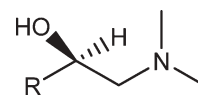
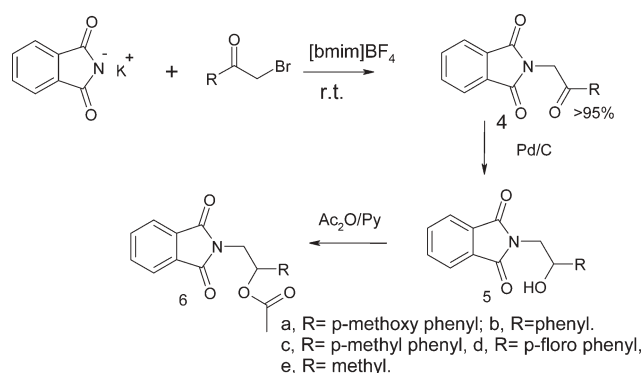


Fig. 2 General formula of masked primary amino alcohols.



**Scheme 1** Synthesis of racemic substrates.

green reaction media for fast chemical transformations at room temperature.<sup>12</sup>

Sodium borohydride reduction of phthalimide ketones in the next step failed to give the desired racemic secondary alcohols due to the hydride attack on the phthaloyl moiety and formation of major side products.<sup>13</sup> However, Pd/C catalysed hydrogenation at room temperature in a suitable solvent or NaCNBH<sub>3</sub> reduction was highly successful. The results of hydrogenation/reduction reactions are shown in Table 1.

In the final step, for the kinetic resolution and preparation of target molecules, enantioselective hydrolysis of racemic  $\alpha$ -phthalimide acetates (**6a–6e**) was carried out with a panel of microorganisms bearing lipases belonging to institute repositories as well as those procured from commercial sources (Table 2, Scheme 2).

The kinetic resolution reactions of **6a** and **6b** were carried out in an aqueous phosphate buffer (0.1 M, pH 7.0), however, the rate of hydrolysis was found to be very slow and enantioselectivity also poor (Table 2).

Therefore, to improve the rate of hydrolysis as well as enantioselectivity, the use of co-solvents was envisaged as a practical option. A biphasic system, using an organic solvent proved to be highly advantageous. Both nonpolar as well as polar solvents in the ratio ranging from 5–30% (v/v) in buffer were used and finally toluene (10% v/v) was found to be the co-solvent of choice as depicted in Table 3. It is evident from these results that addition of only 10% toluene with respect to buffer

**Table 1** Reaction conditions for hydrogenation of  $\alpha$ -phthalimide ketones

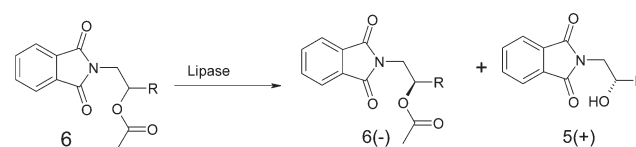
R	Reagent	Solvent	Time/h	Yield <sup>a</sup> (%)
<b>4a</b> (4-OMe-Ph)	Pd/C, 10%	EtOAc	48	0
<b>4a</b> (4-OMe-Ph)	Pd/C, 10%	Ethanol	48	90
<b>4b</b> (Ph)	Pd/C, 10%	EtOAc	6	95
<b>4c</b> (4-Me-Ph)	Pd/C, 10%	Ethanol	40	85
<b>4d</b> (4-F-Ph)	Pd/C, 10%	Ethanol	120	60
<b>4e</b> (Me)	Pd/C, 10%	Ethanol	48	0
<b>4e</b> (Me)	NaCNBH <sub>3</sub>	MeOH	48	85

<sup>a</sup> Isolated yields.

**Table 2** Enzymatic hydrolysis of  $\alpha$ -phthalimide acetates, i.e., ( $\pm$ )-**6a** and ( $\pm$ )-**6b** at 5 gm L<sup>-1</sup> concentration at 25 °C<sup>a</sup>

Sub.	Enzyme	Conv. (%)	Time/h	ee <sub>p</sub> (%)	ee <sub>s</sub> (%)
<b>6a</b>	CCL	34.6	120	8	4.9
<b>6a</b>	MM	38.8	120	0.5	0.4
<b>6a</b>	CRL	ND	120	—	—
<b>6a</b>	CAL	ND	120	—	—
<b>6a</b>	PSL	ND	120	—	—
<b>6a</b>	AS	41.6	48	1.9	0.3
<b>6a</b>	ABL	29.4	24	3.4	3.6
<b>6b</b>	Lipase M	35.1	120	3.8	0.3
<b>6b</b>	PSL	ND	120	—	—
<b>6b</b>	AA	17.8	46	38.2	9.2
<b>6b</b>	AS	2.7	46	25.9	1.3
<b>6b</b>	MM	ND	120	—	—
<b>6b</b>	ABL	46.5	16	8.6	9.2
<b>6b</b>	CCL	24.3	46	13.5	0.9
<b>6b</b>	PSC-II	ND	46	—	—

<sup>a</sup> CCL: *Candida cylindrica* lipase; MM: *Mucor miehei*; CRL: *Candida rugosa* lipase; CAL: *Candida antarctica* lipase; PSL: *Pseudomonas cepacia* Lipase; PSC-II: *Pseudomonas cepacia* lipase on ceramics; ABL: *Arthrobacter sp.* Lipase; Lipase M: *Mucor javanicus*; AA: Amano acylase; AS: Lipase from *Aspergillus niger*; ND = not detected.



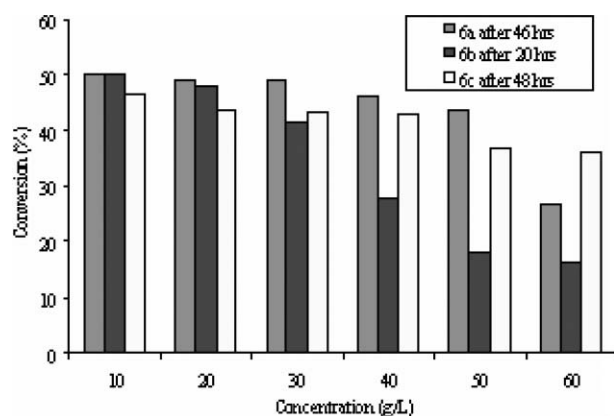
**Scheme 2** Enzymatic hydrolysis of  $\alpha$ -phthalimide acetates.

had a dramatic effect both in terms of rate of hydrolysis and enantioselectivity. Here, a native strain *Arthrobacter sp.* Lipase<sup>14</sup> designated as ABL (MTCC no. 5125) has been identified for its excellent performance in the kinetic resolutions of **6a**, **6b**, **6c** and **6d** (*E* values 1059, 1059, 563 and 1059 respectively). In order to optimize the time space yield, the kinetic resolution reactions were carried out at varied concentrations ranging from 5–60 g L<sup>-1</sup>. It was found that ABL was quite active up to 50 g L<sup>-1</sup>. Selecting *N*-(2-acetoxy-2-phenyl)ethylphthalimide **6b** as a model, the time space yield calculation showed that a concentration of 30 g L<sup>-1</sup> was the optimum. It was also observed that enantiomeric excess remains unchanged i.e. > 99% in the conc. range up to 50 g L<sup>-1</sup>, however, as expected, the rate of hydrolysis decreased with higher concentrations as shown in Fig. 3. For the hydrolysis of **6e**, *Pseudomonas cepacia* lipase-II (Amano) has been found to be the best biocatalyst (*E* = 296) as depicted in Table 3. The advantage of obtaining both the alcohol and the ester mostly with high enantiopurity, can be utilized to convert any one of the products into a single enantiomer by the Mitsunobu inversion.<sup>15</sup> Thus, alcohol (+)-**5** can be *in situ* converted to (-)-**6** via the above reaction while retaining enantiopurity. The enantiomeric excess (ee%) was measured by chiral HPLC on (*R,R*)-Whelk-01 and OD chiral columns using hexane/isopropyl alcohol in the ratio 95 : 5. The enantiomerically pure masked 1,2-amino alcohols thus obtained can easily be converted to 1,2-amino alcohols by the methods (e.g. Ing–Manske Reaction) reported in the literature.<sup>8a,16</sup>

**Table 3** Enzymatic hydrolysis of  $\alpha$ -phthalimide acetates (**6a–6e**) at 5 g L<sup>-1</sup> concentration in biphasic systems<sup>a</sup>

Sub.	Lipase	Co-solvent	Con. (%)	Time/h	<i>E</i>	ee <sub>p</sub> (%)	ee <sub>s</sub> (%)
6a	ABL	Nil	29.4	24	1.1	3.4	3.6
6a	ABL	DIE	10.8	24	3.3	52	5.6
6a	ABL	THF	5.8	24	122	>99	10.6
6a	ABL	Toluene	50.0	24	1059	>99	>99
6b	ABL	Nil	46.5	16	1.3	8.6	9.2
6b	ABL	THF	50.0	16	1059	>99	>99
6b	ABL	DMF	50.0	19	1059	>99	>99
6b	ABL	Dioxan	38.6	30	72	95	57
6b	ABL	Toluene	50.0	16	1059	>99	>99
6b	ABL	DCM	38.8	11	11	74.7	29.5
6b	ABL	DIE	51.0	30	203	95	80
6b	ABL	CCl <sub>4</sub>	30.0	16	28	90	34.7
6b	AAL	Nil	17.8	46	2.4	38.2	9.2
6b	AAL	Acetone	10.8	24	2.1	33.3	8.4
6b	AAL	DMF	11.0	24	2.9	47.7	9.5
6b	AAL	Dioxan	10.0	36	2.5	40	9.3
6b	AAL	Toluene	13.0	24	14.4	84.7	11.1
6c	ABL	Nil	ND	34	—	—	—
6c	ABL	THF	ND	34	—	—	—
6c	ABL	Toluene	35.8	34	346	>99	56
6c	ABL	Benzene	25.3	26	279	>99	33.9
6c	ABL	DIE	2.5	34	51	>99	2.5
6c	ABL	Acetone	ND	26	—	—	—
6c	ABL	DMF	2.0	26	406	99	2.2
6c	ABL	DCM	ND	26	—	—	—
6c	ABL	Toluene	46.5	47	563	>99	90
6c	ABL	Toluene	46.5	60	563	>99	90
6d	ABL	Toluene	50.0	50	1059	>99	>99
6e	ABL	Nil	21.1	3	2.1	31.7	8.5
6e	ABL	Toluene	24.2	3	5.2	62	19.7
6e	ABL	DMF	13.8	3	2.2	34.7	5.5
6e	ABL	DIE	11.0	3	5.8	68.8	8.1
6e	PSC-II	Toluene	29.6	120	296	>99	42
6e	PSC-II	Toluene	40.0	192	68.4	94.5	63
6e	PSC-II	CH <sub>3</sub> CN	5.0	120	105	>99	5.2
6e	PSL	Toluene	30.0	120	22.6	88	23.4

<sup>a</sup> Experimental conditions: All the reactions were performed at 25 °C on a shaker at 320 rpm. ee % was measured by chiral HPLC.



**Fig. 3** Concentration vs. conversion of **6a**, **6b** and **6c** in toluene/buffer using *Arthrobacter sp.* lipase.

## Conclusions

In conclusion, an efficient and green methodology for the preparation of racemic masked  $\beta$ -amino alcohols and their kinetic resolution through lipase catalyzed hydrolysis in the

presence of co-solvents with high enantiomeric purities of the products has been demonstrated.

## Experimental

### Experimental part

<sup>1</sup>H NMR spectra in CDCl<sub>3</sub> were recorded on Bruker 200 MHz spectrometers with TMS as the internal standard. Chemical shifts were expressed in parts per million ( $\delta$  ppm). Reagents and solvents used were mostly LR grade. Silica gel coated aluminium plates coated on alumina from M/s Merck were used for TLC. MS were recorded on a Jeol MSD-300 and Bruker Esquire 3000 LC-mass spectrometer. IR was recorded on a FT-IR Bruker (270–30) spectrophotometer. Optical rotations were measured on Perkin-Elmer 241 polarimeter at 25 °C using sodium D light. Enantiomeric excess (ee) was determined by chiral HPLC on (*R,R*)-Whelk-01 and OD chiral columns. Potassium phthalimide and acetophenone derivatives were purchased from M/s Aldrich Chemicals, Mumbai.  $\alpha$ -Bromo ketones were prepared according to the procedures reported previously.<sup>17</sup>

### Synthesis of $\alpha$ -phthalimide ketones (**4a**, **4b**, **4c**, **4d** and **4e**)

A mixture of potassium phthalimide (1.1 mmol) and bromo ketone (1 mmol) in a 10 mL conical flask, was added to 1 mL ionic liquid [1-butyl-3-methylimidazolium tetrafluoroborate] and the contents were stirred at room temperature for 10–15 minutes. The reaction mixture was extracted from the ionic liquid phase with THF (2  $\times$  5 mL). The organic layer was concentrated and evaporated under reduced pressure. The residue was purified by column chromatography to obtain the corresponding product. The ionic liquid left in the flask was further washed with ethylacetate, dried under vacuum and reused in four to five subsequent reactions without loss in activity.

#### *N*-(4'-methoxybenzoyl)methylphthalimide (**4a**)

IR (KBr) cm<sup>-1</sup>: 1420, 1600, 1716, 1773. <sup>1</sup>H NMR:  $\delta$  3.90 (s, 3H, *OMe*), 5.08 (s, 2H, *CH*<sub>2</sub>), 6.97 (d, *J* = 8.9 Hz, 2H, *ArH*), 7.76–7.78 (m, 2H, *ArH*), 7.86–7.93 (m, 2H, *ArH*), 7.99 (d, *J* = 8.9 Hz, 2H, *ArH*). <sup>13</sup>C NMR:  $\delta$  42.9, 54.6, 113.1, 120.3, 125.5, 128.0, 132.7, 133.1, 163.8, 187.2. ESI-MS (*m/z*): 295.

#### *N*-benzoylmethylphthalimide (**4b**)

IR (KBr) cm<sup>-1</sup>: 1419, 1914, 1962. <sup>1</sup>H NMR:  $\delta$  5.14 (s, 2H, *CH*<sub>2</sub>), 7.51–7.56 (m, 3H, *ArH*), 7.74–7.78 (m, 2H, *ArH*), 7.91–7.93 (m, 2H, *ArH*), 8.00 (d, *J* = 7.1 Hz, 2H, *ArH*). <sup>13</sup>C NMR:  $\delta$  44.3, 123.6, 127.9, 128.2, 132.1, 133.9, 134.1, 134.5, 167.1, 191.1. ESI-MS (*m/z*): 265.

#### *N*-(4'-methylbenzoyl)methylphthalimide (**4c**)

IR (KBr) cm<sup>-1</sup>: 1416, 1689, 1725, 1775. <sup>1</sup>H NMR:  $\delta$  2.44 (s, 3H, *CH*<sub>3</sub>), 5.11 (s, 2H, *CH*<sub>2</sub>), 7.26–7.33 (m, 2H, *ArH*), 7.74–7.79 (m, 2H, *ArH*), 7.86–7.93 (m, 4H, *ArH*). <sup>13</sup>C NMR:  $\delta$  20.8, 43.1, 123.5, 125.7, 128.2, 133.2, 134.1, 134.6, 145.0, 167.9, 187.4. ESI-MS (*m/z*): 279.

***N*-(4'-fluorobenzoyl)methylphthalimide (4d)**

IR (KBr)  $\text{cm}^{-1}$ : 1419, 1510, 1692, 1716, 1775, 2945.  $^1\text{H}$  NMR:  $\delta$  5.04 (s, 2H,  $\text{CH}_2$ ), 7.16–7.26 (m, 2H,  $\text{ArH}$ ), 7.74–7.78 (m, 2H,  $\text{ArH}$ ), 7.87–7.93 (m, 2H,  $\text{ArH}$ ), 8.02–8.09 (m, 2H,  $\text{ArH}$ ).  $^{13}\text{C}$  NMR:  $\delta$  44.4, 116.3, 116.5, 116.7, 124.0, 131.2, 132.6, 134.6, 168.2, 189.9. ESI-MS ( $m/z$ ): 283.

***N*-(2-oxopropyl)phthalimide (4e)**

IR (KBr)  $\text{cm}^{-1}$ : 1415, 1467, 1726, 1773, 2940, 3064.  $^1\text{H}$  NMR:  $\delta$  2.27 (s, 3H,  $\text{CH}_3$ ), 4.50 (s, 2H,  $\text{CH}_2$ ), 7.72–7.78 (m, 2H,  $\text{ArH}$ ), 7.84–7.90 (m, 2H,  $\text{ArH}$ ).  $^{13}\text{C}$  NMR:  $\delta$  27.5, 47.7, 123.6, 132.5, 134.2, 168.0, 203.7. ESI-MS ( $m/z$ ): 203.

**General procedure for the hydrogenation of protected amino ketones (4a, 4b, 4c and 4d)**

Hydrogen gas was purged thoroughly in a solution of  $\alpha$ -phthalimide ketones (1 mmol) and Pd/C (10%) (in catalytic amount) in anhydrous ethanol (10 mL). The final hydrogen pressure was adjusted to 40–70 psi and the reaction mixture was shaken at room temperature. After a certain time the hydrogen pressure was released and the solvent was removed after filtration to obtain the product, which was purified through a silica gel column.

**NaCNBH<sub>3</sub> reduction of 4e**

In a solution of **4e** (2 mmol, 406 mg) in methanol, NaCNBH<sub>3</sub> (5 mmol, 315 mg) was added at 0 °C, and then a trace of Bromocresol green was also added to monitor the reaction. The solution immediately turned to blue and 3N HCl in methanol was added dropwise to restore the yellow color, the solution was stirred for 24 h, the contents were concentrated under reduced pressure and the residue was extracted with diethyl ether. The combined extracts were dried over anhydrous sodium sulfate and concentrated under reduced pressure. The mixture was separated by column chromatography on silica gel to obtain the product **5e** (348 mg, 85%).

***N*-(2-hydroxy-2-(4'-methoxyphenyl)ethyl)phthalimide (5a)**

IR (KBr)  $\text{cm}^{-1}$ : 1462, 1514, 1692, 2923, 3445.  $^1\text{H}$  NMR:  $\delta$  2.84 (brs, 1H, OH), 3.83 (s, 3H, OMe), 3.88–4.10 (m, 2H,  $\text{CH}_2$ ), 5.02–5.10 (m, 1H, CH), 6.90–6.95 (m, 2H,  $\text{ArH}$ ), 7.39–7.43 (m, 2H,  $\text{ArH}$ ), 7.74–7.78 (m, 2H,  $\text{ArH}$ ), 7.86–7.96 (m, 2H,  $\text{ArH}$ ).  $^{13}\text{C}$  NMR:  $\delta$  45.7, 55.3, 72.1, 114.1, 122.6, 127.2, 131.2, 133.3, 134.2, 159.5, 168.8. ESI-MS ( $m/z$ ): 297

***N*-(2-hydroxy-2-phenyl)ethylphthalimide (5b)**

IR (KBr)  $\text{cm}^{-1}$ : 1420, 1457, 1695, 1768, 2899, 3460.  $^1\text{H}$  NMR:  $\delta$  3.88–4.02 (m, 2H,  $\text{CH}_2$ ), 5.01 (dd,  $J$  = 4.2 Hz, 3.3 Hz, 1H, CH), 7.1–7.3 (m, 5H,  $\text{ArH}$ ), 7.73–7.77 (m, 2H,  $\text{ArH}$ ), 7.84–7.86 (m, 2H,  $\text{ArH}$ ).  $^{13}\text{C}$  NMR:  $\delta$  45.8, 72.6, 123.4, 123.5, 125.9, 127.8, 128.5, 128.9, 131.9, 134.0, 134.1, 141.1, 168.8. ESI-MS ( $m/z$ ): 267.

***N*-(2-hydroxy-2-(4'-methylphenyl)ethyl)phthalimide (5c)**

IR (KBr)  $\text{cm}^{-1}$ : 1420, 1605, 1690, 1716, 1775, 2920, 3476.  $^1\text{H}$  NMR:  $\delta$  2.39 (s, 3H,  $\text{CH}_3$ ), 2.85 (brs, 1H, OH), 3.98 (m, 2H,

$\text{CH}_2$ ), 5.05 (m, 1H, CH), 7.02 (d,  $J$  = 8 Hz, 2H,  $\text{ArH}$ ), 7.42 (d,  $J$  = 8 Hz, 2H,  $\text{ArH}$ ), 7.75–7.82 (m, 2H,  $\text{ArH}$ ), 7.84–7.93 (m, 2H,  $\text{ArH}$ ).  $^{13}\text{C}$  NMR:  $\delta$  21.2, 45.4, 72.3, 123.3, 125.9, 129.3, 131.9, 134.1, 137.9, 138.2, 168.8. ESI-MS ( $m/z$ ): 281.

***N*-(2-hydroxy-2-(4'-fluorophenyl)ethyl)phthalimide (5d)**

IR (KBr)  $\text{cm}^{-1}$ : 1510, 1609, 1692, 1709, 2930, 3420.  $^1\text{H}$  NMR:  $\delta$  3.03 (brs, 1H, OH), 3.94–3.99 (m, 2H,  $\text{CH}_2$ ), 5.04–5.07 (m, 1H, CH), 7.04 (t,  $J$  = 8.7 Hz, 2H,  $\text{ArH}$ ), 7.39–7.46 (m, 2H,  $\text{ArH}$ ), 7.71–7.76 (m, 2H,  $\text{ArH}$ ), 7.81–7.88 (m, 2H,  $\text{ArH}$ ).  $^{13}\text{C}$  NMR:  $\delta$  44.6, 71.0, 114.3, 114.7, 119.5, 125.5, 126.5, 129.9, 133.2, 135.0, 165.0. ESI-MS ( $m/z$ ): 285.

***N*-(2-hydroxy)-propylphthalimide (5e)**

IR (KBr)  $\text{cm}^{-1}$ : 1424, 1611, 1718, 1767, 2928, 2964, 3422, 3484.  $^1\text{H}$  NMR:  $\delta$  1.25 (d,  $J$  = 6.4 Hz, 3H,  $\text{CH}_3$ ), 3.74–3.78 (m, 2H,  $\text{CH}_2$ ), 4.15 (m, 1H, CH), 7.72–7.78 (m, 2H,  $\text{ArH}$ ), 7.83–7.89 (m, 2H,  $\text{ArH}$ ).  $^{13}\text{C}$  NMR:  $\delta$  20.3, 44.9, 65.7, 122.4, 130.5, 132.4, 168.0. ESI-MS ( $m/z$ ): 205

**Acylation of protected amino alcohols (5a, 5b, 5c, 5d and 5e)**

Acetic anhydride (1.2 mmol) and a catalytic amount of DMAP were added to a solution of racemic protected amino alcohols (1 mmol) in dry dichloromethane and the reaction mixture kept overnight at room temperature. The contents of the reaction mixture were poured into ice-cold water and extracted with dichloromethane. The organic layer was washed, dried and evaporated to get protected amino acetoxy derivatives in quantitative yield.

***N*-(2-acetoxy-2-(4'-methoxyphenyl)ethyl)phthalimide (6a)**

IR (KBr)  $\text{cm}^{-1}$ : 1424, 1515, 1613, 1716, 1738, 1774, 3444.  $^1\text{H}$  NMR:  $\delta$  2.05 (s, 3H,  $\text{CH}_3\text{CO}$ ), 3.83 (s, 3H, OMe), 3.94 (dd,  $J$  = 4 Hz, 10.2 Hz, 1H, CH), 4.2 (dd,  $J$  = 5.2 Hz, 8.9 Hz, 1H, CH), 6.15 (dd,  $J$  = 3.9 Hz, 5.0 Hz, 1H, CH), 6.96 (d,  $J$  = 5.1 Hz, 2H,  $\text{ArH}$ ), 7.45 (d,  $J$  = 6.8 Hz, 2H,  $\text{ArH}$ ), 7.75–7.79 (m, 2H,  $\text{ArH}$ ), 7.86–7.92 (m, 2H,  $\text{ArH}$ ).  $^{13}\text{C}$  NMR:  $\delta$  20.9, 42.6, 55.1, 72.7, 113.8, 123.2, 127.9, 129.0, 131.7, 133.9, 134.0, 159.6, 167.7, 170.0. ESI-MS ( $m/z$ ): 339. Anal. Calc. for  $\text{C}_{19}\text{H}_{17}\text{NO}_5$ : C, 67.25; H, 5.05; N, 4.13. Found C, 67.09; H, 5.17; N, 4.01.

***N*-(2-acetoxy-2-phenyl)ethylphthalimide (6b)**

IR (KBr)  $\text{cm}^{-1}$ : 1425, 1612, 1716, 1743, 1775, 2361, 2936.  $^1\text{H}$  NMR:  $\delta$  2.03 (s, 3H,  $\text{CH}_3\text{CO}$ ), 3.93 (dd,  $J$  = 10.5 Hz, 3.8 Hz, 1H, CH), 4.17 (dd,  $J$  = 8.9 Hz, 5.3 Hz, 1H, CH), 6.13 (dd,  $J$  = 3.7 Hz, 5.2 Hz, 1H, CH), 7.35–7.45 (m, 5H,  $\text{ArH}$ ), 7.70–7.75 (m, 2H,  $\text{ArH}$ ), 7.84–7.86 (m, 2H,  $\text{ArH}$ ).  $^{13}\text{C}$  NMR:  $\delta$  21.0, 43.0, 73.3, 123.4, 126.6, 128.6, 128.7, 134.1, 137.2, 167.9, 170.3. ESI-MS ( $m/z$ ): 309. Anal. Calc. for  $\text{C}_{18}\text{H}_{15}\text{NO}_4$ : C, 69.89; H, 4.89; N, 4.53. Found C, 69.73; H, 5.03; N, 4.37.

***N*-(2-acetoxy-2-(4'-methylphenyl)ethyl)phthalimide (6c)**

IR (KBr)  $\text{cm}^{-1}$ : 1424, 1718, 1741, 1775.  $^1\text{H}$  NMR:  $\delta$  2.06 (s, 3H,  $\text{CH}_3\text{CO}$ ), 2.39 (s, 3H,  $\text{CH}_3$ ), 3.98 (dd,  $J$  = 3.7 Hz, 10.4 Hz, 1H, CH), 4.22 (dd,  $J$  = 6.2 Hz, 9.0 Hz, 1H, CH), 6.17 (dd,  $J$  = 3.7 Hz, 6.3 Hz, 1H, CH), 7.22 (d,  $J$  = 8 Hz, 2H,  $\text{ArH}$ ), 7.38 (d,



$J = 8.1$  Hz, 2H, *ArH*), 7.75–7.78 (m, 2H, *ArH*), 7.86–7.93 (m, 2H, *ArH*).  $^{13}\text{C}$  NMR:  $\delta$  20.0, 20.1, 41.8, 72.1, 122.3, 125.5, 128.3, 131.3, 133.0, 136.2, 168.2, 170.1. ESI-MS ( $m/z$ ): 323. Anal. Calc. for  $\text{C}_{19}\text{H}_{17}\text{NO}_4$ : C, 70.58; H, 5.30; N, 4.33. Found C, 70.39; H, 5.51; N, 4.21.

#### *N*-(2-acetoxy-2-(4'-fluorophenyl)ethylphthalimide (6d)

IR (KBr)  $\text{cm}^{-1}$ : 1424, 1513, 1607, 1718, 1743, 1775, 2943, 3073.  $^1\text{H}$  NMR:  $\delta$  2.04 (s, 3H,  $\text{CH}_3\text{CO}$ ), 3.90 (dd,  $J = 4.1$  Hz, 10.1 Hz, 1H, *CH*), 4.12 (dd,  $J = 8.6$  Hz, 5.5 Hz, 1H, *CH*), 6.06–6.13 (m, 1H, *CH*), 7.05 (t,  $J = 8.6$  Hz, 2H, *ArH*), 7.39–7.46 (m, 2H, *ArH*), 7.75–7.79 (m, 2H, *ArH*), 7.83–7.87 (m, 2H, *ArH*).  $^{13}\text{C}$  NMR:  $\delta$  20.2, 41.9, 71.5, 114.4, 114.9, 122.4, 127.4, 130.8, 132.0, 133.1, 160.9, 165.5, 168.8. ESI-MS ( $m/z$ ): 327. Anal. Calc. for  $\text{C}_{18}\text{H}_{14}\text{NO}_4\text{F}$ : C, 66.05; H, 4.31; N, 4.28. Found C, 65.95; H, 4.45; N, 4.21.

#### *N*-(2-acetoxy)-propylphthalimide (6e)

IR (KBr)  $\text{cm}^{-1}$ : 1425, 1612, 2958, 3004.  $^1\text{H}$  NMR:  $\delta$  1.27 (d,  $J = 6.6$  Hz, 3H,  $\text{CH}_3$ ), 2.01 (s, 3H,  $\text{CH}_3\text{CO}$ ), 3.83 (d,  $J = 5.3$  Hz, 2H,  $\text{CH}_2$ ), 5.17–5.26 (m, 1H, *CH*), 7.71–7.77 (m, 2H, *ArH*), 7.82–7.88 (m, 2H, *ArH*).  $^{13}\text{C}$  NMR:  $\delta$  17.8, 21.2, 42.0, 68.6, 123.4, 130.1, 134.1, 168.0, 171.0. ESI-MS ( $m/z$ ): 247. Anal. Calc. for  $\text{C}_{13}\text{H}_{13}\text{NO}_4$ : C, 63.15; H, 5.30; N, 5.67. Found C, 63.02; H, 5.47; N, 5.56.

#### General procedure for the hydrolysis of acetyl derivatives of protected amino alcohols

Racemic acetate (50 mg), aqueous phosphate buffer (2.5 mL, 0.1 M, pH. 7.0), toluene (250  $\mu\text{L}$ ) and wet whole cells of *Arthrobacter sp.* lipase (150 mg) were shaken (320 rpm) continuously at  $25 \pm 1$  °C. After a certain degree of conversion ( $\sim 50\%$ ) as indicated by TLC and chiral HPLC, the reaction was terminated by adding ethyl acetate and centrifuging the mixture at 10 000–15 000g to remove the enzyme and the suspended particles. The clear solution was decanted and the centrifuged mass was extracted separately with ethyl acetate ( $3 \times 25$  mL). The organic layer was combined and washed with water. The combined organic layer was then dried and evaporated under reduced pressure to furnish a mixture comprising hydrolyzed alcohol and unhydrolyzed ester, which was separated by column chromatography (100–200 mesh) using a gradient of ethyl acetate in hexane as eluent.

#### (*R*)-*N*-(2-acetoxy-2-phenyl)ethylphthalimide (6b)

HPLC purity > 99%; HPLC ee > 99%;  $[\alpha]_{\text{D}}^{25} -21.7^\circ$  ( $c$  1,  $\text{CHCl}_3$ ); HPLC condition ((*R,R*)-Whelk-01 chiral column, eluent 2-propanol : hexane = 5 : 95, flow rate: 0.8 mL  $\text{min}^{-1}$ ,  $t_1 = 13.9$  min).

#### (*S*)-*N*-(2-hydroxy-2-phenyl)ethylphthalimide (5b)

HPLC purity > 99%; HPLC ee > 99%;  $[\alpha]_{\text{D}}^{25} +23.2^\circ$  ( $c$  1,  $\text{CHCl}_3$ ); {lit.<sup>7a</sup> (for *R*-enantiomer)  $[\alpha]_{\text{D}}^{25} -25.6^\circ$  ( $c$  1,  $\text{CHCl}_3$ )}. HPLC condition ((*R,R*)-Whelk-01 chiral column, eluent 2-propanol : hexane = 5 : 95, flow rate: 0.8 mL  $\text{min}^{-1}$ ,  $t_1 = 19.0$  min).

#### (*R*)-*N*-(2-acetoxy-2-(4'-methoxyphenyl)ethylphthalimide (6a)

HPLC purity > 99%; HPLC ee > 99%;  $[\alpha]_{\text{D}}^{25} -40.8^\circ$  ( $c$  1,  $\text{CHCl}_3$ ); HPLC condition ((*R,R*)-Whelk-01 chiral column, eluent 2-propanol : hexane = 5 : 95, flow rate: 0.8 mL  $\text{min}^{-1}$ ,  $t_1 = 22.4$  min).

#### (*S*)-*N*-(2-hydroxy-2-(4'-methoxyphenyl)ethylphthalimide (5a)

HPLC purity > 99%; HPLC ee > 99%;  $[\alpha]_{\text{D}}^{25} +20.5^\circ$  ( $c$  1,  $\text{CHCl}_3$ ); {lit.<sup>7a</sup> (for *R*-enantiomer)  $[\alpha]_{\text{D}}^{25} -18.8^\circ$  ( $c$  1,  $\text{CHCl}_3$ )}. HPLC condition ((*R,R*)-Whelk-01 chiral column, eluent 2-propanol : hexane = 5 : 95, flow rate: 0.8 mL  $\text{min}^{-1}$ ,  $t_1 = 34.2$  min).

#### (*R*)-*N*-(2-acetoxy-2-(4'-methylphenyl)ethylphthalimide (6c)

HPLC purity > 99%; HPLC ee 90.2%;  $[\alpha]_{\text{D}}^{25} -16.5^\circ$  ( $c$  1,  $\text{CHCl}_3$ ); HPLC condition ((*R,R*)-Whelk-01 chiral column, eluent 2-propanol : hexane = 5 : 95, flow rate: 0.8 mL  $\text{min}^{-1}$ ,  $t_1 = 13.2$  min).

#### (*S*)-*N*-(2-hydroxy-2-(4'-methylphenyl)ethylphthalimide (5c)

HPLC purity > 99%; HPLC ee > 99%;  $[\alpha]_{\text{D}}^{25} +21.5^\circ$  ( $c$  1,  $\text{CHCl}_3$ ); {lit.<sup>7a</sup> (for *R*-enantiomer)  $[\alpha]_{\text{D}}^{25} -23.8^\circ$  ( $c$  1,  $\text{CHCl}_3$ )}. HPLC condition ((*R,R*)-Whelk-01 chiral column, eluent 2-propanol : hexane = 5 : 95, flow rate: 0.8 mL  $\text{min}^{-1}$ ,  $t_1 = 19.4$  min).

#### (*S*)-*N*-(2-hydroxy)-propylphthalimide (5e)

HPLC purity > 99%; HPLC ee > 99%;  $[\alpha]_{\text{D}}^{25} +20.5^\circ$  ( $c$  0.5,  $\text{CHCl}_3$ ); {lit.<sup>7a</sup>  $[\alpha]_{\text{D}}^{25} +41.3^\circ$  ( $c$  1,  $\text{CHCl}_3$ ); lit.<sup>18</sup>  $[\alpha]_{\text{D}}^{25} +15.7^\circ$  (ee = 94%) ( $c$  1.53,  $\text{CHCl}_3$ )}. HPLC condition Chiralcel OD column, eluent 2-propanol : hexane = 5 : 95, flow rate: 0.8 mL  $\text{min}^{-1}$ ,  $t_1 = 39.6$  min).

#### (*R*)-*N*-(2-acetoxy-2-(4'-fluorophenyl)ethylphthalimide (6d)

HPLC purity > 99%; HPLC ee > 99%;  $[\alpha]_{\text{D}}^{25} -32.6^\circ$  ( $c$  1,  $\text{CHCl}_3$ ); HPLC condition ((*R,R*)-Whelk-01 chiral column, eluent 2-propanol : hexane = 5 : 95, flow rate: 0.8 mL  $\text{min}^{-1}$ ,  $t_1 = 16.8$  min).

#### (*S*)-*N*-(2-hydroxy-2-(4'-fluorophenyl)ethylphthalimide (5d)

HPLC purity > 99%; HPLC ee > 99%;  $[\alpha]_{\text{D}}^{25} +18.1^\circ$  ( $c$  1,  $\text{CHCl}_3$ ); {lit.<sup>7a</sup>  $[\alpha]_{\text{D}}^{25} +18.3^\circ$  ( $c$  1,  $\text{CHCl}_3$ )}. HPLC condition ((*R,R*)-Whelk-01 chiral column, eluent 2-propanol : hexane = 5 : 95, flow rate: 0.8 mL  $\text{min}^{-1}$ ,  $t_1 = 24.7$  min).

## References

- S. C. Bergmeier, *Tetrahedron*, 2000, **56**, 2561.
- Daicel Chemical Industries Ltd, *Eur. Pat.*, 0 654 534 A2, Nov. 18, 1994.
- Z. M. Wang, X. L. Zhang and K. B. Sharpless, *Tetrahedron Lett.*, 1993, **34**, 2267.
- S. R. Martha, M. M. Omar, A. P. Cecilia, Q. Leticia and J. Eusebio, *J. Org. Chem.*, 2003, **68**, 2369 and references cited therein.
- C. Palomo, M. Oiarbide and A. Laso, *Angew. Chem., Int. Ed.*, 2005, **44**, 3881.
- D. J. Ager, I. Prakash and D. R. Schaad, *Chem. Rev.*, 1996, **96**, 835.

- 7 (a) C. Bolm, J. P. Hildebrand and K. Muniz, in *Catalytic Asymmetric Synthesis*, ed. J. Ojima, Wiley-VCH, New York, 2nd edn, 2000, p. 399; (b) M. J. McKannon, A. L. Meyer, K. Drautz and M. Schwarm, *J. Org. Chem.*, 1993, **58**, 3568.
- 8 (a) A. Lei, S. Wu, M. He and X. Zhang, *J. Am. Chem. Soc.*, 2004, **126**, 1626; (b) R. Noyori, *Angew. Chem., Int. Ed.*, 2002, **41**, 2008; (c) A. Hu and W. Lin, *Org. Lett.*, 2005, **7**, 455.
- 9 (a) G. Bartoli, M. Basco, A. Carlone, M. Locatelli, P. Melchiorre and L. Sambri, *Org. Lett.*, 2004, **6**, 3973; (b) O. Lohse and C. Spondlin, *Org. Process Res. Dev.*, 1997, **1**, 247 and references cited therein.
- 10 C. H. Wong and G. M. Whitesides, *Tetrahedron Organic Chemistry Series Volume 12: Enzymes in Synthetic Organic Chemistry*, Pergamon, UK, 1994.
- 11 K. Faber, *Biotransformations in Organic Chemistry*, Institute of Organic Chemistry, University of Graz, 4th edn, 2000.
- 12 (a) R. Sheldon, *Chem. Commun.*, 2001, 2399; (b) J. Peng and Y. Deng, *Tetrahedron Lett.*, 2001, **42**, 5917.
- 13 (a) A. Bartovic, B. Decroix and P. Netchitailo, *J. Heterocycl. Chem.*, 2000, **37**, 827; (b) W. N. Speckamp and M. J. Moolenaar, *Tetrahedron*, 2000, **56**, 3817.
- 14 (a) The *Arthrobacter sp.* cell biomass was prepared in shake flasks and in 10 L fermentor containing medium (1% peptone, and 0.5% NaCl and 0.5% beef extract, pH 7.0). The medium was inoculated with an overnight preculture prepared in the same broth. The culture was grown at 30 °C for 16–18 h at 200 rpm. The cell pellet was separated from the broth by centrifugation at 10 000g for 15 min at 4 °C and was preserved at –20 °C till further use. *Arthrobacter sp.* microbial culture (ABL, MTCC no. 5125), isolated at IIIM (RRL) Jammu has been deposited in MTCC culture collection under the Budapest Treaty (2004); (b) S. Koul, S. C. Taneja, R. Parshad and G. N. Qazi, *Tetrahedron: Asymmetry*, 1998, **9**, 3395.
- 15 (a) O. Mitsunobu, *Synthesis*, 1981, 1; (b) A. Steinreiber, K. Edegger, S. F. Mayer and K. Faber, *Tetrahedron: Asymmetry*, 2001, **12**, 2067.
- 16 (a) H. R. Ing and R. H. F. Manske, *J. Chem. Soc.*, 1926, 2349; (b) A. Arffin, M. N. Khan, L. C. Lan, F. Y. May and C. S. Yun, *Synth. Commun.*, 2004, **34**, 4439.
- 17 M. Kapoor, N. Anand, K. Ahmad, S. Koul, S. S. Chimni, S. C. Taneja and G. N. Qazi, *Tetrahedron: Asymmetry*, 2005, **16**, 717.
- 18 T. Fujisawa, H. Hayashi and Y. Kishioka, *Chem. Lett.*, 1987, 129.

# Find a SOLUTION

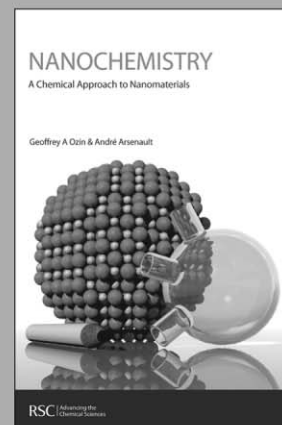
## ... with books from the RSC

**Choose from exciting textbooks, research level books or reference books in a wide range of subject areas, including:**

- Biological science
- Food and nutrition
- Materials and nanoscience
- Analytical and environmental sciences
- Organic, inorganic and physical chemistry

**Look out for 3 new series coming soon ...**

- RSC Nanoscience & Nanotechnology Series
- Issues in Toxicology
- RSC Biomolecular Sciences Series



**RSC** | Advancing the  
Chemical Sciences

[www.rsc.org/books](http://www.rsc.org/books)

28040542

# Iron and vanadium containing molybdophosphoric acid catalyst for selective oxidation of alcohols with molecular oxygen†‡

P. Nagaraju, Nayeem Pasha, P. S. Sai Prasad and N. Lingaiah\*

Received 19th December 2006, Accepted 30th May 2007

First published as an Advance Article on the web 20th June 2007

DOI: 10.1039/b618546k

The Keggin type 12-molybdophosphoric acid is modified by incorporation of vanadium and iron and studied for oxidation of various alcohols using molecular oxygen as oxidant. The molybdophosphoric acid catalyst containing both vanadium and iron is highly active compared with the catalysts containing either vanadium or iron in the Keggin structure. The iron exchanged vanadium incorporated molybdophosphoric acid catalyst is active for the oxidation of various primary and secondary alcohols under mild conditions and reusable without any appreciable loss in activity.

## 1. Introduction

The oxidation of alcohols into aldehydes and ketones is of paramount importance in organic chemistry. Numerous reagents have been reported to accomplish this transformation efficiently and selectively.<sup>1</sup> However most of these oxidants are toxic, hazardous, or required in large excess. From an environmental viewpoint, major efforts have been devoted to the discovery and development of efficient procedures for oxidation employing O<sub>2</sub> (or air) or hydrogen peroxide as oxidant.<sup>2</sup> These systems are particularly interesting as they release only innocuous by-products such as water.<sup>3,4</sup> The oxidation of alcohols employing molecular oxygen requires co-reductants such as *N*-hydroxyphthalimide, diethyl azodicarboxylate, hydroquinone, or nitrasonium ions to accomplish the catalytic cycle with catalysts based on Ru, and Co,<sup>5</sup> Cu,<sup>6</sup> and Zr.<sup>7</sup> Oxidation of alcohols with molecular oxygen is reported on Pt,<sup>8</sup> Rh,<sup>9</sup> Pd,<sup>10</sup> Ru,<sup>11</sup> Co,<sup>12</sup> Os,<sup>13</sup> and heteropoly acid catalysts.<sup>14</sup>

Keggin type heteropoly acids (HPAs) have many advantages that make them economical and environmentally attractive in both academic and industrial applications; they are useful as acid and oxidation catalysts for various reactions since their catalytic features can be varied at a molecular level.<sup>15,16</sup> HPAs like 12-molybdophosphoric acid (MPA) and vanadium containing molybdophosphoric acid are used for alcohol oxidations. These catalysts are soluble in most of the solvents. Few reports exist where it was attempted to overcome the homogeneity of these catalysts by impregnating them on solid supports. The major problem in these supported catalysts is the leaching of the active species. Efforts are being made to overcome the leaching and solubility problem. HPAs are modified by converting them into their corresponding salts or exchanging with different metal ions.

In this article, we report the 12-molybdophosphoric acid based catalysts modified with incorporation of vanadium and iron ions for the oxidation of various alcohols to their corresponding carbonyl compounds with molecular oxygen as oxidant under mild conditions. The oxidation ability of 12-molybdophosphoric acid (MPA), vanadium incorporated 12-molybdophosphoric acid (MPAV<sub>1</sub>), Fe exchanged 12-molybdophosphoric acid (FeMPA) and both vanadium and iron containing 12-molybdophosphoric acid (FeMPAV<sub>1</sub>) are tested. The efficiency of these catalysts are studied for the oxidation reactions using H<sub>2</sub>O<sub>2</sub> or molecular oxygen as oxidant.

## 2. Experimental

Iron exchanged MPA was obtained as a precipitate by adding 1.1 g of iron nitrate in aqueous solution to 5 g of 12-molybdophosphoric acid dissolved in 25 ml of distilled water. The excess water was removed on a water bath and the resultant salt was dried in an oven at 120 °C for 12 h. Finally the catalyst is calcined in air at 300 °C for 2 h. The composition of the final catalyst determined by ICP mass is Fe<sub>0.64</sub>H<sub>0.36</sub>PMo<sub>12</sub>O<sub>40</sub>. This catalyst is denoted as FeMPA.

Vanadium incorporated molybdophosphoric acid was prepared according to the procedure already reported.<sup>17,18</sup> In the synthesis of the catalyst where vanadium was incorporated into the primary structure of MPA *i.e.* H<sub>4</sub>PMo<sub>11</sub>V<sub>1</sub>O<sub>40</sub> (MPAV<sub>1</sub>) hot aqueous solutions of 7.1 g of disodium hydrogen phosphate dissolved in 100 ml of distilled water and 6.1 g sodium metavanadate in 100 ml of water were mixed thoroughly. The mixture was cooled and acidified with 5 ml of concentrated sulfuric acid. To this mixture an aqueous solution of 133 g sodium molybdate dihydrate dissolved in 200 ml of distilled water was added. Then, 50 ml of concentrated sulfuric acid was slowly added while stirring, showing a color change from dark red to light red. The MPAV<sub>1</sub> formed was extracted with diethyl ether as the heteropoly acid was present in the middle layer as heteropoly etherate. Subsequently the ether was removed by passing air through the solution. The orange solid obtained was dissolved in water and concentrated until the crystals appeared.

Catalysis Laboratory, I&PC Division, Indian Institute of Chemical Technology, Hyderabad, 500 007, India.

E-mail: nakkalingaiah@iict.res.in; Fax: +91-40-27160921;

Tel: +91-40-27193163

† IICT Communication No. 070203.

‡ Electronic supplementary information (ESI) available: Elemental analysis of fresh and recycled catalysts. See DOI: 10.1039/b618546k

Iron exchanged vanadium containing MPA (FeMPAV<sub>1</sub>) was prepared by taking appropriate amounts of the above MPAV<sub>1</sub> (4 g) and iron nitrate (1.134 g) in aqueous solution (25 ml). The excess water was removed on a hot water bath and the resultant solid was dried in an oven at 120 °C for 12 h and finally calcined at 300 °C for 2 h in air. The final composition of this catalyst is determined as Fe<sub>0.56</sub>H<sub>0.44</sub>PMo<sub>0.11</sub>V<sub>1</sub>O<sub>40</sub>.

Oxidation of alcohols was carried out in liquid phase at atmospheric pressure under reflux conditions. In a typical experiment a mixture of benzyl alcohol (1 mmol) and catalyst (50 mg) in acetonitrile (5 ml) fixed with an oxygen balloon was refluxed at the boiling point of acetonitrile. The progress of the reaction was monitored by TLC. After completion of the reaction, the catalyst was filtered and the products analyzed by gas chromatography. All the yields are based on the calibration of gas chromatography.

IR spectra of catalysts were taken on a DIGILAB (USA) IR spectrometer by the KBr disc method. XRD patterns were measured on a RIGAKU MINI FLEX diffractometer using Cu K $\alpha$  radiation ( $\lambda = 1.54 \text{ \AA}$ ). The  $2\theta$  angles were scanned from 2–80° at a rate of 2° min<sup>−1</sup>.

### 3. Results and discussion

#### 3.1. Characterization of the catalysts

The results of catalysts characterized by FT-IR are shown in Fig. 1. IR spectra of the catalysts shows that all the catalysts have four strong absorption peaks between 1064 and 785 cm<sup>−1</sup>, attributed to the characteristic bands of heteropoly anion of

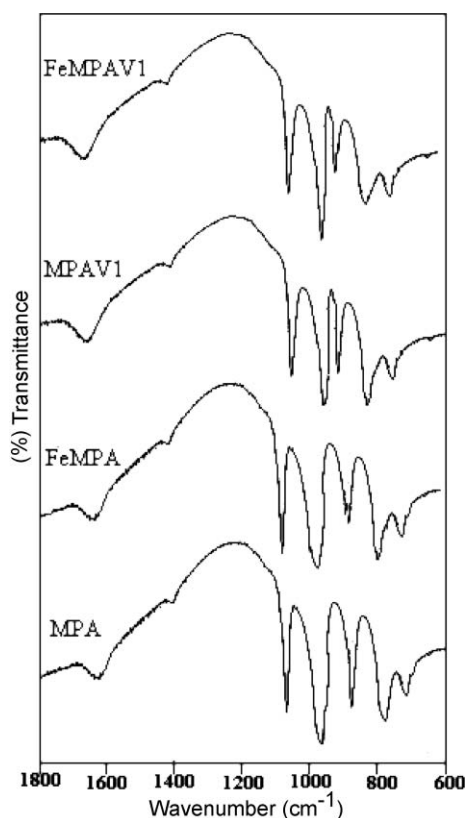


Fig. 1 IR spectra of modified MPA catalysts.

the Keggin structure. The vibration of V–O bond is marked by the very strong absorption of the Mo–O bond.<sup>19</sup> Compared with those of MPA and FeMPA the characteristic absorption peaks of MPAV<sub>1</sub> and FeMPAV<sub>1</sub> are shifted marginally by the presence of V in MPA. The  $\nu(\text{Mo}-\text{O}_b-\text{Mo})$  and  $\nu(\text{Mo}-\text{O}_c-\text{Mo})$  bands exhibit a red shift of about 5 and 8.4 cm<sup>−1</sup> respectively. This red shift of  $\nu(\text{Mo}-\text{O}-\text{Mo})$  band is due to the influence of vanadium on the M–O bond. This shift suggests that vanadium has entered into the primary structure of the Keggin anion.

Fig. 2 shows the XRD patterns of catalysts. The strong characteristic peaks of the Keggin structure of MPA are found in all the samples. The XRD patterns suggest that the Keggin structure is intact even with the exchange of iron and incorporation of vanadium into the Keggin structure.

In order to know the activity of modified molybdophosphoric acid catalysts for oxidation of alcohols initial experiments are carried out for oxidation of benzyl alcohol. The molybdophosphoric acid (MPA) and its modified forms FeMPA, MPAV<sub>1</sub> and FeMPAV<sub>1</sub> catalysts are tested for benzyl alcohol oxidation using H<sub>2</sub>O<sub>2</sub> or molecular O<sub>2</sub> as oxidant and the results are reported in Table 1. The results suggest that oxidation using H<sub>2</sub>O<sub>2</sub> as oxidant afforded smooth reaction on all the modified molybdophosphoric acid catalysts. However, the oxidation using O<sub>2</sub> results in variation of oxidation ability of these catalysts. The basic MPA showed poor activity and its modifications with Fe (FeMPA) or vanadia (MPAV<sub>1</sub>) exhibits considerable yield of the desired product. It is interesting to note that the MPA modified with Fe and V results in very high oxidation ability with O<sub>2</sub> as oxidant within reasonable reaction time. By the inclusion of Fe to the vanadium containing MPA the oxidation product formation is enhanced substantially. It is known that the Mo

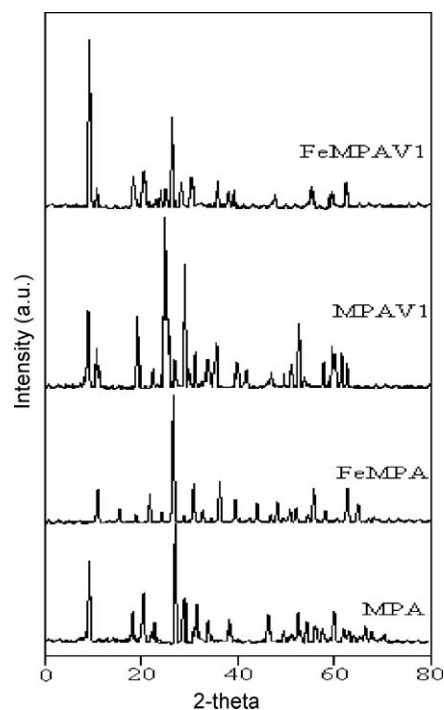


Fig. 2 XRD spectra of modified MPA catalysts.



**Table 1** MPA and modified MPA catalyzed alcohol oxidation of benzyl alcohol with different oxidants<sup>a</sup>

$\text{C}_6\text{H}_5\text{CH}_2\text{OH} \xrightarrow[\text{Oxidant, Reflux}]{\text{Catalyst, CH}_3\text{CN}} \text{C}_6\text{H}_5\text{CHO}$					
Catalyst	Surface area/m <sup>2</sup> g <sup>-1</sup>	Oxidant	Reaction time/h	Yield (%) <sup>b</sup>	Turn over number (TON)
MPA	3.0	H <sub>2</sub> O <sub>2</sub>	6	86	—
		O <sub>2</sub>	20	6	—
FeMPA	8.0	H <sub>2</sub> O <sub>2</sub>	6	92	54.2
		O <sub>2</sub>	20	35	20.6
MPAV <sub>1</sub>	7.0	H <sub>2</sub> O <sub>2</sub>	6	90	45.0
		O <sub>2</sub>	12	24	12.0
FeMPAV <sub>1</sub>	10.0	H <sub>2</sub> O <sub>2</sub>	6	99	115.5
		O <sub>2</sub>	12	92, 90 <sup>c</sup>	107.3, 106.6 <sup>d</sup>

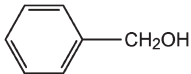
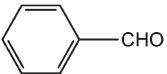
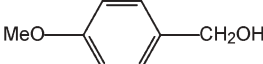
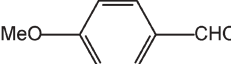
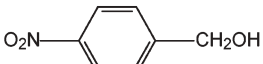

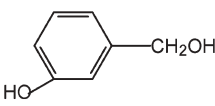
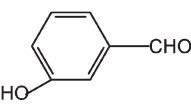
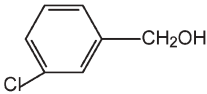
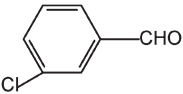
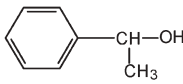
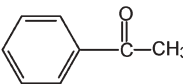
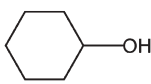
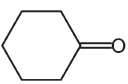
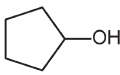
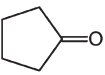
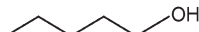
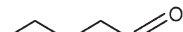


<sup>a</sup> Benzyl alcohol (1 mmol), catalyst (50 mg), acetonitrile (5 ml), reaction temperature: 80 °C. <sup>b</sup> GC yields. <sup>c</sup> Yield after fourth recycle. <sup>d</sup> Turn over number (TON) after fourth cycle.

ions play the main role in the oxidation. However, its activity is enhanced by the presence of both Fe and V.<sup>20</sup> The synergistic role of the presence of iron(III) and vanadium(V)

together is not yet clear, as the presence of either one of the metals is not highly active. The formation of iron oxo species and vanadium hydroperoxide species may be the reason for the high activity. It is known that Fe ions could adjust the Lewis acidity and the redox properties to some extent. The role of vanadium is more important in oxidation catalysis as it is known for its redox properties. It is reported for the vanadium containing MPA that the polyoxometalate [PMo<sub>10</sub>V<sub>2</sub>O<sub>40</sub>]<sup>5-</sup> through transfer of two electrons and two protons from the organic substrate to the catalyst yields the oxidized product and reduced polyoxometalate.<sup>14</sup> The catalyst is reoxidized by molecular oxygen. These results suggest that the modified MPA with vanadium and iron leads to a highly active heterogeneous catalyst for oxidation of alcohols with molecular oxygen.

The activity of the MPA modified with Fe and V catalyst for the oxidation of various alcohols with molecular oxygen are studied. Oxidation of a variety of benzyl alcohol derivatives and aliphatic alcohols are carried out and the results are presented in Table 2. Treatment of an appropriate alcohol (1 mmol) with FeMPAV<sub>1</sub> in acetonitrile afforded the corresponding carbonyl compound after the time indicated

**Table 2** Oxidation of a variety of benzyl alcohol derivatives and aliphatic alcohols using FeMPAV<sub>1</sub> as catalyst<sup>a</sup>

$\text{R-CH}_2\text{OH} \xrightarrow[\text{O}_2, \text{Reflux}]{\text{FeMPAV}_1, \text{CH}_3\text{CN}} \text{R-CHO}$					
Entry	Substrates	Products	Time/h	Yields <sup>b</sup> (%)	TON
1			12	92	107.3
2			12	93	108.5
3			12	89	103.8
4			14	83	96.8
5			12	85	99.0
6			15	94	109.6
7			16	87	101.5
8			18	82	95.6
9			21	64	74.6
10			24	56	65.3

<sup>a</sup> Benzyl alcohol (1 mmol), catalyst (50 mg), acetonitrile (5 ml), reaction temperature: 80 °C. <sup>b</sup> GC yields.

**Table 3** A comparison of the activity of the present catalyst (FeMPAV<sub>1</sub>) with those reported in the literature for benzyl alcohol oxidation

Catalyst	Oxidant	Temperature/°C	Reaction time/h	Yield(%)	Reference
FeMPAV <sub>1</sub>	O <sub>2</sub>	80	12	92	Present work
V <sub>2</sub> O <sub>5</sub>	O <sub>2</sub>	100	24	82	21
1.68%Pd/Al <sub>2</sub> O <sub>3</sub>	O <sub>2</sub>	88	8	62	23
Hydrous RuO <sub>2</sub>	O <sub>2</sub>	80	1.5	16	24
Octahedral molecular sieves (K-OMS-2)	O <sub>2</sub>	110	4	85	25

in Table 2 under reflux conditions. Benzyl alcohol derivatives are converted to the corresponding benzaldehyde derivatives. The yields of the products are very high. The presence of an electron-donating or an electron-withdrawing group on the aromatic ring has no appreciable effect on the reaction times and yields. Primary and secondary aliphatic alcohols are also converted into the corresponding aldehydes and ketones, respectively. In all cases, no over-oxidation products are observed even after extended reaction times. It has been reported that the formation of ester in oxidation of primary alcohols catalyzed by V<sub>2</sub>O<sub>5</sub>.<sup>21</sup> The over oxidation products are observed using quaternary ammonium decatungstate catalyst with hydrogen peroxide under reflux conditions for oxidation of aliphatic n-alcohols.<sup>22</sup> The FeMPAV<sub>1</sub> catalyst is highly active compared to the catalysts reported for the oxidation of cyclic and non-cyclic aliphatic alcohols.<sup>23</sup> The present catalyst is compared with some of the heterogeneous catalysts reported in the literature<sup>21,23–25</sup> and details are shown in Table 3. The FeMPAV<sub>1</sub> catalyst is comparable with the other reported catalysts and showed better yields than some of the catalysts within reasonable reaction time at low reaction temperature.

Carrying the reaction with the same catalyst, which is recovered from the first cycle by simple filtration, establishes the reusability of the catalyst. During the filtration the catalyst is washed several times with acetonitrile and dried in an air oven at 120 °C for 1 h. Four recycle experiments are carried and the yield after the fourth cycle is presented in Table 1. It is noteworthy to mention that the catalyst is active even after fourth recycle.

#### 4. Conclusion

In summary, the oxidation of various alcohols with molecular oxygen as oxidant is achieved using iron-exchanged vanadium incorporated 12-molybdophosphoric acid catalyst. This catalyst is effective for the oxidation of various primary and secondary alcohols. The present catalytic system is inexpensive, easy to handle, non-corrosive and environmentally

benign. This catalyst is reusable and exhibits consistent activity upon recycling.

#### References

- 1 R. C. Larock, *Comprehensive Organic Transformations*, VCH, New York, 1989, p. 604.
- 2 R. A. Sheldon and J. K. Kochi, *Metal catalyzed oxidations of Organic Compounds*, Academic Press, New York, 1981.
- 3 R. A. Sheldon, *Dioxygen Activation and Homogeneous Catalytic Oxidation*, ed. L. L. Simandi, Elsevier, Amsterdam, 1991, p. 573.
- 4 R. A. Sheldon, *Pure Appl. Chem.*, 2000, **72**, 1233.
- 5 S. I. Murahashi, T. Naota and N. Hirai, *J. Org. Chem.*, 1993, **58**, 7318.
- 6 M. F. Semmelhack, C. R. Schmid, D. A. Cortes and C. S. Chou, *J. Am. Chem. Soc.*, 1984, **106**, 3374.
- 7 K. Krohn, I. Vinke and H. Adam, *J. Org. Chem.*, 1996, **61**, 1467.
- 8 C. G. Jia, F. Y. Jing, W. D. Hu, M. Y. Huang and Y. Y. Jiang, *J. Mol. Catal.*, 1994, **91**, 139.
- 9 J. Martin, C. Martin, M. Faraj and M. Bregeault, *Nouv. J. Chim.*, 1984, **8**, 141.
- 10 G. J. ten Brink, I. W. C. E. Arends and R. A. Sheldon, *Science*, 2000, **287**, 1636.
- 11 T. Matsushita, K. Ebitani and K. Kaneda, *Chem. Commun.*, 1999, 265.
- 12 T. Iwahama, S. Sakaguchi, Y. Nishiyama and Y. Ishii, *Tetrahedron Lett.*, 1995, **36**, 6923.
- 13 P. A. Shapley, N. Zhang, J. L. Allen, D. H. Pool and H. C. Liang, *J. Am. Chem. Soc.*, 2000, **122**, 1079.
- 14 R. Neumann and A. M. Khenkin, *Chem. Commun.*, 2006, 2529.
- 15 T. Okuhara and M. Misono, *Adv. Catal.*, 1996, **41**, 113.
- 16 N. Mizuno and M. Misono, *Chem. Rev.*, 1998, **98**, 199.
- 17 G. A. Tsigdinos and C. J. Hallada, *Inorg. Chem.*, 1968, **7**, 437.
- 18 D. Casarini, G. Centi, P. Jiru, V. Lena and Z. Tvaruzkova, *J. Catal.*, 1993, **143**, 325.
- 19 F. Xian, L. Cai and C. Pham, *React. Kinet. Catal. Lett.*, 2002, **75**, 312.
- 20 Q. Deng, S. Jiang, T. Cai, Z. Peng and Z. Fang, *J. Mol. Catal.*, 2005, **229**, 165.
- 21 S. Velusamy and T. Punniyamurthy, *Org. Lett.*, 2004, **6**, 217.
- 22 M. L. Guo, *Green Chem.*, 2004, **6**, 271.
- 23 H. Wu, Q. Zhang and Y. Wang, *Adv. Synth. Catal.*, 2005, **356**, 3471.
- 24 B. Z. Zhan, M. A. White, T. K. Sham, J. A. Pincock, R. J. Doucet, K. V. Raman Rao, K. N. Robertson and T. S. Cameron, *J. Am. Chem. Soc.*, 2003, **125**, 2195.
- 25 Y. C. Son, V. D. Makwana, A. R. Howell and S. L. Suib, *Angew. Chem.*, 2001, **113**, 4410.

# Sustainable production of acrolein: investigation of solid acid–base catalysts for gas-phase dehydration of glycerol

Song-Hai Chai, Hao-Peng Wang, Yu Liang and Bo-Qing Xu\*

Received 12th February 2007, Accepted 1st June 2007

First published as an Advance Article on the web 22nd June 2007

DOI: 10.1039/b702200j

Synthesis of acrolein by catalytic gas-phase dehydration of biomass-derivate glycerol was studied over various solid catalysts with a wide range of acid–base properties. The catalyst acidity and basicity were measured, respectively, by *n*-butylamine and benzoic acid titration methods using Hammett indicators. The most effective acid strength for the selective dehydration of glycerol to form acrolein appeared between  $-8.2 \leq H_0 \leq -3.0$ , with which acrolein was produced at a selectivity of 60–70 mol%. The catalysts having very strong acid sites ( $H_0 \leq -8.2$ ) effected a lower acrolein selectivity (40–50 mol%) due to more severe coke deposition in the reaction. Solid acids holding medium strong and weak acid sites ( $-3.0 \leq H_0 \leq +6.8$ ) were found to be not selective for the acrolein production, the acrolein selectivity being less than 30 mol%. The mass specific catalytic rate for the acrolein production showed a general trend to increase with the fractional acidity at  $-8.2 \leq H_0 \leq -3.0$ . The catalytic data also suggest that Brønsted acid sites were advantageous over Lewis acid sites in catalyzing the selective synthesis of acrolein from glycerol dehydration. Solid base catalysts were shown not to be effective for acrolein production.

## 1. Introduction

The catalytic conversion of biomass-derivate feedstocks for the synthesis of value-added fuels, chemicals and materials has been attracting much attention, as the depletion of non-renewable fossil resources could happen in a few decades.<sup>1–3</sup> Acrolein, an important and versatile intermediate in the chemical industry, is nowadays produced by gas-phase oxidation of petroleum-derived propylene with a Bi/Mo-mixed oxide catalyst. As a sustainable alternative, acrolein can be synthesized by the double dehydration of glycerol, which is a derivate of biomass and is currently a by-product in the transesterification of vegetable oils (biodiesel production) and the saponification of natural fats.<sup>4,5</sup>

There have been a few studies on acrolein production by the dehydration of glycerol using homogenous or heterogeneous solid acid catalysts. In an old patent in 1936, an acrolein yield of 49% was reported by heating an aqueous glycerol solution (6.3 wt%) at 190 °C in the presence of H<sub>2</sub>SO<sub>4</sub> (8 wt%).<sup>6</sup> Glycerol dehydration was also conducted in sub- and supercritical water (250–390 °C and 25–35 MPa) using inorganic acids or salts as the catalysts.<sup>7–9</sup> Acrolein selectivity up to 75 mol% was obtained at 360 °C and 25 MPa when zinc sulfate (470 ppm, g g<sup>−1</sup>) was used as the catalyst.<sup>9</sup> Owing to the known technical and environmental problems, such as reactor corrosion, catalyst reusability and waste management, mineral acids or salts are not the desirable catalysts for practical application.

Solid acids including sulfates, supported phosphates and phosphoric acid (SPA) have been tested as heterogeneous catalysts for the gas-phase dehydration of glycerol under

atmospheric pressure.<sup>10–12</sup> Li<sub>3</sub>PO<sub>4</sub> or FePO<sub>4</sub> supported on pumice, patented by Scheering-Kahlbaum A. G. in 1930,<sup>12</sup> produced an acrolein yield as high as 75–80% for the gas-phase dehydration of glycerol at 400 °C. But, the duplication of the catalytic reaction at Degussa sixty years later<sup>11</sup> showed a much lower acrolein yield (32–36%). Alternatively, an SPA (H<sub>3</sub>PO<sub>4</sub> supported on  $\alpha$ -Al<sub>2</sub>O<sub>3</sub>) catalyst was claimed to produce the highest selectivity to acrolein (65–75 mol% at 100% glycerol conversion) at 250–340 °C when aqueous glycerol solution containing 10–40 wt% glycerol was used as the feedstock (gas hourly space velocity, GHSV, by glycerol was 20 h<sup>−1</sup>).<sup>11</sup> Glycerol dehydration reaction was also tested in liquid phase at 250–300 °C and 70 bar using zeolite HZSM-5 or H-mordenite as a catalyst.<sup>11</sup> The glycerol conversion had to be kept low (15–25%) in order to obtain a high selectivity (71–75 mol%) for acrolein production, since the acrolein selectivity decreased significantly with the increase in glycerol conversion.

In the present work, we studied the glycerol dehydration in the gas phase using various solid catalysts with a wide range of acid–base properties. An attempt has been made to correlate their catalytic performance with the catalyst acidity and/or basicity to understand the nature of active sites for the dehydration reaction, which could help to develop more efficient solid catalysts for a sustainable acrolein production from biomass-derivate glycerol.

## 2. Experimental

### 2.1 Catalyst preparation

Mesoporous SiO<sub>2</sub> (SBA-15) and microporous molecular sieve materials (SAPO-34, H $\beta$  and HZSM-5) were supplied by Dr Zhong-Ming Liu at Dalian Institute of Chemical Physics, Chinese Academy of Sciences. Amorphous Al<sub>2</sub>O<sub>3</sub> and SiO<sub>2</sub>–Al<sub>2</sub>O<sub>3</sub> samples were supplied by Fushun Research Institute of

Innovative Catalysis Program, Key Lab of Organic Optoelectronics & Molecular Engineering, Department of Chemistry, Tsinghua University, Beijing, China 100084. E-mail: bqxu@mail.tsinghua.edu.cn; Fax: +86-10-62792122; Tel: +86-10-62792122

Petroleum and Petrochemicals (FRIPP), SINOPEC. The above catalysts were calcined at 500 °C for 4 h in flowing air before use.

MgO and La<sub>2</sub>O<sub>3</sub> were purchased commercial AR samples. They were calcined in air at 500 °C for 4 h before use. CeO<sub>2</sub> and ZrO<sub>2</sub> were prepared by air calcination of a commercial Ce(NO<sub>3</sub>)<sub>3</sub>·6H<sub>2</sub>O (AR) and homemade zirconyl hydroxide (hydrogel) at 500 °C for 4 h, respectively.

Niobium oxide (Nb<sub>2</sub>O<sub>5</sub>) catalysts with different acidity were prepared by calcining hydrated niobium oxide (Nb<sub>2</sub>O<sub>5</sub>·*n*H<sub>2</sub>O, CBMM HY-340) at various temperatures (350–700 °C) in flowing air. According to the calcination temperature (*T* in °C), these samples were denoted as Nb<sub>2</sub>O<sub>5</sub>-*T* (*T* = 350, 400, 500 and 700).

5 wt% H<sub>3</sub>PO<sub>4</sub>/α-Al<sub>2</sub>O<sub>3</sub>, 5 wt% H<sub>3</sub>PW<sub>12</sub>O<sub>40</sub>/α-Al<sub>2</sub>O<sub>3</sub> and 5 wt% NiSO<sub>4</sub>/α-Al<sub>2</sub>O<sub>3</sub> catalysts were prepared by wet impregnation of a commercial α-Al<sub>2</sub>O<sub>3</sub> with the required amount of aqueous solution of phosphoric acid (H<sub>3</sub>PO<sub>4</sub>), tungstophosphoric acid (H<sub>3</sub>PW<sub>12</sub>O<sub>40</sub>, AR) and NiSO<sub>4</sub>·6H<sub>2</sub>O (AR) at room temperature, respectively. Then, the solution was evaporated in a rotary evaporator at 60 °C; the remaining powder was dried in air at 110 °C overnight.

5 wt% SO<sub>4</sub><sup>2-</sup>/ZrO<sub>2</sub> was prepared by impregnation of the zirconyl hydroxide (hydrogel) with the required amount of aqueous solution of (NH<sub>4</sub>)<sub>2</sub>SO<sub>4</sub> (AR), followed by drying in a rotary evaporator at 60 °C. The final calcination temperature of the catalyst was 600 °C.

The preparation of WO<sub>3</sub>/ZrO<sub>2</sub> was described elsewhere in detail.<sup>13</sup> 15 wt% WO<sub>3</sub>/ZrO<sub>2</sub> catalyst was prepared by impregnation of zirconyl hydroxide (acolgel) with required amount of ammonium paratungstate (N<sub>5</sub>H<sub>37</sub>W<sub>6</sub>O<sub>24</sub>·H<sub>2</sub>O, AR) aqueous solution at 50–60 °C for 4 h. Then the excess water was removed in a rotary evaporator at 60 °C. The remaining powder was dried in air at 110 °C overnight, followed by calcination in air at 900 °C for 4 h. The preparation methods of zirconyl hydroxide hydrogel and acolgel are described in the references.<sup>14,15</sup>

All catalysts investigated in this work were pressed, crushed, and sieved to 20–40 mesh before use.

## 2.2 Measurement of catalyst acidity and basicity

According to the references,<sup>16–18</sup> the catalyst acidity (strength and amount) was measured by the *n*-butylamine titration method using various Hammett indicators (Table 1) with p*K*<sub>a</sub> ≤ +6.8; the catalyst basicity was measured by the benzoic acid titration method using those with p*K*<sub>a</sub> ≥ +7.2. Acid strength was expressed by the Hammett acidity function (*H*<sub>0</sub>)

**Table 1** Hammett indicators used for the measurement of acidity and basicity<sup>a</sup>

Indicators	p <i>K</i> <sub>a</sub>
Neutral red	+6.8
<i>p</i> -Dimethylaminoazobenzene	+3.3
Dicinnamalacetone	−3.0
Anthraquinone	−8.2
2, 4-Dinitroaniline	+15.0
Bromothymol blue	+7.2

<sup>a</sup> Hammett indicators with p*K*<sub>a</sub> = −8.2–+6.8 were used to measure the acidity, while those of p*K*<sub>a</sub> = +7.2–+15.0 were used to measure the basicity of the catalyst samples.

that was scaled by the p*K*<sub>a</sub> values of the indicators with p*K*<sub>a</sub> ≤ +6.8, while the base strength (*H*<sub>−</sub>) was scaled by the p*K*<sub>a</sub> values of the indicators with p*K*<sub>a</sub> ≥ +7.2. Before the measurement, the samples were formulated to 100–180 mesh and pretreated at 315 °C for 4 h in flowing dry nitrogen.

For microporous molecular sieves (SAPO-34, HZSM-5 and Hβ), the acidity measured by *n*-butylamine titration method may be lower than their actual acidity, since their pore sizes (~0.45 nm for SAPO-34, ~0.55 nm for HZSM-5 and ~0.7 nm for Hβ) could be smaller than the dynamic sizes of the indicator molecules (0.5–0.8 nm).

## 2.3 Catalytic reaction

The gas-phase dehydration reaction of glycerol to acrolein was carried out at 315 °C under atmospheric pressure in a vertical fixed-bed quartz reactor (i.d. 9 mm). The catalyst with a constant volume of 0.63 ml was charged in the middle section of the reactor, with quartz wool packed in both ends. 2 ml quartz sand was placed above the catalyst bed in order to preheat and vaporise the feed. Prior to the reaction, the catalyst was pretreated at 315 °C for 1.5 h in a flow of dry nitrogen (30 ml min<sup>−1</sup>). The reaction feed, an aqueous solution containing 36.2 wt% glycerol (molar ratio of glycerol/water = 1/9), was fed into the reactor by a micro-pump. Generally, the catalytic performance of the solid catalysts was evaluated at a gas hourly space velocity (GHSV) by glycerol of 80 h<sup>−1</sup>. For several key catalysts, that retained 100% conversion for 10 h at 80 h<sup>−1</sup>, a higher GHSV of 400 h<sup>−1</sup> was also adopted to investigate the catalyst stability and selectivity. The reaction products were condensed in an ice-water trap and collected hourly for analysis on a HP6890 GC equipped with a HiCap CBP20-S25-050 (Shimadzu) capillary column (i.d. 0.32 mm × 25 m) and a FID detector. The reaction was continued for 10 h and the condensed products during the first hour of the reaction were abandoned due to poor material balance. Glycerol conversion and product selectivity were calculated according to the following equations:

$$\text{Glycerol conversion (\%)} = \frac{\text{Moles of glycerol reacted}}{\text{Moles of glycerol in the feed}} \times 100$$

$$\text{Product selectivity (mol\%)} =$$

$$\frac{\text{Moles of carbon in a product defined}}{\text{Moles of carbon in glycerol reacted}} \times 100$$

The carbon deposits (coke) over the used catalysts were measured by temperature-programmed oxidation (TPO) in flowing air (50 ml min<sup>−1</sup>) from 100 °C to 800 °C at a heating rate of 20 °C min<sup>−1</sup> on a thermal-analyzer (Mettler-Toledo TG/SDTA 851<sup>o</sup>). The weight loss due to carbon oxidation/combustion was detected between 250 °C and 500 °C and normalized to show the amount of carbon deposits on a unit gram of the fresh catalyst.

## 3. Results and discussion

According to the measured highest acid or base strength (*H*<sub>0</sub> or *H*<sub>−</sub>), the catalysts investigated in this work are classified into four groups as follows:



**Table 2** Basic catalysts and their basicity in different base strengths

Catalyst <sup>a</sup>	Basicity/mmol g <sup>-1</sup>		Total
	+7.2 ≤ <i>H</i> <sub>0</sub> ≤ +15.0	+15.0 ≤ <i>H</i> <sub>0</sub>	
Group-1			
CeO <sub>2</sub>	0.10	—	0.10
La <sub>2</sub> O <sub>3</sub>	0.03	0.01	0.04
MgO	0.04	0.34	0.38

<sup>a</sup> Calcination temperature: 500 °C.Group-1 (*H*<sub>0</sub> ≥ +7.2): base catalysts.Group-2 (-3.0 ≤ *H*<sub>0</sub> ≤ +6.8): medium strong and weak acid catalysts.Group-3 (-8.2 ≤ *H*<sub>0</sub> ≤ -3.0): strong acid catalysts.Group-4 (*H*<sub>0</sub> ≤ -8.2): very strong acid catalysts.

Presented in Table 2 are the measured basicity (amount) of group-1 catalysts and in Table 3 the acidity of group-2–4 catalysts in the different base or acid strengths.

### 3.1 Catalytic performance

The gas-phase dehydration reaction of glycerol was carried out at 315 °C with a GHSV by glycerol of 80 h<sup>-1</sup>. For most of the catalysts, the glycerol conversion declined more or less with increasing the reaction time-on-stream (TOS) but the formation of acrolein often showed an induction period (2–8 hours). Summarized in Table 4 are the glycerol conversion and acrolein selectivity data at two intervals of TOS = 1–2 h and 9–10 h, the catalysts are grouped according to their acid and base strength defined as above. Several catalysts were able to maintain a 100% glycerol conversion for longer than 10 h. These “key” catalysts were also evaluated by increasing by five fold the space velocity of glycerol, that is at GHSV = 400 h<sup>-1</sup>, and the results are also listed in Table 4 for comparison. While

the induction period for obtaining the steady acrolein selectivity was shortened using the higher GHSV, the steady acrolein selectivity (*i.e.*, at TOS = 8–9 h) was generally little affected by the variation in glycerol conversion after the induction period.

**3.1.1 Solid base catalysts (group-1).** The solid base catalysts in group-1 were characterised by their low selectivity for the production of acrolein and their relatively slow deactivation rates, shown by the difference in glycerol conversion at the two TOS intervals (Table 4). The highest acrolein selectivity obtainable was only 10–13 mol% when La<sub>2</sub>O<sub>3</sub> was the catalyst. For CeO<sub>2</sub> catalyst, the increase of the reactant GHSV to 400 h<sup>-1</sup> to lower the reactant conversion did not improve the acrolein selectivity but resulted in much heavier carbon deposition.

Table 5 gives the product distribution at TOS = 9–10 h over the basic catalysts. The main products identified were 1,2-propanediol (13 mol% by selectivity) and methanol (8 mol% by selectivity) over the CeO<sub>2</sub> catalyst. These two products, however, were not formed over the La<sub>2</sub>O<sub>3</sub> catalyst, over which the formation of acrolein became relatively favored. When MgO was used as the catalyst, the main products identified were 1-hydroxyacetone (21 mol% by selectivity) and methanol (7 mol% by selectivity). Interestingly, when the reaction was conducted with GHSV=400 h<sup>-1</sup> the product distribution over the CeO<sub>2</sub> catalyst changed to resemble that over MgO at GHSV = 80 h<sup>-1</sup>. A high percentage (>60 mol%) of the reaction products over these base catalysts remained unidentified in this work. Also, significant quantities of CO and H<sub>2</sub> (not quantified) were detected in the uncondensed outlet gas, which was especially remarkable in the first few hours of the reaction and might have relation with the formation of the unidentified products, including carbon deposits.

It is therefore clear that solid base catalysts were not effective for the dehydration glycerol for acrolein production. Solid bases are known as effective dehydrogenation catalysts in the reaction of monohydroxyl alcohols;<sup>16</sup> their ineffectiveness for intra-molecular dehydration of glycerol is not surprising. Clacens *et al.*<sup>19</sup> reported that basic mesoporous MCM-41 materials modified with alkali/alkaline or rare earth metal oxides were effective catalysts for the selective formation of polyglycerols in the liquid-phase etherification of glycerol at 260 °C under atmospheric pressure. However, no significant amount of polyglycerols was detected in the reaction systems examined in this present work. This difference might be due to the fact that the formation of polyglycerols became unfavorable at the much higher reaction temperature of the present study (315 °C).

**3.1.2 Solid acid catalysts (group-2, -3 and -4).** The glycerol conversion experienced, in general, a relatively rapid decline with TOS (Table 4) but the acrolein selectivity went through an induction period in the first few hours over each of the acidic catalysts. The 100% glycerol conversion observed over the Al<sub>2</sub>O<sub>3</sub>, SiO<sub>2</sub>–Al<sub>2</sub>O<sub>3</sub>, SO<sub>4</sub><sup>2-</sup>/ZrO<sub>2</sub> and WO<sub>3</sub>/ZrO<sub>2</sub> catalysts for up to TOS = 10 h in the reactions at GHSV = 80 h<sup>-1</sup> was due to insufficient use of the catalysts, as the same catalysts deactivated when the reactant space velocity was increased to GHSV = 400 h<sup>-1</sup>.

**Table 3** Catalyst acidity at different acid strengths

Catalyst	Acidity/mmol g <sup>-1</sup>			Total
	<i>H</i> <sub>0</sub> ≤ -8.2	-8.2 ≤ <i>H</i> <sub>0</sub> ≤ -3.0	-3.0 ≤ <i>H</i> <sub>0</sub> ≤ +6.8	
Group-2				
SiO <sub>2</sub> (SBA-15) <sup>a</sup>	—	—	0.48	0.48
ZrO <sub>2</sub> <sup>a</sup>	—	—	0.10	0.10
Nb <sub>2</sub> O <sub>5</sub> -700	—	—	0.02	0.02
Group-3				
Al <sub>2</sub> O <sub>3</sub> <sup>a</sup>	—	0.42	0.48	0.90
HZSM-5 <sup>a</sup>	—	0.28	0.36	0.64
Nb <sub>2</sub> O <sub>5</sub> -400	—	0.20	0.14	0.34
15 wt%WO <sub>3</sub> /ZrO <sub>2</sub> <sup>b</sup>	—	0.14	0.32	0.46
Nb <sub>2</sub> O <sub>5</sub> -500	—	0.06	0.10	0.16
5 wt%H <sub>3</sub> PO <sub>4</sub> /α-Al <sub>2</sub> O <sub>3</sub> <sup>c</sup>	—	0.01	0.02	0.03
5 wt%H <sub>3</sub> PW <sub>12</sub> O <sub>40</sub> /α-Al <sub>2</sub> O <sub>3</sub> <sup>c</sup>	—	0.01	0.23	0.24
SAPO-34 <sup>a</sup>	—	0.01	0.05	0.06
5 wt%NiSO <sub>4</sub> /α-Al <sub>2</sub> O <sub>3</sub> <sup>c</sup>	—	0.005	0.025	0.03
Group-4				
5 wt%SO <sub>4</sub> <sup>2-</sup> /ZrO <sub>2</sub> <sup>d</sup>	0.42	0.08	0.18	0.68
SiO <sub>2</sub> –Al <sub>2</sub> O <sub>3</sub> <sup>a</sup>	0.12	0.44	0.20	0.76
Hβ <sup>a</sup>	0.06	0.70	0.30	1.06
Nb <sub>2</sub> O <sub>5</sub> -350	0.04	0.28	0.20	0.52

<sup>a</sup> Calcination temperature: 500 °C. <sup>b</sup> Calcination temperature: 900 °C.<sup>c</sup> Pretreated at 315 °C for 4 h in flowing dry nitrogen. <sup>d</sup> Calcination temperature: 600 °C.

**Table 4** Catalytic performance of solid acid–base catalysts for the gas-phase dehydration of glycerol at 315 °C and glycerol GHSV = 80 h<sup>−1</sup>

Catalyst (0.63 ml)	Catalyst amount/g	TOS = 1–2 h		TOS = 9–10 h		Carbon deposits <sup>c</sup> /mg g-cat <sup>−1</sup>
		X <sup>a</sup> (%)	S <sup>b</sup> (mol%)	X <sup>a</sup> (%)	S <sup>b</sup> (mol%)	
Group-1						
CeO <sub>2</sub>	0.90	100	1	100	1	11
CeO <sub>2</sub> <sup>d</sup>	0.90	96	1	86	1	43
La <sub>2</sub> O <sub>3</sub>	1.06	100	10	100	13	25
MgO	0.36	50	5	40	5	50
Group-2						
SiO <sub>2</sub> (SBA-15)	0.15	71	29	31	30	30
ZrO <sub>2</sub>	0.81	100	1	100	7	31
Nb <sub>2</sub> O <sub>5</sub> -700	0.84	40	26	32	28	4
Group-3						
Al <sub>2</sub> O <sub>3</sub>	0.23	100	16	100	30	384
Al <sub>2</sub> O <sub>3</sub> <sup>d</sup>	0.23	86	36	70	38	309
HZSM-5	0.38	80	36	23	52	54
Nb <sub>2</sub> O <sub>5</sub> -400	0.57	100	37	88	51	108
15 wt% WO <sub>3</sub> /ZrO <sub>2</sub>	0.71	100	48	100	65	82
15 wt% WO <sub>3</sub> /ZrO <sub>2</sub> <sup>d</sup>	0.71	68	66	23	68	88
Nb <sub>2</sub> O <sub>5</sub> -500	0.61	100	29	92	35	74
5 wt% H <sub>3</sub> PO <sub>4</sub> /α-Al <sub>2</sub> O <sub>3</sub>	0.63	81	55	50	59	16
5 wt% H <sub>3</sub> PW <sub>12</sub> O <sub>40</sub> /α-Al <sub>2</sub> O <sub>3</sub>	0.75	69	68	25	70	23
SAPO-34	0.40	55	34	32	48	201
5 wt% NiSO <sub>4</sub> /α-Al <sub>2</sub> O <sub>3</sub>	0.71	87	58	49	63	3
Group-4						
5 wt% SO <sub>4</sub> <sup>2−</sup> /ZrO <sub>2</sub>	0.71	100	2	100	20	189
5 wt% SO <sub>4</sub> <sup>2−</sup> /ZrO <sub>2</sub> <sup>d</sup>	0.71	80	30	64	33	179
SiO <sub>2</sub> –Al <sub>2</sub> O <sub>3</sub>	0.20	100	23	100	40	431
SiO <sub>2</sub> –Al <sub>2</sub> O <sub>3</sub> <sup>d</sup>	0.20	94	43	75	46	375
Hβ	0.23	95	34	60	43	214
Nb <sub>2</sub> O <sub>5</sub> -350	0.57	96	33	75	47	117

<sup>a</sup> Glycerol conversion. <sup>b</sup> Selectivity for acrolein. <sup>c</sup> After the catalyst was reacted for 10 h. <sup>d</sup> The catalytic data were obtained at glycerol GHSV = 400 h<sup>−1</sup>.

Listed in Table 6 are the product distribution at TOS = 9–10 h over the acidic catalysts. The main product of the glycerol dehydration reaction was acrolein over the solid acid catalysts (in group-2, -3, and -4), except for ZrO<sub>2</sub> where 1-hydroxyacetone and acetaldehyde appeared as the main by-products. 1,2-Propandiol and methanol, which were formed in significant amounts over basic MgO and CeO<sub>2</sub> catalysts (Table 5), were hardly detected (<1 mol% by selectivity). Also, the amount of CO and H<sub>2</sub> detected in the uncondensed outlet gas was significantly less than that detected when the solid bases (group-1) were used as the catalysts.

With only a couple of exceptions, the strong acid catalysts in group-3, which have strongest acid strength at  $-8.2 \leq H_0 \leq -3.0$ , generally showed the highest acrolein selectivity, while the medium strong and weak acid catalysts in group-2, with acid strength at  $-3.0 \leq H_0 \leq +6.8$ , showed the lowest selectivity for the production of acrolein. The acrolein

selectivity over the very strong acid catalysts in group-4 was between those over the group-2 and -3 catalysts.

It might be possible that the very different glycerol conversions could make comparison of the acrolein selectivity unreliable. This possibility can almost be excluded when the catalytic data at GHSV = 80 h<sup>−1</sup> were compared with that at GHSV = 400 h<sup>−1</sup> for Al<sub>2</sub>O<sub>3</sub>, 15% WO<sub>3</sub>/ZrO<sub>2</sub> and SiO<sub>2</sub>–Al<sub>2</sub>O<sub>3</sub> catalysts at TOS = 9–10 h (Table 6) because acrolein selectivity over each of these catalysts did not vary significantly, *e.g.*, 65% *versus* 68% over 15% WO<sub>3</sub>/ZrO<sub>2</sub> and 40% *versus* 46% over SiO<sub>2</sub>–Al<sub>2</sub>O<sub>3</sub> catalyst, although the glycerol conversion was reduced remarkably due to the five-fold increase in the reactant GHSV (Table 6). Therefore, a distinct feature of the acid catalysts for the glycerol dehydration reaction is that after being stabilized in the induction period, the catalytic selectivity for acrolein production becomes insensitive to the conversion level of the glycerol reactant.

**Table 5** Product distribution at 315 °C and glycerol GHSV = 80 h<sup>−1</sup> over the investigated solid base catalysts

Catalyst (0.63 ml)	Conversion (%)	Product selectivity at TOS = 9–10 h (mol%)					
		Acrolein	Acetaldehyde	Allyl alcohol	1-Hydroxyl-acetone	Methanol	1,2-Propandiol
Group-1							
CeO <sub>2</sub>	100	1	6	2	3	8	13
CeO <sub>2</sub> <sup>b</sup>	86	1	4	—	21	4	2
La <sub>2</sub> O <sub>3</sub>	100	13	6	—	10	—	—
MgO	40	5	5	—	21	7	2

<sup>a</sup> Selectivity for the unknowns (mol%) = 100 – total selectivity for all identified products. <sup>b</sup> The catalytic data were obtained at glycerol GHSV = 400 h<sup>−1</sup>.

**Table 6** Product distribution at 315 °C and glycerol GHSV = 80 h<sup>-1</sup> over the investigated solid acid catalysts

Catalyst (0.63 ml)	Conversion (%)	Product selectivity at TOS = 9–10 h (mol%)				
		Acrolein	Acetaldehyde	Allyl alcohol	1-Hydroxyacetone	Unknowns <sup>a</sup>
Group-2						
SiO <sub>2</sub> (SBA-15)	31	30	3	2	10	55
ZrO <sub>2</sub> <sup>b</sup>	100	7	6	2	21	64
Nb <sub>2</sub> O <sub>5</sub> -700	32	28	2	5	19	46
Group-3						
Al <sub>2</sub> O <sub>3</sub>	100	30	8	6	12	44
Al <sub>2</sub> O <sub>3</sub> <sup>c</sup>	70	38	6	3	17	36
HZSM-5	23	52	3	2	7	36
Nb <sub>2</sub> O <sub>5</sub> -400	88	51	4	1	12	32
15 wt% WO <sub>3</sub> /ZrO <sub>2</sub>	100	65	3	—	5	27
15 wt% WO <sub>3</sub> /ZrO <sub>2</sub> <sup>c</sup>	23	68	2	1	15	14
Nb <sub>2</sub> O <sub>5</sub> -500	92	35	5	2	14	44
5 wt% H <sub>3</sub> PO <sub>4</sub> /α-Al <sub>2</sub> O <sub>3</sub>	50	59	1	3	14	23
5 wt% H <sub>3</sub> PW <sub>12</sub> O <sub>40</sub> /α-Al <sub>2</sub> O <sub>3</sub>	25	70	2	—	7	21
SAPO-34	32	48	4	2	11	35
5 wt% NiSO <sub>4</sub> /α-Al <sub>2</sub> O <sub>3</sub>	49	63	3	1	13	20
Group-4						
5 wt% SO <sub>4</sub> <sup>2-</sup> /ZrO <sub>2</sub>	100	20	9	2	10	59
5 wt% SO <sub>4</sub> <sup>2-</sup> /ZrO <sub>2</sub> <sup>c</sup>	64	33	7	2	16	42
SiO <sub>2</sub> -Al <sub>2</sub> O <sub>3</sub>	100	40	10	1	12	37
SiO <sub>2</sub> -Al <sub>2</sub> O <sub>3</sub> <sup>c</sup>	75	46	10	—	10	34
Hβ	60	43	8	2	7	40
Nb <sub>2</sub> O <sub>5</sub> -350	75	47	5	1	10	37

<sup>a</sup> Selectivity for unknowns (mol%) = 100 – total selectivity for all identified products <sup>b</sup> Methanol (3 mol%) and 1,2-propandiol (8 mol%) were also present in the product over this catalyst. <sup>c</sup> The catalytic data were obtained at glycerol GHSV = 400 h<sup>-1</sup>.

Another feature disclosed in the present work is that the amount of carbon deposits on the used catalysts (except Al<sub>2</sub>O<sub>3</sub> and SAPO-34) generally increased with increasing the catalyst acid strength. Interestingly, the reaction at GHSV = 400 h<sup>-1</sup> (over Al<sub>2</sub>O<sub>3</sub>, 15% WO<sub>3</sub>/ZrO<sub>2</sub> and SiO<sub>2</sub>-Al<sub>2</sub>O<sub>3</sub> catalysts) did not resulted in more severe carbon deposition over the catalysts when compared with the reaction at GHSV = 80 h<sup>-1</sup>.

### 3.2 Catalyst acid–base property and performance in glycerol dehydration

All catalysts investigated in this work are listed in Fig. 1 according to their acid–base strength and steady acrolein selectivity. Apparently, the strongly acidic catalysts in group-3 and -4 with  $H_0 \leq -3.0$  showed higher acrolein selectivity than those catalysts with weaker acidity, indicating that the intramolecular double dehydration of glycerol for acrolein production requires the participation of acidic sites with  $H_0 \leq -3.0$ . However, the generally highest acrolein selectivity obtained over the strong acid catalysts in group-3 ( $-8.2 \leq H_0 \leq -3.0$ ) would suggest that the most favorable acid strength for the acrolein production is  $-8.2 \leq H_0 \leq -3.0$ .

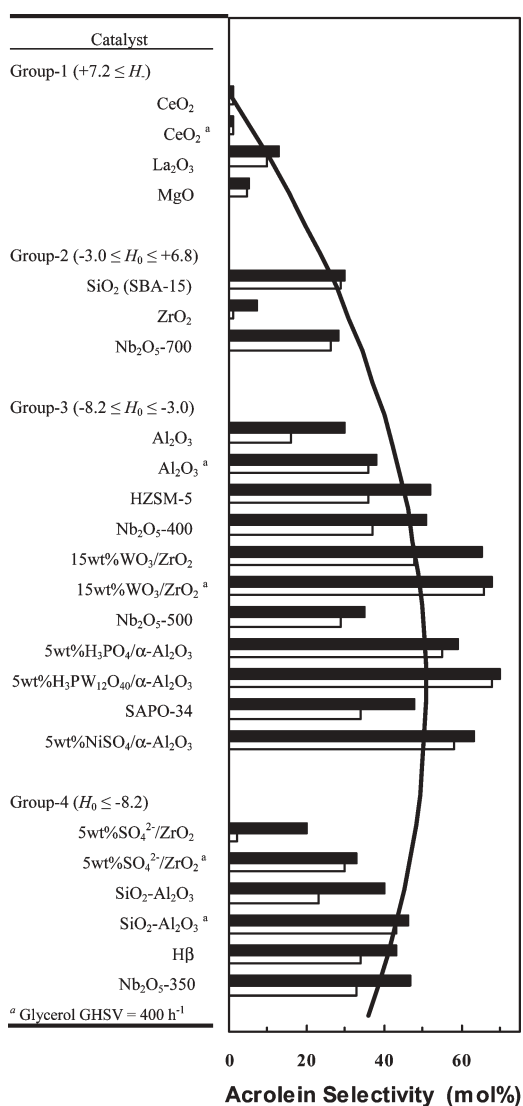
An attempt was made to correlate the catalytic rates at TOS = 9–10 h for glycerol consumption and acrolein formation with the fractional acidity at  $-8.2 \leq H_0 \leq -3.0$ . The average catalytic rates over a single acid site at  $-8.2 \leq H_0 \leq +6.8$  (i.e., TOF) show no clear relationship with the fractional acidity at  $-8.2 \leq H_0 \leq -3.0$ , which could be distorted significantly due to the severe coking on the catalysts.

We then attempted to correlate the catalytic rates based on the catalyst mass with the catalyst acidity, to avoid the disturbance of carbon deposits. As shown in Fig. 2, both of the catalyst mass specific rates for glycerol consumption and for

acrolein production tend to increase with the fractional acidity at  $-8.2 \leq H_0 \leq -3.0$ , which further suggest that the strongly acidic sites at  $-8.2 \leq H_0 \leq -3.0$  are more efficient than those of medium strong and weak acid sites.

The observation that catalysts with a stronger acidity tend to coke more severely than catalysts with a weaker acidity (Table 4) could hint that acrolein molecules formed over the very strong acid catalysts ( $H_0 \leq -8.2$ , group-4) are easily subject to secondary reactions leading to surface carbon deposits. To demonstrate such a possibility, an aqueous acrolein solution was reacted over a fresh SiO<sub>2</sub>-Al<sub>2</sub>O<sub>3</sub> catalyst with the conditions for the glycerol dehydration. The reactant acrolein in the reaction feed was completely converted in the first couple of hours, but the acrolein conversion declined to ca. 40% at TOS = 6 h. The reaction of acrolein appeared very “selective” for the formation of carbon deposits, since almost no product was detected in the condensed liquid at the reactor outlet. Another reaction test was done by adding acrolein to the regular reaction feed (acrolein/glycerol molar ratio being 1.0), this reaction test resulted in a negative formation of acrolein and significantly enhanced deactivation of the catalyst. Therefore, in comparison with the very strong acid catalysts in group-4, the strong acid catalysts in group-3 offer the higher selectivity for acrolein production because their catalytic acid sites of  $-8.2 \leq H_0 \leq -3.0$  were less effective in inducing the secondary reaction of acrolein.

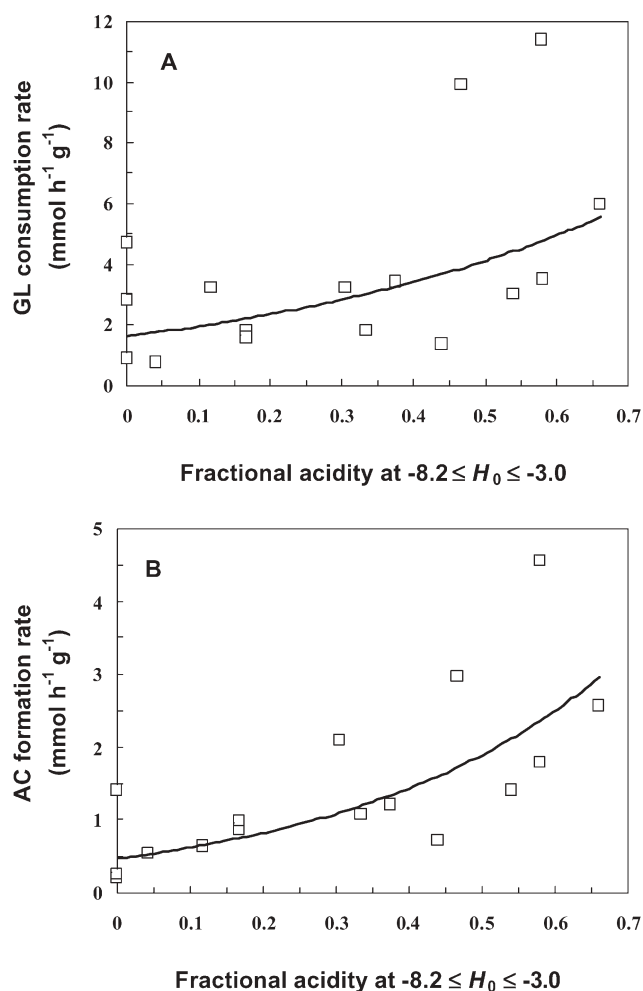
It seems not surprising that the catalyst acidity requirement ( $-8.2 \leq H_0 \leq -3.0$ ) for efficient acrolein production from glycerol is similar to the case of ethanol production from ethylene hydration over solid acid catalysts.<sup>16</sup> A main by-product in the present reaction system was 1-hydroxyacetone, which is a product from a single dehydration of glycerol (Scheme 1). However, the selectivity of this by-product



**Fig. 1** Catalyst highest acid–base strength ( $H_0$  or  $H_-$ ) and acrolein selectivity obtained at TOS = 1–2 h (open columns) and 9–10 h (solid columns). Reaction temperature: 315 °C, glycerol GHSV: 80 h<sup>-1</sup>.

(10–20 mol% in most cases) was not significantly affected (Tables 5 and 6) by the acid–base property of the catalysts investigated in this present study.

Besides acid strength, the nature of acid sites (Brønsted or Lewis type) would play a key role in determining catalytic performance for solid acid catalysts. Among the strong acid catalysts in group-3 ( $-8.2 \leq H_0 \leq -3.0$ ), Al<sub>2</sub>O<sub>3</sub> and Nb<sub>2</sub>O<sub>5</sub>-500 can be taken as typical Lewis acid catalysts;<sup>16</sup> they both showed a poor steady selectivity (<40 mol%) for the acrolein production. The supported phosphoric acid (5% H<sub>3</sub>PO<sub>4</sub>/α-Al<sub>2</sub>O<sub>3</sub>) and heteropoly acid (5% H<sub>3</sub>PW<sub>12</sub>O<sub>40</sub>/α-Al<sub>2</sub>O<sub>3</sub>) are typical Brønsted acids, and they both effected high acrolein selectivity (60–70 mol%). The 5% NiSO<sub>4</sub>/α-Al<sub>2</sub>O<sub>3</sub> and 15 wt% WO<sub>3</sub>/ZrO<sub>2</sub> catalysts would have both Brønsted and Lewis sites,<sup>20,21</sup> and they also both showed a high selectivity (ca. 65 mol%) for the acrolein production. Therefore, in view of the selectivity for the production of acrolein, Brønsted acid sites seem to be superior to Lewis acid sites for the glycerol dehydration reaction. It is likely that the large amount of water



**Fig. 2** Catalyst fractional acidity at  $-8.2 \leq H_0 \leq -3.0$  and mass specific catalytic rates for glycerol consumption (A) and acrolein formation (B) at TOS = 9–10 h. Reaction temperature: 315 °C, glycerol GHSV: 80 h<sup>-1</sup>.

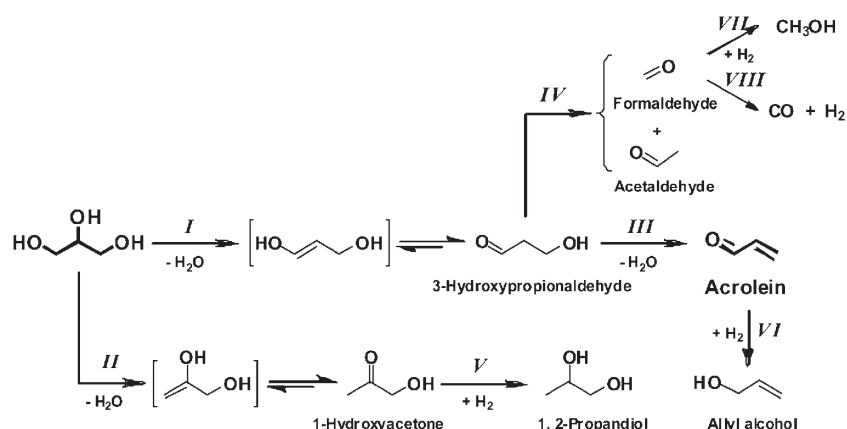
in the present reaction system (the molar water-to-glycerol ratio was 9) could convert at least some Lewis acid sites to Brønsted acid sites,<sup>22</sup> which could in turn induce some acrolein selectivity over the seemingly termed Lewis acid catalysts.

The microporous molecular sieves, such as HZSM-5 and HSAPO-34, are also Brønsted acid catalysts.<sup>23</sup> The relatively low acrolein selectivity (ca. 50 mol%) and glycerol conversion over these catalysts were not proportional to their acidity, which might be a consequence of micro-pore blockage by the carbon deposits during the reaction.

### 3.3 Possible reactions involved in the dehydration of glycerol

Possible reactions involved in the gas-phase dehydration of glycerol are proposed in Scheme 1 based on the products identified in this work. The reaction of glycerol would be initiated by the dehydration involving either the central –OH (step I) or terminal –OH (step II), which result in parallel formation of two enol intermediates. The enols would undergo rapid rearrangement to 3-hydroxypropionaldehyde (3-HPA) or 1-hydroxyacetone, respectively. The 3-HPA, which is often assumed as the reactive intermediate in acrolein synthesis by





**Scheme 1** Reactions leading to the detected products in the glycerol dehydration over solid acid–base catalysts.

aldol condensation reaction of acetaldehyde with formaldehyde,<sup>24,25</sup> would be very unstable at the reaction temperature (315 °C) and can easily give rise to a further dehydration for the production of the desirable acrolein (step III). A secondary hydrogenation reaction of the acrolein product will lead to the formation of allyl alcohol (step VI). The unstable intermediate 3-HPA would also decompose, according to a reversed aldol condensation (step IV), to acetaldehyde and formaldehyde; a follow up hydrogenation or decomposition of formaldehyde would result in met the formation of methanol or CO and H<sub>2</sub> (steps VII and VIII). It seems that hydrogenation of the carbonyl group in 1-hydroxyacetone (step V), which produced 1,2-propandiol, was only possible when the solid bases in group-I were used as the catalysts (Table 5).

No attempt was made in this work to understand side reactions leading to unidentified products including coke on the catalyst. The formation of the unidentified products could involve many complicated side reactions, which would deserve an independent piece of comprehensive research in the future. For example, acrolein itself could be converted to many heavier products including higher aldehydes, olefins, heterocyclic and/or aromatic compounds by a complex reaction network including the reductive coupling, aldol condensation, Diels–Alder reaction, dehydration, and dehydrogenation as well as hydrogenation.<sup>26,27</sup>

## 4. Conclusions

The present data shows that the most selective acid–base catalysts for the production of acrolein by gas-phase glycerol dehydration are those having the strongest acid strength in the range of  $-8.2 \leq H_0 \leq -3.0$ ; the highest steady acrolein selectivity obtained was 70 mol%. The catalysts having further stronger acid sites ( $H_0 \leq -8.2$ ) produce a lower acrolein selectivity (40–50 mol%) due to more severe catalyst coking. The mass specific catalytic rate for the acrolein production tends to increase with the fractional acidity at  $-8.2 \leq H_0 \leq -3.0$ . Brønsted acid sites seem to be superior to Lewis acid sites for the acrolein production. Solid base catalysts are basically not effective for the formation of acrolein.

## References

- D. L. Klass, *Biomass for Renewable Energy, Fuels and Chemicals*, Academic Press, San Diego, 1998.
- H. Van Bakkum and P. Gallezot, *Top. Catal.*, 2004, **27**, 1–2.
- G. W. Huber and J. A. Dumesic, *Catal. Today*, 2006, **111**, 119–132.
- H. S. Kesling, L. J. Karas and F. J. Liotta, *US Pat.*, 5 308 365, 1994.
- D. S. Bradin, *US Pat.*, 5 578 090, 1996.
- H. P. A. Groll, Okaland and G. Hearne, *US Pat.*, 2 042 224, 1936.
- S. Ramayya, A. Brittain, C. DeAlmeida, W. Mok and M. J. Antal, *Fuel*, 1987, **66**, 1364–1371.
- M. J. Antal, Jr., W. S. L. Mok and G. N. Richards, *Carbohydr. Res.*, 1990, **199**, 111–115.
- L. Ott, M. Bicker and H. Vogel, *Green Chem.*, 2006, **8**, 214–220.
- H. Adkins and W. H. Hartung, *Org. Synth., Coll. Vol. 1*, 1941, 15–18.
- A. Neher, T. Haas, D. Arntz, H. Klenk and W. Girke, *US Pat.*, 5 387 720, 1995.
- A. G. Scheering-Kahlbaum, *Fr. Pat.* 695 931, 1930.
- J. Song, H. Wang and B.-Q. Xu, *Chin. J. Catal.*, 2004, **25**, 599–601.
- B.-Q. Xu, J.-M. Wei, Y.-T. Yu, J.-L. Li and Q.-M. Zhu, *Top. Catal.*, 2003, **22**, 77–85.
- B.-Q. Xu, J.-M. Wei, Y.-T. Yu, Y. Li, J.-L. Li and Q.-M. Zhu, *J. Phys. Chem. B*, 2003, **107**, 5203–5207.
- K. Tanabe, M. Misono, Y. Ono and H. Hattori, *New Solid Acids and Bases: Their Catalytic Properties*, Kodansha, Tokyo and Elsevier, Amsterdam, 1989, pp. 247–254 and 260–272.
- H. A. Benesi, *J. Am. Chem. Soc.*, 1956, **78**, 5490–5494.
- H. A. Benesi, *J. Phy. Chem.*, 1957, **61**, 970–973.
- J.-M. Clacens, Y. Pouilloux and J. Barrault, *Appl. Catal., A*, 2002, **227**, 181–190.
- H. Hattori, S. Miyashita and K. Tanabe, *Bull. Chem. Soc. Jpn.*, 1971, **44**, 893–895.
- J. Macht, C. D. Baertsch, M. May-Lozano, S. L. Soled, Y. Wang and E. Iglesia, *J. Catal.*, 2004, **227**, 479–491.
- M. Caus, in *Handbook of Heterogeneous Catalysis*, ed. G. Ertl, H. Knözinger and J. Weitkamp, VCH, Weinheim, 1997, vol. 5, pp. 2370–2380.
- P. Espeel, R. Parton, H. Toufar, J. Martens, W. Holderich and P. Jacobs, in *Catalysis and Zeolites: Fundamentals and Applications*, ed. J. Weitkamp and L. Puppe, Springer-Verlag, Berlin Heidelberg, Germany, 1999, pp. 393–396.
- E. Dumitriu, N. Bilba, M. Lupascu, A. Azzouz, V. Hulea, G. Cirje and D. Nibou, *J. Catal.*, 1994, **147**, 133–139.
- M. Ai, *Bull. Chem. Soc. Jpn.*, 1991, **64**, 1342–1345.
- A. B. Sherrill, h. Idriss, M. A. Barteau and J. G. Chen, *Catal Today*, 2003, **85**, 321–331.
- C. P. Bezouhanova, C. V. Titorenkova and C. Chanev, *J. Mol. Catal. A: Chem.*, 1998, **132**, 87–90.

# An efficient microwave-assisted green transformation of cellulose into levoglucosenone. Advantages of the use of an experimental design approach†

Ariel M. Sarotti, Rolando A. Spanevello and Alejandra G. Suárez\*

Received 12th March 2007, Accepted 25th June 2007

First published as an Advance Article on the web 11th July 2007

DOI: 10.1039/b703690f

The microwave-assisted pyrolysis of cellulose towards its conversion into levoglucosenone is reported. An experimental design approach was used to find the variables involved in this transformation. Using this approach we established the optimal conditions to obtain the maximum yield of product.

## Introduction

Biomass is a widely available raw material which has been recognized as an important source of fuels and chemical products.<sup>1</sup> A substantial amount of research activity is currently undertaken world-wide to identify attractive chemical transformations to convert biomass into highly valuable organic chemicals. By far, carbohydrates are the major annually renewable biofeedstocks from which to develop viable organic chemicals that can compete with or eventually replace those derived from fossil sources.<sup>2</sup> Apart from being more accessible, carbohydrates have many other advantages like functionality, chirality, and structural variation, all features that are not present in petroleum.

Levoglucosenone (1,6-anhydro-3,4-dideoxy- $\beta$ -D-glycero-hex-3-enopyranos-2-ulose) (**1**) is a versatile and readily available member of the carbohydrate derived chiral pool. During the last decade this substrate has been employed as chiral synthon for the synthesis of a wide variety of natural and unnatural products.<sup>3–5</sup> Recently, it was also used as template in the preparation of chiral inductors for asymmetric organic synthesis.<sup>6</sup>

The conventional pyrolysis of cellulose is one of the most frequently used transformations to obtain levoglucosenone as it provides a simple methodology to obtain enantiomerically pure materials.<sup>3,7</sup>

In the last decade, the use of microwave irradiation to accelerate organic reactions has been of growing interest as a type of environmentally friendly process, particularly when it is carried out under solvent-free conditions. One key advantage of using microwaves is the flash heating effect, which often leads to much reduced reaction times, from hours down to minutes.<sup>8</sup> To make the most of this feature, it is essential to

follow an efficient optimisation protocol to rapidly identify the best conditions for the microwave-assisted reaction.<sup>9</sup>

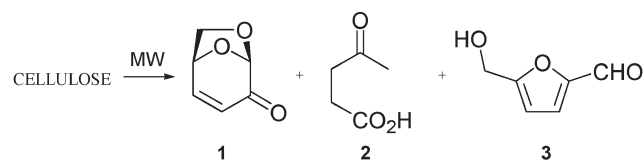
In this study we present the microwave-assisted pyrolysis of cellulose for the production of levoglucosenone under solvent-free conditions. In the course of our studies we found that the use of an experimental design approach allowed the efficient determination of the optimal conditions for microwave-assisted pyrolysis.

## Results and discussion

The conventional pyrolysis of acid pre-treated cellulose in an electrical furnace at 270 °C affords levoglucosenone in 3–5% overall yield. The crude material is generally found with 2-furfuraldehyde as the major impurity.<sup>3,7</sup> Our interest to find a greener procedure to obtain this valuable chiral starting material encouraged us to investigate a microwave-assisted protocol for this reaction to provide the desired product in acceptable yields.

As a starting point for the development of a microwave-assisted methodology we performed the pyrolysis of acid pre-treated cellulose (4.0 g) at 490 W in a household oven over 6.0 min. The condensed crude material obtained was 2.1% of the amount of cellulose pyrolyzed. The analysis of this pyrolytic crude material by <sup>1</sup>H NMR and GC-MS demonstrated that it was formed almost quantitatively by a mixture of levoglucosenone (**1**), levulinic acid (**2**) and 5-hydroxymethylfurfuraldehyde (**3**) in a ratio 92 : 6 : 2 respectively, Scheme 1.

It has been already studied in depth that 5-hydroxymethylfurfuraldehyde decomposed to levulinic acid under acid catalysed conditions.<sup>10</sup> For this reason we considered that the formation of **2** arose from the transformation of **3** under the pyrolytic conditions employed.



Scheme 1

Instituto de Química Orgánica de Síntesis, Facultad de Ciencias Bioquímicas y Farmacéuticas, Universidad Nacional de Rosario – CONICET Suipacha 531, S2002LRK Rosario, Argentina.  
E-mail: asuarez@fbioyf.unr.edu.ar; Fax: 54 341 4370477;  
Tel: 54 341 4370477

† Electronic supplementary information (ESI) available: <sup>1</sup>H NMR spectra of a crude mixture of the pyrolytic product and GC-chromatogram of a crude mixture of the pyrolytic product. See DOI: 10.1039/b703690f

We used the Design-Expert<sup>TM</sup> software to design a set of screening reaction conditions to determine the factors which could have a significant effect on the outcome of the reaction.<sup>11</sup>

It was noted that heat transfer is an important parameter in the pyrolysis of cellulose with conventional heating. Under this condition an inverse relationship between the yield and the sample size was generally found, which was attributed to the poor heat transfer of the substrate.<sup>7b</sup> Therefore, the amount of material to be pyrolyzed and the heat exchange surface is always crucial for the outcome of the reaction. Due to the difference in the microwave heating process, we decided to investigate two different methodologies to treat the sample into the oven. The cellulose was loaded into a glass tube as a thick layer (method X) or spread as a thin layer in an Erlenmeyer (method Y).

It is well known that pyrolysis of cellulose involves a complex series of concurrent and consecutive reactions that afford a variety of products.<sup>7b</sup> For this reason, we considered the different parameters that can affect the yield and purity of levoglucosenone in a microwave-assisted pyrolytic process.

The factors we decided to investigate were: power of microwave irradiation (400–490 W), time of applied irradiation (10–20 min), cellulose mass (4–6 g) and the methodology to carry out the pyrolysis (method X or Y). We employed a full two-level factorial design giving 16 experiments. Table 1 shows the coded selected levels for each factor and the response obtained. The signs + and – are the codification of higher and lower levels.

After these experiments were performed, the application of analysis of variance (ANOVA) allowed us to draw conclusions about the significance of the factors studied. The evidence is

**Table 1** Full two-level factorial design used to evaluate the most important factors for the microwave pyrolysis of cellulose

					Level			
Factor					−1	+1		
A: microwave power/W					400	490		
B: irradiation time/min					10.0	20.0		
C: cellulose mass/g					4.0	6.0		
D: pyrolysis method					Method X	Method Y		
Exp.	A	B	C	D	Yield (%) <sup>a</sup>	1 (%) <sup>b</sup>	2 (%) <sup>b</sup>	3 (%) <sup>b</sup>
1	1	−1	−1	−1	4.85	87.3	10.1	2.6
2	−1	−1	−1	−1	2.86	86.4	11.1	2.5
3	1	−1	−1	1	2.01	85.3	10.5	4.2
4	1	−1	1	−1	5.76	86.8	10.5	2.6
5	−1	1	−1	−1	3.77	85.4	12.1	2.5
6	1	−1	1	1	2.30	86.5	10.2	3.3
7	1	1	−1	−1	3.35	89.0	7.6	3.5
8	−1	1	1	1	1.51	84.1	11.8	4.1
9	−1	1	1	−1	4.80	88.0	10.4	1.6
10	−1	1	−1	1	1.66	82.6	12.6	4.8
11	−1	−1	−1	1	0.06	84.1	8.4	7.5
12	1	1	1	−1	4.50	85.3	12.3	2.5
13	−1	−1	1	−1	4.15	87.6	9.8	2.6
14	1	1	1	1	1.86	80.9	16.0	3.2
15	−1	−1	1	1	0.58	84.1	8.4	7.5
16	1	1	−1	1	2.02	88.2	8.3	3.4

<sup>a</sup> Yield corresponds to the weight of pyrolyzed material from cellulose.

<sup>b</sup> Relative proportions of 1, 2 and 3 in the crude pyrolyzate.

<sup>a</sup> Yield corresponds to the weight of pyrolyzed material from cellulose. <sup>b</sup> Relative proportions of 1, 2 and 3 in the crude pyrolyzate.

**Table 2** Results obtained by applying ANOVA of the selected most significant factors for the microwave pyrolysis of cellulose

Studied factor	Effect	Sum of mean squares	F test	Value of <i>p</i>	Significant <sup>a</sup>
A	0.72	1.04	78.25	0.0030	Yes
B	–0.3	0.18	13.58	0.0346	Yes
C	1.10	2.40	180.98	0.0009	Yes
AB	–1.08	2.33	176.06	0.0009	Yes

<sup>a</sup> The factor was considered significant when the associated probability (*p*) is <0.05.

based on the probability that differences in response, due to the changes introduced by the effects, are greater than the differences that could be expected from random errors. An analysis of the main effects obtained from the results in Table 1 showed that the most important factor was D, being that method X is the one that gives the best yields. The other three factors (A, B, C) were much less significant.

Due to the fact that there was a very important difference in the results by changing the methodology, the eight runs carried out with method Y were excluded, while the other three main factors (A, B, C) were considered and two-factor interactions were evaluated.

In this reduced model, the results of the analysis of variance are shown in Table 2. It was observed that the three factors were significant (*p* < 0.05) and we also found a very important interaction between power and time (AB interaction).

The results of the analysis of variance demonstrates that the value of power and mass should be set at high levels to achieve better yields of levoglucosenone (positive effect of factors A and C). On the other hand, the negative effect of factor B means that a low irradiation time should be preferred. It can be noted in Table 2 that a negative sign affects the interaction between AB factors, which indicates that high power combined with low time should increase the yield of pyrolyzed material. As a result of this analysis, the following pre-optimal working conditions were chosen, Table 3.

After selecting the most significant factors, another optimisation step was undertaken. This was done by applying a surface response methodology to find the optimum combination of factors evaluated. Using a central composite design the microwave-assisted pyrolysis of microcrystalline cellulose was evaluated by a three-factor design with five levels for each factor. In this case, the design requires fourteen experiments plus three in the middle, which were performed in duplicate and were randomly run. The three extra experiments were included to have an estimation of the response in the center of the design. The selected parameters were microwave power (A), irradiation time (B) and cellulose mass (C). Table 4

**Table 3** Results obtained by applying ANOVA of the selected most significant factors for the microwave pyrolysis of cellulose

Studied factor	Level		Pre-optimal
	–1	+1	
A: microwave power/W	400	490	490
B: irradiation time/min	10.0	20.0	10.0
C: cellulose mass/g	4.0	6.0	6.0
D: pyrolysis method	Method X	Method Y	Method X

**Table 4** Central composite design

				Level				
Factor				−1.68	−1	0	1	+1.68
A: microwave power/W				460	490	540	590	620
B: irradiation time/min				1.6	5.0	10.0	15.0	18.4
C: cellulose mass/g				3.0	4.0	5.5	7.0	8.0
Exp.	A	B	C	Yield (%)	1 (%)	2 (%)	3 (%)	
1	−1.68	0	0	5.60	86.1	11.3	2.6	
2	−1	−1	1	5.26	88.8	8.6	2.6	
3	0	0	0	5.09	86.4	11.1	2.5	
4	−1	1	1	6.16	86.7	10.8	2.5	
5	0	0	−1.68	3.67	85.0	12.5	2.5	
6	1	1	−1	6.05	85.9	10.8	3.3	
7	0	0	1.68	6.32	84.5	12.2	3.3	
8	0	−1.68	0	1.25	93.3	2.1	4.6	
9	−1	1	−1	4.71	86.6	11.7	1.7	
10	0	1.68	0	4.62	84.4	11.1	2.5	
11	1	−1	1	4.41	90.5	7.8	1.7	
12	1.68	0	0	5.70	86.1	10.6	3.3	
13	−1	−1	−1	1.28	90.1	8.1	1.8	
14	0	0	0	4.27	87.8	9.7	2.5	
15	0	0	0	4.46	86.2	11.2	2.5	
16	1	1	1	3.70	81.8	15.0	3.2	
17	1	−1	−1	4.83	88.7	8.7	2.6	

lists the design matrix for experiments and the values given to each factor.

The design allowed us to obtain the surface response, fitting the data to the polynomial mathematical model by the linear least-square application shown in the following equation:

$$\xi = b_0 + b_1A + b_2B + b_3C + b_{11}A^2 + b_{22}B^2 + b_{33}C^2 + b_{12}AB + b_{13}AC + b_{23}BC$$

Where  $\xi$  is the response,  $b_0$  is the center point of the system,  $b_i$ ,  $b_{ij}$  and  $b_{ij}$  correspond to coefficients of linear, quadratic and interactive effects respectively.

The regression coefficients and their statistical significance are presented in Table 5.

Analysis of variance indicates that the response models developed for yield, and percentages of **1** and **2**, have a very good fit. However, the model for the percentage of **3** has a poor correlation ( $R^2 = 0.45$ ), which could indicate that the amount of **3** in the crude pyrolyzate is random and has no dependence on the factors studied.

**Table 5** Regression coefficients in terms of coded factors of the model developed for yield and percentage of **1**, **2** and **3** in the mixture

$\xi$	Yield	1	2	3
$b_0$	4.60	86.76	10.67	2.54
$b_1$	0.13	−0.40	0.13	0.27
$b_2$	0.77	−2.34	2.20	−0.11
$b_3$	0.52	−0.32	0.19	0.14
$b_{11}$	0.37	−0.06	0.16	−0.01
$b_{22}$	−0.59	0.90	−1.39	0.22
$b_{33}$	0.14	−0.53	0.64	−0.03
$b_{12}$	−0.48	−0.73	0.44	0.29
$b_{13}$	−1.03	−0.14	0.47	−0.32
$b_{23}$	−0.56	−0.56	0.47	0.09
$F$	14.82	6.28	8.00	0.64
$p$	0.0009	0.0121	0.0060	0.7407
$R^2$	0.95	0.89	0.91	0.45

**Table 6** Regression coefficients in term of coded factors

Predicted		
Yield (%)	1 (%)	2 (%)
7.33	84.9	11.8
Observed		
Yield (%)	1 (%)	2 (%)
7.57	86.4	11.1
7.65	86.5	10.9
7.36	86.2	11.3

**Table 7** Microwave pyrolysis of cellulose (4 g) at 620 W over 12 min

Oven	Yield (%)	1 (%)	2 (%)	3 (%)
MW-1	7.53	86.4	11.1	2.5
MW-2	7.17	84.8	12.7	2.5

The optimal conditions for maximum yield were predicted to be a microwave power of 620 W, 12.0 min of irradiation time and 4.0 g of cellulose. The predicted values of the response under these experimental conditions and the values obtained experimentally are shown in Table 6.

To our delight, the observed values (after three replications) were slightly superior to those predicted. It is important to point out that the model could really predict the combination of factors to give the best response.

These results demonstrate that the microwave pyrolysis of cellulose under the optimised conditions affords levoglucosenone in slightly better yields than those obtained under conventional pyrolytic conditions (3–5%).<sup>3</sup> The levulinic acid can be easily removed by washing the material with dilute  $\text{NaHCO}_3$  solution, recovering 95% of the amount of levoglucosenone.

In order to test the reproducibility of the method developed in a domestic oven (MW-1), we also performed the same experiments in a different microwave oven (MW-2). The representative runs were carried out in duplicate and are shown in Table 7.

The results obtained with two different domestic microwave ovens showed an excellent reproducibility of the results under the optimised conditions.

## Conclusions

We have demonstrated that cellulose can be pyrolyzed under microwave irradiation to produce levoglucosenone. To the best of our knowledge this is the first example of the successful preparation of levoglucosenone under microwave-assisted conditions. An experimental design approach was used to establish the variables (factors) involved in this transformation and to find the optimal conditions that give a maximum yield of product.

## Experimental

### General

Nuclear magnetic resonance spectra were recorded on a Bruker Avance-300 with tetramethylsilane as an internal standard and deuteriochloroform as solvent. GC-mass spectra were carried



out in a Perkin Elmer Autosystem XL gas chromatograph with a Perkin Elmer mass detector model TurboMass. Microwave-assisted reactions were performed in domestic ovens: Whirlpool VIP-20 M-600 (MW-1) or Philco MPR 4020 (MW-2), which were located inside the fume hood. Flash column chromatography were performed using Merck silica gel 60H with ethyl acetate as eluent. The optimisation process was carried out using Design-Expert version 6.0.10 program.

### General procedures

The acid pre-treated cellulose was obtained by suspending 80 g of microcrystalline cellulose 99% (Anedra) in 400 mL of methanol with 2.4 g of  $\text{H}_3\text{PO}_4$ . The suspension was stirred for 30 min and evaporated. This procedure is similar to the one described in the literature.<sup>3</sup>

Microwave-assisted pyrolysis of cellulose was performed by the following methods:

Method X: the corresponding amount of acid pre-treated microcrystalline cellulose was placed in a borosilicate glass tube (2 cm internal diameter and 10 cm long). The tube was introduced into a 125 mL Erlenmeyer and covered with a 40 mL beaker. The equipment was placed into a glass crystalliser and covered with a 500 mL beaker to capture the volatiles that can escape from the first cover.

Method Y: the same equipment was used as in method X, with the only difference being that the cellulose was placed directly as a thin layer in the 125 mL Erlenmeyer.

After the corresponding period of microwave irradiation the glass equipment was removed from the microwave oven and kept inside the fume hood until it reached room temperature. Both glassware and char were washed with EtOAc and filtrated through a short path of silica gel to eliminate the char. The filtrate was evaporated in a vacuum. The yield of the reaction was calculated by the weight of the pyrolyzed material with respect to the amount of cellulose introduced into the oven. The molar fractions of **1**, **2** and **3** were calculated from the  $^1\text{H}$  NMR spectra.

The spectroscopic and physical data of these products were in good agreement with those reported in the literature.<sup>7</sup>

Calibration of the microwave field strength was accomplished by measuring the temperature rise in 1 kg of water exposed to microwave irradiation for a fixed period of time. This technique is described as Method 1015A by the U. S. Environmental Protection Agency.<sup>12</sup>

### Acknowledgements

This research was supported by Agencia Nacional de Promoción Científica y Tecnológica and CONICET,

Argentina, the International Foundation for Science, Sweden and the Organization for the Prohibition of Chemical Weapons, The Netherlands. We thank Prof. A. C. Olivieri for helpful discussions. AMS thanks CONICET and Fundación Josefinia Prats for the award of a fellowship.

### References

- 1 D. L. Klass, *Biomass for Renewable Energy, Fuels and Chemicals*, Academic Press, New York, USA, 1998.
- 2 F. W. Lichtenthaler, *Acc. Chem. Res.*, 2002, **35**, 728.
- 3 *Levogluconone and Levoglucosans: Chemistry and Applications*, ed. Z. J. Witczak, ATL Press, Mount Prospect, USA, 1994.
- 4 *Carbohydrate Synthons in Natural Products Chemistry. Synthesis, Functionalization, and Applications*, ed. Z. J. Witczak and K. Tatsuta, *ACS Symp. Ser. 841*, American Chemical Society, Washington, DC, USA, 2003.
- 5 For examples see: (a) L. Awad, R. Demange, Y. H. Zhu and P. Vogel, *Carbohydr. Res.*, 2006, **341**, 1235; (b) T. Nishikawa, D. Urabe and M. Isobe, *Angew. Chem., Int. Ed.*, 2004, **43**, 4782; (c) M. Gómez, J. Quincoces, K. Peseke, M. Michalik and H. Reinke, *J. Carbohydr. Chem.*, 1999, **18**, 851; (d) J. S. Swenton, J. N. Freskos, P. Dalidowicz and M. L. Kerns, *J. Org. Chem.*, 1996, **61**, 459.
- 6 (a) A. M. Sarotti, R. A. Spanevello, C. Duhayon, J. P. Tuchagues and A. G. Suárez, *Tetrahedron*, 2007, **63**, 241; (b) A. M. Sarotti, R. A. Spanevello and A. G. Suárez, *Org. Lett.*, 2006, **8**, 1487; (c) A. M. Sarotti, R. A. Spanevello and A. G. Suárez, *Tetrahedron Lett.*, 2005, **46**, 6987; (d) A. M. Sarotti, R. A. Spanevello and A. G. Suárez, *Tetrahedron Lett.*, 2004, **45**, 8203.
- 7 (a) Y. Halpern, R. Riffer and A. Broido, *J. Org. Chem.*, 1973, **38**, 204; (b) F. Shafizadeh, R. H. Furneaux and T. T. Stevenson, *Carbohydr. Res.*, 1979, **71**, 169.
- 8 (a) A. M. Sarotti, R. A. Spanevello, M. M. Joullie and A. G. Suárez, *Org. Lett.*, 2006, **8**, 5561; (b) R. M. Palau, *Química en Microondas*. CEM Publishing, USA, 2006; (c) A. de la Hoz, A. Díaz-Ortiz and A. Moreno, *Chem. Soc. Rev.*, 2005, **34**, 164; (d) C. O. Kappe, *Angew. Chem., Int. Ed.*, 2004, **43**, 6250; (e) M. Nüchter, B. Ondruschka, W. Bonrath and A. Gum, *Green Chem.*, 2004, **6**, 128; (f) B. L. Hayes, *Microwave Synthesis. Chemistry at the Speed of Light*, CEM Publishing, Matthews, NC, 2002; (g) P. Lidstrom, J. P. Tierney, B. Wathey and J. Westman, *Tetrahedron*, 2001, **57**, 9225.
- 9 (a) T. Pena, L. Pensado, C. Casais, C. Mejuto, R. Phan-Tan-Luu and R. Cela, *J. Chromatogr., A*, 2006, **1121**, 163; (b) C. E. Domoni, M. Hidalgo, F. Marken and A. Canals, *Anal. Chim. Acta*, 2006, **561**, 210; (c) E. Fuentes, M. E. Báez and D. Reyes, *Anal. Chim. Acta*, 2006, **578**, 122; (d) H. Tye and M. Whittaker, *Org. Biomol. Chem.*, 2004, **2**, 813.
- 10 (a) B. Girisuta, L. P. B. M. Janssen and H. J. Heeres, *Green Chem.*, 2006, **8**, 701; (b) C. Chang, M. Xiaojian and P. Cen, *Chin. J. Chem. Eng.*, 2006, **14**, 708.
- 11 (a) G. Capello, H. C. Goicoechea, H. F. Miglietta and V. E. Mantovana, *Chem. Educator*, 2003, **8**, 1; (b) E. Morgan, *Chemometrics: Experimental Design*, Wiley, New York, USA, 1995.
- 12 *Microwave assisted acid digestion of aqueous samples and extracts*, US Environmental Protection Agency, 1998, [www.epa.gov/epaoswer/hazwaste/test/pdfs/3015a.pdf](http://www.epa.gov/epaoswer/hazwaste/test/pdfs/3015a.pdf).

## An efficient synthesis of 1,5-benzodiazepine derivatives catalyzed by silver nitrate

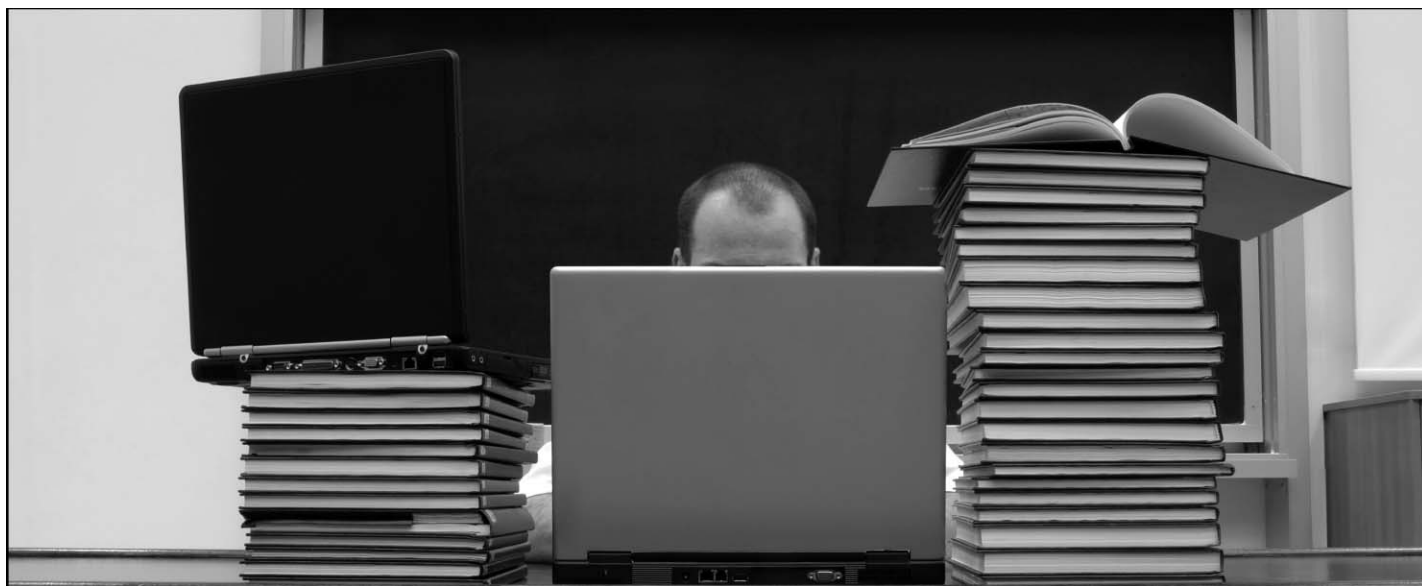
Rupesh Kumar, Preeti Chaudhary, Surendra Nimesh, Akhilesh K. Verma and Ramesh Chandra

*Green Chem.*, 2006, **8**, 519–521, (DOI: 10.1039/b601993e)

Our attention has been drawn to the elegant work of Kaupp, Pogodda and Schmeyers entitled ‘Gas/Solid Reactions with Acetone’ (*Chem. Ber.*, 1994, **127**, 2249–2261) who use a somewhat different strategy for making the salt of benzodiazepine *via* a gas phase reactor with acetone. Our paper complements this work and provides an alternative route to the product, which may well be optimised in the future to give similar yields.

The Royal Society of Chemistry apologises for these errors and any consequent inconvenience to authors and readers.

**Additions and corrections can be viewed online by accessing the original article to which they apply.**



## There is an easier way to keep up with research in your field...

An integral part of managing your career as a scientist is staying on top of the news and developments in your field of research and related areas. A good knowledge of your industry is a key component to your success, but finding the time to keep up with the latest research news can pose the greatest challenge.

**The solution?** By signing up for e-alerts from one of our free news services, you can receive updates about newsworthy and significant research appearing in RSC journals in a quick and easily digestible monthly alert.

**Free access.** From each news item you can link directly to the source research paper, which is completely free to access and download for a limited period.

**New tools to help you.** In addition to research news, our news services also feature

- **Instant insights** – whirlwind tours of exciting research areas you should know about
- **Interviews** – leading scientists share their opinions

**Chemical  
Technology**

[www.rsc.org/chemicaltechnology](http://www.rsc.org/chemicaltechnology)

**Chemical  
Science**

[www.rsc.org/chemicalscience](http://www.rsc.org/chemicalscience)

**Chemical  
Biology**

[www.rsc.org/chembiology](http://www.rsc.org/chembiology)

RSC Publishing

[www.rsc.org/ej\\_alert](http://www.rsc.org/ej_alert)

Registered Charity Number 207890

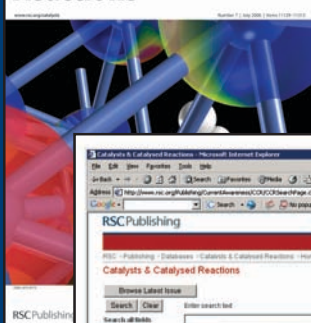
# Specialised searching



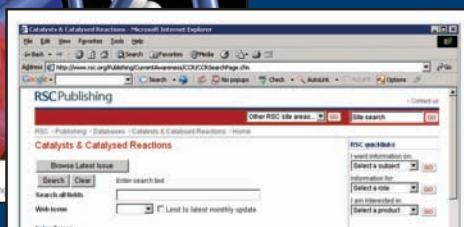
The graphical abstracting services at the RSC are an indispensable tool to help you search the literature. Focussing on specific areas of research they review key primary journals for novel and interesting chemistry.

## requires specialised tools

### Catalysts & Catalysed Reactions

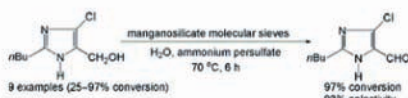


Catalysts and Catalysed Reactions covers all areas of catalysis research, with particular emphasis on chiral catalysts, polymerisation catalysts, enzymatic catalysts and clean catalytic methods.



The online database has excellent functionality. Search by: authors, products, reactants and catalysts, catalyst type and reaction type.

11086 The green catalytic oxidation of alcohols in water by using highly efficient manganosilicate molecular sieves  
H. G. Manyar, G. S. Chaure, A. Kumar\*  
Green Chem., 2006, 8(4), 344-348



With Catalysts and Catalysed Reactions you can find exactly what you need. Search results include diagrams of reaction schemes. Also available as a print bulletin.

Registered charity Number 207890

For more information visit

RSC Publishing

[www.rsc.org/databases](http://www.rsc.org/databases)



# See Science Come Alive



23010761

## Introducing Project Prospect

### Features include

- IUPAC Gold Book terms linked*
- Hyperlinked compound information in text*
- Ontology terms linked to definitions and related papers*
- RSS feeds with ontology terms and compound structures*

### Benefits

- Completely free service*
- At a glance HTML view with additional features accessed by toolbox*
- Downloadable compound structures*
- Printer friendly*

Scientists trawling through the thousands of research papers published every month must wish their computer could do the job for them. This could soon be a reality thanks to **Project Prospect**, an initiative developed by RSC Publishing together with academic partners. Readers can click on named compounds and scientific concepts in an electronic journal article to download structures, understand topics, or link through to electronic databases. Powerful functionality instantly helps researchers to find, understand and share (bio)chemical knowledge with each other quicker than ever before. See the science in journal articles *come alive*: visit the **Project Prospect** website for FAQs, examples, contact information and latest news.

RSC Publishing

[www.projectprospect.org](http://www.projectprospect.org)

Registered Charity Number 207890